UTS UNIVERSITY OF TECHNOLOGY SYDNEY

ENGINEERING THE POLYAMIDE SELECTIVE LAYER OF THIN FILM COMPOSITE MEMBRANES FOR OSMOTIC POWER GENERATION

by Ralph Rolly Gonzales

Thesis submitted in fulfilment of the requirements for the degree of

Doctor of Philosophy

under the supervision of **Professor Ho Kyong Shon** and **Dr. Sherub Phuntsho**

University of Technology Sydney
Faculty of Engineering and Information Technology

January 2021

Certificate of Original Authorship

I, *Ralph Rolly Gonzales*, declare that this thesis, is submitted in fulfilment of the requirements for the award of *Doctor of Philosophy*, in the *Faculty of Engineering and IT* at the University of Technology Sydney.

This thesis is wholly my own work unless otherwise referenced or acknowledged. In addition, I certify that all information sources and literature used are indicated in the thesis.

This document has not been submitted for qualifications at any other academic institution.

This research is supported by the Australian Government Research Training Program.

Signature: Production Note:
Signature removed prior to publication.

Date: 29 January 2021

I dedicate this thesis and my PhD degree to my family,

Rolito, Ruby, Ruelle Ela, and Raphael Lorenz,

for the love and the faith;

and to my precious nephews, my favourite persons in the world,

Kaelan Raphael and **Kristoff Reese**,

may you never grow tired of learning.

My success is nothing without you.

At the end of this journey, this is not just my PhD, this OUR PhD.

ACKNOWLEDGEMENTS

My PhD would not be possible without several people and institutions, to whom I shall express my gratitude through these acknowledgements.

First of all, this PhD thesis would not come into fruition without the support, guidance, and mentorship of my supervisors, Professor Ho Kyong Shon and Dr. Sherub Phuntsho. During my PhD, I have lost focus and determination many times, but the constant drive, passion, and management of Prof. Shon have kept me going. The fortnightly groups meetings and occasional personal meetings have proved effective in keeping my progress in check, and have helped me to constantly perform beyond expectations. I would also like to thank Prof. Shon for the scholarship provision during my entire PhD candidature, and for the opportunity to involve in a number of collaborative projects and a research experience in Kobe, Japan. Thank you also, Dr. Phuntsho, for allowing me to be part of the organising committee of 2020 MSA ECR Membrane Symposium; the experience taught me a lot and inspired me to be more involved in my professional network and research community.

Aside from my supervisors, I have been fortunate to have been guided and contantly cheered on by other people in our NanoMemPro research group who, despite not being my supervisors, have proved to be great help in completing my PhD work. Thank you, Dr. Leonard Tijing, Dr. Myoung Jun Park, Dr. Jungeun Kim, Dr. Donghan Seo, and Dr. Laura Chekli. Special thanks to Dr. Tijing for being instrumental in me doing my PhD in UTS under Prof. Shon – if we had not met in CESE in 2015, I would have done my PhD in an entirely different group, university, or country.

My research on development of PRO membranes was made possible through a grant from the Qatar National Research Fund, under its National Priorities Research

Program, and through our collaborators at Texas A&M University at Qatar (Professor Ahmed Abdel-Wahab) and Conoco-Phillips (Dr. Samer Adham).

It is comforting to know that I am not in this journey alone, I feel quite lucky that our research group had been among the largest one in the school, that I constantly did not feel alone. I would like to thank the whole NanoMemPro research group, for the shared times in and out of the laboratory. It is quite difficult to list everyone down in this acknowledgement, but I would like to particularly thank the 4SeaBrothers and the offspring dining club, for all the good food, good conversations, and good company shared: Dr. David Inhyuk Kim, Dr. Federico Volpin, Dr. Syed Muztuza Ali, Dr. Van Huy Tran, Dr. Pema Dorji, Dr. Minwei Yao, Dr. Nawshad Akther, Dr. Jiawei Ren, and Dr. Ugyen Dorji.

I also would like to acknowledge the help in the laboratory by Dr. Md Abu Hassan Johir, Dr. Nirenkumar Pathak, and Dr. Sungil Lim, as well as the administrative support of Ms. Van Le, Ms. Maya Tanaka, Ms. Trish Dimasi, Mr. Alex Chen, Ms. Minnie Wan, and Mr. Samuel Ho. Doing my PhD had taken its toll on my health, and I also wish to thank the UTS Health Service, specifically Dr. Leonie Matthews, Dr. Melissa Noetel for guiding me in taking care of my physical, emotional, and mental health.

The last chapter of my thesis was wholly done at Kobe University, Japan, wherein I conducted my overseas research collaboration program. This would not have been possible without the support of Professor Hideto Matsuyama and the Center on Membrane and Film Technology.

I always look back at the rigorous research training I received from the Environmental Processes and Materials Laboratory (now situated in Yonsei University; previously the Environmental Energy Research Laboratory at Daegu

University), headed by Professor Sang-Hyoun Kim, which provided the foundation of academic research career and the opportunities which led me to where I am now.

I am very grateful to my cousin and her family, Kimberly Miana, Christian Miana, and their children Cataleya and Cornelius, for providing me a home and for making sure that I did not encounter any problems during my stay in Sydney. Through them, I also found other families in Sydney, the Gutierrez and the Paras families, with whom I have celebrated milestones and personal victories.

Many people say that friends are family you choose. I would then like to thank my chosen family. Living in another country is tough, but it always gets better knowing you are not alone. Thank you to my Filipino friends in Australia: Dr. Joshua Tapas, Dr. Yami Bautista, Mara Gonzales, Dr. Nina Versoza, Dr. William Infante, Kami Navarro, Dr. Jeff Hora, Dianne Relojo, Justelle Tuiza, Faith Santos, Patrick Santos, Sarah Genelsa, Elmer Austria, Ross Anne Yumol, Nikki Natividad, Vhon Garcia, Anthon Repollo, Billy Uy, Mia Pavia, Mika Sioson, Dr. Bobby Katigbak, and Dr. Stephanie Chua, among others. Thank you also to my Korean circle at UTS – Dr. Seongchul Ryu, Weonjung Sohn, Dr. Yonghyun Shin, Dr. Youngkwon Choi, and Yunju Jo – for adopting me as a part of your group, despite not being Korean. Thank you as well to my Engineering PhD friend circle, for the random dinners and fun times, Dr. Alex Phuong, Dr. Kireesan Sornalingam, Dr. Sara Farahmandian, and Dr. Hannah Sun. During my stay in Sydney, I have found myself living in several shared houses, and I have been lucky to have met housemates, who despite not being graduate students in Sydney or staying for a short time due to working holiday visa conditions, have shown me kindness and generosity: Yoongi Shim, Yunje Jung, Dongil Shin, Hongseon Lee, and Junsik Lim. Lastly, thank you to all my friends in the Philippines and Korea,

who have made time to meet me during my short trips to these countries during my PhD candidature.

I was only supposed to stay in Japan for a few months, but ended up staying longer due to CoViD-19. I was able to get by through a few people who make my stay here more bearable, despite being alone in a foreign country. I am fortunate to have Filipino friends, whom I have known for over ten years, here in Japan, Dr. Mellissa Alcantara, Dr. Alvin Acebedo, and Dr. Lubai Punzalan-Enriquez. I also gained a few friends in my current research group: Titik Istirokhatun, Kyoko Miyake, Dr. Lei Zhang, Dr. Kecheng Guan, Dr. Yuqing Lin, Yuki Kawabata, Kai Ushio, Takafumi Ueda, and Wataru Kushida. Outside the university, I met these people and gained great friends: Isao Ohara, Fuminori Nagae, Andy Limas, Kenichi Kawahira, and Yoshio Yoshimura.

Last but not the least, I offer my eternal gratitude and love to my family for their overwhelming support during my entire PhD. They are mainly the reason why I constantly thrived and continued, despite numerous setbacks and issues. I did not give up primarily because I did not want to disappoint them, but I ultimately persevered because I felt empowered by their constant care and love. Thank you, Papa, Mama, Ela, Lorenz, and babies, and I love you!

Ralph Rolly Gonzales

LIST OF PUBLICATIONS RELATED TO THESIS DURING CANDIDATURE

1. **Gonzales, R.R.**, Park, M.J., Bae, T.-H., Yang, Y., Abdel-Wahab, A., Phuntsho, S. & Shon, H.K. 2019. 'Melamine-based covalent organic framework-incorporated thin film nanocomposite membranes for enhanced osmotic power generation', *Desalination*, vol. 459, pp. 10-19. (**Chapter 4)**
2. **Gonzales, R.R.**, Yang, Y., Park, M.J., Bae, T.-H., Abdel-Wahab, A., Phuntsho, S. & Shon, H.K. 2020. 'Enhanced water permeability and osmotic power generation with sulfonate functionalised porous polymer-incorporated thin film nanocomposite membranes', *Desalination*, vol. 496, pp. 114756-114765. **(Chapter 5)**
3. **Gonzales, R.R.**, Abdel-Wahab, A., Adham, S., Phuntsho, S., Suwaileh, W., Hilal, N. & Shon, H.K. 2020. Salinity gradient energy generation via pressure retarded osmosis: A review', *Desalination*, vol. 500, pp. 114841-114852. **(Chapter 2)**
4. **Gonzales, R.R.**, Abdel-Wahab, A., Phuntsho, S., Matsuyama, H. & Shon, H.K. 2020. 'Aliphatic polyketone-based thin film composite membrane with mussel-inspired polydopamine interlayer for high performance osmotic power generation'. **(Chapter 7)**
5. **Gonzales, R.R.**, Abdel-Wahab, A., Matsuyama, H., Phuntsho, S. & Shon, H.K. 2020. 'Control of the antagonistic effects of chlorine oxidative degradation on pressure retarded osmosis thin film composite membrane surface'. **(Chapter 6)**

PhD Candidate Credit Statement: Conceptualisation; Methodology; Formal analysis; Investigation; Data curation; Writing of original draft; Review and editing; Visualisation

LISTS OF OTHER PUBLICATIONS DURING CANDIDATURE

1. **Gonzales, R.R.**, Park, M.J., Tijing, L., Han, D.S., Phuntsho, S. & Shon, H.K. 2018, 'Modification of support layer for thin film composite forward osmosis membranes via layer-by-layer polyelectrolyte deposition', *Membranes*, vol. 8, no.3, pp. 70-84.
2. Park, M.J., **Gonzales, R.R.**, Abdel-Wahab, A., Phuntsho, S. & Shon, H.K. 2018. 'Hydrophilic polyvinyl alcohol coating on hydrophobic electrospun nanofiber membrane for high performance thin film composite forward osmosis membrane', *Desalination*, vol. 426, pp. 50-59.
3. Volpin, F., **Gonzales, R.R.**, Lim, S., Pathak, N., Phuntsho, S. & Shon, H.K. 2018. 'GreenPRO: A novel fertiliser-driven osmotic power generation process for fertigation', *Desalination*, vol. 447, pp. 158-166.
4. Park, M.J., Lim, S., **Gonzales, R.R.**, Phuntsho, S., Han, D.S., Abdel-Wahab, A., Adham, S. & Shon, H.K. 2019. 'Thin-film composite hollow fiber membrane incorporated with graphene oxide in polyethersulfone support layer for enhanced osmotic power density', *Desalination*, vol. 464, pp. 63-75.
5. Kim, D.I., **Gonzales, R.R.**, Dorji, P., Gwak, G., Phuntsho, S., Hong, S. & Shon, H.K. 2020. 'Efficient recovery of nitrate from municipal wastewater via MCDI using anion-exchange polymer coated electrode embedded with nitrate selective resin', *Desalination*, vol. 484, pp. 11425-11433.
6. Park, M.J., Wang, C., Seo, D.H., **Gonzales, R.R.**, Matsuyama, H. & Shon, H.K. 2021. 'Inkjet-printed single walled carbon nanotube as an interlayer for high performance thin film composite nanofiltration membrane', *Journal of Membrane Science*, in press.

7. **Gonzales, R.R.**, Phuntsho, S., Matsuyama, H. & Shon, H.K. 2021. ‘Facile development of comprehensively fouling-resistant and self-cleaning reduced aliphatic polyketone-based thin film composite forward osmosis membranes for treatement of oily wastewater’.
8. Zhang, L., **Gonzales R.R.**, Shon, H.K., & Matsuyama, H. 2021. ‘In situ engineering of an ultrathin polyampholyte layer on polyketone-based thin film composite forward osmosis membrane for comprehensive anti-fouling performance’.

CONFERENCE PRESENTATIONS DURING CANDIDATURE

1. **Gonzales, R.R.**, Park, M.J., Bae, T.-H., Yang, Y., Abdel-Wahab, A., Phuntsho, S. & Shon, H.K. 2018. 'Melamine-based covalent organic framework-incorporated thin film nanocomposite membranes for enhanced osmotic power generation', *The 11th Conference of the Aseanian Membrane Society*, Queensland, Australia, 3-6 July 2018.
2. **Gonzales, R.R.**, Yang, Y., Park, M.J., Bae, T.-H., Abdel-Wahab, A., Phuntsho, S. & Shon, H.K. 2019. 'Enhanced water permeability and osmotic power generation with sulfonate functionalised porous polymer-incorporated thin film nanocomposite membranes', *The 12th Conference of the Aseanian Membrane Society*, Jeju Island, South Korea, 2-5 July 2019.
3. **Gonzales, R.R.**, Abdel-Wahab, A., Phuntsho, S. & Shon, H.K. 2020. 'Control of antagonistic chemical modification effects of chlorine and ionic liquids on thin film composite membranes for enhanced osmotic power generation', *The 12th International Conference on Membranes & Membrane Processes*, London, United Kingdom (online), 7-11 December 2020.

LIST OF ABBREVIATIONS

AEMA	2-aminoethyl methacrylate hydrochloride
APTMS	3-aminopropyltrimethoxysilane
APS	Ammonium persulfate
ANOVA	Analysis of variables
AFM	Atomic force microscopy
AL-DS	Active layer facing the draw solution (also known as, PRO mode)
AL-FS	Active layer facing the feed solution (also known as, FO mode)
ATR	Attenuated total reflectance
BattMix	Battery mixing
BTDA	3,3',4,4'-benzophenone tetracarboxylic dianhydride
BET	Brunauer-Emmett-Teller theory
CapMix	Capacitive mixing
CNT	Carbon nanotube
CQD	Carbon quantum dots
CA	Cellulose acetate
CTA	Cellulose triacetate
CCD	Central composite design
COF	Covalent organic frameworks
CP	Concentration polarisation
DI water	Deionised water
DCE	1,2-dichloroethane
DCM	Dichloromethane
***p*-DCX**	α-α'-dichloro-*p*-xylene
DMF	N,N-dimethylformamide
DMSO	Dimethylsulfoxide
DS	Draw solution (i.e., solution of higher solute concentration)
ERD	Energy recovery device
EDTA	Ethylenediaminetetraacetic acid
ECP	External concentration polarisation
FE-SEM	Field emission scanning electron microscopy
FO	Forward osmosis
FS	Feed solution (i.e., solution of lower solute concentration)
FTIR	Fourier transform infrared spectroscopy
GMVP	Global MVP project
GA	Glutaraldehyde
GO	Graphene oxide
HNT	Halloysite nanotube
HTI	Hydration Technologies, Inc.
HPI	Hydroxypolyimide
HPG	Hyperbranched polyglycerol
ICP	Internal concentration polarisation

IP	Interfacial polymerisation
LbL	Layer-by-layer
LIS	Liquid-phase ion stripping
LPRO	Low-pressure reverse osmosis
MPD	*m*-phenylenediamine
MBR	Membrane bioreactor
MD	Membrane distillation
MPC	2-methacryloxyloxyethylphosphorylcholine
MDI	Methylene diamine
MPDI	Methylphenylene diamine
MED	Multi-effect distillation
NF	Nanofiltration
NOM	Natural organic matter
NIPS	Nonsolvent-induced phase separation
OHE	Osmotic heat engine
PAO	Pressure assisted osmosis
PAA	Poly(acrylic acid)
PAN	polyacrylonitrile
PAH	Poly(allylamine hydrochloride)
PA	Polyamide
PAI	Polyamide-imide
PBI	Polybenzoxaxole-co-imide
PDA	Polydopamine
PEi	Polyetherimide
PES	Polyethersulfone
PE	Polyethylene
PEG	Polyethylene glycol
PET	Polyethylene terephthalate
PEI	Polyethylenimine
POSS	Polyhedral oligomeric silsesquioxane
PI	Polyimide
PK	Polyketone
PSf	Polysulfone
PVA	Polyvinyl alcohol
PVP	Polyvinylpyrrolidine
POPs	Porous organic polymers
PP	Porous polymer
PRO	Pressure retarded osmosis
PWP	Pure water permeability
RED	Reverse electrodialysis
RO	Reverse osmosis
RSF	Reverse salt flux
RSM	Response surface methodology
SNW	Schiff-based network
SWRO	Seawater reverse osmosis
TA	Terephthalaldehyde
THF	Tetrahydrofuran

TEOS	Tetraorthyl orthosilicate
TFC	Thin film composite
TFN	Thin film nanocomposite
TIPS	Thermal-induced phase separation
TOC	Total organic carbon
TMP	Transmembrane pressure
TBP	Tributylphosphate
TMC	Trimesoyl chloride
UF	Ultrafiltration
XPS	X-ray photoelectron spectroscopy

LIST OF SYMBOLS

a_s	Activity coefficient
A_m	Area, membrane (m^2)
C_i	Concentration at active layer interface
$C_{d,b}$	Concentration of bulk draw solution
$C_{f,b}$	Concentration of bulk feed solution
$C_{d,m}$	Concentration of draw solution at membrane active layer interface
$C_{f,m}$	Concentration of feed solution at support and active layer interface
C_f	Concentration of the feed solution during RO experiments
C_p	Concentration of the permeate solution during RO experiments
μ	Chemical potential
d_h	Diameter, cross-flow cell hydraulic
ΔH_{mix}	Enthalpy of mixing (J kg^{-1})
ΔS_{mix}	Entropy of mixing (J K^{-1})
G_B	Gibbs free energy of brackish water (J mol^{-1})
G_F	Gibbs free energy of freshwater (J mol^{-1})
ΔG_{mix}	Gibbs free energy of mixing freshwater and salt water
G_S	Gibbs free energy of salt water
ΔP	Hydraulic pressure, applied; transmembrane pressure (bar)
R	Ideal gas constant (8.314 x 10^{-2} bar L K^{-1} mol^{-1})
L	Length, channel
k	Mass transfer coefficient (m s^{-1})
n	Number of solute molecules (mol)
π	Osmotic pressure (bar)
π_d	Osmotic pressure, draw stream (bar)
π_f	Osmotic pressure, feed stream (bar)
$\Delta\pi$	Osmotic pressure difference (bar)
μ_p	Pore diameter, mean
V_{micro}	Pore volume, microporous
V_{total}	Pore volume, total
ε	Porosity, membrane support
W	Power density, membrane
W_{max}	Power density, membrane, maximum
P/P^o	Pressure, relative
σ	Reflection coefficient
β_{iji}	Regression interactive coefficient
β_i	Regression linear coefficient
β_{ii}	Regression quadratic coefficient
β_0	Regression y-intercept
Y	Response, response surface methodology
J_s	Reverse salt flux (g m^{-2} s^{-1})
Re	Reynolds number
R_{ms}	Ridge elevation, root mean square
R_a	Roughness, mean
Sc	Schmidt number
Sh	Sherwood number
D_s	Solute diffusion coefficient
B	Solute permeability constant (m s^{-1}; L m^{-2} h^{-1})
R	Solute rejection

K	Solute resistivity, membrane support (s m^{-1})
σ_p	Standard deviation, geometric
S	Structural parameter, m
S_{BET}	Surface area, BET theory
S_{micro}	Surface area, microporous
T	Temperature (K)
t	Thickness, membrane support (m)
τ	Tortuosity, membrane support
i	Van't Hoff factor
$\bar{V}_s$	Volume, moral
V_w	Volume, solvent
ΔV	Volume change
J_w	Water flux (L m^{-2} h^{-1})
A	Water permeability constant (m s^{-1} bar^{-1}; L m^{-2} h^{-1} bar^{-1})

LIST OF TABLES

LIST OF FIGURES

TABLE OF CONTENTS

ABSTRACT

Population increase and economic growth have played huge parts in the continuously increasing global energy consumption, which has led to the fossil fuel reserves decline and greenhouse gas emissions. Thus, there is a significant increase in interest in alternative renewable energy sources, among which is osmotic power or salinity gradient energy. Osmotic power is harnessed upon the mixing of water streams with different solute concentrations and osmotic pressures (typically, freshwater and saltwater). Pressure retarded osmosis (PRO) is a process which exploits the osmotic pressure difference between the water streams and allows water to pass through a selectively permeable membrane from the less concentrated stream to the pressurised more concentrated stream. While PRO presents itself as an environmentally benign energy-harnessing process, its wide-scale implementation and technological development are hindered by challenges, among which is the available of suitable and high-performance membranes. Thin film composite (TFC) membranes are conventionally utilised for PRO, due to their porous membrane substrate and dense thin film selective layer, which, together, can exhibit outstanding separation performance and withstand the application of hydraulic pressure during PRO operation. In this thesis, TFC membrane development for PRO was conducted by engineering specifically the polyamide thin film selective layer. Several techniques were conducted in this thesis, which include: (1) nanomaterial filler incorporation; (2) surface functionalisation via nanomaterial incorporation; (3) chemical treatment; and (4) substrate-and-selective-layer interface modification.

First, melamine-based covalent organic framework nanomaterial, Schiff base network-1 (SNW-1), was incorporated into the polyamide selective layer to develop a

thin film nanocomposite (TFN) PRO membrane. This material was chosen due to its size, porosity, and intrinsic hydrophilicity, and these properties could further enhance the performance of the TFC PRO membrane. SNW-1 deposition during interfacial polymerisation (IP) was first investigated, and it was observed that the secondary amine functional groups of SNW-1 react with the carbonyl groups of the acyl chloride IP precursor, effectively reducing the available reactive groups for the amine precursor; thus, SNW-1 was incorporated through the amine precursor, *m*-phenylenediamine (MPD). Upon incorporation, the porosity and intrinsic hydrophilicity of SNW-1 facilitated water transport across the membranes, while maintaining satisfactory salt rejection ability, resulting in enhanced water flux and power density. The best performing membrane with 0.02 wt% loading of SNW-1 exhibited an initial water flux of 42.5 L m^{-2} h^{-1} and a maximum power density of 12.1 W m^{-2}.

The second study on functionalisation of the polyamide selective layer was achieved via the incorporation of a sulfonate-functionalised porous polymer, PP-SO_3H. Following the successful development of SNW-1, another nano-sized porous material was chosen due to its size, porosity, hydrophilicity, and functionality. The sulfonate functional group of the material was hypothesised to provide better affinity with water molecules and resistance with solute particles. PP, a hydrophobic porous organic polymer synthesised via *Friedel-Crafts* alkylation of dichloro-*p*-xylene, was reacted with chlorosulfonic acid to produce the hydrophilic sulfonate-functionalised PP-SO_3H. Not only did the presence of the highly hydrophilic functional group assist in the nanomaterial compatibility with the aqueous amine precursor during IP, it was also able to extend its functionality with the selective layer, enhancing the membrane water permeability, porosity, and osmotic energy harvesting capability. The best performing

membrane with 0.002 wt% loading of PP-SO_3H exhibited an initial water flux of 46.3 L m^{-2} h^{-1} and a maximum power density of 14.6 W m^{-2}.

TFC membranes are known to be highly susceptible to constant exposure to chemicals, such as chlorine, present in the water streams, which damage the membrane selective layer after continuous exposure. After TFC membrane modification via nanomaterial incorporation was performed for the first two technical chapters of this thesis, TFC membrane modification was then performed using chemical agents. Exploiting the chemical reactions of the polyamide with chemical agents and controlling the antagonistic effects were hypothesised to improve the water permeability performance of the TFC membranes. In the third study, the TFC membranes were placed in control oxidative degradation conditions using active chlorine in aqueous NaOCl solution. Chlorine and heat can thin out the dense selective layer, and when controlled and optimised, can tune the membrane surface properties and separation performance. Optimisation was performed in terms of chlorine exposure (a factor of both exposure time and chlorine dosage), solution pH, and subsequent heat treatment time. The resultant membranes exhibited various levels of polyamide degradation and increase in water permeability, at the expense of salt rejection performance. Response surface methodology (RSM) was performed to maximise the water permeability and power density and the antagonistic effects of the chlorine modification on the TFC membrane rejection capability was controlled. The RSM results showed that modification of the TFC membrane using 4000 ppm Cl_2·h, pH 10.9, and 216 s (3.6 min) heating time would yield the highest water flux of 84.7 L m^{-2} h^{-1}, specific reverse solute flux of 1.8 g L^{-1}, and power density of 4.7 W m^{-2} at 5 bar. These results indicate the usability of chlorine modification for TFC PRO

membranes for specific and niche PRO applications, especially those which does not require a high hydraulic pressure and high membrane selectivity.

The relationship of the membrane substrate morphology and the formation of the polyamide selective layer during IP was lastly investigated. This study aimed to bring together both chemical modification and nanomaterial incorporation to enhance the PRO membrane performance. The membrane substrate-and-selective-layer interface was modified by the introduction of bio-inspired polydopamine (PDA) interlayer. Two types of PDA layer were prepared and compared in this study: (1) the conventional PDA layer formed from the self-polymerisation of dopamine, and (2) the PDA nanoparticle layer formation formed from ammonia-initiated dopamine polymerisation. The difference in the interlayer morphology revealed differences in the way the polyamide selective layer was formed during IP, leading to difference in osmotic performance, as well. While the smooth interlayer was known to be preferred due to the ability to form thinner and less dense polyamide, the nanoparticle interlayer exhibited the formation of a looser polyamide, similar to nanomaterial-incorporated TFN membranes, with the PDA nanoparticles providing enhanced hydrophilicity and additional channels for water molecule transport. The best performing membrane with nanoparticulate PDA layer formed at pH 9.0 exhibited an initial water flux of 40.8 L m^{-2} h^{-1} and a maximum power density of 17.1 W m^{-2}.

The four studies presented in this thesis show how vital the engineering of the polyamide selective layer is in enhancing the separation performance and osmotic energy harvesting capability of TFC PRO membranes. These techniques prove not only facile and effective, these are also versatile and applicable for a variety of membrane substrates and even larger-scale membrane development.

1. Introduction

1.1 Thesis

This thesis aims to prepare mechanically strong, stable, and suitable **membranes** for **pressure retarded osmosis** (PRO), a process known to generate power from the osmotic pressure difference of water streams with different salinities. This particular **membrane fabrication** study involves the engineering of the selective layer of the **thin film composite (TFC)** membrane, using a variety of methods, including **nanomaterial** incorporation, **surface functionalisation**, **chemical treatment**, and **TFC membrane interlayer** modification.

The following terms are defined as follows:

Membrane is a selective barrier which allows certain selected materials to pass through.

Membrane fabrication is a current field of study focused on preparation of suitable membranes for various membrane technology processes.

Nanomaterial is a material whose single unit is sized between 1 to 100 nanometres.

Pressure retarded osmosis is an osmotic technique used to separate a solvent (i.e., fresh water) from another solution with higher solute concentration (i.e. salt water) and applied pressure; a technique used to generate power from the salinity gradient energy obtained from the salt concentration difference between the fresh and salt water.

Surface functionalisation is the introduction of a functional group on the membrane surface, done by either chemical treatment, grafting, or incorporation of functionalised materials.

Thin film composite membrane is a semipermeable membrane, typically made from a thin polyamide layer deposited on top of a porous polymeric layer, whose properties include high rejection of undesired materials, high filtration rate, and good mechanical strength.

TFC membrane interlayer is the interface between the membrane support and selective layers.

1.2 Background

The world is currently experiencing rapid population growth, industrialization, and economic development, which lead to a higher demand for accessible energy (Chung, Li, et al. 2012; Gonzales & Kim 2017). The global energy use is highly dependent on fossil fuels, which are not only renewable, but also a primary cause of greenhouse gas emissions and global warming. Among the fossil fuels from which our energy is typically sourced are petroleum, coal, and natural gas (Shafiee & Topal 2009), and the amount of fossil fuel reserves is exponentially declining (Kruyt et al. 2009). Moreover, the worldwide surface temperature has in fact faced an increase in the last century. This has led to an increase in coastal erosion, flooding frequency, vegetation and livestock mortality, food shortage, illness prevalence, and destruction of several terrestrial and marine ecosystems (Root et al. 2003). Currently, several technologies have been continuously in study to provide sustainable and efficient solutions for the energy crisis. Technologies for more efficient production, processing, and distribution of energy are currently in various stages of development and implementation. Furthermore, a shift in the population's lifestyle has started to be noticeable, as societies, people, and enterprises have become more mindful of how energy use plays a vital role in the total energy requirement and crisis.

Due to the world demand for environmentally sustainable renewable energy, interest in cost-efficient, clean, and sufficient alternative sources has increased. Currently, these non-conventional renewable energy sources include solar, tide, wave, geothermal, wind, and biomass (Gonzales, Kim & Kim 2019; Gonzales et al. 2017; Kalogirou 2005; Touati & Tadeo 2017). While research on these alternative sources and technologies has been consistently done, widespread use of these renewable energy sources is impeded by uneven availability of the resources and high cost of installation and maintenance (Sgouridis & Csala 2014). Should the use of renewable energy sources be widely developed and implemented, this will lead to benefits which include, but are not limited to, environmental and economic sustainability and environmental safety (Kim, Choi & Lee 2012).

Another renewable and sustainable energy source is salt gradient power (Post et al. 2007). The mixture of two streams, freshwater and saltwater, produces this energy. The free energy is released as driven by the chemical potential difference between the two water streams (Alvarez-Silva & Osorio 2015). According to previous studies, the potential power which can be harnessed worldwide from the mixing of river water and saltwater will exceed 2 TW (Burheim et al. 2012; Lin, Straub & Elimelech 2014). Filtration and membrane technology have played a huge part in provision of fresh and clean water supply from a number of sources, such as surface runoff, aquifers, freshwater, brackish water, saltwater, and even wastewater and industrial effluents (Kim, Gonzales, et al. 2020; Nicolaisen 2003). Membrane-based technologies do not only have the ability to treat water and recover valuable materials, but also manage treatment with less number of unit operations and high viability for a larger scale application (Guo, Ngo & Li 2012). Membranes for such processes are characterized on the basis of the mechanical and chemical properties, as well as

permeability and selectivity (Strathmann 2001). In recent, studies on membrane-based technologies are continuously evolving, with researchers coming up with better approaches on the processes and better membranes for more efficient separation and suitability in various applications. It is highly predicted that membrane technology can sustainably manage the earth's water resources, especially in areas of high aridity (Elimelech & Phillip 2011). It is then remarkable to be able to find a membrane-based technology which can augment the world's requirements for both fresh water and energy altogether. A number of membrane-based technologies have surfaced to harness salinity gradient power, such as reverse electrodialysis (RED), capacitive mixing (CapMix), battery mixing (BattMix), and pressure retarded osmosis (PRO) (Straub, Deshmukh & Elimelech 2016; Yip & Elimelech 2014).

PRO is a process currently being developed to provide solutions for worldwide problems in finding alternative renewable energy sources (Achilli & Childress 2010; Yip & Elimelech 2014). While also capable of desalination and wastewater treatment, PRO mainly generates osmotic power, or the energy generated by the mixture of salt concentration difference between two streams, commonly freshwater and saltwater (Helfer, Lemckert & Anissimov 2014). Moreover, desalination of concentrated brine can also be performed using PRO. PRO utilizes a semi-permeable membrane which is positioned between these two streams, allowing fresh water to flow from the less concentrated stream towards the direction of the more concentrated one, in order to achieve concentration gradient equilibrium between the two streams. Electricity is then produced using hydro turbines, like how hydropower energy is produced. The similarity between osmotic energy and hydropower ends there, since a hydropower plant utilizes river water and dam, whereas PRO utilizes, as earlier mentioned, osmotic pressure gradient between two streams of different salinities. In PRO, the hydro turbine

depressurizes the permeate to obtain power. This energy-generating aspect of PRO is highly promising in harnessing renewable energy to significantly lessen our dependency on fossil fuels and the high carbon footprint associated with it.

Nevertheless, membrane fouling/scaling is a crucial problem when using wastewater feed or seawater. Fouling of membranes can be divided into organic, inorganic and biofouling which influence the efficiency of the desalination technology (D. Johnson 2015). The use of wastewater concentrate containing various foulants and scalants causes fouling problem. The fouling becomes severe when the wastewater is against the porous membrane sublayer rather than the active layer of the thin film composite (TFC) PRO membrane (Chun et al. 2017). It was realized that when using wastewater concentrate feed in the PRO process, calcium phosphate salt becomes the predominant fouling. To mitigate fouling/scaling tendency of the PRO membrane, a suitable pre-treatment method is necessary. Researchers have developed different mitigation strategies for PRO membrane to reduce fouling problem (D. I. Kim 2015; K. Yang 2010; Nagy et al. 2018). These strategies can minimize the operating cost relating to membrane cleaning and ensure long term performance of the PRO membrane.

1.3 Aims, objectives, and significance

1.3.1 Aims

PRO is an environmentally viable process to produce osmotic energy. Being an osmotic process, it requires a suitable membrane for its use. Commercial polymeric asymmetric membranes may be widely available; however, these membranes are limited in terms of performance and suitability for PRO. Development of mechanically

stable and highly robust PRO membranes will significantly make the PRO process much more efficient in delivering clean water and osmotic power.

1.3.2 Objectives

In this thesis, I will deliver and design high performance PRO thin film composite membranes via various engineering methods on the polyamide selective layer. Success of the research entails the ability to generate power from high-salinity water using the fabricated polyamide-engineered TFC membranes. The approaches and methods performed in this thesis could serve as pointers for future industrial applications, as well as large-scale PRO membrane development. The following are the specific objectives of this thesis:

- Investigate the effect of incorporation of highly porous and hydrophilic nanomaterials in the polyamide selective layer on PRO performance;
- Evaluate the feasibility of polyamide functionalisation via the incorporation of a functionalised nanomaterial and its effect on PRO performance;
- Exploit and control the antagonistic effects of chemical modification to maximise water permeability with satisfactory solute rejection during PRO operation; and
- Explore the effect of introduction of a nano-sized particulate intermediate layer on the formation of polyamide selective layer and PRO membrane performance.

1.3.3 Significance of the study

1. Fabrication of suitable membrane for PRO will not only enhance the water treatment aspect of the process, but also its efficiency in harnessing power.

2. Membranes can serve as “green materials” which are low-cost, environmental-friendly, and easily available. With the use of membrane technology, not only can we obtain fresh, usable water, but also, we eliminate the use of excessive energy and resources.

3. Even though thin film composite membranes have been prepared for PRO, the mechanism of water and salt transport remains to be insufficiently studied. This thesis hopes to draw more knowledge on this area. This thesis aims to engineer the porosity, hydrophilicity, functionality, chemistry, and structure of the polyamide selective layer through the methods chosen.

4. There are no clear guidelines in engineering the polyamide selective layer specifically for TFC PRO membranes. Most PRO membrane fabrication studies involved applying the same fabrication procedures for other water treatment membranes. In this thesis, the methods performed for engineering the polyamide selective layer were chosen due to their applicability in conventional and emerging niche applications of PRO.

1.4 Thesis structure

The thesis will be consisted of eight chapters:

Chapter 1 provides the background of this thesis and the research motivation, as well as the aims and objectives.

Chapter 2 provides a comprehensive review on the theory, history, and current state of pressure retarded osmosis and the membrane development specifically for this process.

Chapter 3 presents the general methods conducted during membrane development, as well as the membrane performance evaluation and characterisation methods.

Chapter 4 presents the first method chosen for polyamide selective layer engineering: incorporation of a highly porous and hydrophilic nanomaterial, melamine-based covalent organic framework SNW-1, in the polyamide selective layer.

Chapter 5, inspired by the successful results of SNW-1 incorporation in the polyamide selective layer, describes the functionalisation of the TFC membrane surface via incorporation of sulfonate-functionalised porous polymer, PP-SO_3H.

Chapter 6 then describes the modification of the polyamide selective layer with a chemical agent, chlorine. This chapter optimises the chlorine oxidative degradation and heat treatment of polyamide.

Chapter 7 shows the effect of alteration of the polyamide selective layer via introduction of bio-inspired polydopamine intermediate layer between the substrate and selective layer on the performance of TFC membranes.

Chapter 8 summarises how nanomaterial incorporation, surface functionalisation, chemical modification, and intermediate layer introduction could alter the properties of the polyamide selective layer of the TFC PRO membrane and affect osmotic performance. The recommendations for future study are also presented.

Figure 1.1 shows the graphic abstract of the methods for engineering of the polyamide selective layer of TFC PRO membranes presented in this thesis.

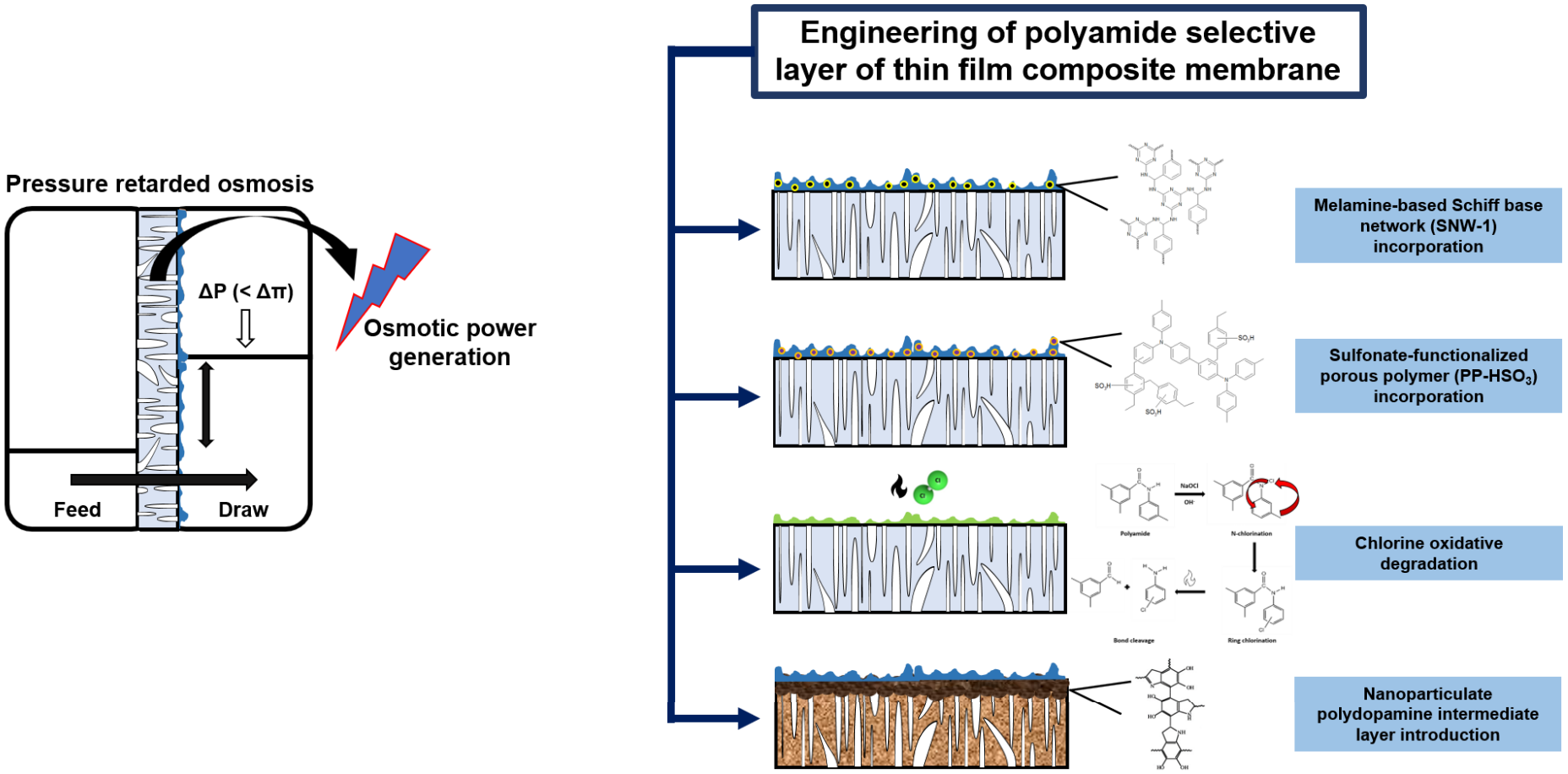

Figure 1.1 Graphical abstract of this thesis on engineering of polyamide selective layer of thin film composite membranes for osmotic power generation

2 Literature review

This chapter provides a comprehensive review on the theory, history, and current state of pressure retarded osmosis and the membrane development specifically for this process. A portion of this chapter was published as a review article in *Desalination*: **Gonzales, R.R.**, Abdel-Wahab, A., Adham, S., Phuntsho, S., Suwaileh, W., Hilal, N. & Shon, H.K. 2020. Salinity gradient energy generation via pressure retarded osmosis: A review', *Desalination*, vol. 500, p. 114841.

2.1 Theory

2.1.1 Engineered osmosis

A stream with lower solute concentration, known as the feed solution (FS), is separated from the draw solution (DS), another stream with higher solute concentration, by a semi-permeable membrane, which is only permeable for the solvent and impermeable for the solute. Due to the difference in the solute concentration of the two streams, both the FS and DS have different chemical potentials, μ. The osmotic pressure π between the FS and DS rises due to the concentration difference between these two streams, and the solvent (water, in this case) flows from the low-concentrated FS to the high-concentrated DS until equilibrium is reached. The transport of water through the semi-permeable membrane is known to be osmosis (Chung et al. 2015; Gerstandt et al. 2008; Logan & Elimelech 2012). Water transport from one side to the other causes an increase in the total volume of the DS, causing a difference in hydrodynamic pressure, which is known as the osmotic pressure difference, $\Delta\pi$. During the osmotic phenomenon, the DS is effectively diluted by the FS and the feed is concentrated simultaneously, until the chemical potential of the two streams across the membrane approaches equilibrium state. The osmotic

pressure (π) of a solution can be obtained from the amount of the solute particles (n, mol), the solvent volume (V_w, L), and temperature (T, K), as shown in:

$$\pi = \frac{n}{V_w} iRT \quad \textbf{2.1}$$

where R is the ideal gas constant (8.314 x 10^{-2} bar L K^{-1} mol^{-1}) and i is the dimensionless Van't Hoff factor (Loeb & Mehta 1978).

The transport of water through the semi-permeable membrane during osmosis is described using water flux, J_w, as shown in this equation:

$$J_w = A(\sigma\Delta\pi - \Delta P) \quad 2.2$$

where J_w, A, σ, $\Delta\pi$, and ΔP are water flux (L m^{-2} h^{-1}), pure water permeability constant of the membrane (L m^{-2} h^{-1} bar^{-1}), reflection coefficient, osmotic pressure difference (bar), and applied hydraulic pressure (bar), respectively (Cath, Childress & Elimelech 2006a). Pure water permeability constant A can be calculated as:

$$A = \frac{\Delta V}{A_m \Delta t \Delta P} \quad 2.3$$

where ΔV, A_m, and Δt are permeate volume, effective membrane area, and sampling time, respectively (Gonzales et al. 2018).

Reverse solute diffusion is the transport of solute (commonly, salt) from the DS to the FS across the semi-permeable membrane. Influenced by the concentration gradient across the membrane, reverse solute diffusion occurs naturally in osmotically-driven membrane processes. Due to the salt transport, the solute concentration of the FS effectively increases, thus the effective osmotic pressure difference of the FS and DS across the membrane decreases (Achilli & Childress 2010). The solute permeability of a membrane is a factor of the membrane's salt rejection, R, given by:

$$R = 1 - \frac{C_p}{C_f} \quad 2.4$$

where C_p *and* C_f are the solute concentrations in the permeate and feed solutions, respectively, during RO experiments. Using *R*, the solute permeability coefficient, *B*, of a membrane can be determined:

$$B = \frac{A(1-R)(\Delta P - \Delta\pi)}{R} \qquad \textbf{2.5}$$

The osmotic pressure difference energy is the free energy released during the spontaneous mixing of the FS and the DS (Loeb 1976; Yip et al. 2011). This free energy can be theoretically calculated from basic thermodynamics (Gerstandt et al. 2008), wherein the Gibbs free energy of mixing (ΔG_{mix}) freshwater and salt water is given by:

$$\Delta G_{mix} = G_B - (G_F + G_S) \qquad 2.6$$

where G_B, G_F, *and* G_S are the Gibbs free energies (J mol^{-1}) of brackish water resulting from the mixing of freshwater and salt water, freshwater, and salt water, respectively. The amount of Gibbs free energy which can be harnessed is basically a factor of the salinity difference between the two solutions mixed. As mentioned earlier, the reversible spontaneous mixing of freshwater and saltwater results in the production of work. Helfer et al. listed the maximum extractable energy from the mixing of freshwater with high salinity solutions from different sources, such as seawater, seawater reverse osmosis (SWRO) brine, salt-dome solution, Great Salt Lake, and the Dead Sea (Helfer, Lemckert & Anissimov 2014). Sea water obtained from the Dead Sea, known to be the most saline body of water, has an osmotic pressure of 507 bar, and, when mixed with water, can provide a theoretical maximum extractable energy of 14.1 kWh for every 1 m^{-3} of fresh water. On the other hand, seawater, which typically has a concentration equivalent to 0.55 M NaCl, mixed with fresh water can theoretically produce 0.75 $kWhm^{-3}$.

For an ideal solution, ΔH_{mix} = 0, thus ΔG_{mix} can simply be derived from temperature and ΔS_{mix}, which is the total molar entropy of the freshwater, saltwater, and the resultant brackish water streams during the mixing process. The calculated Gibbs free energy of mixing is known to be the theoretical maximum energy which can be produced during the mixing process (Volpin et al. 2018). When the water flux transports from the saline feed stream to the concentrated draw stream at almost constant pressure, the PRO process converts the osmotic pressure into hydraulic pressure. This results in an increase of the permeate volume generating a high amount of Gibbs free energy of mixing (ΔG_{mix}) (N. Hilal 2020). The general equation of ΔG_{mix} of the two different salinity solutions in an ideal process can be expressed as (Loeb, Van Hessen & Shahaf 1976):

$$-d(\Delta G_{mix}) = -RT\ ln(a_s dn_s) = \pi_{ss}\bar{V}_s dn_s \qquad \textbf{2.7}$$

in which, T and R denote the absolute temperature and the gas constant. a_s, n_s, π_{ss}, and $\bar{V}_s$ are the activity coefficient of the product solution, the number of moles of the product solution, the osmotic pressure of the salty solution, and the molar volume of the final solution.

Processes which utilise osmotic pressure difference include reverse osmosis (RO), forward osmosis (FO), pressure assisted osmosis (PAO), and PRO. However, not all of these can be considered as osmotically driven processes. It is because these membrane processes may be classified according to the applied hydraulic pressure on the system; and these processes may either be pressure-driven (i.e., ΔP is greater than $\Delta\pi$) or osmotically-driven (i.e., ΔP is zero or less than $\Delta\pi$). A pressure-driven process results to a state wherein the pressure increase beyond the net osmotic pressure between the two streams causes water to flow from the more concentrated DS to the less concentrated FS (Xie et al. 2015), which is the case in RO. On the other

hand, FO, PAO, and PRO are osmotically driven processes, during which water spontaneously moves across a semi-permeable membrane from the stream of lower solute concentration to the stream of higher solute concentration. These four processes are compared schematically in Figure 2.1 (Cath, Childress & Elimelech 2006a; Yun et al. 2014).

During RO operation, high hydraulic pressure is supplied on the concentrated DS by a high-pressure pump. The applied trans-membrane pressure ΔP is significantly much higher than $\Delta\pi$, thus reversing the direction of water transport. The applied pressure is required to facilitate the reverse flow of the solvent from the more concentrated stream to the less concentrated one (Cath, Childress & Elimelech 2006a). Due to this, water passes through the semi-permeable membrane from the concentrated DS, leaving behind an even more concentrated brine. The RO process has been the most extensively performed process for seawater desalination; however, energy is heavily utilised during this process.

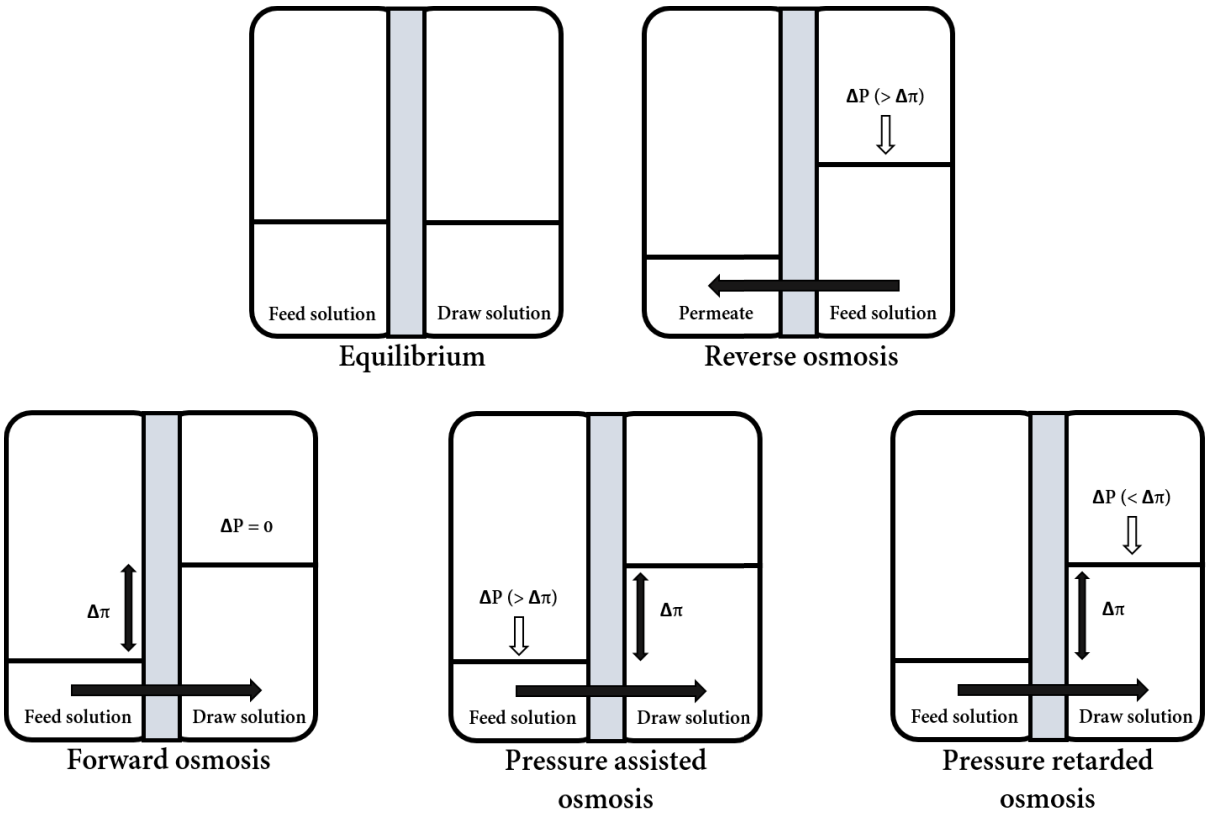

Figure 2.1 Schematic diagrams of the operational conditions of reverse osmosis, forward osmosis, pressure assisted osmosis, and pressure retarded osmosis

The naturally occurring FO makes use of the difference in salinity and osmotic pressure between the FS and DS streams, and thus, unlike RO, does not require the application of an external hydraulic pressure for it to occur. As seen in Figure 2.1, hydraulic pressure is nearly zero during FO operation, and water spontaneously passes through the semi-permeable membrane from the FS to the DS driven by $\Delta\pi$ (Cath, Childress & Elimelech 2006a). Unlike pressure-driven RO, FO is regarded as less energy-intensive, and less susceptible to membrane fouling (Chekli et al. 2016; Park et al. 2018). A typical FO system is shown in Figure 2.2.

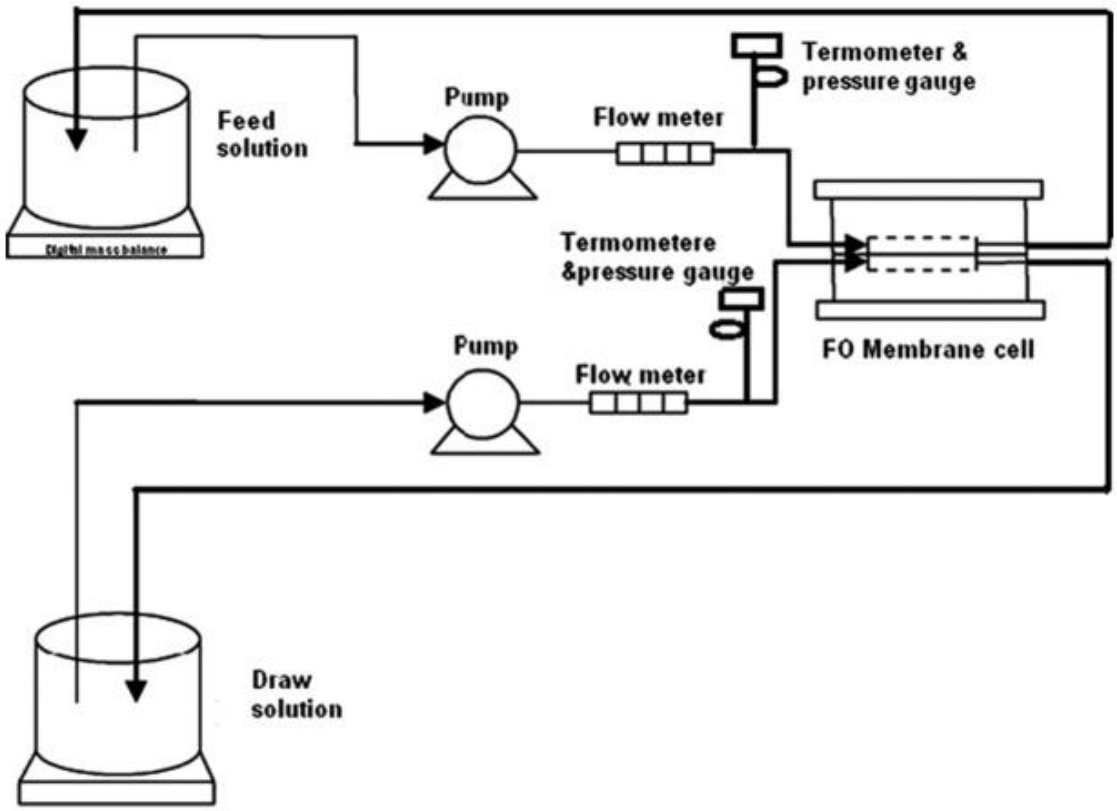

Figure 2.2 Schematic diagram of a conventional FO system (Amini, Jahanshani & Rahimpour 2013)

PAO is a process that involves properties of both FO and RO. Applied hydraulic pressure, which is less than the osmotic pressure difference, is present on the FS region to further facilitate the water transport driving force during this process. During PAO operation, the water moves due to the applied pressure on top of the osmotic pressure driving force between the DS and the FS (Oh et al. 2014; Yun et al. 2014). The application of additional hydraulic pressure serves two purposes: first is to facilitate water transport, and second is to mitigate the reverse diffusion of the solute.

Lastly, PRO is similar to both FO and PAO since the main driving force of this process is the osmotic pressure difference; however, during PRO, the water moves from the FS towards the DS against a hydraulic pressure applied on the DS stream side (She, Jin & Tang 2012). Due to the applied hydraulic pressure against the water flow, PRO is regarded as an intermediate process between FO and RO. The applied

hydraulic pressure effectively hinders the flow of the permeate water, thus retarding the osmotic flow, hence the name, pressure retarded osmosis. When the ΔP is between 0 and $\Delta\pi$, water transport from the FS to the DS is possible due to the osmotic pressure difference, but water permeation stops once $\Delta P = \Delta\pi$. Despite the application of hydraulic pressure, PRO still exploits the osmotic pressure difference between the two water streams, and, just like FO, water from the lower concentrated FS passes through the semi-permeable membrane toward the pressurised more concentrated DS (Mehta & Loeb 1978). The water flux across the membrane was prevented by the pressurisation of the DS stream, hereby retarding the water transport, hence the name "pressure retarded osmosis."

2.1.2 Power generation via pressure retarded osmosis

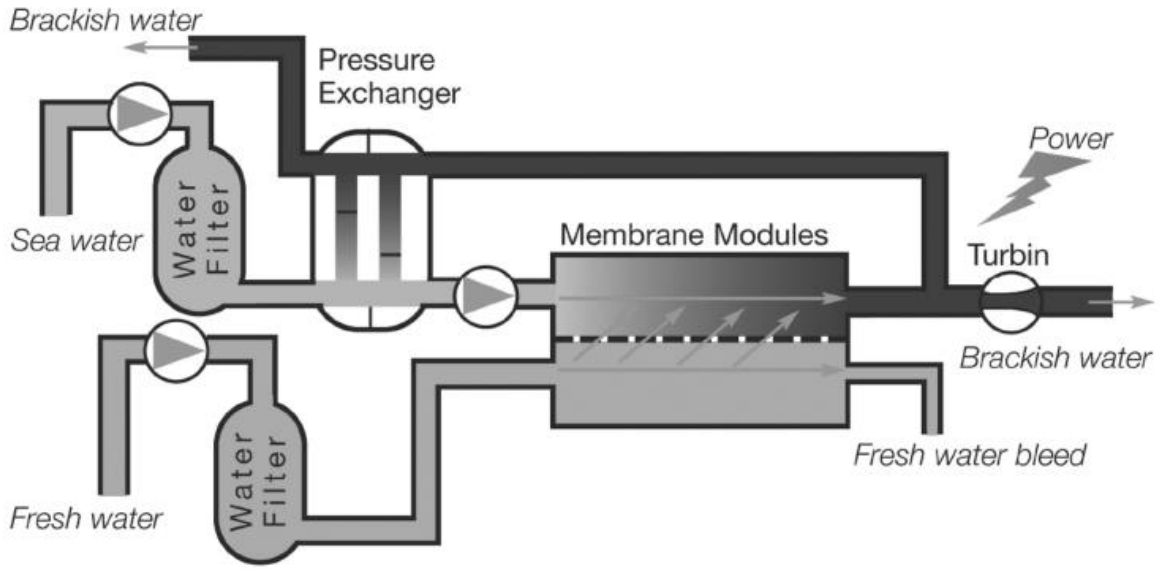

Figure 2.3 Schematic diagram of the conventional PRO process (Skilhagen, Dugstad & Aaberg 2008)

As earlier mentioned, the spontaneous mixing of freshwater and saltwater results to production of work, should the mixing be reversible. The spontaneity of mixing is

given by the Gibbs free energy, ΔG_{mix}, which is a function of the enthalpy of mixing (ΔH_{mix}) and entropy of mixing (ΔS_{mix}):

$$\Delta G_{mix} = \Delta H_{mix} - T\Delta S_{mix} \quad 2.8$$

For an ideal solution, ΔH_{mix} = 0, thus ΔG_{mix} can be simply derived from temperature and ΔS_{mix}, which is the total molar entropy of the freshwater, saltwater, and the resultant brackish water streams during the mixing process. The calculated Gibbs free energy of mixing is known to be the theoretical maximum energy which can be produced during the mixing (Volpin et al. 2018).

Figure 2.3 shows the schematic diagram of the PRO process. The FS first undergoes pretreatment using filtration and organics removal prior to use for PRO to reduce the presence of impurities and possible foulants. The FS is then placed in a non-pressurised compartment opposite the support layer of the semi-permeable membrane, while the DS is pumped through a pressure exchanger and placed in a pressurised compartment facing the active layer of the membrane. PRO operation usually occurs with the membrane orientation at PRO mode, or the membrane active layer facing the DS (AL-DS). FO and PAO, on the other hand, are operated via FO mode, or the membrane active facing the FS (AL-FS). Fresh water flows spontaneously across the membrane due to the osmotic driving force from the FS to the DS. Increase in both pressure and volume in the pressurised draw stream will be observed, as resulted by the water flow. The effective osmotic driving force, the difference of $\Delta\pi$ *and* ΔP, pushes the movement of water through the membrane at a steady water flux, J_w:

$$J_w = \frac{\Delta V}{A_m} \quad \mathbf{2.9}$$

where ΔV and A_m are the change in volume and membrane area, respectively. The increase in volume of the pressurised DS effectively increases the pressure. The

resultant diluted DS (brackish water) during the PRO process is then directed toward two different streams: (1) hydro-turbine, for energy production, and (2) pressure exchanger, for energy recovery (Kim & Elimelech 2013; Skilhagen, Dugstad & Aaberg 2008).

In PRO, power generated per unit membrane area (W m^{-2}) is known as the power density, *W*, given by this equation:

$$W = J_w \Delta P = A(\Delta\pi - \Delta P)\Delta P \qquad \textbf{2.10}$$

where *W* is the product of the water flux and the hydraulic pressure applied across the membrane (Lee, Baker & Lonsdale 1981). Upon differentiation of Equation 2.10 with respect to *ΔP*, the maximum power density can be obtained when *ΔP* is equal to half of the osmotic pressure difference across the membrane, as shown by:

$$W_{max} = A\frac{\Delta\pi^2}{4} \qquad \textbf{2.11}$$

The W_{max} during a PRO operation is directly proportional to the pure water permeability (PWP), *A*, and the square of the osmotic pressure difference across the membrane, thus the maximum power generation can be obtained when PRO is operated at a pressure close to $\frac{\Delta\pi}{2}$, as shown in Figure 2.4.

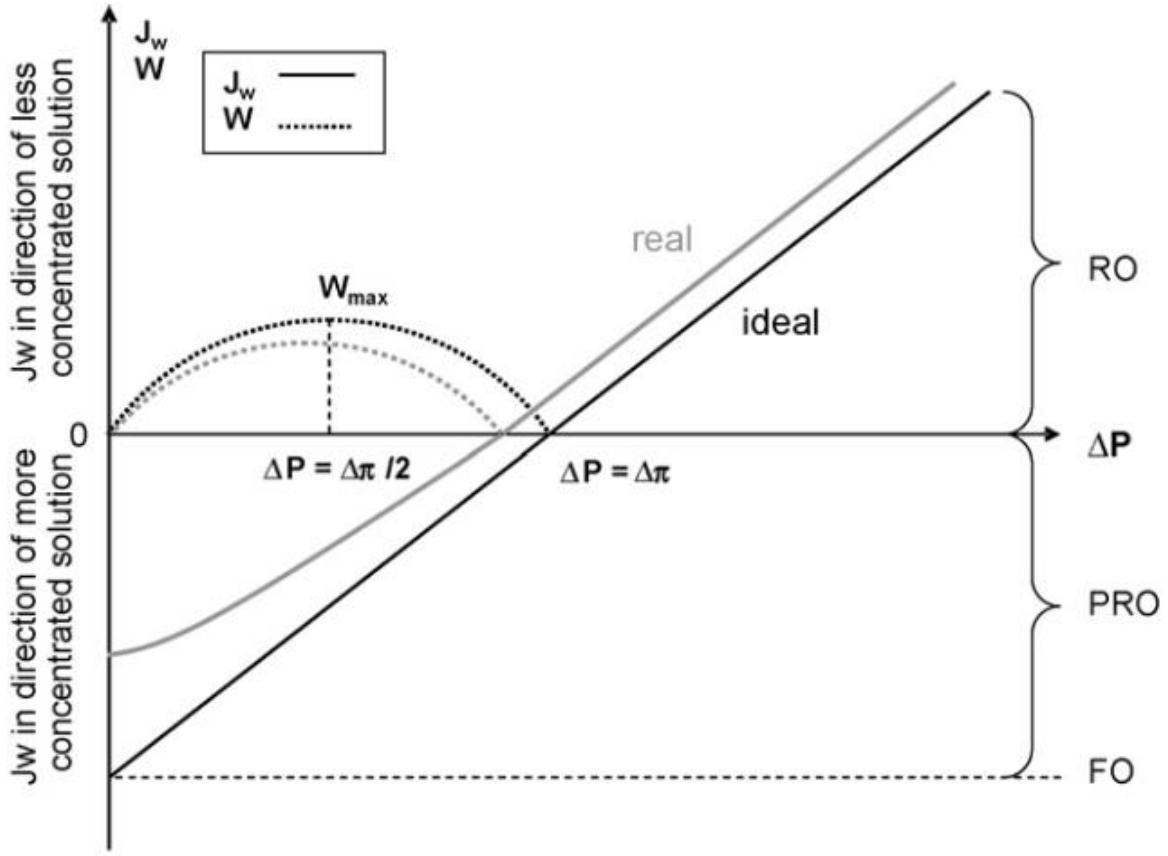

Figure 2.4 Ideal water flux (J_w) and power density (W) during PRO operation as a function of applied hydraulic pressure (ΔP). The conditions surrounding FO, PRO, and RO operation are also shown (Achilli, Cath & Childress 2009)

2.1.3 Reverse salt flux

Due to the non-ideality of the semi-permeable membrane, it is possible that solute can permeate from the DS toward the FS, in a phenomenon known as reverse salt flux (RSF). RSF leads to a decrease in effective osmotic pressure. RSF is a factor of another intrinsic membrane parameter, the solute permeability coefficient (B), which is determined from membrane salt rejection, R. R and B can be determined from the following equations (Gonzales et al. 2018):

$$R = \left(1 - \frac{C_d}{C_f}\right) \quad \textbf{2.12}$$

$$B = J_w \left(\frac{1-R}{R}\right) e^{-\frac{J_w}{k}} \quad 2.13$$

where C_d, C_f, and k are the DS solute concentration, FS solute concentration, and mass transfer coefficient, respectively (Tiraferri et al. 2011b). k can be determined from the Sherwood number (Sh), solute diffusion coefficient (D_s), and the cross-flow cell hydraulic diameter (d_h), which are based on the hydrodynamic conditions during an engineered osmosis process, and these parameters can be calculated from the following equations:

$$k = \frac{Sh \cdot D_s}{d_h} \qquad 2.14$$

$$Sh = 1.85 \left(Re \cdot Sc \frac{d_h}{L} \right)^{0.33} \; if \; Re < 2000 \qquad \mathbf{2.15}$$

$$Sh = 0.04 \cdot Re^{0.75} \cdot Sc^{0.33} \; if \; Re > 2000 \qquad 2.16$$

where Re, Sc, and L are Reynolds number, Schmidt number, and channel length, respectively (Tan & Ng 2013).

Upon determination of B, RSF, denoted as J_s, can be determined by this equation (Touati & Tadeo 2016):

$$J_s = B \, (C_d - C_i) \qquad \mathbf{2.17}$$

where C_i is the solute concentration at the active layer interface.

2.1.4 Concentration polarisation

During PRO operation, an amount of salt is able to permeate through the semi-permeable membrane due to RSF, significantly affecting the concentration gradient across the membrane. This then leads to the extraction of lower power density compared to the theoretical power density. The change in concentration gradient across the membrane causes reduction of water flux across the membrane; however, another phenomenon responsible for water flux decline during osmotic operation is concentration polarisation.

Concentration polarisation (CP) is a naturally occurring phenomenon during osmotically driven membrane processes. CP is the accumulation of solute particles on or near the membrane interface, resulting to the concentration of the solute on the membrane surface facing the feed stream (concentrative CP) and dilution on the side facing the draw stream (dilutive CP). CP especially occurs during processes utilizing asymmetric composite membranes, where a thin dense polyamide selective layer is on top of a porous membrane support. Solute particles tend to accumulate on the dense layer side (external CP, or ECP), or internally, on the interface between the membrane support and selective layer (internal CP, or ICP). Due to the occurrence of CP, the actual osmotic pressure difference across the membrane is less than the osmotic pressure difference of the bulk fresh and draw streams, and the consequence of which is water flux decrease (McCutcheon & Elimelech 2006). It is true that CP is not only influenced by the membrane design and transport properties, it is also influenced by the system specifications and design, hydrodynamics, and operating parameters. Figure 2.5 shows the concentration profile in a PRO membrane during PRO orientation due to CP.

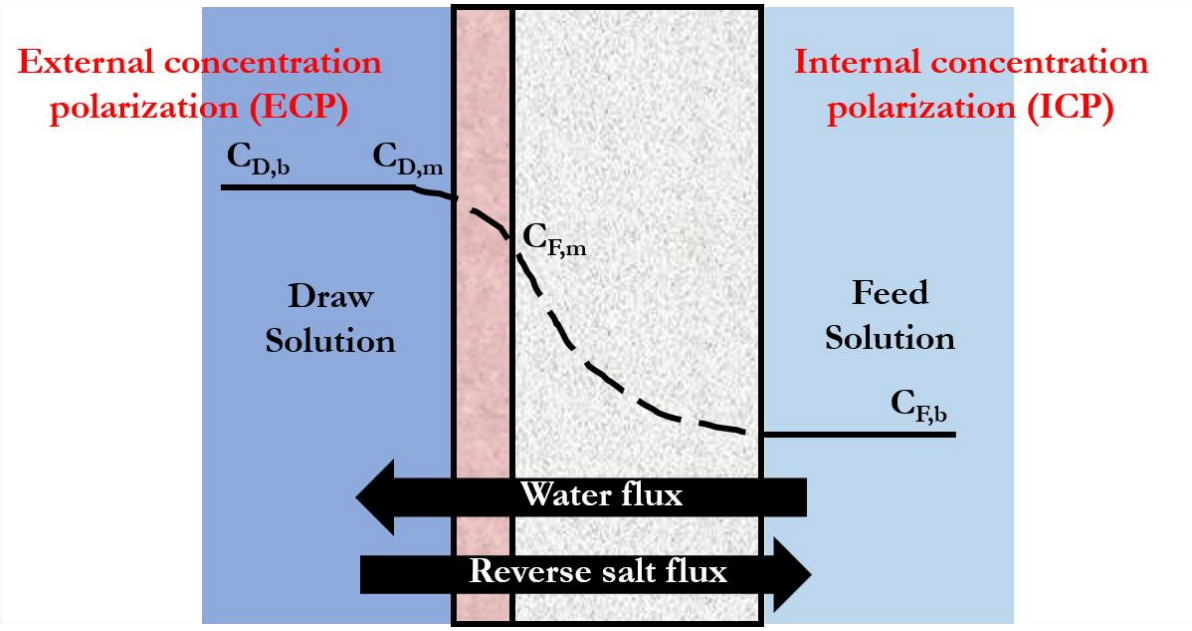

Figure 2.5 Concentration profile of the membrane during PRO operation as influenced by ECP and ICP. $C_{D,b}$, $C_{D,m}$, $C_{F,m}$, and $C_{F,b}$ are the concentration of the bulk draw solution, concentration of the draw solution at the membrane active layer interface, concentration of the feed solution at the support and active layer interface, and concentration of the bulk feed solution, respectively

One main factor affecting the occurrence of CP in osmotic processes is the membrane orientation. Asymmetric membranes typically have a porous support and a solute-rejecting active layer. For osmosis-driven processes, the active layer can have either one of the following orientations: (1) active layer facing the FS (AL-FS), or (2) active layer facing the DS (AL-DS). In the case of PRO, operation is conventionally performed with AL-DS membrane orientation, meanwhile other osmotic-driven processes, such as forward osmosis (FO) and pressure assisted osmosis (PAO) are typically operated at AL-FS membrane orientation.

Generally, ICP is caused by the inability of the solute particles to pass through the membrane active layer; therefore, ICP is heavily influenced by solute molecular size and diffusivity. ICP specifically occurs within the porous membrane support layer as the solutes of the DS accumulates at the interface of the support and the active layers, due to the inability of the solute particles to penetrate and pass through the

dense active layer (Zhou, Lee & Chung 2014). An immobile area is formed inside the membrane support, decreasing the osmotic driving force (McCutcheon & Elimelech 2008; Tow, McGovern & Lienhard V 2015).

The effect of ICP on the PRO performance is given by this equation (Lee, Baker & Lonsdale 1981):

$$J_w = A\left[\pi_{D,m}\frac{1-\frac{C_{F,b}}{C_{D,m}}e^{J_wK}}{1+\frac{B}{J_w}(e^{J_wK}-1)}\right]- \Delta P \qquad \textbf{2.18}$$

where $C_{F,b}$ and $C_{D,m}$ are the salt concentrations of the bulk FS and DS at the membrane surface, respectively. This model suggests that ICP generally occurs due to the presence of the membrane substrate layer. *K* is the solute resistivity of the porous membrane support for the diffusion of solute particles, and can be determined using the following equation (W. A. Suwaileh 2018):

$$K = \frac{t\tau}{D_s\varepsilon} = \frac{S}{D_s} \qquad \textbf{2.19}$$

where *t, τ, D_s, ε,* and *S* are the membrane support porosity, membrane support thickness, membrane support tortuosity, diffusion coefficient of the solute in the DS, membrane support porosity, and structural parameter, respectively. *S* is an important transport parameter in osmotic processes, as it provides a singular parameter describing the membrane porosity, thickness, and tortuosity, which could all influence the membrane permeability. By incorporating the solute resistivity (*K*), the concentration of the FS ($C_{F,b}$), the concentration of the DS ($C_{D,b}$), and ICP expression, the water flux equation can be rewritten as (Loeb, Van Hessen & Shahaf 1976):

$$J_w = A\left[\pi_{D,b}\frac{1-\frac{C_{F,b}}{C_{D,b}}\exp(J_wK)}{1+\frac{B}{J_w}[\exp(J_wK)-1]}-\Delta P\right] \qquad \textbf{2.20}$$

It can therefore be said that these properties of the porous membrane support layer affect the occurrence of ICP during PRO operation, and, consequently, affect the water flux.

ECP inhibits water flow due to the change in osmotic pressure at the membrane active layer surface. ECP can either be concentrative or dilutive, depending on the position of the active layer surface. If the active layer faces the feed side, the solute is concentrated at the membrane surface, resulting in concentrative ECP. On the other hand, dilutive ECP occurs when the solute is diluted around the membrane active layer facing the DS side. Eventually, the water flux and reverse solute flux across the PRO membrane can be influenced significantly by the mass transfer characteristics of the membrane. The physicochemical properties of the selected membrane are other crucial elements that deteriorate both the water flux and the RSF. Not only they could acerbate the reverse solute flux and the ICP, they may also critically lower the osmotic driving force for power extraction (A. Altaee 2017). Consequently, the development of high-performance PRO membranes with excellent water permeation and minimum reverse solute flux has increasingly attained attention in PRO research.

2.2 History and timeline of pressure retarded osmosis

PRO started as an idea of reversible osmotic mixing of freshwater and saltwater to produce power (Pattle 1954). PRO has gained attention since then; however, it was not fully developed until the late 20th century due to the limitations of the existing membranes and the underlying costs and economic challenges associated with process installation, especially during the efforts for process commercialisation (Jellinek & Masuda 1981; Lee, Baker & Lonsdale 1981; Sarp, Li & Saththasivam 2016).

In 1974, an osmotic energy converter was proposed to operate such that freshwater passes through a semi-permeable membrane toward a pressurised seawater chamber, after which, when the volume of the chamber is exceeded, water can runoff and operate a water wheel to operate a generator (Norman 1974). While technologically feasible, this proposal was considered to be uneconomical and expensive at the time. Loeb then proposed an osmosis process using high salinity streams from sources such as Dead Sea brine or the Great Salt Lake, during which existing RO equipment at the time which could apply hydraulic pressure up to 40 bar could be used. It was during this time, too, that the term “pressure retarded osmosis” was coined (Loeb & Norman 1975). This proposal was further validated using experimental data obtained from PRO operation using RO hollow fibre membranes, with freshwater and Dead Sea brine delivered onto the bore and shell sides, respectively (Loeb 1976). The experimental data were further supported by technical and economic evaluations to further demonstrate its feasibility (Loeb, Van Hessen & Shahaf 1976), albeit the poor osmotic performance during PRO operation attributed to the use of the RO hollow fibre membrane. The first PRO model was developed to account for water flux as a function of the osmotic pressures of the DS and the FS, separated by a porous permeator of a certain thickness *t*, as shown in this equation (Loeb 1976; Loeb & Mehta 1978; Loeb & Norman 1975):

$$J_w = A\left(\pi_d - \pi_f e^{\frac{t}{D_S}} - \Delta P\right) \qquad \textbf{2.21}$$

where π_d and π_f are the osmotic pressures of the DS and FS.

Loeb, in 1975, also proposed the concept of a closed-loop osmotic heat engine (OHE) (Loeb 1975). While this particular system does not exactly demonstrate production of renewable energy, it was considered a system to generate sustainable energy due to the huge availability of water resources which can be applied for PRO.

In this OHE, the fresh water passes through a selectively permeable membrane to dilute a pressurised concentrated DS, until the DS volume increases and flows through a turbine. To then separate the draw from the feed, a thermal distillation process is applied, and the heat energy was converted into mechanical work.

The first PRO model assumed that J_s and the effects of CP are negligible. The influence of CP on osmotic power generation via PRO was then examined (Mehta & Loeb 1978). This led to the development of the second PRO model, which considered the influence of ICP, while neglecting the effects of ECP, given in Figure 2.5 (Lee, Baker & Lonsdale 1981). Further mathematical simulations on PRO were conducted to further understand the mass transfer of solute and water and how these are influenced by the membrane properties, such as pure water permeability A, solute permeability B, and solute diffusivity D_s (Reali, Dassie & Jonsson 1990). During the late 1990s and early 200s, the focus on PRO study has shifted towards practical applications and further proof of the technological feasibility of PRO, producing salinity gradient power upon utilisation of brine from Dead Sea (Loeb 1998) and Great Salt Lake (Loeb 2001), and it was found out that produced energy from these sources cost $ 0.058 and $ 0.091 per kWh, respectively. From these findings, a larger-scale PRO implementation was conducted using spiral RO modules and river water and seawater (FS and DS, respectively), and it was found that the energy harnessed from PRO, given the marginal production costs, could offset the operational energy requirements of the RO plants, provided operating the limited PRO plant size and capacity (Loeb 2002).

Larger scale implementation of PRO was further conducted in various countries, with the objective of increasing the power density of the membranes, until Statkraft was able to achieve a power density of 3 W m^{-2} (Skråmestø, Skilhagen & Nielsen

2008). The first PRO osmotic power plant in the world was built by Statkraft in Norway in 2009. The PRO plant had an energy generation capacity of 10 kW and the generated power could reach at least 5 W m^{-2}. Statkraft decided to discontinue its operation of the PRO plant in 2014, citing the unlikeliness of the technology to be further developed within the market outlook at the time (International Renewable Energy Agency 2014). This failure of Statkraft to show the feasibility of PRO as a commercially-viable process lead to a shift in the direction of PRO, which is to develop hybrid processes involving PRO to augment the high energy consumption of more commercially-viable processes, such as SWRO.

In 2010, Japanese company Kyowakiden Industry Co. in collaboration with Kyushu University, Nagasaki University, Tokyo Institute of Technology, and Mega-ton Water System studied the implementation of a large-scale osmotic power plant and developed a PRO prototype plant which was envisioned to produce 9 W m^{-2} and a maximum power density of 13.5 W m^{-2} using concentrated SWRO brine and pre-treated wastewater as DS and FS, respectively (Saito et al. 2012; Tanioka 2016). The Mega-ton operation ended in 2014.

In 2017, a consortium of Korean researchers and industry partners, with the financial support of the Korean government, demonstrated the feasibility of an integrated SWRO and PRO hybrid process. The project, named Global MVP (GMVP), aimed to reduce the energy consumption of SWRO by recovering energy from the salinity gradient of SWRO brine and membrane bioreactor (MBR) permeate (Lee, Park, et al. 2020).

2.3 Fouling, scaling, and mitigation

One of the limitations of PRO is the occurrence of membrane fouling, which can be influenced by the membrane orientation and application of hydraulic pressure during PRO operation. Typical feed streams for PRO contain huge amounts of colloidal particles, organic, inorganic, and biological matter that could induce fouling and affect membrane performance, *i.e.*, flux and power density reduction. Upon occurrence of fouling, there is a decrease in the membrane performance, which, in turn, limits the power generation and increases power consumption. Fouling can be caused by a number of fouling substances, or foulants, which can be classified into any of the following: inorganic, organic, colloidal, and biological. In PRO process, fouling mainly occurs in any one of these fouling mechanisms: (1) pore plugging, (2) pore narrowing, and (3) film or cake formation. Pore plugging occurs when larger foulant particles plug the membrane pores. In the case of smaller or finer foulant particles, these can be absorbed into the membrane porous structure and accumulate inside the pores, effectively narrowing the pore size. Finally, film or cake formation occurs when the foulants are not absorbed into the pore, but accumulate on the membrane surface instead, effectively blocking the pore.

2.3.1 Fouling studies for PRO

Among the earliest PRO fouling studies was conducted by Yip et al., who investigated the influence of natural organic matter (NOM) (Yip & Elimelech 2013) on membrane performance. It was found out that NOM, which is highly present in river water, could cause severe water flux decline to over 46%, following the adsorption of the foulants at the interface between the active layer and membrane substrate, resulting in higher transport resistance (Yip & Elimelech 2013). Thelin et al. also

studied the effect of NOM, wherein the effect of NOM concentration and ionic strength in the feed stream was investigated (Thelin et al. 2013). The researchers found that the PRO membrane fouling propensity was independent of the NOM concentration, and instead was influenced by the increased ionic strength brought about by RSF and ICP.

Fouling due to organic substances, specifically, alginate, was found to be a major issue during PRO operation (She, Wong, et al. 2013). It was also found out in this study that alginate fouling was more severe when the DS contained large amounts of divalent cations, like Ca^{2+} and Mg^{2+}. Interactions of inorganic species with organic foulants enhanced organic fouling, especially at higher DS concentrations. Similarly, gypsum, or calcium sulfate dihydrate, was another foulant investigated and found to affect PRO operation performance (Zhang et al. 2014). Gypsum, formed from the interaction of calcium and sulfate present both in the feed and draw streams, was found to clog the pores of the membrane substrate and cause severe ICP.

Colloidal fouling, specifically, silica, was studied by Kim et al. (Kim, Park, et al. 2016). The researchers found that colloidal fouling due to silica occurs through a cake layer buildup at the surface of the membrane. Furthermore, salt diffusion increased fouling occurrence due to the interaction of the salt with the cake layer, effectively reducing the osmotic driving force.

Mixed gypsum scaling and sodium alginate fouling was examined in a study, which concluded that in combined fouling studies, the membranes are initially conditioned or fouled more easily by a single foulant (Chen, Wan & Chung 2015). After the conditioning, the membrane surface chemistry changes, which accelerates the fouling occurrence of the other foulants. The presence of both gypsum and alginate during PRO operation allows the initial occurrence of alginate fouling, due to the lower

gypsum scaling propensity due to reverse diffusion of Na^+; thus, alginate fouling conditions the membrane first, followed by the formation of gypsum scaling.

Combined fouling was investigated using real wastewater concentrate FS, using which, the main types of fouling include organic (humics and alginate) and inorganic (calcium phosphate and gypsum) fouling (She et al. 2017). Similar to the study which used model foulants, the scaling caused by inorganic foulants contributed mainly to the decline in membrane performance. RO retentate was also used as feed stream in an earlier study, and it was found that calcium phosphate scaling and silica fouling were the biggest fouling problems, affecting the innermost layer and the outmost surface of hollow fiber membranes, respectively (Chen, Amy & Chung 2016).

Biofouling propensity was investigated in another study, and it was found that biological population in the wastewater, when used as feed, could cause severe fouling both on the membrane substrate and feed spacer, and eventually cause severe flux decline (Bar-Zeev et al. 2015).

2.3.2 Pre-treatment processes and fouling mitigation

Kim and Elimelech (Kim & Elimelech 2013) were among the first ones to propose PRO configurations which include pretreatment of the feed stream to prevent the occurrence of membrane fouling, especially when municipal wastewater effluent would be used as feed instead of river water.

Abbasi-Garravand et al. proposed the use of a multimedia sand filter and ultrafiltration (UF) as pretreatment to eliminate total organic carbon (TOC), turbidity, and hardness of the FS prior to PRO operation (Abbasi-Garravand et al. 2016). Using the multimedia sand filter, 68.6% turbidity and 1.5% TOC were removed, while 100% turbidity and 41% TOC were removed using UF.

UF, nanofiltration (NF), and low-pressure reverse osmosis (LPRO) were conducted in another study as pretreatment procedures of wastewater retentate, prior to use as feed stream in another study (Yang, Wan, et al. 2019). Among the three processes, while LPRO was found to be able to most effectively mitigate fouling, NF was found to be the most effective in rejection of species such as calcium and phosphate ions which could form hydroxyapatite, a well-known scalant during PRO. Low-pressure NF was also performed by Chen et al., and they found that low-pressure NF could remove multivalent ions and NOM, which are both persistent foulants during PRO; however, silica fouling was not effectively prevented using this process (Chen et al. 2017).

Coagulation was performed as a pretreatment in a recent study (Wan, Jin & Chung 2019). Two coagulants, acidic $AlCl_3$ and alkaline $NaAlO_3$ were used to coagulate with phosphate to eliminate this particular species from the concentrated wastewater and prevent the formation of $Ca_3(PO_4)_2$. While both coagulants were effective in PO_4^{3+}, $AlCl_3$ was less effective in removal of silica, which leads to lower water flux recovery after hydraulic backwashing.

Fouling caused by the use of real concentrated wastewater as FS for PRO was mitigated in a study which employed different pretreatments to remove foulants from the feed (Chen, Amy & Chung 2016). Both pH adjustment by adding HCl and removal of anti-scalant via chelation with ethylenediaminetetraacetic acid (EDTA) were successful in mitigating fouling, even after backwashing. Another study demonstrated similar findings when anti-scalant pretreatment and pH adjustment were found to be both effective for fouling control (Han et al. 2016).

Kim et al. (Kim, Kim & Hong 2016) investigated the possibility of PRO operation with the membrane active layer facing the feed stream (AL-FS), instead of the

conventional membrane AL-DS membrane orientation, or the active layer facing the draw stream. They were able to demonstrate lower RSF during AL-FS operation, reduced pretreatment cost, and better fouling control due to the high shear flux caused by the water permeation from the FS toward the DS. While promising, this research was not followed up due to intrinsically lower membrane performance at AL-FS mode and issues with membrane deformation due to hydraulic pressure.

For continuous PRO operation, physical backwashing proves to be highly effective in removing fouling species from the porous support layer, leading to high recovery of membrane performance (Yip & Elimelech 2013). In another study, air bubbling was also found to be even more effective in removal of foulants on the membrane surface (Chen, Amy & Chung 2016). Various membrane cleaning agents were employed and compared for membrane cleaning and performance recovery ability. Among deionized water (DI water), alkaline solution, acidic solution, and chelating solution, the chelating agent EDTA was found to be the most effective in recovering the performance of the membrane used for PRO with wastewater effluent as feed (Li, Cai, et al. 2017).

Chemical-in-place was introduced as a cleaning strategy for a laboratory-scale SWRO-PRO pilot study (Lee et al. 2017). This chemical-free cleaning strategy uses continuous circulation of tap water directed to both the outer surface and inner surface of hollow fiber membranes. This particular strategy resulted to excellent water permeability recovery, without affecting its operational duration, especially during intermittent chemical-in-place cleaning.

Larger scale demonstrations using larger membrane modules may perform chemical-involving maintenance cleaning for the membranes by flushing the fouled membranes with low-concentration acidic or alkaline solution, with tap water circulated

concurrently. This treatment, however, is longer than chemical-in-place, due to several cycles of recirculation and soaking (Lee et al. 2017).

2.3.3 Anti-fouling PRO membranes

Several PRO membrane development studies were conducted focusing on mitigation of the fouling propensity during PRO operation.

Alginate fouling, influenced by Na^{2+}, was reduced by using annealed PBI/POSS/PAN hollow fiber membranes (Chen, Fu & Chung 2014). The membrane selectivity was enhanced, since reverse diffusion of NaCl results in increased alginate fouling. Since then, anti-fouling membrane development studies have mainly focused on chemical modification or incorporation of nano-sized materials with intrinsic hydrophilicity and functionality, whose interaction with foulants could control fouling. Chemical modifications of membranes used various agents, among which are polyvinyl alcohol and polydopamine (Zhang, Zhang & Chung 2016), polyelectrolytes (Li, Qi, et al. 2017), zwitterions (Cai et al. 2016; Han et al. 2018; Zhao et al. 2016), aminosilane (Zhang et al. 2016), hyperbranched polyglycerol (Li, Cai & Chung 2014; Zhang et al. 2018), and hyperbranched poly(ionic liquid) (Li et al. 2019). Among the nano-sized materials in literature are carbon quantum dots (Zhao, Das & Chung 2017), carbon nanotubes (Kim, Yang, et al. 2020), titanium dioxide (Kim, Suh, et al. 2016), graphene oxide, and halloysite nanotubes (Lim et al. 2018). Silver nanoparticles, known for their biocidal properties, have been also incorporated in membranes specifically designed for biofouling mitigation (Liu, Foo, et al. 2016). There are a number of studies which used different membrane preparation technique, such as double polyamide active layers for both ICP and fouling mitigation (Han, Cheng &

Chung 2017). More information on PRO membrane development will be discussed in the succeeding subsection.

2.4 Membrane development for pressure retarded osmosis

An immensely vital aspect of the PRO process is the use and development of suitable and highly efficient membranes, such that it was deemed practically and economically not feasible to proceed with PRO commercialisation and further development without suitable membranes (She, Jin & Tang 2012). Due to the similarities of PRO with RO (i.e., application of hydraulic pressure and membrane orientation), asymmetric RO membranes were used during the initial studies on PRO (Loeb & Mehta 1978; Loeb, Van Hessen & Shahaf 1976; Mehta & Loeb 1978; Mehta & Loeb 1979). Immensely low performance was obtained from the earliest studies due to the thick supports of those membranes, which caused ICP to occur and lead to low water flux and power density.

Initially, cellulose-based membranes were used for the initial PRO studies, due to its commercial availability, as well as hydrophilicity and satisfactory tensile strength. A flat-sheet cellulose acetate membrane was prepared and was developed specifically for desalination (Loeb 1981). These integrated skinned cellulose-based membranes were either cellulose acetate (CA) or cellulose triacetate (CTA). Hydration Technologies Inc. (HTI) developed a cellulose-based membrane for FO and PRO applications, which was utilised in the earlier PRO simulations (Achilli, Cath & Childress 2009; Kim & Elimelech 2013) The HTI membrane became the standard commercially available membrane, until targeted osmotic energy requirements during large-scale PRO implementation could not be achieved by the HTI membrane, and

therefore requiring the use of a different type of membranes (Gerstandt et al. 2008; Thorsen & Holt 2009).

Several studies on membrane development have been performed, and a significant number has been used for industrial applications. Since then, advanced materials and sophisticated methods have paved the way to continuous improvement of membrane properties and performance. A vast improvement in the membranes' chemical and thermal stability, as well as transport properties, can be observed on the membranes currently in development, compared to the very first membrane for an osmotic process. Based on the various mathematical simulation of PRO, PRO membrane design has specifically focused on the following membrane characteristics: (1) hydrophilicity, for enhanced water flux and fouling mitigation; (2) selectivity of the thin, dense active layer for satisfactory solute rejection; and (3) high tensile strength to withstand the application of hydraulic pressure. Development of suitable PRO membranes made it possible to achieve higher power density values, which further shows the feasibility of PRO for wider-scale applications.

2.4.1 Flat sheet TFC PRO membranes

Thin film composite (TFC) membranes, known to be asymmetric, are consisted of two layers: (1) a microporous membrane substrate, and (2) a dense, selective thin film, typically polyamide formed *in situ* on the membrane substrate surface via interfacial polymerisation (IP). The membrane supports are conventionally prepared either via nonsolvent-induced phase separation (NIPS) or electrospinning of polymeric substances. During NIPS, the polymer solution was made in contact with a nonsolvent, resulting in coagulation and phase separation of the polymer.

Interfacial polymerisation (IP) is the reaction taking place between two monomers dissolved in immiscible solutions (aqueous and organic), such that when the two solutions are mixed together *in situ* on the membrane substrate surface, the polymerisation reaction occurs at the liquid-liquid interface. Typically, an amine monomer dissolved in aqueous phase reacts with an acyl chloride dissolved in an organic solvent (e.g., hexane, heptane) to form polyamide (PA). The most common PA active layer for PRO TFC membranes is formed from the following monomers: *m*-phenylenediamine (MPD) and trimesoyl chloride (TMC) (Alsvik & Hägg 2013; Chou et al. 2010).

Figure 2.6 shows the typical morphology of a flat sheet TFC PRO membrane, whose substrate is prepared via NIPS. Flat sheet membranes gained popularity due to ease in preparation of the membranes, as well as the application for plate-and-frame and spiral wound modules.

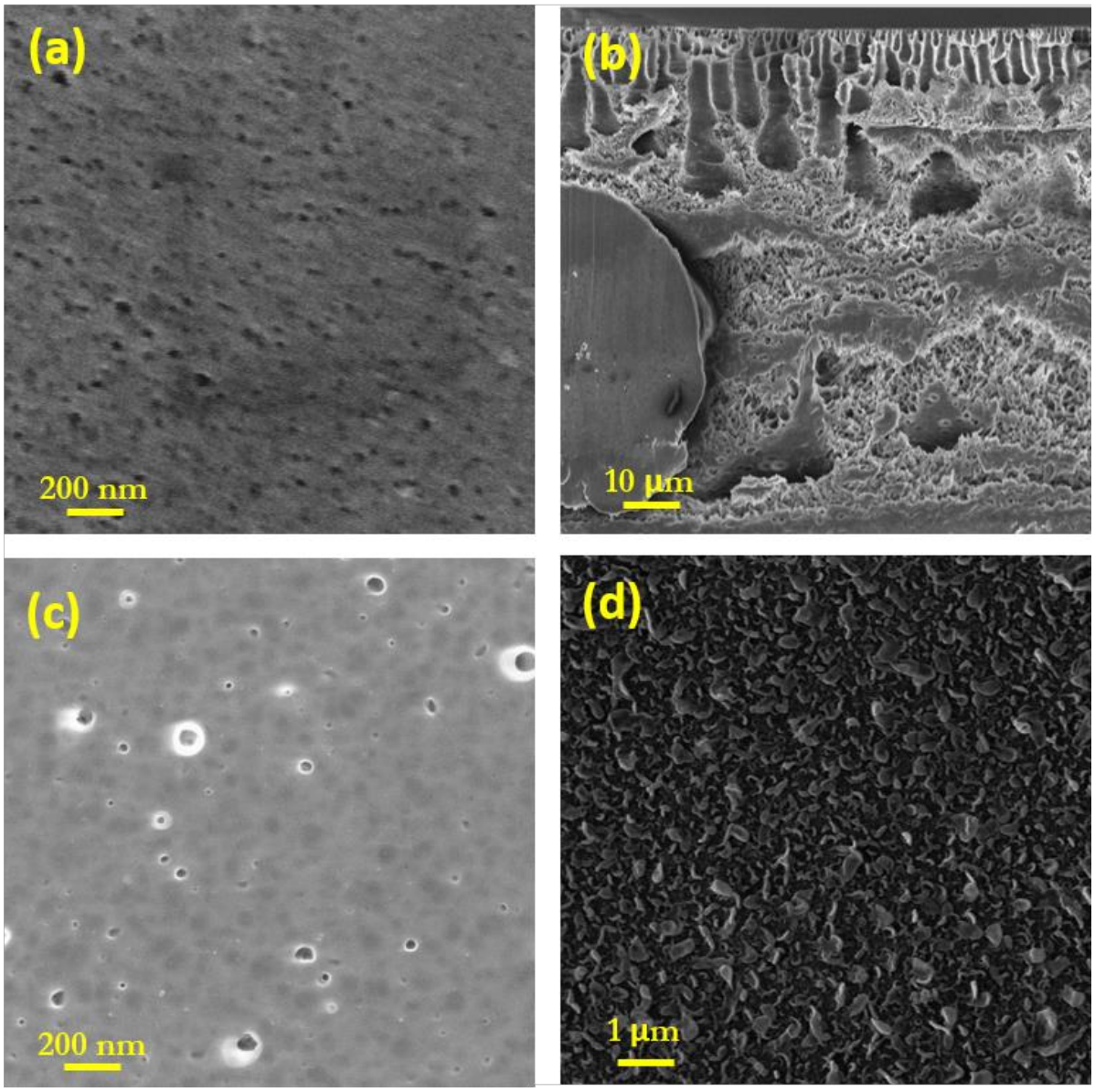

Figure 2.6 Scanning electron microscope images showing the morphology of the (a) membrane substrate top surface, (b) membrane cross section, (c) membrane substrate bottom surface, and (d) membrane polyamide active layer surface of a flat sheet TFC PRO membrane

Table 2.1 lists the flat-sheet PRO TFC membranes in literature.

The first TFC membrane used for PRO application was PA on a polysulfone (PSf) substrate, backed with a polyethylene terephthalate (PET) nonwoven fabric (Yip et al. 2011). This membrane has exhibited the suitable morphology for PRO TFC membranes and has become the guideline for succeeding TFC PRO membrane development studies. Polyetherimide (PEI), another commonly-used polymer, was

used as the polymeric material in a study which yielded 12.8 W m^{-2} at 17.2 bar using 10 mM NaCl and 1 M NaCl as feed and draw, respectively (Li, Wang, Qi, et al. 2015).

Deformation of TFC membranes is a huge issue which needs to be addressed during membrane development, such that use of commercial high-mechanical strength polymeric materials and reinforcement of the support layer were performed by a number of PRO TFC membrane researchers. In order to develop a more robust and more mechanically strong membrane, a different class of polymer known as polyimide (PI), more commonly known with trade name Matrimid® 5218, was used for PRO membrane development (Cui, Liu & Chung 2014; Han et al. 2013), wherein a porous substrate with sponge-like structure was prepared, and the PA layer was modified with certain agents. Another commercially-available polymer is polyamide-imide (PAI), whose trade name is Torlon®, which was used in PRO membrane studies after modification with polydopamine (PDA) (Li et al. 2013). Similarly, reinforcement of the PRO TFC supports have been performed in various PRO membrane development studies. She et al. (She et al. 2016) tested different types of fabric as fabric reinforcement materials for PRO TFC membranes, and found that tricot fabric has the best potential for PRO membrane preparation, due to its resistance to tensile stretching, as compared to woven and non-woven fabric, and this TFC membrane exhibited a power density of 7.1 W m^{-2} at 18.4 bar. Macromolecular additives can be added to control the porosity of the membrane substrate, and thus increase the free volume of the membrane for more effective water transport. Polyvinylpyrrolidone (PVP) was mixed in PSf dope solution and the influence of PVP was tested on PRO TFC membranes, and the best performing membrane showed 12.9 W m^{-2} power density at 22 bar using 1 M NaCl draw. This has led to further studies which examined

the role of reinforcing materials on PRO TFC membrane performance (Idarraga-Mora, Ladner & Husson 2018; Sun et al. 2018).

Chemical modification of membranes has potentially various benefits for TFC membranes, which include tailoring of the mechanical strength, pore structure, hydrophilicity, and functionality of the membranes. A TFC PRO membrane with polyacrylonitrile (PAN) substrate was developed after chemical treatment of the PAN substrate with ethanol (Zhang, Fu & Chung 2013). Chemical treatment of the TFC membranes improved the water flux and mechanical stability of the membrane, while it is able to swell the polymeric chains, which results in the formation of a thinner and smoother PA layer with a larger free volume, which led to higher water flux.

In recent, membrane researchers have exploited the properties of functional nano-sized materials to develop nanocomposite membranes with enhanced porosity, hydrophilicity, anti-fouling property, and energy-harnessing capability. Son et al. incorporated functionalised carbon nanotube (CNT) in the polyethersulfone (PES) support (Son et al. 2016). The CNT effectively increased the membrane porosity, pore size, and hydrophilicity of the TFC membrane. A dual-layered TFC PRO membrane, whose membrane substrate was incorporated with graphene oxide (GO) and halloysite nanotube (HNT) was prepared using a dual-blade casting technique to enhance water flux and antifouling property. The membranes exhibited better fouling mitigation and the membrane with the optimal GO and HNT loading exhibited a power density of 12.1 W m^{-2} at 21 bar using 1.0 M NaCl as draw (Lim et al. 2018). A new class of nanomaterials known as covalent organic framework (COF) was also incorporated in the polyamide layer of a PRO thin film nanocomposite (TFN) membrane.

A recently reported membrane with unprecedented thinness and high water permeability was reported (Kwon et al. 2021). A fabric support-free PRO TFC membrane was developed using porous polyethylene (PE) separators typically used for lithium-ion battery applications coated with polyvinyl alcohol (PVA) and cross-linked with glutaraldehyde (GA), prior to toluene-assisted IP. The hydrophilized PE battery separators exhibited structural parameter values of around 235 μm. The pure water permeability of the membrane was found to be 8.8 L m^{-2} h^{-1} bar^{-1}, which corresponded to the highest reported power density for TFC membranes in literature of 35.7 W m^{-2} at 20 bar.

Table 2.1 Flat-sheet PRO TFC membranes in literature

Membrane substrate	Feed solution	Draw solution	Pressure (bar)	Power density (W m^{-2})	Note	Reference
PSf on PET	DI water	0.5 M NaCl	12	10.0	PA modified with NaOCl, $NaHSO_3$, heat	(Yip et al. 2011)
PI	DI water	1.0 M NaCl	15	12.0	PA modified with NaOCl, $NaHSO_3$, MeOH	(Han et al. 2013)
PI	DI water	1.0 M NaCl	22	18.1	TFC membrane modified with DMF	(Cui, Liu & Chung 2014)
PAN on PET	DI water	3.5% (w/w) NaCl	10	2.6	PAN modified NaOH, HCl; PA modified with NaOCl, $NaHSO_3$, EtOH	(Zhang, Fu & Chung 2013)
PAI on PET	DI water	3.5% (w/w) NaCl	13	7.1	PAI was coated with PDA; PA modified with NaOCl, $NaHSO_3$, EtOH	(Li et al. 2013)
PEI	10 mM NaCl	1.0 M NaCl	17.2	12.8		(Li, Wang, Qi, et al. 2015)
PSf on tricot PET	10 mM NaCl	1.0 M NaCl	18.4	7.1		(She et al. 2016)
PES/CNT	DI water	0.5 M NaCl	6	1.6	PA modified with NaOCl, $NaHSO_3$, heat	(Son et al. 2016)
PSf	DI water	1.0 M NaCl	22	12.9		(Wei et al. 2016)
PES on PET	DI water	1.0 M NaCl	25	12.1		(Idarraga-Mora, Ladner & Husson 2018)
PSf/GO and PSf/HNT (dual layer) on PET	DI water	1.0 M NaCl	21	12.1		(Lim et al. 2018)
PK on PET	DI water	0.6 M NaCl	28	6.1		(Sun et al. 2018)
PVA-coated PE	DI water	1.0 M NaCl	20	35.7	Toluene-assisted IP	(Kwon et al. 2021)

Another type of flat sheet membranes can be prepared from electrospun polymeric supports. Electrospinning is the application of the polymer solution driven by electrostatic force, forming nano-sized polymer fibres, which are collected on a rotating collector whose electric potential is significantly lower (Gonzales et al. 2018). The nanofibre mat produced after the electrospinning exhibits high porosity and tortuosity (Kim, Han, et al. 2015). Electrospun nanofibre mats can be used as either the membrane support layer of a TFC membrane or a replacement for the non-woven polyester fabric base. This subsection focuses on the TFC PRO membrane development studies which used electrospun nanofibre mats for either purpose, as listed in Table 2.2.

PAN-SiO_2 nanofibres were electrospun on a nonwoven PET fabric, prior to active layer formation via IP in the first nanofibre-supported PRO membrane development study (Song, Liu & Sun 2013). SiO_2 was synthesised in the PAN solution before electrospinning via the reaction of tetraethyl orthosilicate (TEOS) and acetic acid. Another set of nanofibre-supported PRO TFC membranes was prepared using PAN on nonwoven PET fabric. Two different kinds of membranes was formed during IP: (1) the typical TFC membrane with PA from the reaction of MPD and TMC; and (2) TFC membrane with PA formed from polyethyleneimine (PEI) and isophthaloyl chloride (IPC) (Bui & McCutcheon 2014). A tiered nanocomposite membrane support made of polyetherimide (PEi) was reinforced with functionalised CNT to deliver a TFC membrane with an outstanding power density of 17.3 W m^{-2} at a pressure of 16.9 bar (Tian et al. 2015).

A limitation of nanofibre-supported membranes is the poor mechanical strength of the nanofibre substrate, that is why usually a nonwoven backing support is required. Another method in literature which can significantly enhance the robustness and

strength of nanofibre-supported membranes is thermal rearrangement of the polymeric material. In three studies, hydroxypolyimide (HPI) nanofibres were electrospun and then placed in a furnace to allow thermal rearrangement to polybenzoxazole-co-imide to occur (Kim et al. 2018; Moon, Kim, et al. 2020; Moon, Lee, et al. 2020). In one of these studies (Moon, Lee, et al. 2020), the nanofibres were also crosslinked to further improve the mechanical strength of the membranes.

Studies involving electrospun nanofibre support for PRO membrane development show the material's applicability; however, its limitation in terms of mechanical strength still exists (Bui et al. 2011). During application of high hydraulic pressure during PRO, nanofibre-based membranes are expected to sustain damage. To continue the development of nanofibre-based PRO TFC membranes, it is important to control the structure and use other materials to reinforce the mechanical strength and stability of the membranes.

Table 2.2 Nanofibre-based PRO TFC membranes in literature

Material	Feed solution	Draw solution	Pressure (bar)	Power density ($W\ m^{-2}$)	Note	Reference
PAN/SiO_2; PET	0.9 mM NaCl (synthetic river water)	1.06 M NaCl (synthetic seawater brine)	15.2	10.3	Substrate coated with PVA; PA modified with NaClO, NaOH	(Song, Liu & Sun 2013)
PAN; PET	DI water	0.6 M NaCl	10	8.0	PA formed from MPD and TMC	(Bui & McCutcheon 2014)
			8.3	6.2	PA formed from IPC and PEI	
PEi/fCNTs	DI water	1.0 M NaCl	16.9	17.3	Tiered nanofibre structure	(Tian et al. 2015)
HPI thermally rearranged to PBO	DI water	1.0 M NaCl 3.0 M NaCl	14 18	17.9 39.5	Substrate coated with PDA, NAOH; PA treated with DMF	(Kim et al. 2018)
HPI thermally rearranged to PBO	DI water	3.0 M NaCl	27	87.2	Fluorinated	(Moon, Kim, et al. 2020)
HPI thermally rearranged to PBO	DI water	1.0 M NaCl	21	26	Substrate treated with DMSO; PA treated with NaOCl	(Moon, Lee, et al. 2020)

2.4.2 Hollow fibre TFC PRO membranes

Hollow fibre membranes are self-supporting, tubular shaped membranes which are typically prepared through phase separation spinning process, either via NIPS or thermal induced phase separation (TIPS). During TIPS, the polymer was mixed with a diluent, and is made in contact with a quenching bath at a high temperature. Like NIPS, the diluent and the quenching bath are incompatible with each other and the phase separation is heavily influenced by the heat transfer. Hollow fibre membranes are known to have higher surface area compared to flat sheet membranes. This is highly important, especially for productivity and scaling up of the membrane development process and the subsequent commercialisation. Furthermore, hollow fibre membranes are known to have better mechanical support and convenience in modulation, as the hollow fibre membrane module can have a high packing density and does not require the use of feed spacers (Peng et al. 2012; Sivertsen et al. 2012, 2013). Figure 2.7 shows the typical morphology of a hollow fibre TFC PRO membrane, whose substrate is prepared via NIPS. The elimination of the use of spacers for hollow fibre membrane modules minimises the interactions between the membrane and the spacer, as well as the energy loss in the feed flow channel due to these interactions (Han, Zhang, et al. 2015).

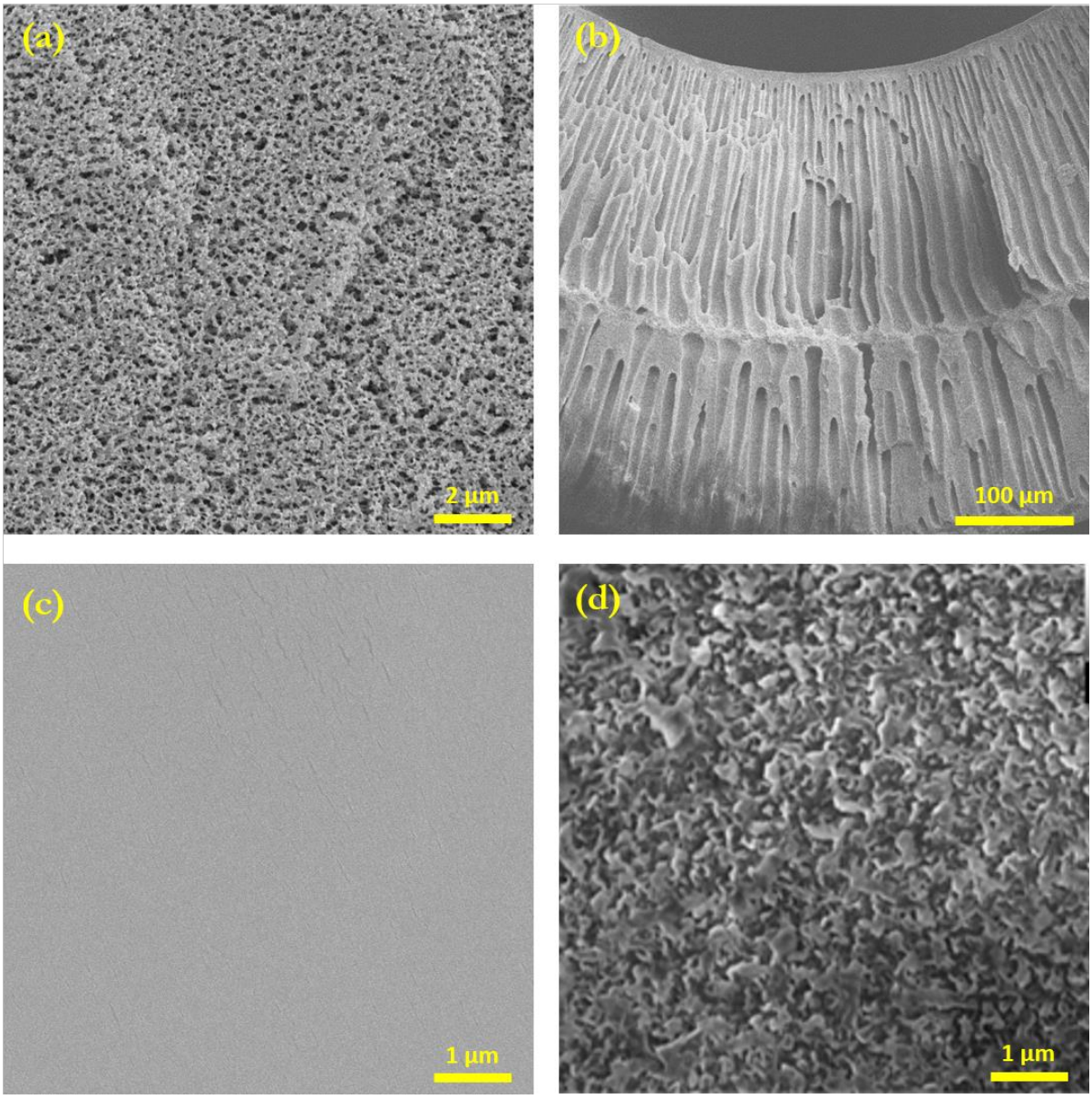

Figure 2.7 Scanning electron microscope images showing the morphology of the (a) membrane substrate top surface, (b) membrane cross section, (c) membrane substrate bottom surface, and (d) membrane polyamide active layer surface of a hollow fibre TFC PRO membrane

During hollow fibre spinning, a viscous polymer solution pumped through a spinneret at the same time as a non-solvent bore solution pumped through another tube into the spinneret delivered into a non-solvent coagulation bath. The formed fibres are then collected using a rotary winder. A number of parameters can be controlled

during hollow fibre preparation, such as bore and polymer solution flow rate, air residence time or air gap distance, and take-up rate.

Chou et al. (Chou et al. 2012a) developed the first hollow fibre TFC PRO membrane reported in literature. The PES hollow fibre TFC membrane exhibited a power density of 11 W m^{-2} using model river and sea water brine as feed and draw, respectively, at 8.4 bar. This membrane suffered from weak mechanical strength, having burst at only 9 bar, so the same group developed hollow fibre membrane using PEI (Chou, Wang & Fane 2013). The resultant membrane had an enhanced mechanical strength, that a maximum power density of 20.9 W m^{-2} was achieved at 15 bar using the same set of FS and DS. PES and PEI were still widely used as the polymer for hollow fibre membranes. Zhang et al. (Zhang, Sukitpaneenit & Chung 2014) manipulated the co-extrusion method to prepare a tailored PES hollow fibre membrane support, and the TFC membrane achieved a power density of 24.0 W m^{-2} at 20 bar, using DI water as feed and 1 M NaCl as draw. Other studies continued using PES and PEI hollow fibre substrates for the TFC membranes, each time trying to further enhance the membrane properties and performance, as well as modification (Chen et al. 2018; Cheng et al. 2017; Gai et al. 2016; Wan et al. 2017). Ingole et al. (Ingole, Choi, Kim, Jo, et al. 2014; Ingole, Choi, Kim, Park, et al. 2014; Ingole, Kim, et al. 2014) started fabricating a plain PES hollow fibre TFC PRO membrane, and to improve the performance of the membrane after certain modifications and treatments, like PDA coating and treatment with tributylphosphate (TBP). Li et al. used a novel co-polyimide polymer, 3,3',4,4'-benzophenone tetra-carboxylic dianhydride and 80% methylphenylenediamine + 20% methylene diamine (BTDA-TDI/MPDI/MDI) as the membrane substrate material, and the membrane exhibited a power density of 12 W m^{-2} at 21 bar.

Following their initial work with PI flat sheet PRO TFC membranes, researchers from the National University of Singapore developed PI hollow fibre PRO TFC membranes. Han et al. (Han & Chung 2014) prepared hollow fibre membranes using PI, which exhibited 16.5 W m^{-2} power density at 15 bar for feed of 10 mM NaCl and draw of 1 M NaCl. The same group also introduced the outer-selective hollow fibre membranes, wherein the polyamide selective layer was formed on the shell side of the fibres. Outer-selective hollow fibre membranes have higher surface area, compared to inner-selective ones; however, these membranes are not easy to make into modules and the IP process usually encounters challenges. Sun et al. (Sun & Chung 2013) employed vacuum-assisted IP to form on the shell side of PI hollow fibre substrates coated with PDA. The membranes exhibited super mechanical strength, with a burst pressure over 20 bar, and a maximum power density of 7.63 W m^{-2} at 20 bar with DI water and 1 M NaCl, respectively, as feed and draw. Cheng et al. (Cheng et al. 2016) and Le et al. (Le et al. 2016) followed a similar approach in fabrication of outer-selective hollow fibre membranes.

Fu et al. conducted two dual-layer hollow fibre PRO TFC studies using polybenzimidazole (PBI). Their first study used PAN as the inner layer material, and a thin outer layer of PBI mixed with polyhedral oligomeric silsesquioxane (POSS), to prevent the PBI from delaminating, prepared *via* co-extrusion (Fu et al. 2013). This membrane exhibited 2.5 W m^{-2} at 7 bar using 1.0 M NaCl as draw. This first study on dual-layer hollow fibre membranes yielded low flux due to the macromolecular additive PVP entrapped within the inner layer. A second study tried to correct this by subjecting the membranes into ammonium persulfate (APS) treatment to remove the PVP and improve the water permeability of the membranes. After treating the dual layer PAN and PBI/POSS hollow fibre with APS, the maximum power density was improved to

5.1 W m^{-2} at 15 bar. A TFC membrane with double polyamide layer was prepared by Han et al. (Han, Cheng & Chung 2017) to mitigate both ICP and fouling, with the membranes exhibiting 10.7 W m^{-2} at 15 bar with 1 M NaCl and DI water as draw and feed, respectively.

Chemical modified hollow fibre TFC PRO membranes were developed in several studies. Li et al. (Li, Cai & Chung 2014) grafted hyperbranched polyglycerol (HPG) onto a PES hollow fibre substrate, prior to IP. This membrane, with enhanced antifouling capability, exhibited a power density of 6.7 W m^{-2} at 16 bar with 3.5% NaCl as draw against DI water as feed. Sulfonate hyperbranched polyglycerol Grafting of aminosilane, specifically 3-aminopropyltrimethoxysilane (APTMS), was also performed by Zhang et al. (Zhang et al. 2016) to improve the fouling resistance of the membrane. Municipal wastewater was used as the FS in a study of Zhao et al. (Zhao et al. 2016) wherein they prepared antifouling membranes modified with zwitterionic 2-methacryloyloxyethylphosphorylcholine (MPC) which exhibited 7.7 W m^{-2} power density at 15 bar. MPC was then reacted with 2-aminoethyl methacrylate hydrochloride (AEMA) *via* a single-step free radical polymerisation to synthesise the P[MPC-co-AEMA] copolymer, which was grafted on a hollow fibre substrate made from blend of PES and PAI, and the membrane exhibited a power density of 13.5 W m^{-2} at 20 bar (Han et al. 2018). Li et al. exploited the properties of poly(allylamine hydrochloride) (PAH) to modify TFC PRO membranes. First, they used layer-by-layer (LbL) polyelectrolyte deposition of PAH and poly(acrylic acid) (PAA) (Li, Qi, et al. 2017). Another study involved the crosslinking of PAH onto the surface of the PAI hollow fibre substrate using glutaraldehyde (GA).

Nanocomposite hollow fibre membranes were also prepared *via* the incorporation of nanomaterials. Zhao et al. (Zhao, Das & Chung 2017) grafted carbon

quantum dots (CQDs) on PDA-coated PES hollow fibre membranes and achieved a power density of 11.0 W m^{-2} at 15 bar. CQDs were then incorporated in the selective polyamide layer of PRO hollow fibre TFN membranes by Gai et al. (Gai, Zhao & Chung 2018) exhibiting 34.2 W m^{-2} power density at 23 bar. GO was then mixed by Park et al. (Park et al. 2019) in PES hollow fibre substrate to prepare a TFC membrane with 14.6 W m^{-2} power density at 16.5 bar.

Thermally-assisted nonsolvent-induced phase separation (T-NIPS) was introduced by Cho et al. (Cho et al. 2019) to tailor the structure of a CTA/CA hollow fibre membrane with a dense outer layer and isoporous inner layer.

Table 2.3 shows a summary of the hollow fibre TFC PRO membranes in literature.

Table 2.3 Hollow fibre PRO TFC membranes in literature

Membrane substrate	Active layer	Feed solution	Draw solution	Pressure (bar)	Power density (W m^{-2})	Note	Reference
PES	PA on lumen side	10 mM NaCl	1.0 M NaCl	9	10.6		(Chou et al. 2012a)
PEI	PA on lumen side	10 mM NaCl	1.0 M NaCl	15	20.9		(Chou, Wang & Fane 2013)
PAN (inner layer)	PBI/POSS (outer layer)	10 mM NaCl	1.0 M NaCl	7	2.5	Fibres treated with thermal annealing	(Fu et al. 2013)
PAN (inner layer)	PBI/POSS (outer layer)	10 mM NaCl	1.0 M NaCl	15	5.1	Fibres treated with APS	(Fu et al. 2014)
PI	PA on lumen side	10 mM NaCl	1.0 M NaCl	15	16.5		(Han & Chung 2014)
PI	PA on shell side (outer-selective)	DI water	1.0 M NaCl	20	7.6	PDA intermediate layer was formed	(Sun & Chung 2013)
PES	PA on lumen side	DI water	0.6 M NaCl	6	1.5		(Ingole, Choi, Kim, Jo, et al. 2014)
PES	PA on lumen side	DI water	0.6 M NaCl	7	3.0	PDA intermediate layer was formed	(Ingole, Choi, Kim, Park, et al. 2014)
PES	PA on lumen side	DI water	0.6 M NaCl	8	3.9	PDA intermediate layer was formed; PA treated with TBP	(Ingole, Kim, et al. 2014)
PES	PA on lumen side	DI water	3.5% (w/w) NaCl	16	6.7	PDA-coated support grafted with HPG	(Li, Cai & Chung 2014)
PES	PA on lumen side	Wastewater retentate	0.81 M NaCl	20	18.8	PDA-coated Support grafted with SHPG, TEA	(Zhang et al. 2018)
BTDA-TDI/ MDPI/MDI	PA on lumen side	DI water	1.0 M NaCl	21	12		(Li & Chung 2014)

PES	PA on lumen side	DI water	1.0 NaCl	M	24	21		(Zhang, Sukitpaneenit & Chung 2014)
PES	PA on shell side (outer-selective)	DI water	1.0 NaCl	M	20	7.8		(Cheng et al. 2016)
PES	PA on lumen side	DI water	1.0 NaCl	M	20	22.1		(Gai et al. 2016)
PES	PA on lumen side	DI water	1.0 NaCl	M	22	10.1		(Cheng et al. 2017)
PES	PA on lumen side	DI water	1.0 NaCl	M	20	22.0		(Wan et al. 2017)
PES	PA on lumen side	DI water	1.2 NaCl	M	30	38		(Wan et al. 2018)
PEI	PA on lumen side	DI water	1.0 NaCl	M	15	8.9		(Chen et al. 2018)
PEI	PA on shell side (outer-selective)	DI water	1.0 NaCl	M	17	9.6		(Le et al. 2016)
PEI	PA on shell side (outer-selective)	DI water	1.0 NaCl	M	13	13	Modified with APTMS	(Zhang et al. 2016)
PES	PA on shell side (outer-selective)	Municipal wastewater	0.81 NaCl	M	15	7.7	Substrate modified with PDA and MPC	(Zhao et al. 2016)
PES	PA on both sides (dual layer)	DI water	1.0 NaCl	M	15	10.7	Dual selective layer	(Han, Cheng & Chung 2017)
PEI	PA on lumen side	DI water	1.0 NaCl	M	15	16.2	LbL deposition of PAH and PAA on substrate	(Li, Qi, et al. 2017)

PES	PA on lumen side	DI water	0.81 M NaCl	15	11	CQDs grafted on shell side	(Zhao, Das & Chung 2017)
PES	PA on lumen side	DI water	1.0 M NaCl	23	34.2	CQDs incorporated in PA layer	(Gai, Zhao & Chung 2018)
PES/GO	PA on lumen side	DI water	1.0 M NaCl	16.5	14.6		(Park et al. 2019)
PES/PAI	PA on lumen side	DI water	1.0 M NaCl	20	13.5	Substrate modified with P[MPC-co-AEMA]	(Han et al. 2018)
PAI	PA on lumen side	Wastewater RO retentate	1.0 M NaCl	13	4.3	Substrate modified with crosslinking of PAH, GA	(Li, Zhao, Setiawan, et al. 2018)
CTA/CA	-	DI water	1.0 M NaCl	18	5.5	Hollow fibre fabricated using T-NIPS	(Cho et al. 2019)

2.4.3 Free-standing PRO membranes

To minimise the occurrence of ICP during PRO operations, a new class of membranes were being developed, known as free-standing membranes. These membranes eliminate the use of membrane substrate or support layer to be able to achieve high water flux. The first reported free-standing membrane was reported by Patel et al. (Patel et al. 2014). A poly(vinyl chloride)-g-poly(3-sulfopropyl methacrylate) graft copolymer was synthesised and cast using NIPS, similar to flat-sheet membrane substrates. This membrane was able to generate 0.88 W m^{-2} power density at 14 bar using model seawater as draw. Tong et al. (Tong et al. 2018) prepared free-standing GO membranes for PRO, wherein GO sheets were filtered onto an inorganic porous filter. Using 3 M NaCl and 0.017 M NaCl as draw and feed, respectively, a power density of 24.62 W m^{-2} was achieved at an applied pressure of 6.90 bar. Following this study, Gao et al. (Gao et al. 2020) mixed together GO and two-dimensional MXene $Ti_3C_2T_x$ material to prepare the freestanding membrane which was able to achieve a power density of 56.4 W m^{-2} at 9.66 bar using 2.0 M NaCl as draw and 0.017 M NaCl as feed.

While the development of free-standing membranes seems attractive due to the high power density and water flux values achieved, the ability of these membranes to sustain hydraulic pressure application has yet to be optimised, since elimination of the membrane substrate significantly affects the mechanical strength and stability of the membranes. Moreover, the free-standing membranes in literature both use nanomaterials, which may not be the most economical choice for membrane materials, and, thus, can affect the larger-scale development of these membranes.

2.5 Module and spacer development for pressure retarded osmosis

A number of PRO studies have expressed concern for problematic module and spacer designs, which were found to significantly affect the membrane integrity, process performance and efficiency (Kim & Elimelech 2012; She, Hou, et al. 2013; Straub, Lin & Elimelech 2014). Initially, RO modules were used for PRO studies due to the similarity in use of applied hydraulic pressure; however, due to the basic differences between the two processes, RO modules were found to be not-suitable for PRO (Cath, Childress & Elimelech 2006a). RO only has feed circulation on one side, whereas PRO requires simultaneous feed and draw circulation, thus the PRO module should be able to maximise flow and circulation efficiency, while being able to mitigate fouling tendency (Chen et al. 2018; Straub, Lin & Elimelech 2014). FO modules were then tested due to the availability of four ports for inlet and outlet of feed and draw streams; however, most FO modules could not sustain the hydraulic pressure applied during PRO operation.

2.5.1 PRO module development

Due to the pressure tolerance requirements of the PRO process, PRO membrane modules are only limited to either spiral-wound module for flat sheet membranes or hollow fibre membrane module. Figure 2.8 shows a representation of these membrane module configurations. Module-scale PRO studies, thus far, could not achieve the performance of bench-scale PRO experiments, mainly due to the membrane module hydrodynamics and inconsistency in pressure and osmotic driving force distribution inside the module, as well as the inevitable dilution of the DS (Kim, Kim, et al. 2013).

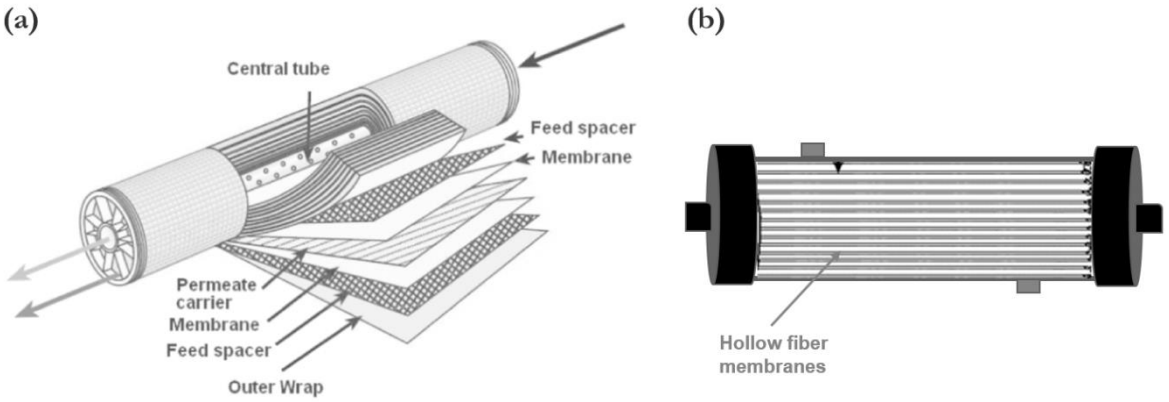

Figure 2.8 Representations of the commercial membrane modules for PRO: (a) spiral-wound and (b) hollow fibre

One of the modular configurations for TFC membranes is the spiral-wound module, which can be applied for flat-sheet membranes. The spiral-wound module is the preferred membrane module configurations for flat sheet PRO membranes. The spiral-wound module is composed of membrane sheets placed in between spacers housed in a module casing. The membrane sheets are glued together with spacers in between each sheet to form a leaf. The leaves are afterwards rolled around to form FS and DS channels inside the membrane module. Spiral-wound modules are suitable for flat sheet membranes due to high packing density which could be achieved from this configuration, compared with other flat sheet module configurations. A challenge in the development of spiral-wound modules for PRO is the loss of pressure inside the membrane module, due to the feed channel spacers, which are designed to enhance mass transfer within the module (Schwinge et al. 2004). Furthermore, this module configuration requires suitable spacers for PRO operation. The spiral-wound configuration can be used for most osmotic processes; however, for PRO implementation, the spacer design of conventional spiral-

wound modules was found to be not suitable, as the spacers could cause membrane damage and pressure drop. Kim et al. (Kim, Kim, et al. 2013) operated an HTI PRO using a spiral-wound module with two different flow paths, axial and spiral, and two different spacers, net-type for the draw stream and tricot for the feed stream. Toray Chemicals, a textile and polymer manufacturing company, also came up with a PRO TFC spiral-wound module, which was used for the GMVP project in Korea. Due to these efforts, module development for PRO has continued to advance.

On the other hand, hollow fibre modules are composed of hollow fibres bundled and housed together in a compact housing, with surface-to-volume ratios and packing densities higher than that of the spiral-wound module. Other advantages of hollow fibre modules include strong pressure resistance with proper and consistent flow distribution within the module (Kishimoto et al. 2019). During one PRO module study, a pilot CTA hollow fibre module for PRO was evaluated for performance and use for PRO (Higa et al. 2017); but since then, TFC PRO hollow fibre membranes have posed problems regarding modulation and membrane creeping (Chen, Alanezi, et al. 2019; Chen et al. 2018). The biggest challenge in the development of hollow fibre modules is the optimisation of the quantity of the hollow fibres and the suitable potting process to prepare the membrane modules with minimal defects. Defects in the PRO module could result in membrane creeping and membrane bursts during higher pressure operation. Another limitation of the hollow fibre module is the pressure tolerance, as feed and draw pressures are usually limited for this module type. Following this PRO hollow fibre module work, a number of modulation studies to solve the perceived modulation problems and provide outstanding water and solute transport mechanisms.

Sivertsen et al. simulated various configurations of hollow fibre modules for PRO application, and found that overall PRO performance was similar regardless the module configuration (Sivertsen et al. 2013) and the thermodynamics and mass transfer in hollow fibre modules were simulated by Xiong et al. (Xiong et al. 2017). Commercialisation of hollow fibre modulation for PRO, however, has still not progressed significantly, albeit with a number of laboratory-scale studies (Chen et al. 2018; Wan et al. 2017). In fact, commercialisation of hollow fibre membranes for PRO has only been achieved by Japanese company Toyobo, whose PRO hollow fibre modules were used for the Mega-ton project in Japan.

Table 2.4 lists the performance of commercial PRO membranes in literature.

Table 2.4 Commercial PRO membrane modules in literature

Company	Module type	Draw solution	Operating pressure (bar)	Power density (W m^{-2})	Reference
Flat-sheet					
HTI	OsMem™ 2521 spiral wound	0.52 M NaCl	4.0	0.57	(Attarde et al. 2015)
		1.03 M NaCl		1.10	
		0.60 M NaCl	9.8	1.10	(Kim, Kim, et al. 2013)
		1.03 M NaCl	4.0	3.29	(She, Jin & Tang 2012)
Toray Chemical Korea	8040 spiral wound	0.60 M NaCl	10.4	1.77	(Lee et al. 2016)
Hollow fibre					
Toyobo	5 inch	1.0 M NaCl	30	17.1	(Kurihara et al. 2016)
		1.0 M NaCl		13.3	
	10 inch	1.0 M NaCl	25	7.7	(Saito et al. 2012)
		1.0 M NaCl	29	4.4	

2.5.2 PRO spacer development

In the same manner, spacer development for PRO has not reached any significant milestone. Spacer development for a specific process is important as it is able to influence not only the operational efficiency, but the membrane lifetime as well. With the use of non-suitable spacers, membrane deformation and damage could possibly occur, affecting membrane performance and often leading to membrane collapse (She, Hou, et al. 2013; She, Jin & Tang 2012). It was observed that the application of high hydraulic pressure on the draw stream could cause membrane deformation due to the use of feed channel spacer (Kim & Elimelech 2012). This led to the assessment of different types of spacers suitable for use with PRO membranes.

2.6 Integration of PRO with membrane pretreatment techniques

PRO is highly versatile process, since a wide variety of possible DS and FS can be exploited to achieve the necessary salinity gradient required for osmotic power generation. This has led to the use of freshwater, wastewater effluent, and pre-treated seawater as feed, and seawater and concentrated brine as draw. As a result of the perceived versatility of PRO and the questions on feasibility of PRO as a stand-alone process, PRO was integrated with other membrane-based technologies to be able to exploit high salinity concentrations of by-products (i.e., brine), augment energy and operational costs, and mitigate environmental impact of direct ocean discharge (Altaee & Hilal 2014; Chae et al. 2019). Soon, the PRO research community found that hybrid processes involving PRO and conventional desalination processes, such as RO and FO, have great potential, and thus, recently, the direction of PRO research has significantly shifted to hybrid processes.

While desalination processes, such as SWRO, have already been commercialised or applied at a larger scale, these processes are concerned more about the production of freshwater at a higher efficiency and production rate. In doing this, operational cost and energy expenditure are likewise increasing. This is where PRO can be integrated, as it is a process which is able to perform desalination, but more importantly, at the same time, reduce the energy consumption through power generation (Chae et al. 2019; Chae et al. 2018).

2.6.1 Reverse osmosis and pressure retarded osmosis hybrid

Integration of SWRO and PRO mainly aims to lessen energy expenditure and operating costs, and there are two mechanisms through which SWRO-PRO hybrid systems can achieve this: (1) generation of power through a hydro-turbine, and (2) circulation of energy through a pressure-exchanger. The former has a low energy generation efficiency; however, the electricity produced from this system can also be used for other purpose, not just to provide energy for the desalination plant. Inversely, the use of pressure-exchanger is highly efficient, but the energy or pressure recovered through this mechanism can only be used to augment the energy requirements of SWRO (Prante et al. 2014). The pressure recovered through the pressure exchanger is provided to the seawater influent, thus less energy could be used for pressurise the stream.

The most notable integrated PRO hybrid process was Japan's Mega-ton Water System, which integrated SWRO and PRO and whose schematic is shown in Figure 2.9. For this hybrid installation, SWRO brine from a desalination plant and wastewater effluent from a regional sewage treatment facility were used as draw and feed, respectively, and

10-inch Toyobo CTA PRO hollow fibre modules were used (Saito et al. 2012; Tanioka 2016). This SWRO-PRO prototype power plant was able to achieve 13.8 W m^{-2} power density at 30 bar applied hydraulic pressure. In this system, which aimed to produce energy through a turbine and to circulate energy, there were four open ports situated in the PRO hollow fibre module, to provide passage for the feed inlet, draw inlet, permeate outlet, and feed water discharge directed to the effluent tank. The feed water discharge was placed to provide circulation for the feed and mitigate the presence of leaked solute and the occurrence of ICP. During operation, the maximum power density was found to be 13.3 W m^{-2} and energy savings of 10-30% (Tanioka, Kurihara & Sakai 2018).

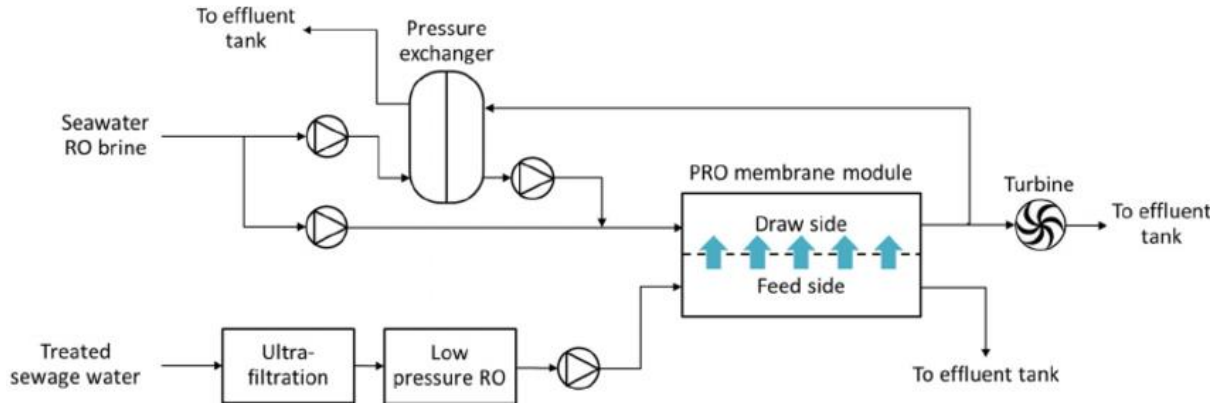

Figure 2.9 Schematic of the integrated Mega-ton RO-PRO hybrid system (Kim, Jeong, et al. 2015; Tanioka, Kurihara & Sakai 2018)

Following the halt in operations of Mega-ton, the GMVP project continued the large-scale implementation of the PRO hybrid processes. Wastewater treatment plant effluent and SWRO brine were used to achieve a low-cost seawater desalination operation (Lee, Kim & Park 2018). Instead of focusing on just energy production, GMVP also aimed to recover the pressure from the pressurised DS to augment the pressure demand of

seawater desalination. Osmotic power was generated and recovered using a hydraulic turbine and an energy recovery device (ERD), as shown in Figure 2.10. The SWRO-PRO demonstration plant was able to treat 240 m^3 d^{-1} of seawater. The maximum power density for this implementation was 18.3 W m^{-2} and the energy expenditure was reduced to 80%.

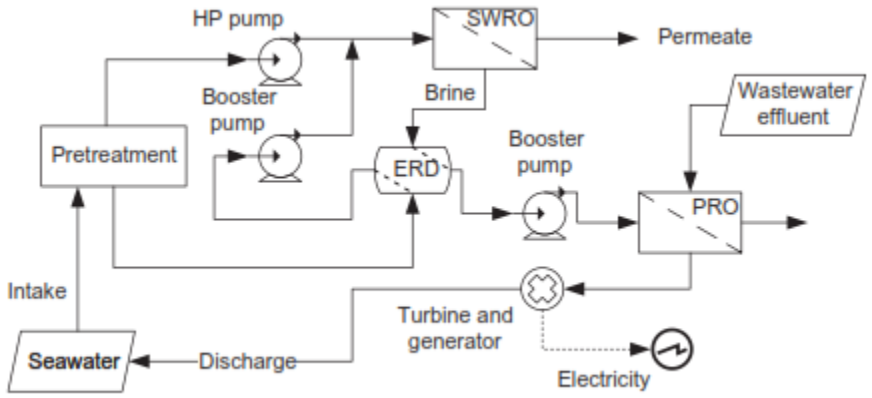

Figure 2.10 Schematic of the integrated GMVP RO-PRO hybrid system (Lee, Kim & Park 2018)

Kim et al. (Kim, Park, et al. 2013) assessed the efficiency of four different configuration of the hybrid RO-PRO system, as shown in Figure 2.11, which all aimed to focus more on either power generation or fresh water production.

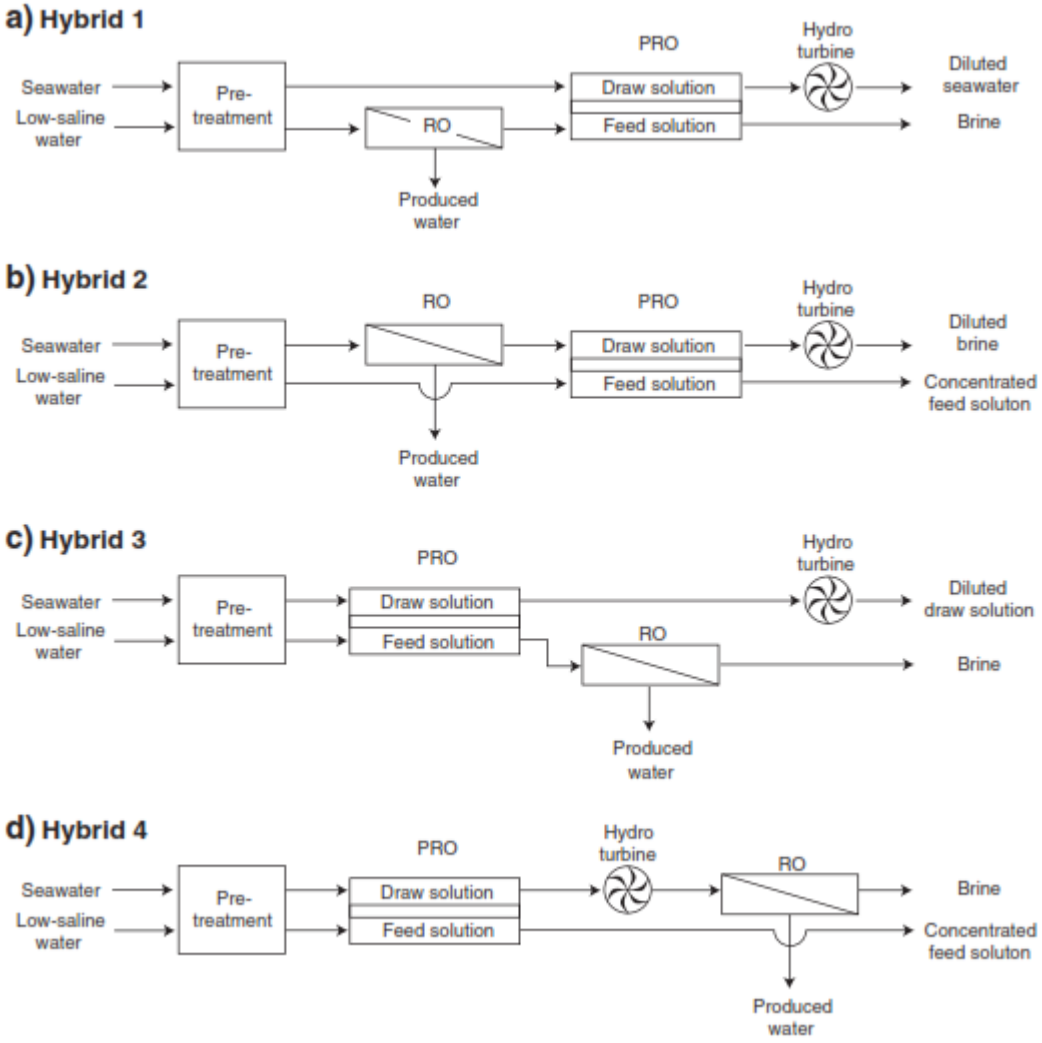

Figure 2.11 Schematic of four proposed RO-PRO hybrid system configurations (Kim, Park, et al. 2013)

Achilli et al. (Achilli et al. 2014) installed and operated a pilot-scale RO-PRO system using three spiral-wound RO modules connected in series, delivering concentrated seawater brine to an ERD to reduce the pressure prior to use as the draw for the PRO system with a spiral-wound PRO module. Seawater was first pressurised using a pressure exchanger, delivered to the first RO module, and the concentrated seawater brine from each module was used as the feed for the succeeding module, until the brine

reaches the ERD and used as draw for PRO, with wastewater effluent as feed. This particular configuration of the integrated RO-PRO system was able to demonstrate efficient energy production and energy consumption, as the seawater brine generated during RO was then diluted back to seawater concentration during PRO, and thus can be reused.

Altaee et al. (Altaee, Zaragoza & Sharif 2014) proposed an integrated power generation and seawater desalination process, wherein PRO was first operated to generate energy using seawater as draw and low-quality water as feed. The diluted seawater was then delivered into a turbine, and afterwards to the RO module for desalination.

There are several other studies conducted to investigate and determine the feasibility of the RO-PRO hybrid process, aiming to reduce the specific energy consumption (Wan & Chung 2016a), maximise the profit from commercial operation (Wan & Chung 2016b), and optimise the process performance (Touati et al. 2017).

A combined integrated system involving PRO, RO, and NF was proposed by Touati et al. (Touati et al. 2020). As shown in Figure 2.12, wastewater effluent was first pre-treated using NF, and the permeate proceeded to the PRO system to be used as feed. Seawater, on the other hand, passed through RO operation first and the concentrated brine was used as draw. The treated water in this hybrid system can be used for irrigation, thus this particular system has shown the potential of a combined water treatment, seawater desalination, and energy production to augment requirements for food-water-energy nexus.

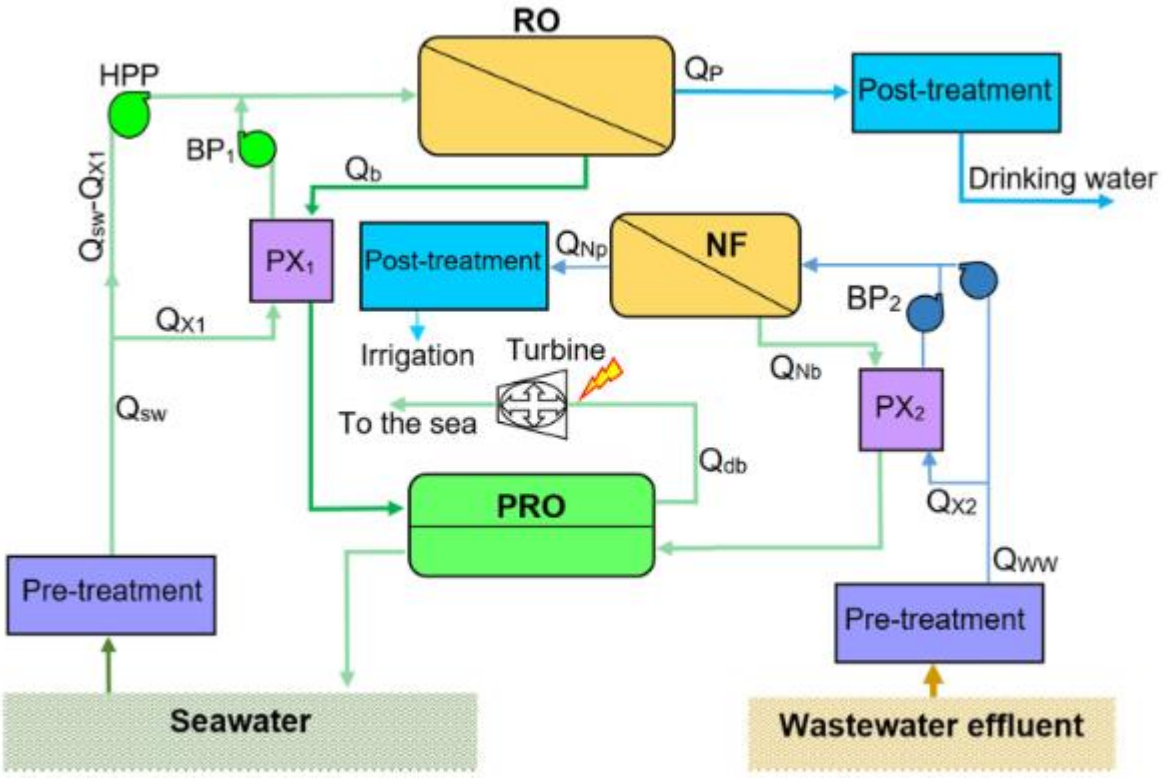

Figure 2.12 Schematic of proposed combined water treatment, seawater desalination, and energy production RO-NF-PRO hybrid process (Touati et al. 2020)

2.6.2 Forward osmosis and pressure retarded osmosis hybrid

Two configurations of PRO integrated with FO-PRO-FO and FO-PRO were evaluated in a previous study (Altaee & Hilal 2014). Two similar modules were installed, which both could perform either FO or PRO depending on the configuration, and treated hypersaline solution and wastewater effluent as draw and feed, respectively. An integrated process wherein PRO was operated first followed by FO proved to be more efficient in terms of power generation.

Integrated FO-PRO was also conducted by Cheng et al. (Cheng, Li & Chung 2018) to mitigate membrane fouling during PRO. The use of real wastewater effluent as FS for

PRO posed problems regarding membrane fouling, thus FO was first conducted as a pre-treatment step to exploit the several advantages of the FO process: low fouling propensity, simple membrane cleaning strategies, and minimum energy requirement.

PRO was also proposed to be integrated with a biological wastewater treatment process (Meng, Liu & Wang 2020). Wastewater was first treated by the membrane bioreactor (MBR) and the effluent was used as the feed for PRO. While this system suffered from severe fouling, simultaneous contaminant removal from the wastewater and power production were achieved in this study.

2.6.3 Membrane distillation and pressure retarded osmosis hybrid

PRO was integrated with membrane distillation (MD) in a study conducted by Han et al (Han, Zuo, et al. 2015), whose configuration is not similar to a closed loop OHE. PRO was first conducted and the diluted DS after PRO operation was used for MD. This configuration was found to have a high water recovery rate and osmotic power, with minimal membrane fouling.

Lee et al. (Lee et al. 2015) proposed an integrated vacuum MD and PRO system. This system is consisted of a recycling flow vacuum MD scheme operated for continuous production of fresh water and concentrated brine, which was then used as the draw for PRO, as shown in Figure 2.13.

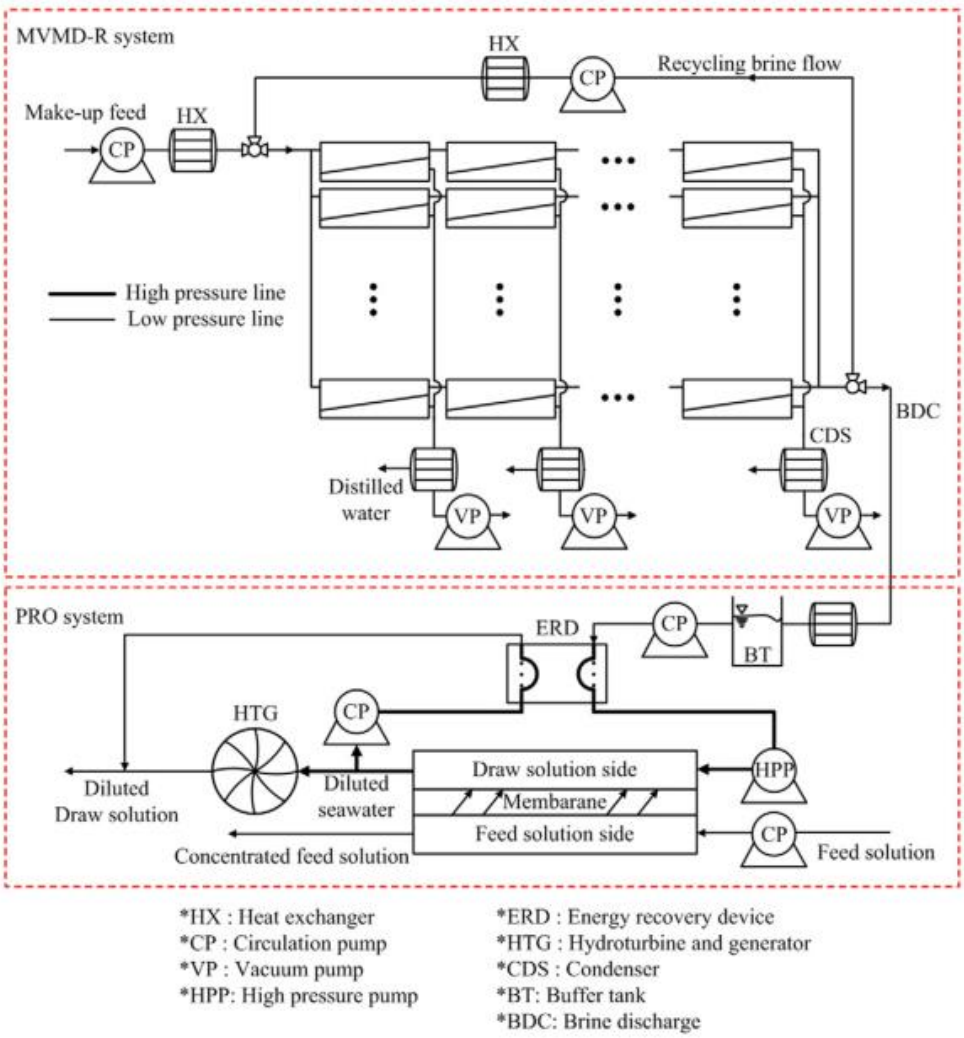

Figure 2.13 Schematic of the proposed integrated vacuum MD-PRO process (Lee et al. 2015)

2.6.4 Liquid phase ion stripping - pressure retarded osmosis hybrid

A new concept of an integrated process involving PRO was introduced by Wang et al. (Wang et al. 2020). Liquid-phase ion-stripping (LIS) was used to generate salinity gradient with only low temperature and integrated with PRO. As shown in Figure 2.14, the saline solution undergoes a thermal cycle, and with organic solvent, ions are rejected to produce fresh water and concentrated brine, which respectively become the feed and

draw for PRO. This proposed hybrid process was found to have high energy efficiency, solvent extraction efficiency, and heat recovery system efficiency.

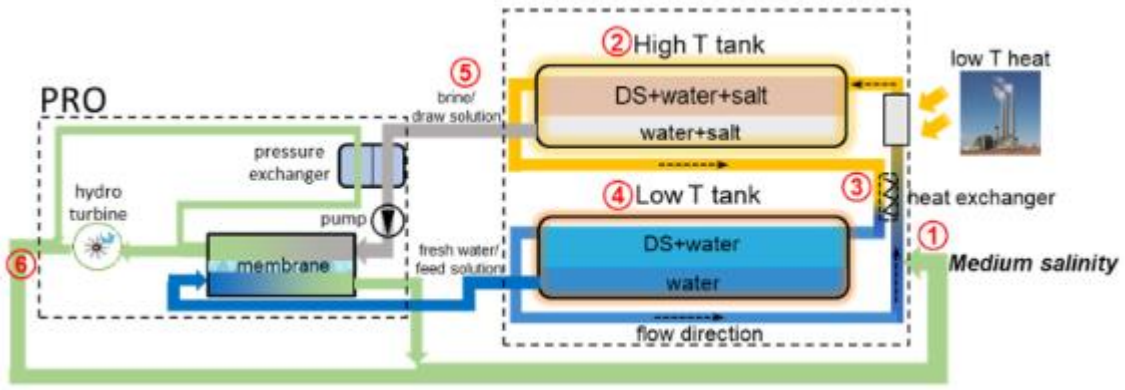

Figure 2.14 Schematic of the proposed integrated LIS-PRO hybrid system (Wang et al. 2020)

2.7 Novel configurations and niche applications of pressure retarded osmosis

Following the versatility of PRO in terms of configuration and DS and FS choice, novel configurations and niche applications of PRO have been proposed and gained attention in recent.

2.7.1 Closed-loop osmotic heat engine

The concept of a closed-loop OHE was first introduced and patented by Sidney Loeb in 1975 (Loeb 1975), but it is not until three decades after when PRO researchers started assessing its feasibility and performance.

Hickenbottom et al. (Hickenbottom, Vanneste & Cath 2016) exploited the concept of OHE, that is the coupling of PRO with a thermal separation process, i.e., MD. They pointed out that this process will only work when the PRO process is able to achieve high

power density, to minimise operational and capital costs, while the MD process must have high water flux to be able to reconcentrate the diluted DS better. Various inorganic and ionic organic DS were tested and assessed in terms of PRO and MD performance, as well as equipment corrosion potential.

McGinnis et al. (McGinnis, McCutcheon & Elimelech 2007) then tried a novel DS for their own application of the closed-loop OHE. Concentrated ammonia-carbon dioxide (from the mixing of NH_4HCO_3 and NH_4OH) was chosen and used as the DS, with DI water as the feed. Heat was introduced to the engine to separate the draw solute from the fresh water. The use of the combination of DS and FS allowed lower temperature for draw and feed separation, while using high concentrations of the draw ensured high power density.

To further enhance thermal separation efficiency, DS prepared with an organic solvent were used in an OHE demonstration (Shaulsky et al. 2015). LiCl was chosen as a draw solute and it was mixed in methanol, to exploit the high volatility and lower heat capacity of this particular organic solvent during the MD draw solute reconcentration. Operation using a DS of 3 M LiCl in methanol yielded water flux of 47.1 L m^{-2} h^{-1} and power density of 72.1 W m^{-2}, with high heat recovery and energy efficiency.

Another configuration of a closed loop OHE was proposed to utilise low-grade thermal energy using MD coupled with PRO (Lin et al. 2014). Using different heat source temperatures and working DS concentrations, energy efficiency was assessed and the process with optimised, and it was found out that at lower working temperatures of 60 and 20 ºC, use of a higher working concentration of draw would enhance the process efficiency.

Instead of MD, multi-effect distillation (MED) was performed for thermal separation in the OHE process proposed by Altaee et al. (Altaee et al. 2017). They proposed two different configurations of the OHE: a single stage conventional OHE, and the dual-stage closed-loop process. MED was chosen due to the deemed free source of waste heat utilisable for thermal regeneration. With their simulation, they were able to show that dual-stage closed loop PRO was 20% more efficient than the single-stage OHE.

2.7.2 Dual-stage PRO

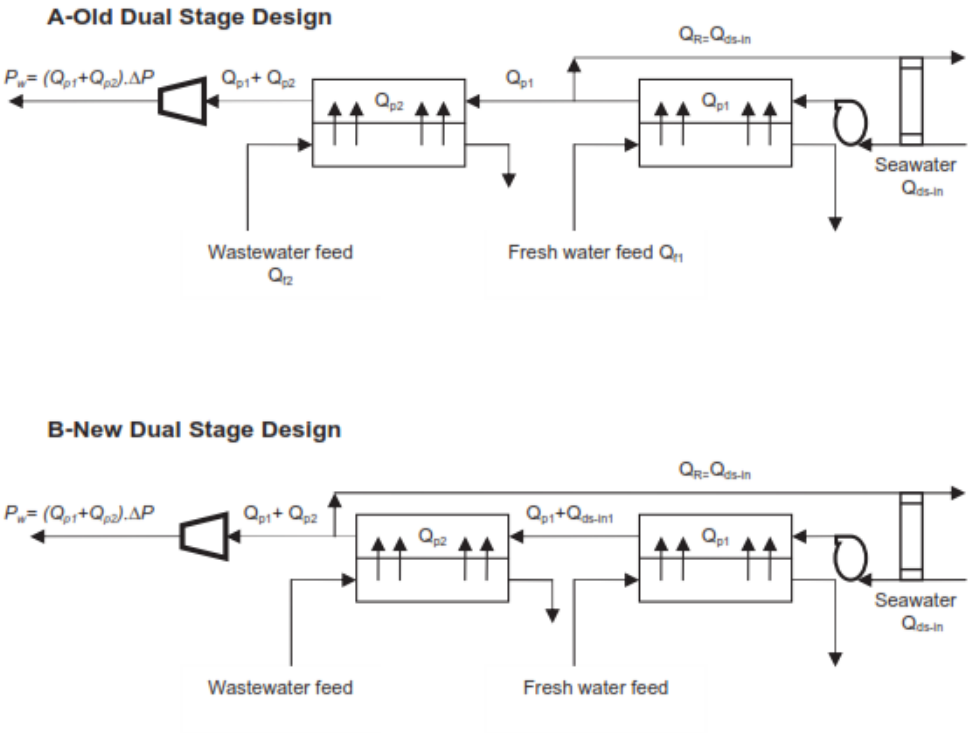

Figure 2.15 The conceptual schematic of dual-stage PRO operation using two different feed streams (Altaee et al. 2014)

Among the earlier novel configurations of PRO is the installation of a dual-stage PRO system. Introduced in 2014 by Altaee et al. (Altaee et al. 2014), the dual-stage PRO

process aimed to utilise two different feed streams: brackish/fresh water and wastewater, as shown in Figure 2.15. The feed streams were delivered separately into the PRO modules, with the pressurised seawater delivered continuously into the two PRO modules in series. The diluted DS recovered after the second stage PRO treatment was depressurised by a turbine for power generation. This configuration was found to generate higher power higher power density; however, capital costs of the system were also significantly higher due to the employment of two PRO modules. Following the results of the first study, the dual-stage PRO process was then further optimised to enhance process performance, leading to the proposition of a new design configurations of the dual-stage PRO process, also shown in Figure 2.15. In the old configuration, the diluted DS from the first stage was delivered onto the second stage; in the modified configuration, the seawater flow goes from the first stage to the second stage simultaneously from the pressurised DS chamber. This configuration significantly improved the PRO performance, due to the higher water flux obtained at the second stage.

Another group proposed the enhanced energy recovery using a two-stage PRO system. He et al. (He, Wang & Shaheed 2015) proposed four different configurations of the dual-stage PRO system, as shown in Figure 2.16: (a) CDCF; (b) DDDF; (c) CDDF; and (d) DDDF. For CDCF, the draw and feed streams are connected in series through two PRO modules. DDDF, on the other hand, delivers draw and feed from the same source tank separately into two PRO modules. Comparing these two configurations, DDDF showed worse energy harnessing performance than that of the single, conventional PRO operation. For CDDF, and DDCF, either the draw or the feed was

supplied continuously, while the other was treated separately. These two configurations showed better performance than DDDF.

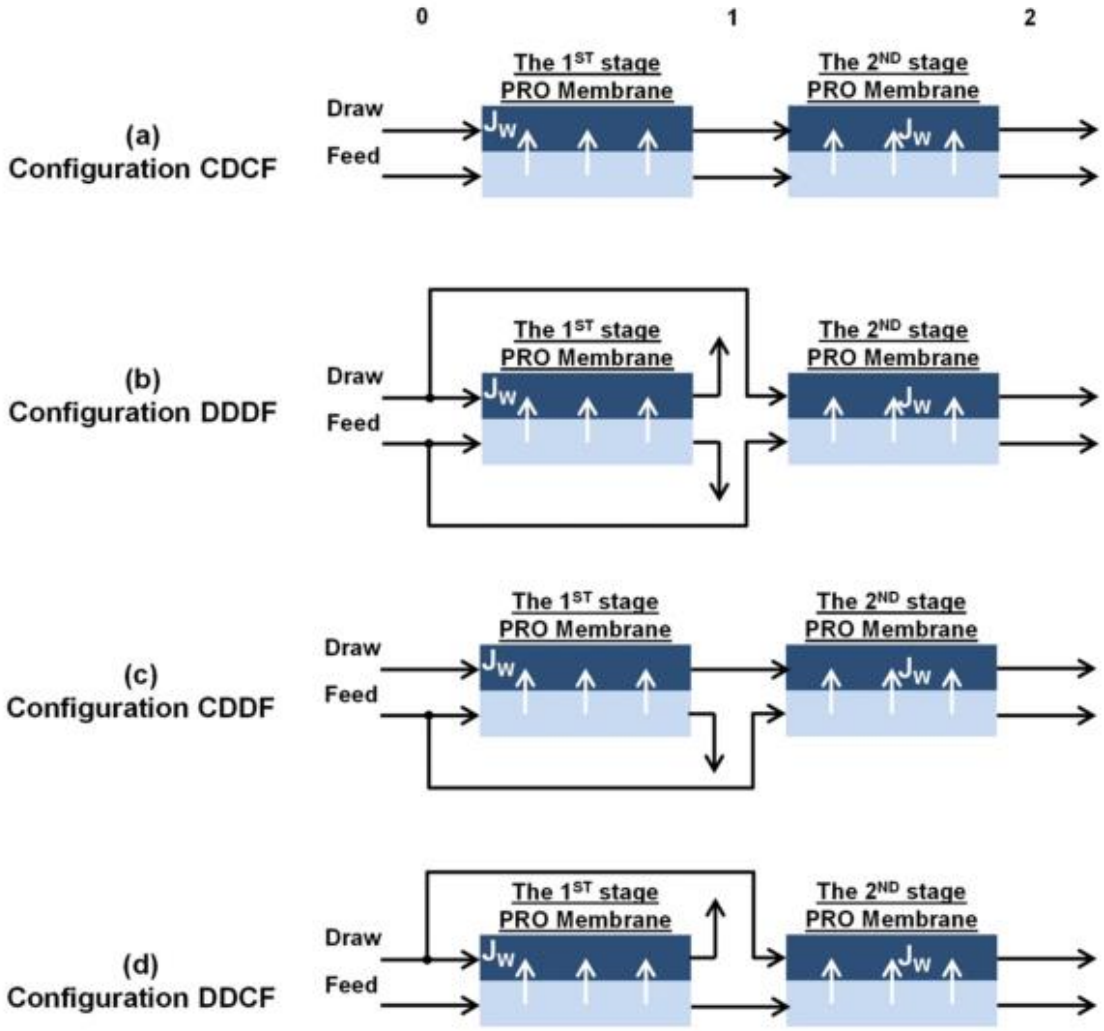

Figure 2.16 Four different proposed configurations of a dual-stage PRO system: (a) CDCF (continuous draw and feed); (b) DDDF (divided treatment of draw and feed); (c) CDDF (continuous draw and divided feed); and (d) DDCF (divided draw and continuous feed) (He, Wang & Shaheed 2015)

2.7.3 Pool PRO

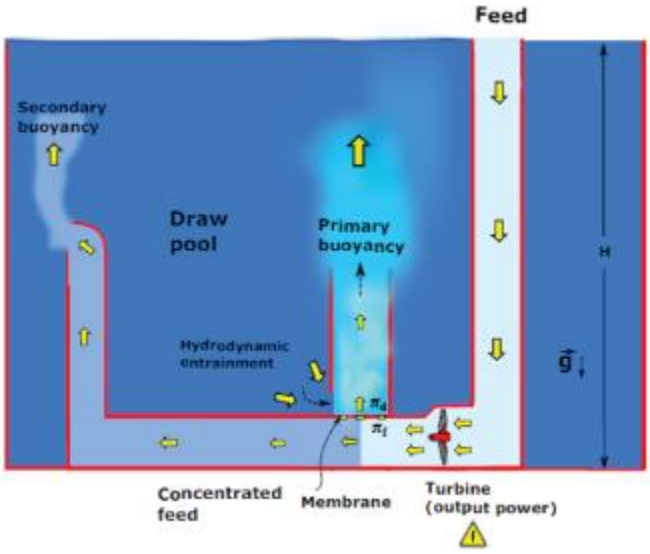

Figure 2.17 Proposed pool PRO system (Arias & De Las Heras 2020)

One of the inherent limitations of PRO is its requirement of various mechanical parts, which all require energy to function. One of these mechanical parts is the pressure exchanger, which transfers pressure from the pressurised stream to a non-pressurised stream. The pool PRO system eliminated the use of pressure exchanger, as shown in Figure 2.17 (Arias & De Las Heras 2020). In the pool PRO system, the DS is placed in a pool, and the feed was supplied into a stream, until it approaches the semi-permeable membrane, which allows the permeance of fresh water and the buoyancy of the mixed feed and draw will allow the diluted draw to be pulled instantaneously as it is formed. The buoyancy of the diluted draw was expected due to a change in the density of the draw. Due to the pulling away effect of the buoyancy of the diluted draw, the need for the pressure exchanger to pressurise the diluted draw stream was eliminated. No further

study was done on pool PRO, but based on the simulations, the pool configuration could prove to be highly beneficial when there is a large amount of DS available.

2.7.4 Facultative RO/PRO system

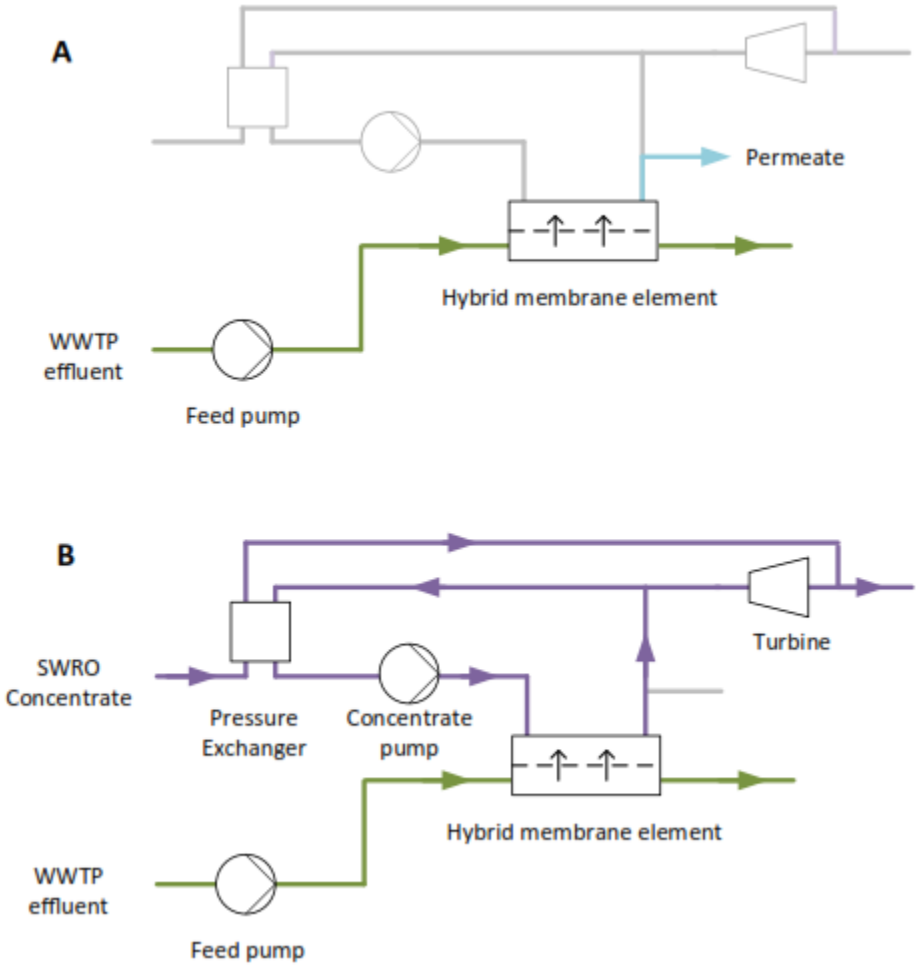

Figure 2.18 Schematic of the proposed facultative RO-PRO system, which can do both (a) RO operation and (b) PRO operation, but not at the same time, as the system switches between the two operating modes (Blankert et al. 2020)

To improve the economic efficiency of a stand-alone PRO system, Blankert et al. (Blankert et al. 2020) proposed a facultative RO and PRO system which does both

operations, but not at the same time, as the system switches between the two operating modes, depending on the presence of the DS (Figure 2.18).The RO mode is activated when only the FS containing wastewater treatment plant effluent is available, resulting in the production of high-quality water. The PRO mode, on the other hand, is activated in the presence of SWRO brine DS, whose salinity difference with the wastewater effluent can be converted into osmotic energy. While this system does not specifically develop PRO as an energy-harnessing process, it is able to provide solutions to improve the process, and find a way to facilitate wastewater treatment along with energy generation.

2.7.5 GreenPRO

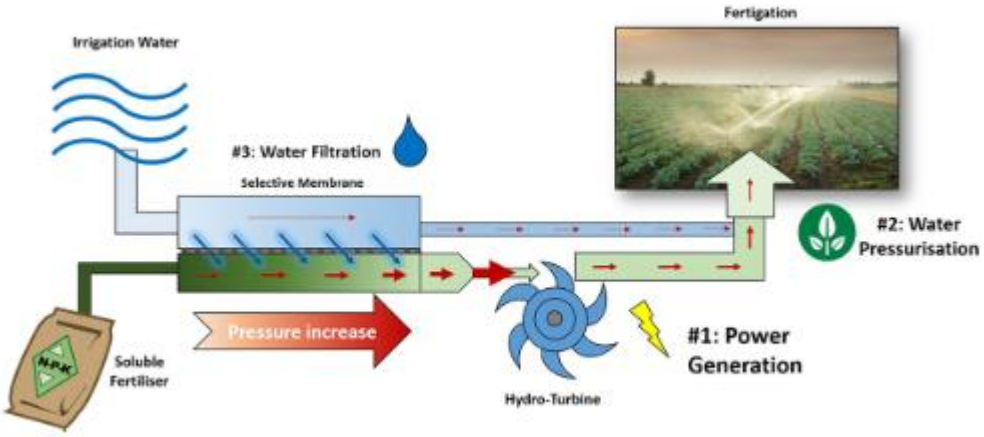

Figure 2.19 The proposed fertiliser-driven PRO process, GreenPRO (Volpin et al. 2018)

A niche application of PRO was the use of agricultural fertilisers as the draw solute, for a process known as GreenPRO (Volpin et al. 2018). This process was envisioned to be able to generate power, pressurise irrigation water, and treat water, as shown in Figure 2.19. Pure and mixed agricultural fertilisers were utilised as the draw and irrigation water

(river water) was used as the feed in this study. Theoretical thermodynamic simulation results were validated with experimental data to demonstrate that the dilution of agricultural fertilisers to make these suitable for fertiliser-based irrigation could release chemical potential energy, which could then be harnessed during PRO.

2.7.6 PRO for enhanced oil recovery

A consortium of researchers from Qatar, Australia, and US has an ongoing work on the use of PRO for oil recovery and treatment of produced water from conventional oil sources (Adham et al. 2018). The hypersaline nature of produced water from oil sources (amounting to up to 290,000 mg L^{-1} salinity, around 8 times higher than seawater) makes it a suitable DS choice, with seawater or desalination plant brine as the FS. This work is currently ongoing, with a main focus on the following: (1) pretreatment requirements of produced water for PRO DS use, (2) development of suitable membranes which could withstand high pressures required for obtaining peak power densities from the hypersaline produced water, and (3) application of waterflooding with PRO.

Waterflooding is a practice performed in large-scale petroleum industries, wherein the produced water is injected into the oil source to displace the oil, hereby increasing oil production at the wellhead. PRO can be applied alongside waterflooding, as shown in Figure 2.20. This process is able to reuse the diluted produced water from PRO while simultaneously reducing required pumping energy requirements, reducing waste stream, enhancing injectivity, generate energy, and enhance oil production.

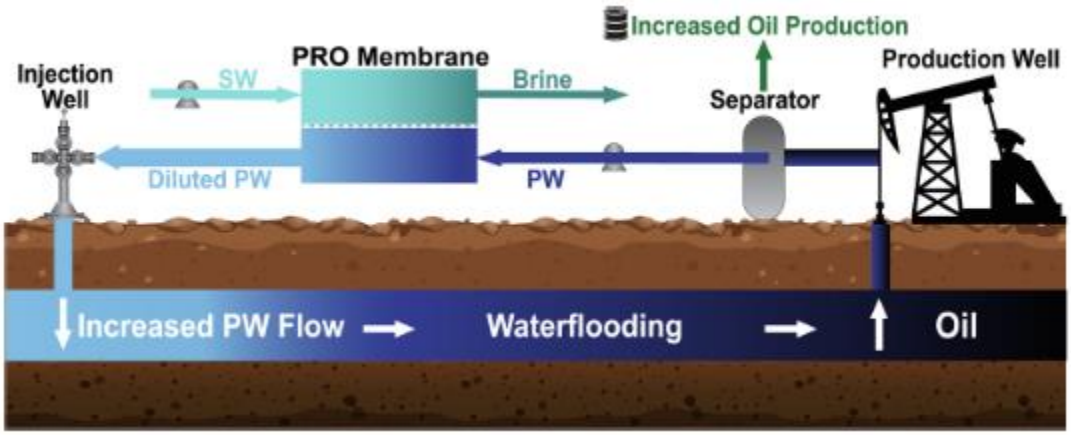

Figure 2.20 The proposed integrated PRO and waterflooding process, for enhanced oil recovery (Janson et al. 2020)

2.7.7 Geothermal PRO

A new renewable energy system combining geothermal heat and PRO was recently developed. Named SaltPower, the system uses high salinity geothermal brine in an osmotic power installation coupled with geothermal heat production (Madsen et al. 2020). As shown in Figure 2.21, geothermal brine passes through a heat exchanger, in this case, the geothermal heat plant, prior to PRO operation, using various feed sources, such as wastewater. The geothermal heat plant can be used for district heating, while the electricity produced by the PRO operation can be used either for household or geothermal plant use.

Using the geothermal PRO system, single and multi-stage operation designs were investigated. The authors believed that a larger amount of osmotic potential is required to increase salinity gradient production, thus a multi-stage PRO operation could prove useful. Two multi-stage designs were investigated and the efficiency and performance of these designs were compared with that of the single-stage operation. A single-stage operation was only able to extract 35% of the theoretical extractable salinity gradient

energy. One multi-stage PRO design made use of two different membrane modules operated at different pressures, with the DS output of the first stage (operated at 50 bar) proceed to both a hydro turbine and the second stage operated at 30 bar. This design resulted to an enhanced salinity gradient energy extraction of 46%. The other multi-stage operation aimed to reduce the loss in the pressure exchanger by using two membranes connected in series, operated at an equal pressure of 50 bar to generate more permeate directed toward the same turbine. The energy extraction capacity improved to over 60% following this approach.

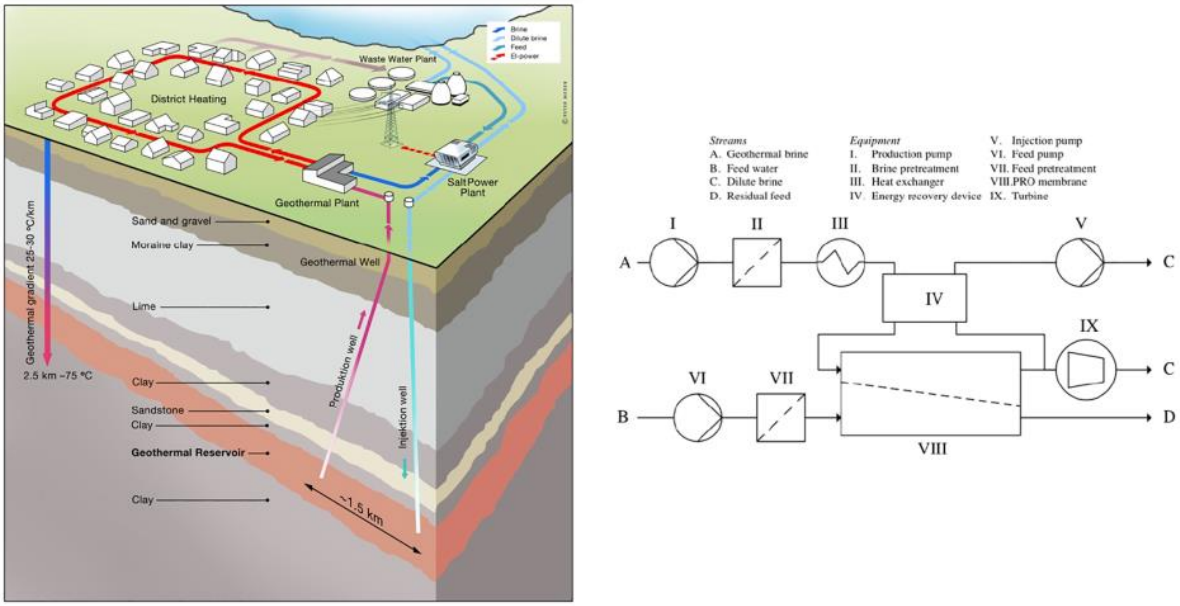

Figure 2.21 (L) Illustration of the combined PRO and geothermal heat plant system of SaltPower, showing how geothermal heat production and PRO could work together to provide both district heating and electricity; (R) Schematic diagram of how the geothermal plant acts as the heat exchanger in this system (Madsen et al. 2020)

2.8 Technical challenges, feasibility, and future perspectives

2.8.1 Technical challenges and feasibility

The current biggest challenge of PRO is the feasibility of the process. PRO researchers have now started to accept that the theoretical energy-harnessing potential of PRO is flawed and there are limitations in the actual demonstration of the process, affecting the maximum thermodynamic energy which can be harnessed from the process, especially when energy expenditures for pre-treatment, pressurisation, and delivery are to be considered. Straub et al. (Straub, Deshmukh & Elimelech 2016) calculated that the maximum Gibbs free energy extractable from the mixing of seawater (0.6 M NaCl) and river water (0.015 M NaCl) was only 0.26 kWh m^{-3}. Taking in consideration the energy requirements for pre-treatment (0.1-0.4 kWh m^{-3}), pressurisation (0.05-0.1 kWh m^{-3}), and pumping (0.02-0.05 kWh m^{-3}), the amount of net energy will be fractional, that the whole process could be considered futile (Lee, Chae, et al. 2020; Lin, Straub & Elimelech 2014; Straub, Lin & Elimelech 2014). However, these energy expenditure assumptions, as well as the cost and economic analysis, do not depict a clear picture of the feasibility of the PRO process, as full-scale PRO power plants are not operated to validate these findings. With the implementation of a full-scale PRO power plant, PRO researchers can also gain insight with the underlying capital, operational, and maintenance costs of the plant.

These information lead to the question of the feasibility and viability of the process. Can the limitations and the underlying costs of PRO operation be offset by the amount of energy harnessed by the process?

Aside from commercialisation of the process, large-scale development and commercialisation of PRO membranes also remain to be fully achieved. Due to the lack

of commercialised membranes for PRO, the unit price of each module is too high, that the total capital cost of PRO operation is also affected. Furthermore, membranes and modules have only a specific lifetime, that during continuous PRO operation of a plant, the replacement, cleaning, and maintenance of the membranes should also be considered. Also, membrane cost may be inversely proportional to membrane durability and efficiency, such that, cheaper membranes may not deliver better performance and longer lifetime, hereby further increasing operational costs (Achilli & Childress 2010). Membrane performance is also highly important in determining the feasibility of the PRO process. Similarly, membranes with low power density values would require larger membrane size to augment the limited energy harnessing capability of the membrane, thus, increasing capital expenditure. High performance membranes for PRO are expected to be able to decrease energy cost due to the higher energy production of better membranes. If PRO membranes are able to increase power density, membrane life, and minimise energy production cost, then revenues for PRO demonstration would increase.

The recent research direction that PRO is gearing towards is the integrated hybrid processes involving PRO and other applications of PRO. Previous studies have shown that PRO installations as part of a hybrid process are cheaper than a stand-alone PRO power plant, mainly due to the use of already available infrastructure for PRO operation, and the cheaper installation and operational costs of already established and commercial processes, like SWRO and MD (Stenzel & Wagner 2010; Tanioka, Kurihara & Sakai 2018). The issues hindering the full-scale implementation and commercialization of PRO has not changed in the past five years. This is the reason why recent research on process development for PRO has gone from pilot-scale applications to development of hybrid

PRO processes and finding niche applications for PRO. Development of hybrid PRO processes and niche applications for PRO could then use the extractable energy of PRO to augment energy requirements of other processes or find suitable applications for PRO, which would not require expensive infrastructure construction or intensive energy consumption due to pumping and pressurization.

2.8.2 Future perspective

The PRO process is a promising technology to harness renewable power from natural salinity gradient. Through utilizing a suitable membrane to control the spontaneous mixing of the saline solutions, the salinity gradient energy can be extracted in terms of electricity using the PRO system with reduced environmental impacts. The concept of this PRO process has been reported in the last decade, however, due to failure in both sustainable large-scale PRO implementation and development of suitable membranes and modules, PRO research has not significantly advanced as many researchers had hoped. Different PRO configurations, as well as multi-stage or hybridized process designs, have been recently investigated to improve the overall process efficiency while minimizing energy requirements and operational cost. Also, recently, bench-scale membrane development studies have achieved outstanding PRO performance with membranes prepared by a variety of techniques, which include chemical modification and material incorporation. While these membranes were able to achieve excellent bench-scale performance, the real challenge is cost-effective and consistent fabrication of such membranes at a larger scale, potentially for modulation. In literature, nano-sized material incorporation and chemical modification have become

popular membrane development research trends to alter the properties and separation performance of the membrane; however, the material synthesis cost and the process optimization for effective and consistent incorporation and modification are some of these technique's limitations. Furthermore, module development is the next necessary step. High-performance membranes are required for PRO; however, membrane modulation was found to be more important in a sustainable PRO process operation (Straub, Lin & Elimelech 2014). Membrane modules should be designed such that pressure drop is limited, the membrane weak points are minimized, and the membranes do not sustain damage over constant operation at a higher pressure (Altaee & Cipolina 2019).

New emerging trends involve advanced configurations and niche applications of the PRO process. Due to these processes, salinity gradient energy can be harnessed using a wide variety of DS and FS. Not only that, integrated processes are able to perform more than just salinity gradient energy generation, but also seawater desalination, wastewater treatment, heat recovery, and valuable resource recovery. These technologies can effectively be utilized for maximizing the power density with excellent heat recovery and energy efficiency when coupled with other membrane desalination technology. The dual-stage closed loop PRO process is a potential method that can achieve more efficient performance than the single-stage PRO process due to high water permeation in the second stage. Furthermore, future PRO studies should also focus on the further development of hybrid processes and large-scale installation of pilot plants. Following the efforts of the Mega-ton and GMVP projects in Japan and South Korea, respectively, it was found that SWRO-PRO demonstration plant can achieve maximum power density of

about 18.3 W m^{-2} and the energy consumption can be decreased by 80% when desalinating 240 m^3 d^{-1} of seawater.

It is also believed that the pretreatment strategies can reduce PRO membrane fouling, decrease the need for chemical cleaning and module replacement, and increase the membrane life time. The RO-NF-PRO hybrid process is an outstanding system, which integrates these membrane processes to simultaneously attain three objectives: (1) pre-concentration of DS for higher extractable salinity gradient energy, (2) pretreatment of the feed, and (3) salinity gradient energy harnessing. Other pretreatment conditions can also be considered, depending on the nature of the FS and DS.

Despite the difficulty in proving the feasibility of PRO as a commercially viable process, this process still has a huge commercial potential. The failure of Statkraft and the lack of follow-up after the high-profile Mega-ton and GMVP SWRO-PRO pilot plant projects prove to be discouraging; however, these projects were able to provide significant insights regarding the implementation of PRO. Based on these pilot-scale implementations, the stand-alone PRO process has proven difficult to be implemented, and would require a more systemic process design and optimization to address the inherent limitations of the process, as well as more careful evaluation of economic potential. On the other hand, integration with other membrane-based processes has shown promising results, and with better configurations and operating conditions, the GMVP project will definitely not be the last full-scale implementation for PRO, as many membrane engineers and researchers are finding ways to exploit this process and improve its efficiency. In fact, the Middle East is starting to look at PRO to augment the diminishing fresh water supply in the region, while generating salinity gradient energy.

Also, SaltPower has recently shown the feasibility of its geothermal PRO system installation in simultaneous district heating and energy generation. With continuous effort in development of PRO processes, membranes, and modules, the economically feasible extractable power density requirement of 5 W m^{-2}, originally set by Statkraft, could be achieved in the future.

3 General Methods

3.1 Introduction

In this thesis, PRO TFC membranes were prepared using a variety of methods and approaches. In order to demonstrate the versatility of the techniques performed for polyamide selective layer engineering, different PRO TFC membrane substrates, i.e., flat-sheet and hollow fibre, via NIPS were first prepared prior to the IP to form the thin film polyamide layer.

The TFC membranes developed were then characterised for morphology, chemistry, mechanical strength, porosity, and wettability. To gain insights about the membrane separation performance, the intrinsic transport properties, *A*, *B*, and *S*, were evaluated during RO operation. The PRO performance was then evaluated at a single DS concentration of 1.0 M NaCl and a range of applied hydraulic pressures to determine the J_w, J_s, and W of the membranes.

This chapter describes the general methods for TFC membrane development, characterisation, and osmotic performance evaluation. Methods specific for certain studies are detailed in the succeeding chapters.

3.2 TFC membrane preparation

3.2.1 TFC membrane substrate preparation

The TFC membrane substrates were prepared using conventional NIPS process. Flat sheet membrane substrates were casted on a flat surface while hollow fibres were spun using a hollow fibre spinning machine.

A polymer dope solution with a known concentration of polymer and additives dissolved in organic solvent was first prepared. The polymer solution was afterwards degassed prior to casting or spinning.

3.2.1.1 Flat-sheet

3.2.1.1.1 Polyamide-imide (Torlon®)

Polyamide-imide (PAI, Torlon® 4000 T-MV) was supplied by Solvay Chemicals Co. Ltd., South Korea. A 15 wt% PAI solution was prepared with *N,N*-dimethylformamide (DMF, 99.8%, anhydrous, Sigma-Aldrich, Australia) and tetrahydrofuran (THF, 99.9%, anhydrous, Sigma-Aldrich, Australia) as solvents (6:4 weight ratio of DMF and THF). The solution was stirred at 300-500 rpm at 60ºC for 24 h. The solution was degassed and brought to room temperature prior to casting. The polymer dope solution was poured onto the 63 µm thick open mesh PET (PETEX®, Sefar Pty. Ltd., Australia) fabric attached on a glass plate and, using a casting blade set at a 200 µm thickness and a casting machine (Elcometer 4340 Automatic Film Applicator, Elcometer Asia Pte. Ltd., Singapore), was spread into a film. The nascent polymer film was immediately immersed in a water coagulation bath maintained at room temperature for 20 min, and afterwards stored in DI water overnight to ensure complete removal of organic solvents.

3.2.1.1.2 Aliphatic polyketone

The membrane substrate was prepared using aliphatic polyketone (PK, M_w = 200000 g mol^{-1}, Asahi Kasei Co., Japan) and PET nonwoven fabric (90HP, Awa Seishi Co., Japan). To prepare the PK polymer dope solution, resorcinol (> 99.0%) and DI water

were used as solvents. Methanol (> 99.8%), acetone (> 99.8%) and hexane (> 99.8%) were used during flat sheet membrane casting. A 10 wt% PK solution was prepared by dissolution of the polymer in a resorcinol/DI water (65:35) solvent mixture at 80 ºC for 4-6 h with constant stirring. The polymer solution was degassed at 50 ºC overnight. The solution was poured onto the nonwoven PET fabric attached on a glass plate and was spread with a casting thickness of 200 µm using a stainless-steel casting knife. The PK film was afterwards immersed in a 35% aqueous methanol coagulation bath for 20 min for phase separation to occur. The membrane substrate was then placed in steel frames to avoid shrinkage before successive 20 min immersion cycles in acetone and hexane baths. The membrane substrate was air-dried afterwards until further use.

3.2.1.2 Hollow fibre

Polyethersulfone (PES, Veradel® 3000P, M_w = 62000 – 64000 g mol^{-1}, Solvay Specialty Polymers, Republic of Korea) was the polymer for the membrane substrate. N-methyl-2-pyrrolidone (NMP, Merck, Australia) was the polymer solvent and LiCl and polyethylene glycol 400 (PEG 400, M_w = 400 g mol^{-1}, Merck, Australia) were the pore-forming agents. The hollow fibre membrane substrate was prepared by a wet-wet spinning process using a hollow fibre spinning machine (Sepratek, Republic of Korea), as shown in Figure 3.1.The polymer dope solution was prepared with the following composition: 22 wt% PES, 30 wt% PEG 400, 45 wt% NMP, 1.5 wt% LiCl, and 1.5 wt% DI water. The bore and polymer dope solutions were supplied separately into their respective channels in the spinning machine. After transferring the polymer dope solution into the syringe pump, the solution was degassed at ambient temperature for 24 h before hollow

fibre spinning took place. Both the dope and bore solutions were delivered by a syringe pump (Teledyne ISCO, Teledyne Technologies Company, USA) and extruded by the spinneret at the same time from a designed air gap distance and immediately immersed in a coagulation water bath at ambient temperature. The rotary drum-type winder collected the fibres at a designed take-up speed. The spinning conditions of the hollow fibre substrate include the following: polymer dope solution flow rate, bore solution flow rate, air gap distance, and the take-up rate, as shown in Table 3.1. The as-spun fibres accumulated on a drum-type rotary winder at a set take-up speed, at an almost free-fall condition. The hollow fibres were afterwards stored in DI water to eliminate solvent residue for approximately 2 d. The spun substrates were then placed in a solution containing 1:1 (w/w) water/glycerol for post-treatment and preservation, followed by air-drying for 2 d, prior to storage, module preparation, and use.

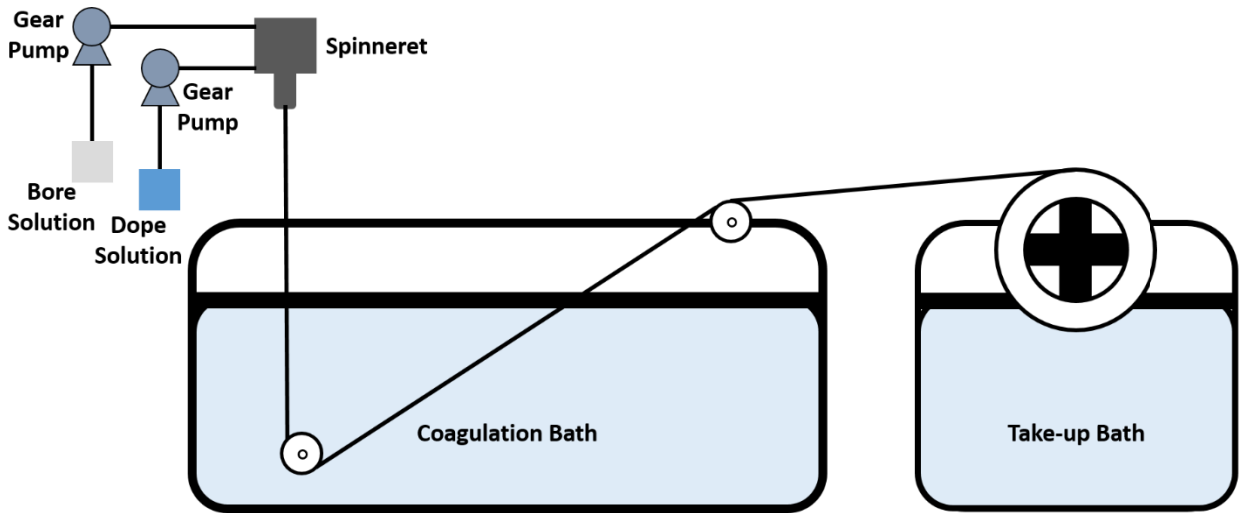

Figure 3.1 Hollow fibre spinning machine

Table 3.1 PRO hollow fiber membrane substrate spinning conditions

Parameter	
Polymer dope solution (wt%)	PES:PEG:NMP:LiCl:DI (22:30:45:1.5:1.5)
Bore solution	DI:NMP (1:1)
Flow rate, dope solution (mL min^{-1})	3.0
Flow rate, bore solution (mL min^{-1})	1.2
Air gap distance (cm)	5.0
Take-up rate (m min^{-1})	1.45 - 1.50
Non-solvent coagulant	Tap water

3.2.2 Interfacial polymerisation

Polyamide was formed on the surface of the membrane substrate during IP upon the reaction of an amine (MPD, 99%, Sigma-Aldrich, Australia) and an acyl chloride (TMC, 98%, Sigma-Aldrich, Australia).

3.2.2.1 Flat-sheet

The flat sheet membrane substrates were placed in an acrylic frame, to facilitate the introduction of the IP precursors onto only one side of the membrane substrate. The aqueous 2 wt% MPD solution was first poured onto the membrane substrate surface, and drained after a designed time, followed by complete removal of the MPD solution using air knife. The MPD-immersed surface was then made to react with the 0.15 wt% TMC solution for a designed time. The excess TMC solution was drained off and the membrane was air-dried before it was placed in an oven set at 90 ºC for 10 min for heat curing.

3.2.2.2 Hollow fibre

A certain number of hollow fibre membrane substrates were placed together in a module specifically designed for PRO membrane performance tests. The ends of the

modules were potted with epoxy resin prior to IP and the subsequent membrane performance evaluation.

The polyamide selective layer was synthesised on the lumen (inner surface) of the hollow fibre substrates via IP. Both ends of the modules were tethered to a peristaltic pump (Masterflex HV-77926-10, Cole-Parmer, Australia) to specifically place only the lumen in contact with the precursors of the IP process. The modules were fixed in a vertical position and the IP precursors were delivered into the lumen side of the hollow fibres in an upward direction. The aqueous 2 wt% MPD solution was first allowed to flow through the membrane lumen for a fixed period of time and a designed flow rate. Excess MPD solution was removed by purging N_2 gas at a pressure of 0.1 bar for 5 min; after which, 0.15 wt% TMC in heptane was then passed through the lumen at a designed flow rate for a certain period to allow complete reaction with the MPD in the pores of the membrane lumen. The TMC unreacted with MPD was afterwards purged out using N_2 gas at a pressure of 0.1 bar for 1 min. The modules were subsequently placed in DI water without any more post-treatment. The membrane modules were stored in cool conditions prior to osmotic tests and characterisation.

3.3 Membrane characterisation

A number of characterisation techniques were performed to obtain morphological, structural, and chemical information of the prepared membranes. Table 3.2 summarises the membrane characterisation techniques used in this thesis.

Table 3.2 Membrane characterisation technique employed in this thesis

Parameter	Technique
Membrane morphology	Field emission scanning electron microscopy
Chemical structure	Attenuated total reflectance-Fourier transform infrared spectroscopy
Chemical composition	X-ray photoelectron spectroscopy
Membrane surface roughness	Atomic force microscopy
Membrane wettability (water contact angle)	Optical tensiometry
Porosity and pore size	Capillary flow porometry
Mechanical strength	Tensile testing

3.3.1 Field emission scanning electron microscopy

The surface and cross-section morphology of the membranes were examined under a field emission scanning electron microscope (FE-SEM, Zeiss SUPRA 55-VP, Carl Zeiss AG, Germany) operated at 5-10 kV. Prior to FE-SEM analysis, the membrane samples were dried before sputter-coated with 10 nm of gold and palladium. For cross-section morphology analysis, the membrane samples were frozen using liquid nitrogen and snapped immediately prior to sputter-coating.

3.3.2 Attenuated total reflectance-Fourier transform infrared spectroscopy

Fourier transform infrared (FTIR) spectroscopy (IRAffinity-1, Shimadzu, Kyoto, Japan) equipped with a single reflection attenuated total reflectance detector (ATR, MIRacle 10, Shimadzu, Kyoto, Japan) was used to analyse the chemical composition of the membrane. Multiple measurements were conducted within the wavelength range of 4000 – 600 cm^{-1} for a minimum of 32 scans with a signal resolution of 4 cm-.

3.3.3 X-ray photoelectron spectroscopy

X-ray photoelectron spectroscopy (XPS, ESCALAB250Xi, Thermo Fisher Scientific, USA) was used to determine surface elemental composition. The monochromatised spectrometer has an Al Kα radiation probe at 1500 eV.

3.3.4 Atomic force microscopy

Surface roughness were analysed by atomic force microscopy (AFM) using a scanning probe microscope (Dimension 3100, Bruker, Germany) operated on tapping mode (scanning area of 5 μm × 5 μm).

3.3.5 Optical tensiometry

The hydrophilicity of the membrane was measured using an optical tensiometer (Attension Theta, Biolin Scientific, Gothenberg, Sweden), employing the sessile drop method. A 5-μL water droplet was made to contact the membrane, and contact angle values were recorded through OneAttension software (Biolin Scientific, Gotherberg, Sweden). The average of five measurements on different spots of the membrane was reported.

3.3.6 Capillary flow porometry and other membrane porosity characterisation

Capillary flow porometry was conducted using a porometer (Porolux 100, Porolux, Belgium). Analysis was performed with dried samples under dry-up/wet-up mode using a wetting agent (Porefil surface tension = 16 dynes cm^{-1}).

Membrane porosity was determined via gravimetric analysis (Park et al. 2018). Pre-weighed dried samples were soaked in water for 24 h at 30 °C, and the wet samples were re-weighed. Porosity (ε) was calculated through Equation 3.1:

$$\varepsilon = \frac{(m_2 - m_1)/\rho_w}{(m_2 - m_1)/\rho_w + m_2/\rho_p} \quad \textbf{3.1}$$

where m_1, m_2, ρ_w, and ρ_p are weight of the dry sample, weight of the wet sample, density of water, and density of the polymer, respectively.

3.3.7 Mechanical strength determination via tensile testing

Mechanical strength of the membrane was determined using an advanced material testing system (Lloyd Materials Testing LS1, Ametek, Berwyn, PA, USA) with a 1 kN load cell. The flat sheet membrane samples were cut into 30 mm × 10 mm prior to the test. For hollow fibre membrane samples, a pair of wire grip with bollard and vice clamp (2 kN) was used.

3.4 Membrane intrinsic transport property evaluation

Membrane parameters, pure water permeability (*A*) and solute permeability coefficient (*B*) were determined using a cross-flow reverse osmosis (RO) filtration system (Sterlitech Co., Kent, WA, USA), with an effective membrane area of 42 cm^2. Prior to the flux test, the membranes were placed in DI at 5 bar for 1 h to eliminate possibility of membrane compaction.

Pure water flux through the membrane was measured at various transmembrane pressures (TMP) from 1 to 10 bar with a flow rate and cross-flow velocity of 1.5 L min^{-1} and 0.25 m s^{-1}, respectively. *A* was calculated using Equations 3.2 and 3.3:

$$J_w = \frac{\Delta V}{A_m \Delta t} \quad \textbf{3.2}$$

$$A = \frac{J_w}{\Delta P} \quad \textbf{3.3}$$

where ΔV, A_m, Δt, and ΔP are permeate volume, effective membrane area, sampling time, and applied pressure, respectively (Park et al. 2015).

Salt rejection (R) and solute permeability coefficient were determined after performing a flux test for 1 h with 1000 mg L^{-1} NaCl solution as DS at 25 °C and 10 bar. R and B are calculated using Equations 3.4 and 3.5:

$$R = \left(1 - \frac{C_d}{C_f}\right) \quad \textbf{3.4}$$

$$B = J_w \left(\frac{1-R}{R}\right) exp\left(-\frac{J_w}{k}\right) \quad \textbf{3.5}$$

where C_f, C_d, and k are the solute concentrations of the FS and DS, and mass transfer coefficient, respectively (Tiraferri et al. 2011b). k is a function of the solute diffusion coefficient (D), hydraulic diameter (d_h) of the cross flow cell, and the Sherwood number (Sh), which is calculated based on the hydrodynamic conditions of the FO system, as shown in these equations:

$$\boldsymbol{k = \frac{Sh \cdot D}{d_h}} \quad \textbf{3.6}$$

$$\boldsymbol{Sh = 1.85\left(Re \cdot Sc \frac{dh}{L}\right)^{0.33} \; if \; Re < 2000} \quad \textbf{3.7}$$

$$\boldsymbol{Sh = 0.04\left(Re^{0.75} \cdot Sc^{0.33}\right) \quad if \; Re > 2000} \quad \textbf{3.8}$$

where Re, Sc, and L are Reynolds number, Schmidt number, and length of the channel, respectively (Tan & Ng 2008, 2013).

The membrane structural parameter (S) was determined after performing an FO test on the membrane, and calculated using Equation (10):

$$\boldsymbol{S = KD} \quad \textbf{3.9}$$

where *K* is the solute resistance to diffusion within the membrane support layer (Gerstandt et al. 2008; Li et al. 2010).

3.5 Membrane performance evaluation

3.5.1 Experimental

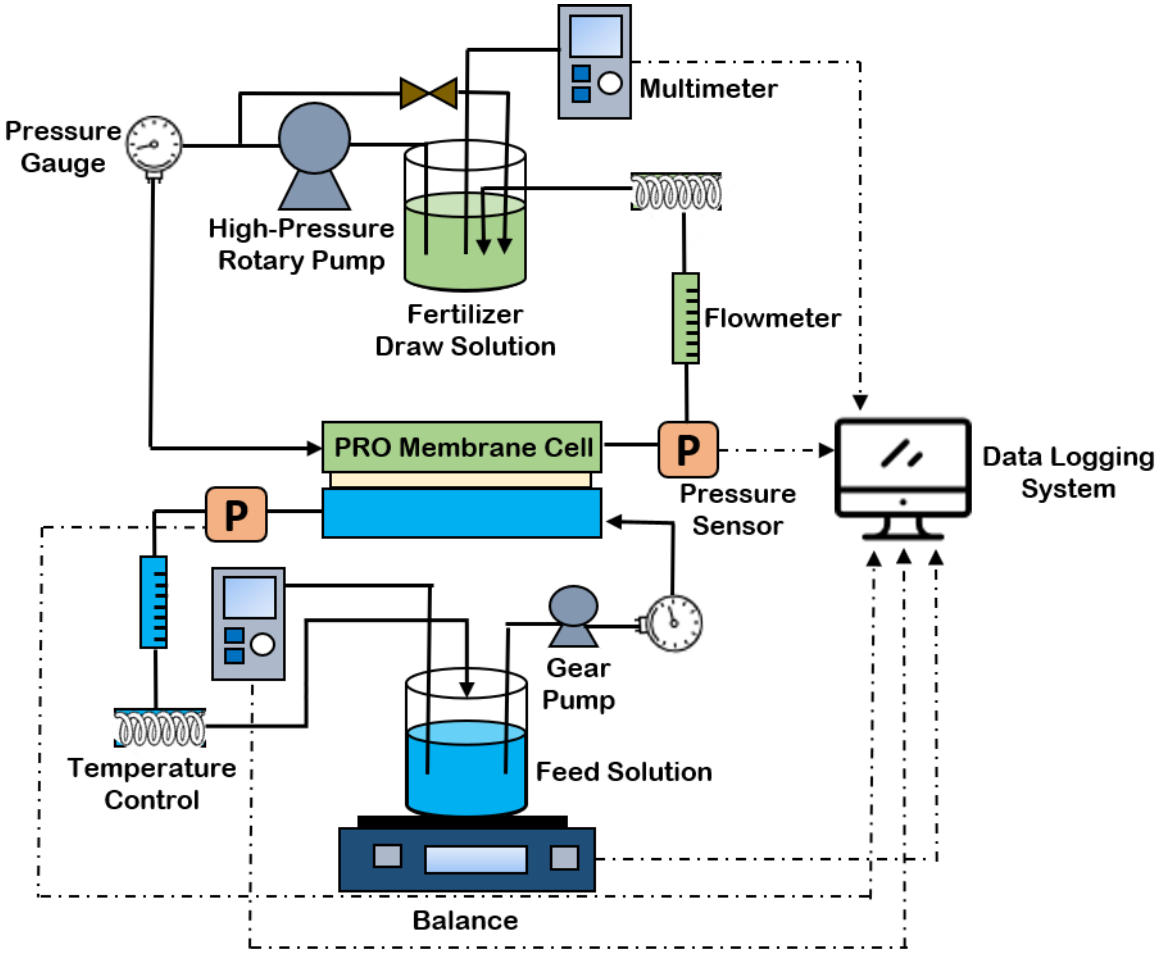

Figure 3.2 Bench-scale PRO system used in membrane osmotic performance evaluation in this thesis

PRO experiments were carried out using a bench-scale PRO system (Cheon Ha Heavy Industries Co. Ltd., Gwangju, Republic of Korea), as shown in Figure 3.2. The

system is consisted of stainless-steel-based membrane test cell containing two water channels permitting counter-current operation. A gear pump (Cole Parmer, USA) was used to flow the FS while a high-pressure plunger pump (BM-4.18, BTLN, China) was used to deliver and pressurise the DS. Behind the high-pressure pump, a customised buffer chamber (Cheon Ha Heavy Industries Co. Ltd., Gwangju, Republic of Korea) was installed in the PRO unit in order to alleviate the pulsation caused by the pump, so that the applied pressure was constantly maintained during the course of PRO operation. The FS was contained in a vessel, whose weight is measured using an analytical balance (CAS CUW4200HX, CAS, Republic of Korea) and monitored using the data auto-logging system. Conductivity measurements were monitored by a conductometer (Horiba LAquaact D-74, Horiba Scientific, Japan).

The channel on the FS side has the following dimensions: 2.6 cm width, 7.7 cm length, and 0.25 cm depth. The FS flowed tangential to the flat-sheet membrane, which has an active area of 20.02 cm^2. The flow rate for both FS and DS were set accordingly. Mesh spacers were placed on the feed channel to support the membrane. For hollow fibre membrane module testing, the module was connected with the FS and DS channels, replacing the flat sheet membrane cell.

The membrane was firstly stabilised and pre-compacted at 10 bar for 30 min. After pre-compaction, the DS was pressurised from 0 bar stepwise until the maximum applied hydraulic pressure sustained by the membrane. All experiments were performed at a fixed system temperature of 23 ± 1 ºC.

3.5.2. Calculation

Water flux (J_w, L m^{-2} h^{-1}) was calculated using Equation 3.10:

$$J_w = \frac{\Delta m}{S_m \Delta t \rho_w} \quad \textbf{3.10}$$

where Δm, S_m, and Δt, are change in mass of FS, effective membrane surface area, and change in time, respectively. Reverse salt flux (J_s, g m^{-2} h^{-1}), on the other hand, was calculated using Equation 3.11:

$$J_s = \frac{\Delta(C_t V_t)}{S_m \Delta t} \quad \textbf{3.11}$$

where C_t and V_t are salt concentration and feed volume at time t, respectively. The specific salt flux is the ratio of reverse salt flux and water flux, J_s/J_w.

The power density (W) was obtained from this equation:

$$W = J_w \Delta P \quad \textbf{3.12}$$

where ΔP is the pressure difference across the PRO membrane.

3.6 Response surface methodology and statistical analysis

Response surface methodology (RSM) designs experimental procedures which allow to determine the interactions and the quadratic effects of various factors in an experiment. Statistical analysis and modelling can also be performed using RSM, as well as the evaluation of the significance of the individual experimental factors and of the experimental conditions (Chi et al. 2012). A central composite design (CCD) contains centre points and axial points, which allow estimation of the process response surface.

A central composite face-centred experimental design with replicate centre trials and axial centre points for the three factors, pH, chlorine exposure, and heat treatment period, was used in this study. A total of 20 experimental trials, consisted of eight trials for cubic points, six for axial points, and six centre points, were performed in this study.

The individual and synergistic effects of the oxidation and heat treatment factors were investigated.

The responses and the synergistic influences of the experimental factors were correlated using the following general quadratic general equation (Gonzales, Kim & Kim 2019):

$$\boldsymbol{Y = \beta_0 + \sum_{i=1}^{k} \beta_i X_i + \sum_{i=1}^{k} \beta_{ii} X_i^2 + \sum_{i<j} \beta_{ij} X_i X_j} \qquad \textbf{3.13}$$

where Y is the response, β_0 is the y-intercept, β_i is the linear coefficient, β_{ii} is the quadratic coefficient, and β_{ij} is the interactive coefficient. Statistical analysis and modelling were conducted using Design-Expert software (Stat-Ease, USA). Analysis of variables (ANOVA) is used to calculate the statistical parameters in RSM. ANOVA is used for graphical analyses of the experimental responses to define the interaction between the experimental variables and the responses. Using ANOVA, responses could be used to optimise the statistical parameters. Experimental data are first analysed using regression analysis, the response surfaces are afterwards drawn, and the contour plot could be obtained for any optimised condition. To check for the statistical significance of the model, F-test is conducted and evaluated using the probability value (P-value) at 95% confidence interval, and the accuracy of the fitted polynomial model was determined by the R^2 value.

4 Melamine-based covalent organic framework-incorporated thin film nanocomposite membrane for enhanced osmotic power generation

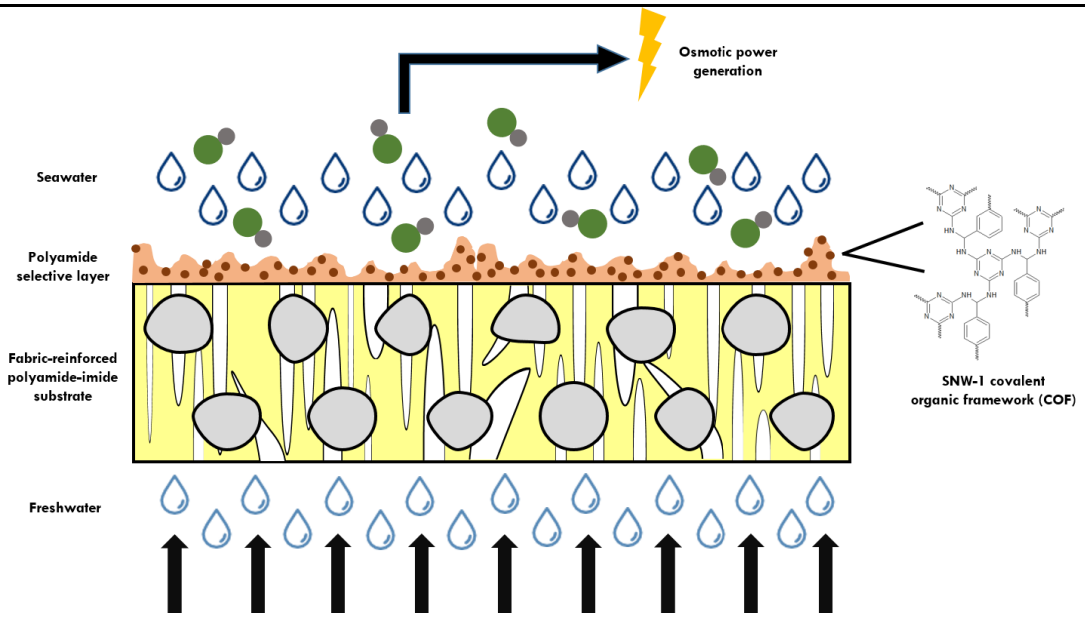

The first technical chapter of this thesis describes the incorporation of a highly porous and hydrophilic nanomaterial, melamine-based Schiff base-network covalent organic framework (SNW-1), into the polyamide selective layer of the TFC PRO membrane. This chapter was published in *Desalination*:

Gonzales, R.R., Park, M.J., Bae, T.-H., Yang, Y., Abdel-Wahab, A., Phuntsho, S. & Shon, H.K. 2019. 'Melamine-based covalent organic framework-incorporated thin film nanocomposite membranes for enhanced osmotic power generation', *Desalination*, vol. 459, pp. 10-19.

4.1 Introduction

Population, industrialisation, and economy have all seen exponential growth, leading to a worldwide concern regarding environmental sustainability and climate

change. The demand for clean water and renewable energy is therefore rising exponentially (Cath, Childress & Elimelech 2006b; Chung, Zhang, et al. 2012; Geise et al. 2010; Gonzales, Sivagurunathan & Kim 2016; Shannon et al. 2008). Desalination and wastewater reuse play significant roles in meeting the continuously increasing fresh water demand. However, current technologies such as thermal desalination and RO are considered to be energy-intensive, thus not sustainable, despite recent efforts to significantly reduce energy consumption (Greenlee et al. 2009). Thus, a desalination process which is less energy-intensive, less costly, and more environment-friendly needs to be developed. Aside from the high level of interest in fresh water production through seawater desalination and wastewater reuse, as a result of the alarming rate of fossil fuel depletion, there is also a significant surge in interest in non-conventional renewable energy, which include solar, geothermal, wind, and biomass (Gonzales & Kim 2017; Gonzales et al. 2017; Gonzales et al. 2016; Han, Zhang, et al. 2015; Kim, Jeong, et al. 2015).

Osmosis occurs through a semipermeable membrane, wherein water is transported from the FS to the DS (Chung, Li, et al. 2012). The membrane should be able to allow only water to pass through and retain most solute molecules or ions in each solution. π between the two solutions is the main driving force of osmosis. This natural phenomenon has been engineered to apply for a number of applications, including desalination, wastewater treatment, and osmotic power harnessing. The advantages of osmosis as a desalination technique are its low-energy requirement (as the process works using natural driving force), low cost, and low fouling propensity (Chekli et al. 2012; Kim, Kim, et al.

2015; Phuntsho et al. 2012), unlike RO process which has to operate at high hydraulic energy.

Besides desalination, osmosis has also been engineered for generating osmotic power using the chemical potential difference by PRO (Achilli, Cath & Childress 2009; Chung et al. 2015; She, Jin & Tang 2012; Yip & Elimelech 2011). The osmotic energy is generated due to the continuous pure water transport across the membrane thereby expanding the volume of the DS and when this happens in a closed restricted DS chamber, it can generate energy in the form of hydraulic pressure (Achilli, Cath & Childress 2009; Klaysom et al. 2013; Straub, Deshmukh & Elimelech 2016; Straub et al. 2015; Volpin et al. 2018). The increased DS volumetric flow with high pressure can be used to run a hydro-turbine and this mechanical energy can be converted into electrical energy using a generator (Han, Zhang, et al. 2015).

Power density is one of the most important parameter in determination of osmotic power generation viability by PRO process. When the available driving force (concentration differences) is fixed, membranes properties play a significant role in the power density. Membranes with high power density are therefore more suitable for osmotic power generation; however, despite PRO process being a potential renewable energy process, the technology is yet to be fully commercialised.

Membrane properties such as permeability, selectivity, hydrophilicity and their robustness to fouling are some of the most important parameters for the power density of the membrane. Traditional polymeric membranes for osmotic processes are often limited since both water permeability and solute selectivity cannot be simultaneously improved, thus finding an optimal membrane fabrication method and membrane configuration still

presents a challenge. Furthermore, membrane fabrication methods should also be environmentally-friendly and cost-effective. Recently, the synthesis of ideally thin, mechanically strong, highly water-permeable, and selective TFC membranes for PRO process has been reported (Han, Wang & Chung 2013; Huang, Arena, et al. 2016; Ingole, Choi, Kim, Jo, et al. 2014; Yip et al. 2011). A number of studies have shown that improvement of the TFC membranes can significantly achieve higher water flux than the first generation of commercially-available membranes, the HTI's symmetric cellulose acetate membranes (Tiraferri et al. 2011a; Wei et al. 2011).

TFC are composite membranes with a thick porous polymer substrate with a thin film of salt rejecting active layer made of polyamide. The membrane substrate for TFC PRO membranes are typically prepared first, followed by the *in situ* selective layer formation on the membrane substrate surface. Porous membrane substrate is normally casted on the nonwoven fabric by NIPS while the thin polyamide selective layer is formed by IP (Alsvik & Hägg 2013). A major factor that limits performance of PRO and any other engineered osmotic processes is the concentration polarisation affects in the membrane. During PRO process, the support and selective layers of the membrane face the FS and DS, respectively. This is known as the PRO mode, or AL-DS membrane orientation, during which concentrative ICP may occur within the substrate. The osmotic driving force and resulting in significantly reduced water flux and power density (Straub, Lin & Elimelech 2014). Thicker membranes are associated with higher structural parameter and more severe ICP and therefore, the TFC PRO membranes must be designed to be of high porosity, strength, and minimum thickness.

One of the new approaches of fabricating osmotic membranes in order to enhance both permeability and selectivity is to incorporate nanomaterial as fillers into the membranes. Mixed matrix membranes (MMMs) consist typically of organic polymer bulk phase and the homogeneously dispersed inorganic particle phase (Choi, Son & Choi 2017; Wang, Song, et al. 2015; Zornoza et al. 2013). These MMMs have shown highly enhanced porosity, water permeability and selectivity compared to traditional polymer membranes. The filler nanoparticles affect the morphology, hydrophilicity and thus performance of the membrane. In conventional MMMs, porous inorganic materials are generally incorporated into the polymeric dope solution prior to membrane fabrication. Ideally, the addition of a small fraction of inorganic fillers may lead to a significant increase in overall water permeability and selectivity. TFN membranes, on the other hand, are prepared by incorporating the nanoparticles on the active polyamide layer instead of the substrate (Amini, Jahanshani & Rahimpour 2013; Emadzadeh, Lau & Ismail 2013). Incorporation of nanomaterials into PRO membranes to form either MMMs or TFN membranes has shown enhancement in its porosity and hydrophilicity, leading to higher water flux and osmotic power during PRO process. Among the hydrophilic nanomaterials reported in literature are graphene oxide (Lim et al. 2017; Park et al. 2015; Soroush et al. 2015; Wang, Ou, et al. 2015), zeolite (Ma et al. 2012), carbon nanotubes (Tian, Wang & Wang 2015; Wang et al. 2013), titanium dioxide (Emadzadeh, Lau, Matsuura, Ismail, et al. 2014; Emadzadeh, Lau, Matsuura, Rahbari-Sisakht, et al. 2014), and silica (Tian et al. 2017).

Recently, a new type of nanomaterial called porous coordination polymer (PCP) has been synthesised and used in the fabrication of membranes for various applications, such

as gas separation, gas adsorption, ion exchange, drug delivery, catalysis, and liquid separation (Gao et al. 2014; Sorribas et al. 2013; Tiscornia et al. 2010; Zornoza et al. 2013). Covalent organic frameworks (COF) and metal organic frameworks (MOF) are three-dimensional PCPs, which are currently receiving growing interest in the aforementioned research areas (Kitagawa, Kitaura & Noro 2004).

While MOF are comprised of metal ions and organic ligands forming a porous framework structure, COF are nano-sized diversified framework structured PCPs composed of light elements (C, H, N, O, and B) (Ding & Wang 2013) in organic functional groups linked by covalent bonds, whose exceptional porosity, high surface area, and thermal stability make them highly advantageous compared to most inorganic nanomaterials for incorporation in membranes. Synthesis of COF, therefore, is a widely practical and promising field, especially now that there is an immense need for new materials that can be used for a wide variety of applications (Gao et al. 2014).

In this study, TFN PRO membranes were fabricated by incorporating lab-scale synthesised COF on the polyamide selective layer. The permeability, power density, porosity, and selectivity of the TFN membranes were evaluated in comparison to the conventional TFC membrane, as a function of COF loading rate. To the best of the authors' knowledge, no previous COF-incorporated TFN membranes have been prepared specifically for PRO application.

4.2 Materials and methods

4.2.1 Materials

Melamine (Sigma-Aldrich, USA), terephthalaldehyde (TA, Sigma-Aldrich, USA), dimethylsulfoxide (DMSO, Sigma-Aldrich, USA), THF, and methanol (MeOH, Sigma-Aldrich, USA) were utilised for nanomaterial synthesis.

4.2.2 Schiff-based synthesis of SNW-1

The synthesis of the covalent organic framework SNW-1 was adapted and modified from previous studies (Schwab et al. 2009; Wang et al. 2017). 6.26 g (49.7 mmol) melamine was solubilised in a mixture containing 10 g (74.6 mmol) g TA and 230 mL DMSO. The solution was degassed with Ar and continuously heated at 180°C and stirred vigorously for 72 h under nitrogen atmosphere, at which formation of precipitates was observed. The solution was cooled down to room temperature and the precipitate was collected via vacuum filtration; after which it was washed with DMF and THF in succession, and finally purified using Soxhlet extraction with MeOH and THF. The yield SNW-1 precipitate was dried under vacuum conditions and temperature of 120°C for 24 h.

SNW-1 is an N-rich melamine-based COF nanoparticle which can be dispersed homogeneously in water and most organic solvents. It is a triazine-based framework, which is typically characterised by lower crystallinity and higher chemical and thermal stability (Ding & Wang 2013). Synthesised from melamine, composed of three exocylic primary amine functional groups, and TA, an industrial aldehyde, this particular nanomaterial has a number of amino groups which can provide reactivity, as well as hydrophilicity. The SNW-1 synthesised in this study exhibits a three-dimensional

framework, with a particle size of 35-50 nm and major pore size of 5 Å, which is larger than the molecular size of water (3 Å), but smaller than the typical seawater solute NaCl (5.64 Å). Covalent C-N bonds present in the monomeric products of TA and melamine link the monomers together to form the framework structure of SNW-1. This nanomaterial has BET and Langmuir specific surface area values of 725 and 965 m^2g^{-1}, respectively, and a total pore volume of 2.556 cm^3g^{-1}, due to a high degree of cross linking.

4.2.3 Interfacial polymerisation and SNW-1 incorporation

The selective polyamide layer was formed on one side of the PAI substrate through IP. Due to its stability both in aqueous and organic phases, various loading rates (from 0.01 to 0.1 wt%) of the SNW-1 were dispersed in both DI water and heptane, to prepare SNW-1-incorporated aqueous MPD and organic TMC solutions, respectively. Before soaking the membrane in both solution, solvents remaining on the surface were removed using air knife. The membrane substrates were first soaked in 2 wt% MPD aqueous solution for 2 min and then in 1.5 wt% TMC solution in heptane solution for 1 min. The excess TMC solution was drained and the membranes were dried in air for 3 min and oven-dried at 90°C for another 3 min. The prepared membranes were placed in DI water until tested.

The mode of incorporation of SNW-1 was first tested wherein a loading of 0.01 wt% of SNW-1 was used to prepare MPD and TMC solutions. The fabricated TFN membranes were denoted according to the COF-incorporation medium, i.e. TFN-M and TFN-T, for MPD and TMC, respectively. Upon comparing the morphology, characteristics, and performance of both membranes, the mode of incorporation at which a better

performance was observed was further used for the succeeding experiments, wherein the SNW-1 loading was increased from 0.01 wt% to 0.02, 0.05, and 0.10 wt%. A control TFC membrane was prepared without nanomaterial incorporation.

4.3 Results and Discussion

4.3.1 SNW-1 covalent organic framework material

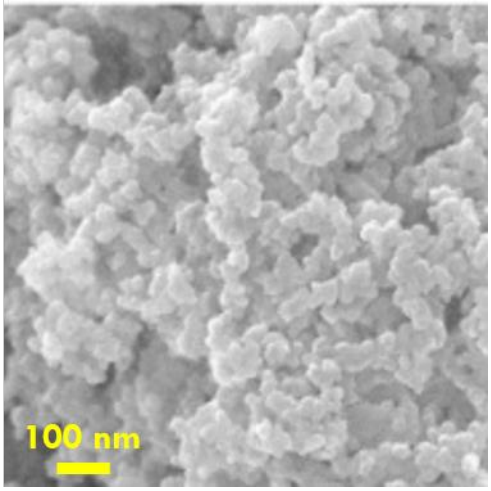

Figure 4.1 FE-SEM image of the synthesised SNW-1 covalent organic framework nanoparticles

FE-SEM was used to determine the size and characterise the synthesised SNW-1. Figure 4.1 shows that the SNW-1 particles are spherical in shape, and each particle has a size of approximately 35-50 nm, making it possible to be incorporated in both the membrane substrate and polyamide selective layers, which are approximately 150 μm and 150 nm thick, respectively. The small size of the particles also allows it to be easily dispersed homogeneously in a solution.

4.3.2 Mode of incorporation of SNW-1

One of the aims of this study is to determine the best way to incorporate the SNW-1 nanoparticles into the polyamide layer. The nanoparticles can be introduced onto the membrane selective layer through either one of the polyamide precursors. The MPD precursor is introduced onto the membrane surface through an aqueous solution, while TMC is dissolved in an organic solvent (i.e., heptane). SNW-1 both have hydrophilic (-NH) and hydrophobic groups (C=O and aromatic groups), that it is neither fully soluble in water nor in organic solvents, in fact it is stable in both and exhibited good dispersion.

The polyamide selective layer is formed from the reaction between the amine functional groups of MPD with the carbonyl carbon of acyl halide TMC (Qiu et al. 2009). Amines act as the nucleophile due to the presence of the lone electron pair on N (Brotzel, Chu & Mayr 2007), thus a nucleophilic attack on the carbonyl carbon occurs. The double bonds between C and O break, and the O atoms obtain a partially-negative charge, while N becomes partially positive due to the presence of four bonds on it. A proton is then transferred between N and O. The lone pair on the oxygen then forms the carbonyl C=O bond.

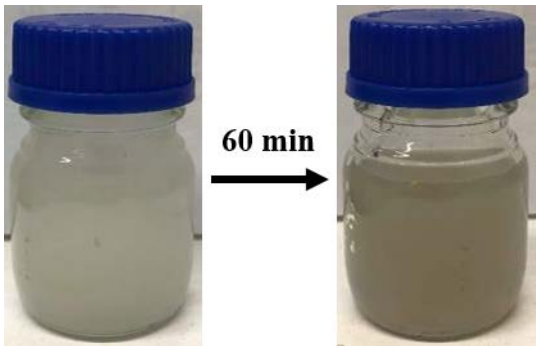

Figure 4.2 Observed change in solution colour of benzene-1,3,5-tricarbonyl chloride and SNW-1 after 60 min, indicating a reaction between the two substances

SNW-1 is known to contain secondary amine (-NH) groups, which are also able to react with acyl halides to form amides. Upon dispersion of the COF nanoparticles, a similar nucleophilic substitution reaction between amine and carbonyl groups occurs and forms amide, albeit slowly. The dispersion solution of SNW-1 and TMC in heptane was initially clear; however, the solution turned milky grey as time passed (shown in Figure 4.2), most likely due to the formation of amide from the reaction of SNW-1 and TMC.

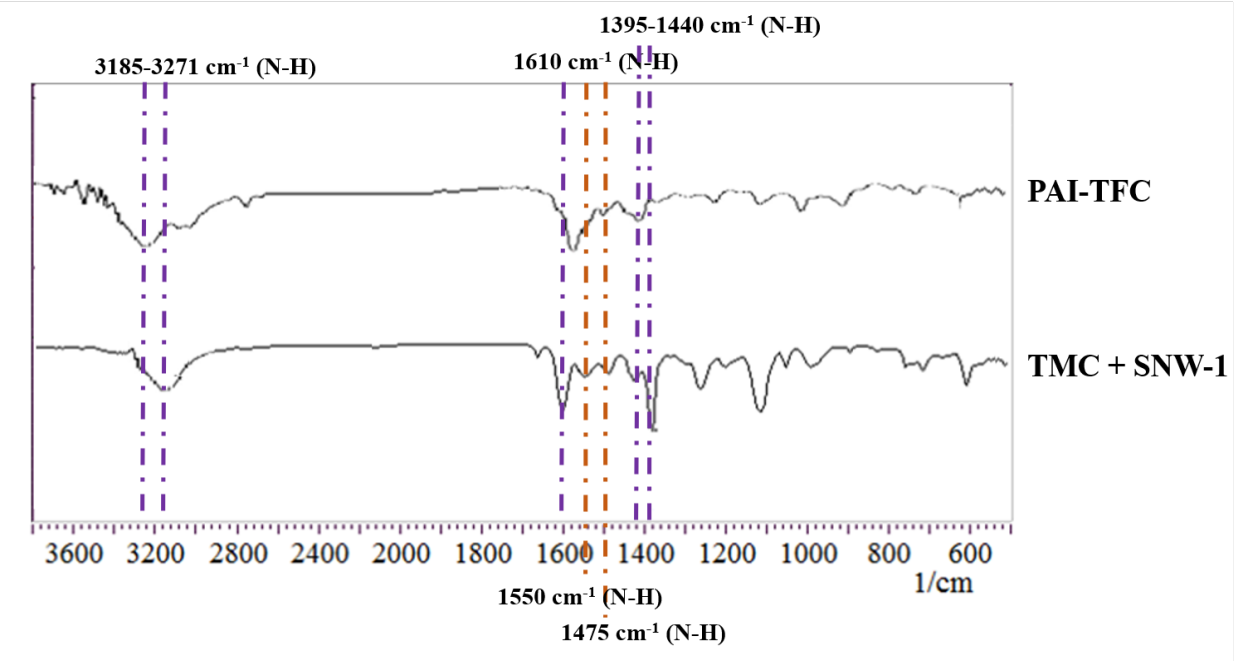

Figure 4.3 FTIR spectra of (a) TFC polyamide and (b) product formed after the reaction of SNW-1 and benzene-1,3,5-tricarbonyl chloride

To confirm the formation of amide, FTIR analysis was conducted on a membrane substrate wherein only the TMC solution with SNW-1 was contacted with the surface (sans MPD). The IR spectrum was then compared with that of a TFC membrane, whose

polyamide is formed from the reaction of MPD and TMC, and as shown in Figure 4.3, both exhibited similar peaks at 3185-3271 cm^{-1}, 1395-1440 cm^{-1}, and 1610 cm^{-1}, which all correspond to the presence of amide (Belfer, Purinson & Kedem 1998). This confirms that the reaction of TMC and SNW-1 is highly similar to the polyamide polymerisation reaction which occurs during IP.

While the SNW-1 COF nanomaterial is stable in both aqueous and organic phases, its reaction with TMC makes it not suitable to be incorporated through TMC during polyamide selective layer formation. The reaction between TMC and SNW-1 is similar to that of the polymerisation reaction during IP, due to SNW-1's secondary amine groups. Nucleophilic substitution of amine occurs at the carbonyl carbon of TMC, leading to the formation of amide groups. Mixing TMC and SNW-1 together will then effectively react in solution, decreasing the integrity of the TMC solution prior to formation of polyamide during IP. Therefore, MPD was chosen as the mode of incorporation of SNW-1 in PRO TFN membrane preparation.

4.3.3 TFC and TFN membrane characterisation

The surface chemical composition of the TFC and TFN membranes were characterised using FTIR spectroscopy; the spectra of the membrane surfaces are shown in Figure 4.4. The TFC membrane showed absorption peaks at 3271 cm^{-1}, 1440 cm^{-1} and 1610 cm^{-1}, which are indicative of the carbonyl group of an amide functional group, showing that polyamide formation via IP was successful. The peaks around 1440 cm^{-1} and 1610 cm^{-1} are likewise visible in the spectra of these membranes; however, the peak at 3271 cm^{-1} was not visible in the TFN membrane spectra, which show that the intensity

of the hydroxyl group peak decreased upon incorporation of SNW-1. This can be attributed to the electrostatic interactions that occurred between the polyamide precursors and the COF nanoparticles (Yang et al. 2016). Additional peaks at 1475 cm^{-1} and 1550 cm^{-1}, which are characteristic of the triazine group of SNW-1 (Wang et al. 2017), indicating that SNW-1 is incorporated into the polyamide layer.

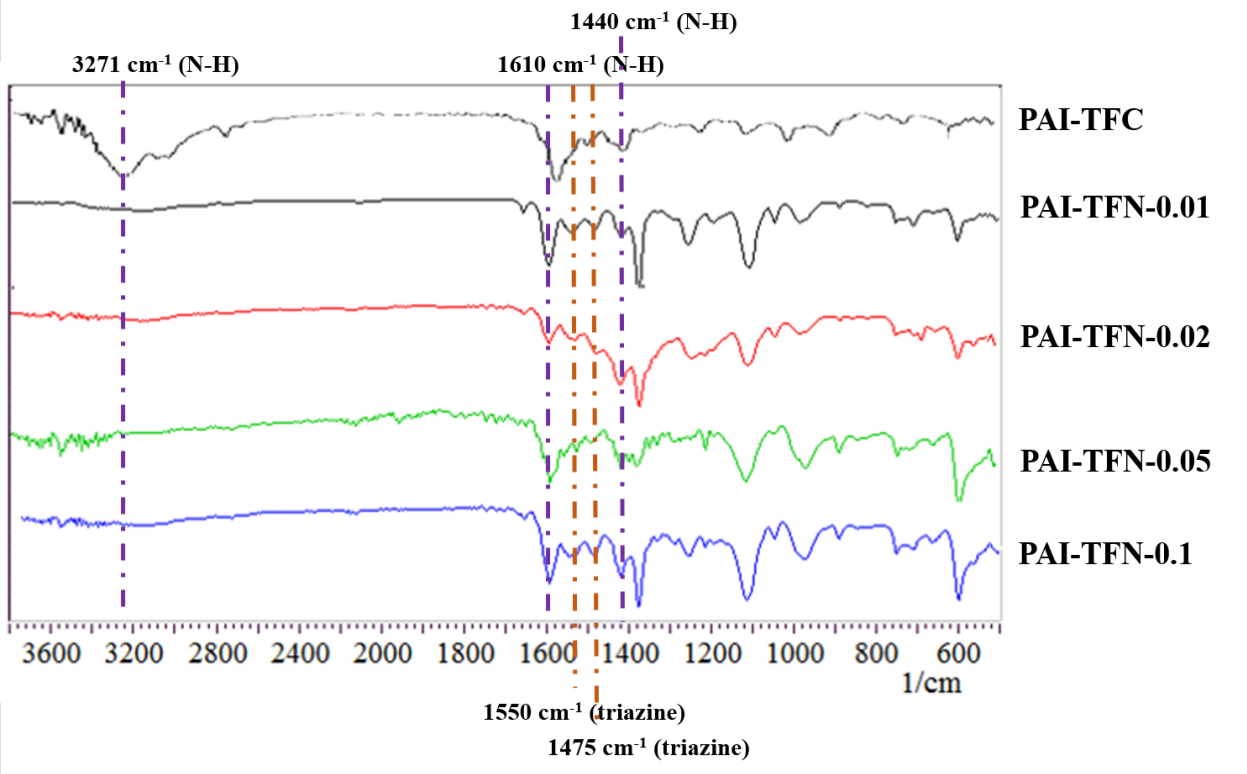

Figure 4.4 FTIR spectra of the TFC and SNW-1-incorporated TFN membranes

Aside from determination of the functional groups present in the membrane surfaces using FTIR spectroscopy, elemental analysis of membrane surface was also performed using XPS. XPS spectra of the TFC and TFN membranes are shown in Figure 4.5. To provide a simpler comparison, the TFN membranes with the lowest and highest SNW-1

loadings were chosen as the representative samples for XPS analysis. Chemical composition values of carbon, nitrogen, and oxygen, were shown in Table 4.1.

Table 4.1 Chemical composition of the TFC and SNW-1-incorporated TFN membrane surfaces

Membrane	C (%)	N (%)	O (%)	Others (%)
TFC	71.83	9.59	17.88	0.70
TFN-0.01	73.68	11.31	14.55	0.46
TFN-0.1	72.72	14.04	12.70	0.54

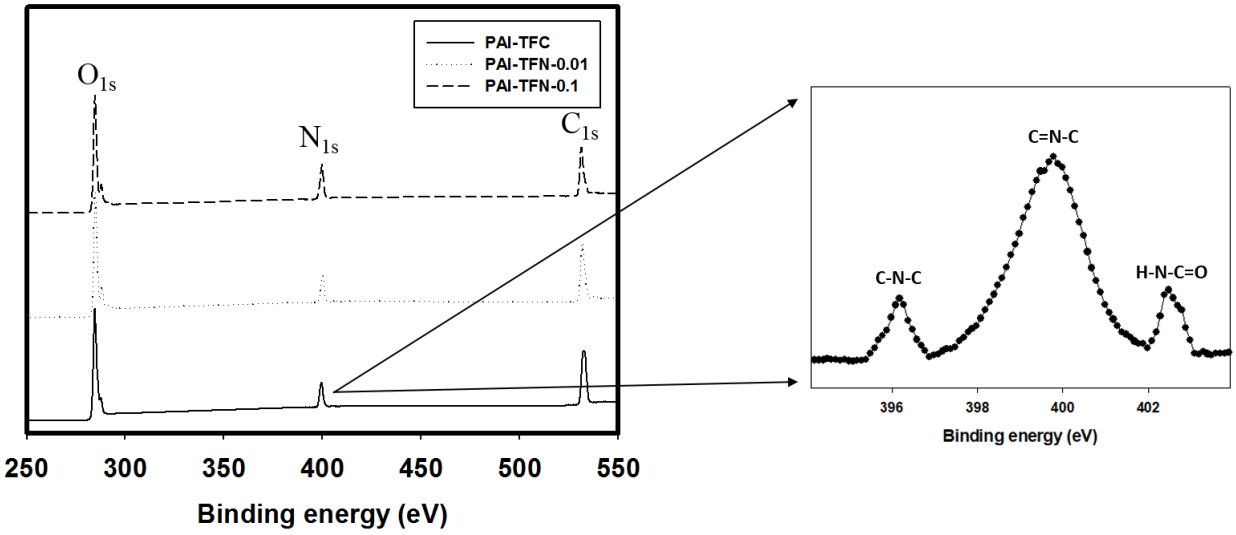

Figure 4.5 XPS spectra of the TFC and SNW-1-incorporated TFN membranes

The XPS results indicate that nitrogen content further increased with the presence of the SNW-1 COF nanoparticles, with TFN-0.1 having the highest % N (14.04%), confirming the successful incorporation of SNW-1 in the polyamide selective layer. Figure 4.5 also shows the resolved N1s peak of the TFN membrane. The TFN membrane exhibits peaks at 396.18 and 402.48 eV binding energies, corresponding to C-N-C and H-N-C=O, which both correspond to the groups found in polyamide. A peak at 399.78 eV,

that corresponds to C=N-C present in the triazine structure of SNW-1 (Wang et al. 2017), is also found, indicating the presence of SNW-1 in the TFN membrane.

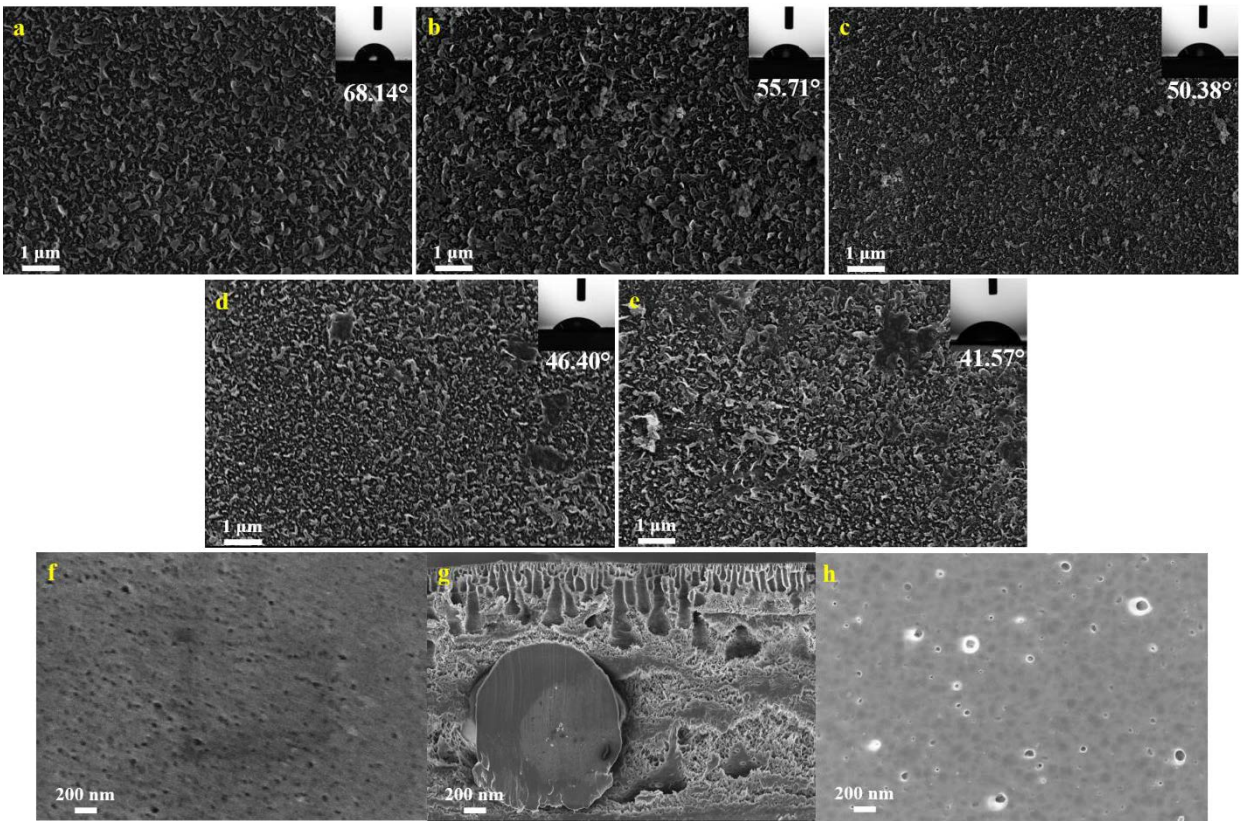

Figure 4.6 Surface morphologies of the (a) TFC, (b) TFN-0.01, (c) TFN-0.02, (d) TFN-0.05, (e) TFN-0.01 PRO, (f) substrate top surface, (g) substrate cross section, and (h) substrate bottom surface membranes, respectively, taken through FE-SEM imaging; Contact angle measurements of each membrane were also included inset

The membrane surface and cross-section morphology were analysed using FE-SEM, as shown in Figure 4.6. Polyamide, typically characterised by ridge and valley structures, was formed on top of the PAI substrate (Chou et al. 2012a). This signifies that since the SNW-1 nanoparticles are incorporated with the TMC solution, the particles remained mostly on the surface, and not embedded in the polyamide layer. This change

in morphology of the polyamide layers of the TFN membranes may play a major role in modifying other properties of the membranes, i.e. porosity, roughness, hydrophilicity, water permeability, and selectivity. The top and bottom surface, as well as cross-section, SEM images show that the TFC and TFN membranes exhibit a mixture of sponge-like and finger-like porous structures.

One of the direct effects of incorporation of SNW-1 on the polyamide layer is the enhanced surface hydrophilicity and affinity to water. Furthermore, enhanced surface hydrophilicity is integral in the improvement of water flux of PRO membranes (Bui & McCutcheon 2014). To be able to evaluate surface hydrophilicity of the membranes, static water contact angle was measured. However, contact angle is not only a function of hydrophilicity, but also surface smoothness (Park et al. 2015), wherein smoother surfaces normally have lower contact angles. As seen from Figure 4.6, the water contact angle measurements at the membrane surface were observed to decrease slightly as the nanomaterial loading increased. Polyamide has both hydrophobic carbonyl (C=O) and hydrophilic N-H groups, making the TFC membrane selective layer exhibit properties of both. Upon incorporation of SNW-1, the amine groups of SNW-1 further react with TMC and form amide groups, resulting the membranes to exhibit low hydration energy and have more affinity with water. Incorporation of the porous and hydrophilic SNW-1 would have definitely improved the overall hydrophilicity of the membranes; however, the contact angle differences were not significantly high. This is because incorporation of the nanomaterials also resulted in increased surface roughness as most nanoparticles are exposed to the surface of PA layer (Liu et al. 2018). Overall, there were considerable improvements observed in hydrophilicity in the membranes after the selective polyamide

selective layer formation on the PAI substrate and the subsequent incorporation of nanomaterials. The relative hydrophobicity and low surface energy of PAI caused the high contact angle measurement observed for the substrate (Park et al. 2018). The observed increase in the surface hydrophilicity after incorporation of SNW-1 is due to the presence of the secondary amine functional groups (-NH) left unreacted with TMC (Wang et al. 2017).

Membrane surface roughness was characterised by AFM analysis. Figure 4.7 shows the three-dimensional AFM images of the membrane surfaces for the TFC and TFN samples. The mean roughness (R_a, nm) and root mean square ridge elevation (R_{ms}, nm) are also presented. The R_a and the R_{ms} of 8.16 nm and 10.4 nm, respectively, were observed for the TFC membrane. The R_a values were seen to increase as the loading of the nanomaterial increased. It is also noteworthy that the TFN-T membranes exhibited higher surface roughness than their TFN-M counterparts, as seen by the AFM images which show agglomeration of the COF nanoparticles, hereby increasing the overall roughness.

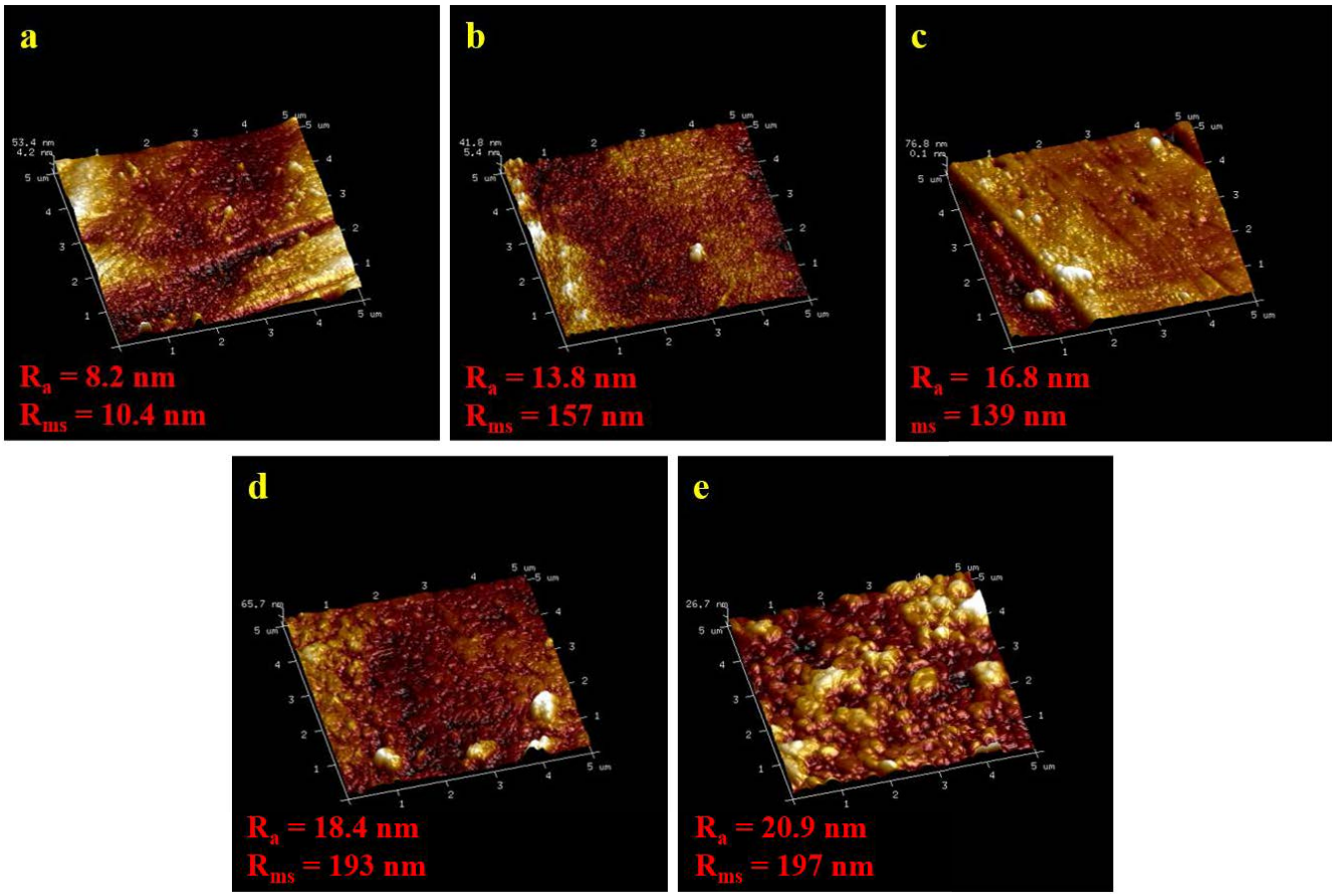

Figure 4.7 Surface roughness of TFC and TFN membranes obtained by atomic force microscopy (AFM) analysis of (a) TFC, (b) TFN-0.01, (c) TFN-0.02, (d) TFN-0.05, and (e) TFN-0.1 PRO membranes

4.3.4 Membrane intrinsic transport properties

PWP, as shown in Table 4.2**,** increased with SNW-1 loading, regardless whether COF material was introduced through MPD or TMC. This is highly consistent with the enhanced surface hydrophilicity observed earlier. Incorporation of a porous and highly-hydrophilic material, such as SNW-1, facilitates passage of water molecules through the composite membrane. Furthermore, similar to other TFN membranes in which nanoparticles are incorporated through the polyamide layer, the interface between the nanoparticles and the polymer also provides additional passageway for water to pass

through (Wang et al. 2017; Yin et al. 2012). As expected, the high porosity of the nanoparticles does not only allow the passage of water molecules, but solute particle passage as well. This resulted in a significant increase in B (solute permeability coefficient) of the TFN membranes as compared to the TFC. Furthermore, enhancement of membrane hydrophilicity brought about by SNW-1 incorporation significantly decreased the structural parameter *S* (Arena et al. 2011; Lim et al. 2017; Park et al. 2018; Park et al. 2015).

Table 4.2 Intrinsic transport properties of TFC and COF-incorporated TFN membranes

Membrane	***A*** **(L m^{-2} h^{-1} bar^{-1})**	***B*** **(L m^{-2} h^{-1})**	***B/A*** **(bar)**	**R (%)**	***S*** **(μm)**
TFC	1.72	0.45	0.26	96.3	430
TFN-0.01	2.71	0.82	0.30	95.7	340
TFN-0.02	3.23	1.20	0.38	94.7	280
TFN-0.05	3.72	1.59	0.43	94.0	240
TFN-0.1	3.87	1.83	0.47	93.4	240
Toray PRO TFC	1.23	0.39	0.32	96.2	410

In comparison with the commercial PRO TFC membrane from Toray Chemicals, all the membranes prepared in this study showed better PWP. However, the commercial membrane exhibited better selectivity compared to the TFN membranes due to SNW-1, which did not just improve water permeability, but also reverse salt permeability.

4.3.5 PRO membrane performance

The PRO performance of the TFC and TFN membranes were evaluated by J_w, J_s/J_w, and *W*, all of which are shown in Figures 4.8 and 4.9. The tests were performed using DI water and 1.0 M NaCl as feed and draw, respectively. As indicated by the PWP values,

water flux of the membranes improved significantly upon incorporation of the SNW-1 nanoparticles. Increasing the loading of SNW-1 allows the creation of more water-selective channels. This shows that enhancement of the membrane hydrophilicity would lead to enhanced membrane wetting and water transport (Liu, Li, et al. 2016). This confirms that hydrophilicity plays a significant role in the enhancing the water flux and PRO membrane performance. Furthermore, SNW-1 has an ability to adsorb water molecules due to the H-bonding occurring between SNW-1's –NH functional groups and O-H of water (Yang et al. 2016). The enhanced hydrophilicity and selectivity of SNW-1 towards water molecule further enhance water continuity and transfer of water molecules across the membrane.

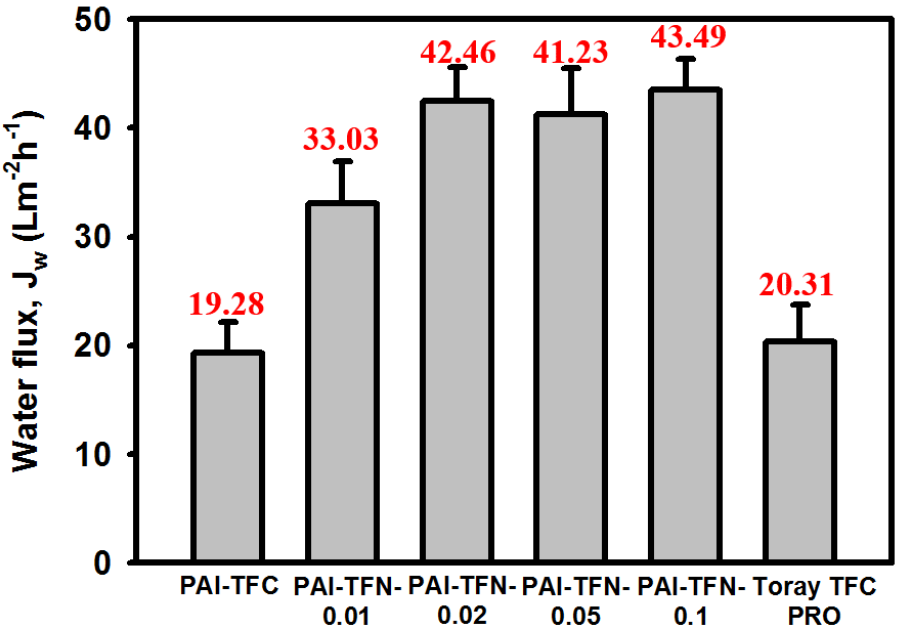

Figure 4.8 Water flux (J_w) of the TFC and TFN PRO membranes in comparison with Toray TFC PRO membrane at 0 bar hydraulic pressure. (Feed solution: DI water; Draw solution: 1.0 M NaCl; Flow rate: 200 mL min-1)

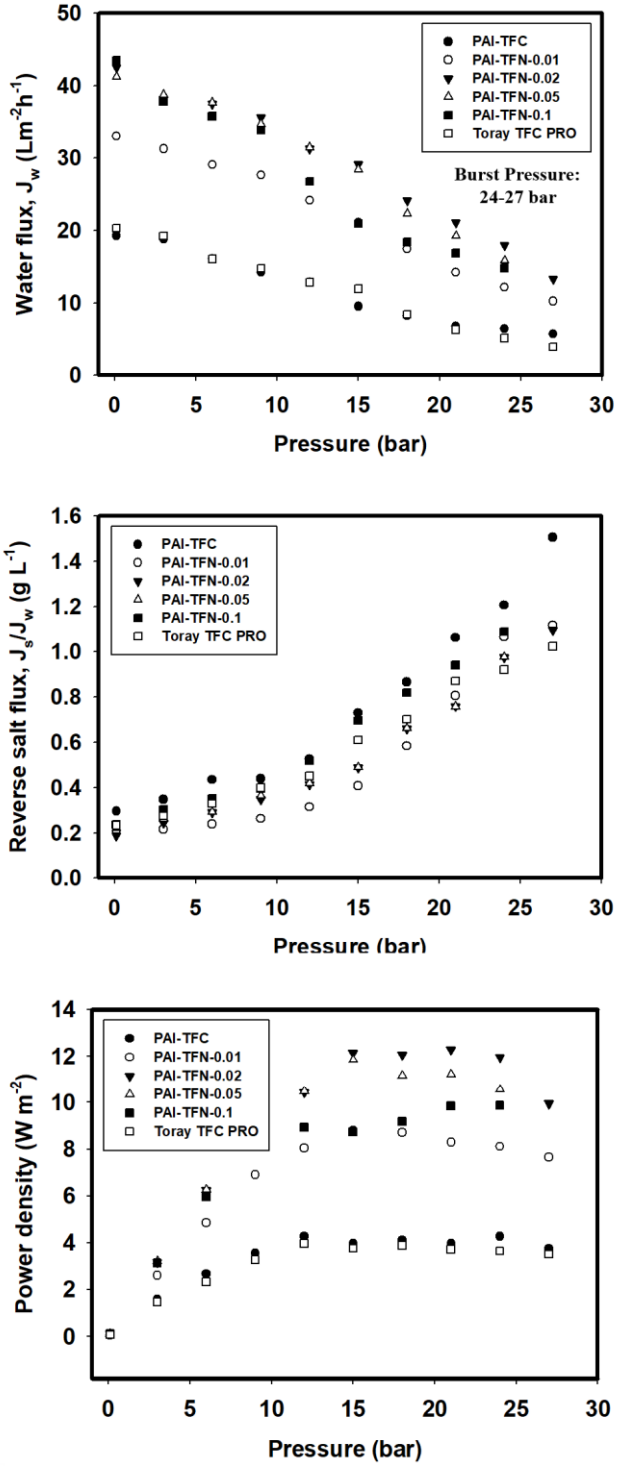

Figure 4.9 Water flux (J_w), reverse salt flux (J_s), and power density of the membranes at various hydraulic pressures. (Feed solution: DI water; Draw solution: 1.0 M NaCl; Flow rate: 200 mL min^{-1})

As mentioned earlier, the pores of SNW-1 have a major pore size of 5Å, which is significantly larger than the size of the water molecule (3Å), thus it can easily allow water to pass through. Incorporation of SNW-1 in the dense polyamide layer simply provides free channels for water to pass through despite the dense property of polyamide. Furthermore, not only does the internal core of SNW-1 provide nanochannels for water transport, but also the gap between the interface of the nanomaterial and the polyamide allowed water transport to occur (Li, Zhao, Tian, et al. 2018). The enhanced fractional free volume due to the porous nanomaterials increases the membrane permeability. Although this can also undermine the membrane selectivity however, the size of the pores and the molecules, as well as the selectivity of SNW-1 towards water, take part in limiting reverse salt diffusion through the membranes (Yang et al. 2016). The sieving property of the nanomaterial also comes into play, such that once water molecules have penetrated through the micro-sized pores of the COF material, no other molecule is able to penetrate further. Had the nanomaterial loading been increased further, aggregation of the particles may occur, which can lead to decreased permeability, due to blockage.

The water flux of the membranes was observed to decrease as the applied hydraulic pressures increased and it was a function of membrane compaction (Han & Chung 2014), as shown in Figure 4.9. The compaction caused an increased effective membrane area resulted from stretching and thinning of the membrane polyamide selective layer (Choi, Vigneswaran & Lee 2016). The gradual decrease of water flux suddenly became a rapid increase at a point when the membranes have already sustained enough irreversible defects and damage, this point is known as the burst pressure. The highest J_w at ΔP = 0 bar was observed for TFN-0.1 (43.5 L m^{-2} h^{-1}), incorporated with 0.1 wt% SNW-1, marking

a significant improvement as compared to water flux of TFC (19.3 L m^{-2} h^{-1}). Even addition of 0.01 wt% of the COF increased the water flux to 33.0 L m^{-2} h^{-1} for TFN-0.01. It is, however, noticeable that the water flux did not follow a linear trend as SNW-1 loading increased, instead, a hyperbolic trend was observed. This is influenced by the membrane surface roughness, which offsets the enhanced hydrophilicity of the membranes. Moreover, the water fluxes of all TFN membranes with loading of at least 0.02 wt% SNW-1 are similar to each other. Thus, it can be suggested that 0.02 wt% is the optimum SNW-1 loading for future studies.

On the other hand, J_s/J_w of TFC-PRO membranes at ΔP=0 bar was observed to increase as both SNW-1 loading and applied hydraulic pressure increase. These trends are consistent with the intrinsic properties of those TFC membranes from *A* and *B* values presented in Table 4.2. The results indicate that enhancement of hydrophilicity and porosity significantly enhanced both water and solute diffusivity. As hydraulic pressure increases, the membranes are subject to being damaged, which would cause more water and solute molecules to pass through.

The robustness of the membranes is evaluated by the burst pressure, or the pressure at which the membranes sustain damage. At this pressure, water and solute simply pass through the membrane. It is important to determine the burst pressure of membranes, especially for long-term PRO operation (Chen et al. 2016). The membranes showed to have a burst pressure of 27 bar, except for TFN-0.05 and TFN-0.1, which burst at 24 bar. It is suggested that in future studies involving SNW-1-incorporated TFN membranes, pre-stabilisation of the membranes at a pressure lower than the burst pressure must be performed prior to PRO operation to enhance the PRO performance of

the membranes (Gai et al. 2016). Furthermore, these results also indicate that higher loading of the SNW-1 nanomaterial can lead to instability of the membranes when operated for PRO at higher pressures, and 0.02 wt% of SNW-1 is the optimal loading at which the membranes can be operated at 27 bar. In the PRO process, a straightforward evaluation of membrane performance can be correlated with the power density (W m^{-2}). From Figure 4.9, the maximum power density of 12.1 W m^{-2} at the pressure of 20 bar was achieved with TFN-M2, much higher than that obtained with the TFC membrane which was 4.28 W m^{-2}.

4.4 Conclusions

Novel PET open mesh fabric-reinforced SNW-1 COF-incorporated TFN PRO membranes were fabricated in this study. The mode of incorporation of SNW-1 was also investigated using two different precursors of the interfacial polymerization process. The following conclusions were drawn from this study:

1. Incorporation of the porous and hydrophilic nanomaterial resulted in significant enhancement of the surface hydrophilicity and water flux of the TFN membranes, due to the hydrophilic secondary amine functional groups of SNW-1;
2. The hydrophilicity and porosity of the nanomaterial facilitated the water transport across the membranes, while maintaining satisfactory salt rejection ability;
3. SNW-1 cannot be incorporated through TMC due to the reaction between the two, which is highly similar to that of polyamide formation;
4. Maximum PWP was 3.87 $Lm^{-2}h^{-1}bar^{-1}$ for the membrane with 0.1 wt% SNW-1 incorporated through the MPD solution;

5. 0.02 wt% was considered to be the optimum loading of the nanomaterial, beyond which the loading affects the stability of the membrane at higher applied pressures; and
6. The highest water flux and power density for the membrane incorporated with 0.02 wt% SNW-1 through MPD were 42.5 $Lm^{-2}h^{-1}$ and 12.1 Wm^{-2} (at 20 bar), respectively.

These results indicate that the incorporation of a porous and hydrophilic COF nanomaterial such as SNW-1 is a promising method to fabricate high performance TFN PRO membranes.

5 Enhanced water permeability and osmotic power generation with sulfonate-functionalised porous polymer-incorporated thin film nanocomposite membranes

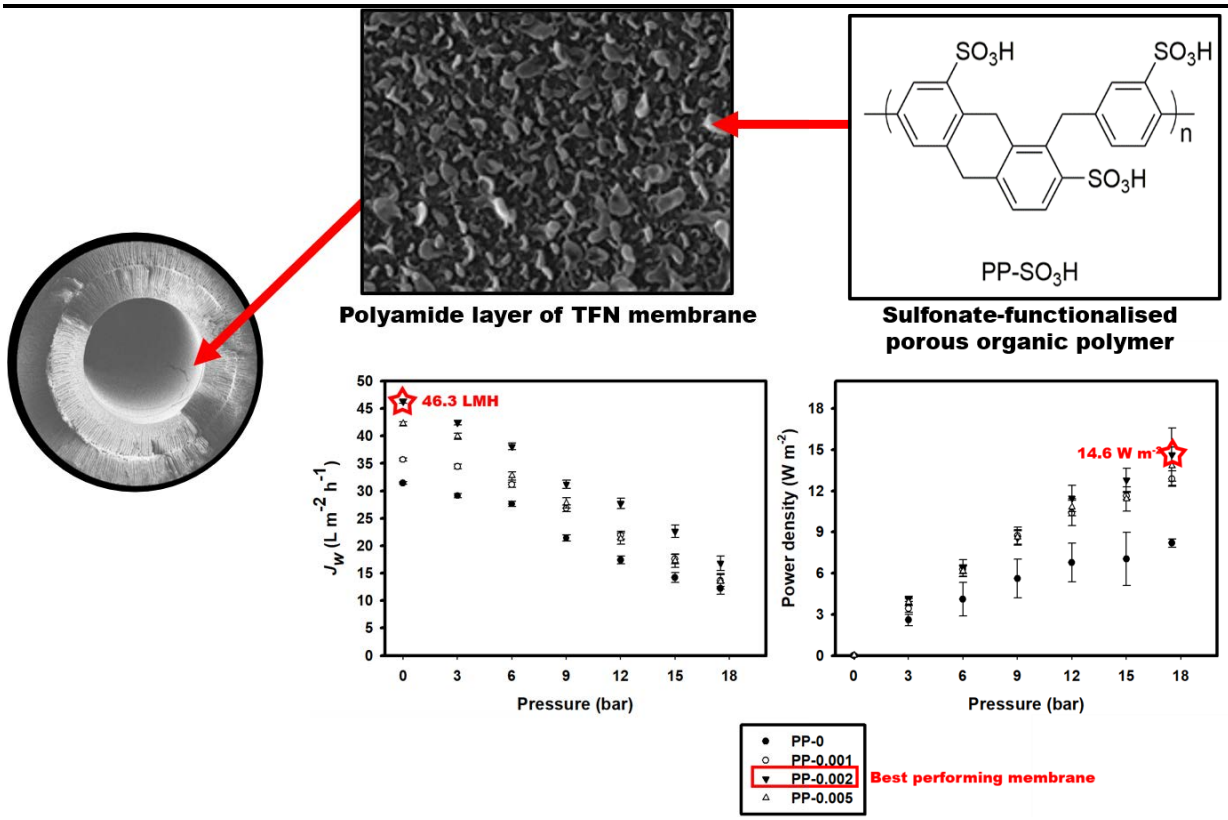

Following the successful incorporation of a highly porous and hydrophilic nanomaterial in the polyamide selective layer of TFC PRO membrane as described from the previous technical chapter, this chapter describes the surface functionalisation of the TFC PRO membrane surface after incorporation of a functionalised porous organic polymer. This chapter was published in *Desalination*:

Gonzales, R.R., Yang, Y., Park, M.J., Bae, T.-H., Abdel-Wahab, A., Phuntsho, S. & Shon, H.K. 2020. 'Enhanced water permeability and osmotic power generation with sulfonate functionalised porous polymer-incorporated thin film nanocomposite membranes', *Desalination*, vol. 496, pp. 114756-114765.

5.1 Introduction

There has been an increase recently in the demand for new sustainable renewable energy sources due to the impending depletion of fossil fuels and their adverse contribution to global warming and subsequent climate change. The interest in sustainable renewable energy leads to the development and continuous research on alternative sources like solar, wind, biomass, geothermal sources, and osmotic energy (Gonzales, Kim & Kim 2019; Straub, Deshmukh & Elimelech 2015; Volpin et al. 2018). Osmotic energy is one such potential energy source that can be generated from the Gibbs free energy of mixing solutions (Straub, Deshmukh & Elimelech 2015). Furthermore, industrialisation and the exponential increase of the world's population do not only increase the demand for energy, there is also an increased demand for clean, fresh water (Kim, Gonzales, et al. 2020).

PRO is a process known to have a great potential in renewable energy harvesting by utilising the concentration and/or osmotic pressure difference between two streams of varying salinity, where water from the low-concentrated feed solution passes through a dense selective membrane towards the direction of the higher-concentrated DS by natural osmosis. While largely similar to the FO process, hydraulic pressure is applied against the osmotic pressure direction in the PRO process, and while slightly retarding the movement of water towards the DS. The spontaneous mixing of the two streams of different salinity leads to the production of free energy of mixing which is then converted into mechanical energy as it passes through a hydro-turbine which then generates electrical energy (Klaysom et al. 2013). Not only can PRO augment the world's need for alternative energy sources, PRO, as an osmotic process, can also be applied for

desalination or wastewater reuse, which both can provide solutions to the world's water crisis.

Lack of a suitable semi-permeable membranes solely for PRO process is one of the major challenges in the commercialisation of the PRO technology. Ideal PRO membranes must possess the following properties: high hydrophilicity and porosity to facilitate water flux, high selectivity, low structural parameter, and satisfactory mechanical strength to resist hydraulic pressure throughout PRO operation (Zhang, Sukitpaneenit & Chung 2014). Typical PRO membranes are made up of a TFC membranes consisting of a highly porous membrane support layer prepared by polymer NIPS method and a dense thin film selective layer formed by polymerisation reaction on the interface of the membrane support (Chou et al. 2012b; Yip et al. 2011). While significant progresses have been achieved on PRO membrane development in recent times (Han, Zhang, et al. 2015), membrane performance remains limited by issues, such as membrane fouling and ICP. In the PRO process, ICP refers to the concentration increase of the less concentrated feed within the membrane support layer structure. ICP occurs due to the asymmetric nature of TFC membranes wherein the membrane selective layer faces the DS in the PRO process. Thicker and denser membrane support layer exacerbates ICP effects thereby hindering water flux during PRO operation. Hence the occurrence of ICP is a huge impediment in osmotic performance of TFC membranes because of which a number of studies have focused on ICP mitigation for osmotic membrane development (Huang, Arena, et al. 2016; Song, Liu & Sun 2013).

A relatively new approach in membrane development is the incorporation of nanomaterials, which can enhance the porosity, permeability, and reactivity of the

membranes. These nanomaterials may be either dispersed and immobilised in the membrane support or the selective layer, and form either a MMM or a TFN membrane, and may serve to modify the morphology and other properties of the membrane (Amini, Jahanshani & Rahimpour 2013; Choi, Son & Choi 2017; Wang, Song, et al. 2015). Some of the nanomaterials in previous membrane development studies include carbon nanotubes (Amini, Jahanshani & Rahimpour 2013; Deng et al. 2020; Song et al. 2015), silica (Tian et al. 2017), titanium dioxide (Ghanbari et al. 2015), titania nanosheets (Ahmad et al. 2020), silver (Liu et al. 2013), graphene oxide (Hegab et al. 2015; Kang et al. 2019; Soroush et al. 2016), and metal organic frameworks (Kadhom, Hu & Deng 2017; Ma et al. 2017). Recently, a new class of nano-sized materials known as porous organic polymers (POPs) has gained interest for various applications (Kitagawa, Kitaura & Noro 2004). POPs are porous framework molecules but are only composed of covalently-bonded organic functional groups containing H, C, N, and O, which are considered light elements (Zou et al. 2017).

Compared to other nanomaterials, POPs exhibit outstanding porosity as well as thermal and chemical stability. Moreover, the hydrophilicity, which is a critical surface property for improving water permeability of a membrane, can be readily improved by either post- or pre-synthetic sulfonate functionalisation (Chandra et al. 2016; Lu et al. 2011). All these imply that POPs can be good candidates for the fabrication of high performance TFN membrane featuring high water permeability with an excellent stability. To this end, herein, a specific porous polymer (denoted as PP) reported in our previous work has been synthesised, sulfonated and then incorporated into a TFN membrane to

develop a PRO membrane with outstanding osmotic performance (Yang, Chuah, et al. 2019).

The PP can be facilely prepared from commercially-available monomer *α,α'*-dichloro-*p*-xylene (*p*-DCX) via a one-pot *Friedel-Crafts* alkylation reaction catalysed by inexpensive $FeCl_3$. PP, which has a high porosity and a robust hydrocarbon structure, can be functionalised by a post-synthetic sulfonation reaction while maintaining the structural integrity. It is noteworthy that, to the best of the authors' knowledge, PP-SO_3H has never been explored as a filler for any TFN membrane. In this study, the PP-SO_3H was incorporated into the selective polyamide layer of an inner-selective TFC hollow fibre PRO membrane. The properties of the PP-SO_3H-incorporated inner-selective TFN hollow fibre PRO membranes and their PRO process performances were evaluated in terms of the nanomaterial loading rates.

5.2 Experimental

5.2.1 Materials

1,4-bis(chloromethyl)benzene (*α,α'*-dichloro-*p*-xylene, *p*-DCX, Sigma Aldrich, Singapore), ferric chloride ($FeCl_3$, anhydrous, Sigma Aldrich, Singapore), 1,2-dichloroethane (DCE, Sigma Aldrich, Singapore), chlorosulfonic acid (Tokyo Chemical Industry Co., Ltd., Singapore), methanol (MeOH, VWR Chemicals, Singapore), dichloromethane (DCM, VWR Chemicals, Singapore), and THF (VWR Chemicals, Singapore) were used for the synthesis of PP-SO_3H.

5.2.2 Synthesis of PP

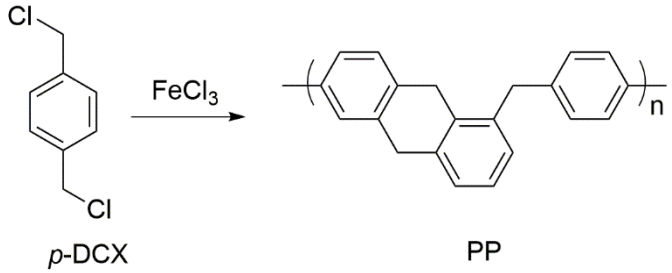

Figure 5.1 Self-polymerisation of p-DCX to synthesise PP

Synthesis of PP was first performed according to a method (Figure 5.1) reported previously (Yang, Chuah, et al. 2019). 3.50 g *p*-DCX was mixed in 130 mL DCE to form 20.0 mmol *p*-DCX solution. Anhydrous $FeCl_3$ (3.24 g, 20.0 mmol) was added in the mixture under nitrogen atmosphere. The mixture was placed in vigorous stirring conditions for 1 h at 45°C and 2 h at 80°C. The brown-coloured precipitate formed during the reaction was afterwards filtered and thoroughly washed with MeOH and THF alternately until a clear filtrate could be obtained. The PP precipitate was then placed in a vacuum oven at 60°C for 1 d for drying.

5.2.3 Sulfonate-functionalisation of PP

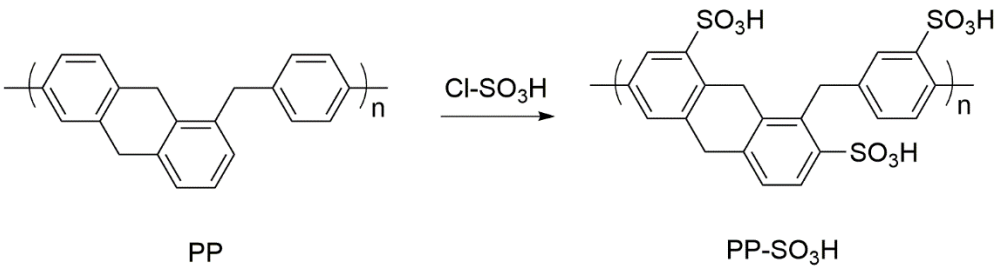

Figure 5.2 Functionalisation of PP with chlorosulfonic acid to synthesise PP-SO_3H

The PP underwent functionalisation modification with an excess amount of chlorosulfonic acid, following a modified method in literature (Figure 5.2) (Li, Wang, Chen, et al. 2015). 3.0 g of the PP solid was placed with 60 mL DCM in a thoroughly dried flask fitted with a condenser under nitrogen atmosphere. The mixture was stirred until the solution was homogeneous. A mixture containing 20 mL chlorosulfonic acid in 60 mL DCM was added dropwise into the flask at 0°C, after which, the solution was vigorously mixed at room temperature (25°C) for 24 h. The resultant product was collected by vacuum filtration and rinsed thoroughly with DCM and MeOH. The PP-SO_3H solid was afterwards dried at 80°C for 1 d.

5.2.4 PP-SO_3H characterisation

FESEM and FTIR were used to characterise the synthesised PP-SO_3H nanomaterial. N_2 physisorption studies were performed at 77 K using an Autosorb-6B instrument (Quantachrome, Anton-Paar, Singapore) to determine the surface areas and pore volumes.

5.2.5 Interfacial polymerisation and PP-SO3H incorporation

The selective polyamide layer was formed on the lumen side of the PES hollow fibre substrate through IP. Various loading rates (from 0 to 0.005 wt%) of PP-SO_3H were dispersed in DI water, to prepare PP-SO_3H-incorporated aqueous 2 wt% MPD solution. The membrane substrates were first soaked in 2 wt% MPD aqueous solution for 2 min and then in 1.5 wt% TMC solution in heptane solution for 1 min. The excess TMC solution

was drained and the membranes were dried in air for 3 min and oven-dried at 90°C for another 3 min. The prepared membranes were placed in DI water until tested.

5.3 Results and Discussion

5.3.1 PP-SO_3H characterisation

PP obtained by *Friedel-Crafts* alkylation of DCX was then converted into a sulfonated nanomaterial through a post-synthesis functionalisation with chlorosulfonic acid to synthesise PP-SO_3H. Figure 5.3 shows the morphology of the synthesised PP-SO_3H. The spherically shaped PP-SO_3H each has a size of approximately 90-100 nm; thus, it is suitable for incorporation within the polyamide selective layer, which typically has a thickness of 150 nm.

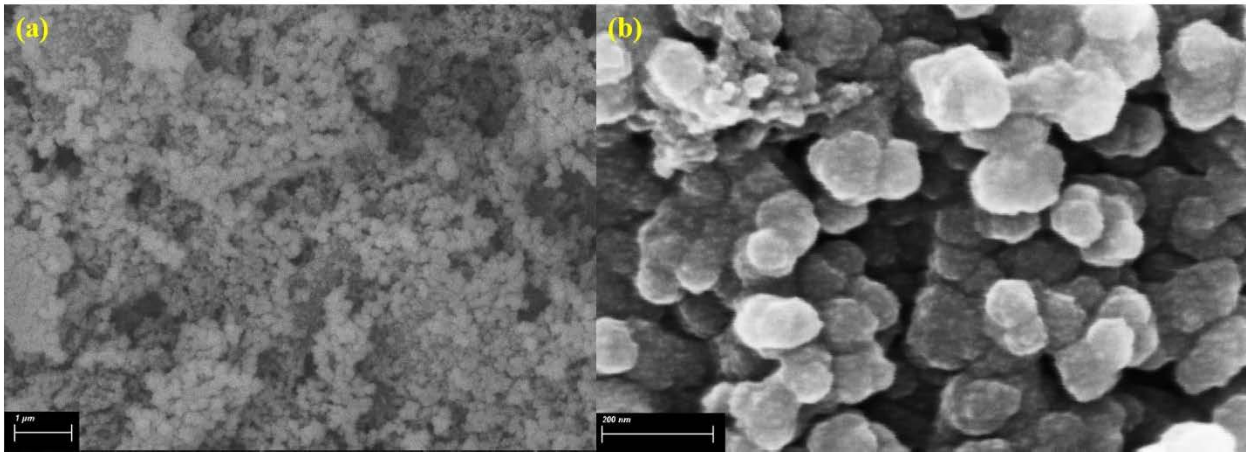

Figure 5.3 FESEM images of PP-SO_3H at two different magnifications

The FTIR spectrum of PP-SO_3H is shown in Figure 5.4. A –CH stretching at 2920 cm^{-1} and a sharp peak between 1600 and 1500 cm^{-1} were observed, corresponding to the saturated –CH2– and –C=C– groups, respectively. The stretching vibrations

appearing between 1050 and 1040 cm^{-1} are assigned to O=S=O, indicating the successful introduction of sulfonate groups. The surface area and pore volume values calculated from the N_2 physisorption studies at 77 K, tabulated in Table 5.1, show the microporous and mesoporous characteristic of PP-SO_3H.

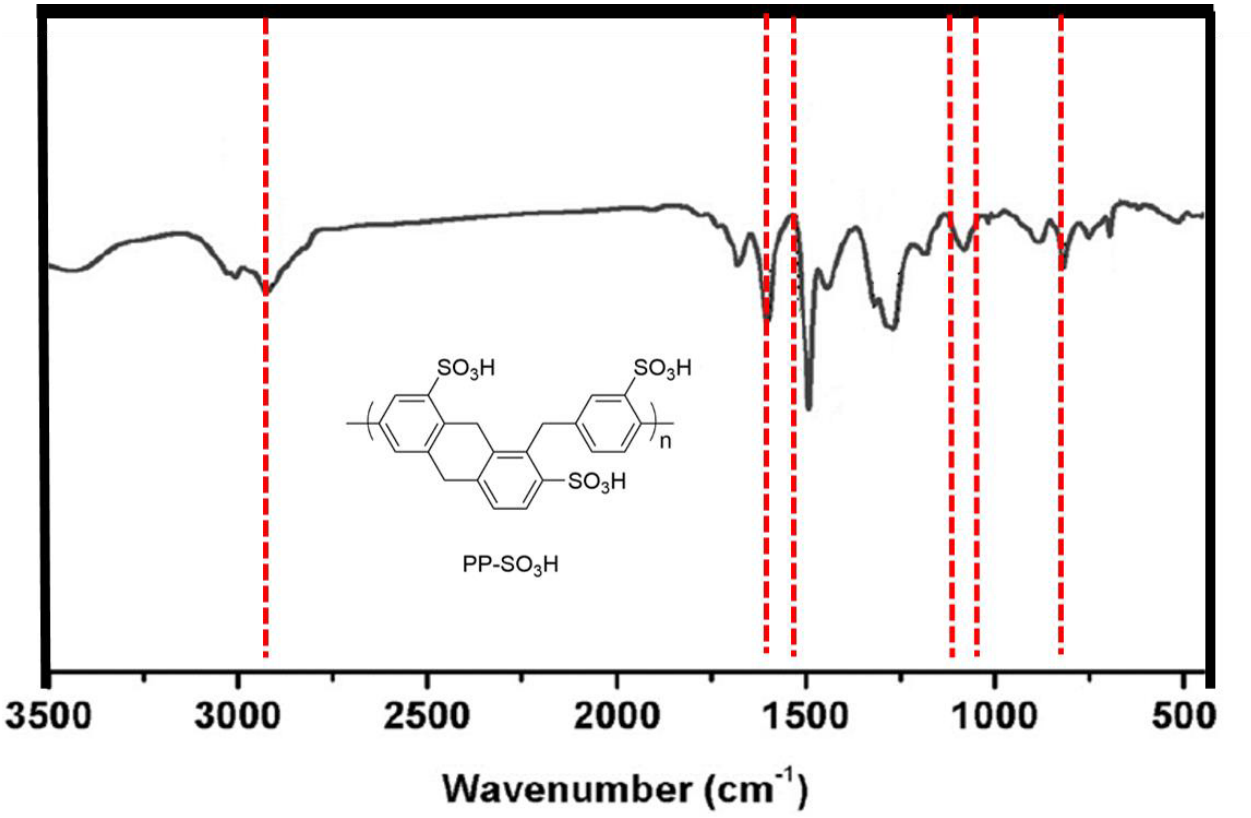

Figure 5.4 The FTIR spectrum of the synthesised PP-SO_3H, after the sulfonate functionalisation of PP; Chemical structure of PP-SO_3H is also shown inset

Table 5.1 The surface area and pore volume values of PP-SO_3H

Parameter	S_{BET}[a]	S_{micro}[b]	V_{micro}[c]	V_{total}[d]
	1090 m^2 g^{-1}	680 m^2 g^{-1}	0.313 cm^3 g^{-1}	1.481 cm^3 g^{-1}

[a] Surface area determined over the relative pressure (P/P^0) range of 0.05-0.2 using Brunauer-Emmett-Teller method.
[b] Microporous surface area and pore volume determined over P/P^0 range of 0.4-0.6 using *t*-plot method analysis for micropores.
[c] Total pore volume determined at P/P^0 of 0.99.

5.3.2 Membrane characterisation

The surface of the membranes was characterised using FTIR spectroscopy to determine the effect of incorporation of PP-SO_3H on the surface chemistry. As shown in Figure 5.5, FTIR spectrum suggests the presence of the polyamide selective layer on all the TFC (PP-0) and TFN (PP-0.001, PP-0.002, and PP-0.005) membranes. The carbonyl C–N group of the polyamide was evident for all the membrane samples, due to the presence of stretching at 1615 cm^{-1}, as well as the vibrations around 1440 cm^{-1}. Vibrations between 1600 and 1450 cm^{-1} indicate the unsaturated –C=C– and $–CH_2$ groups. The TFN membranes were observed to exhibit the O=S=O stretching vibrations between 1050 and 1040 cm^{-1}, indicating the presence of the sulfonate-functionalised PP-SO_3H. FTIR spectroscopy was able to show the successful incorporation of PP-SO_3H in the TFN PRO membranes.

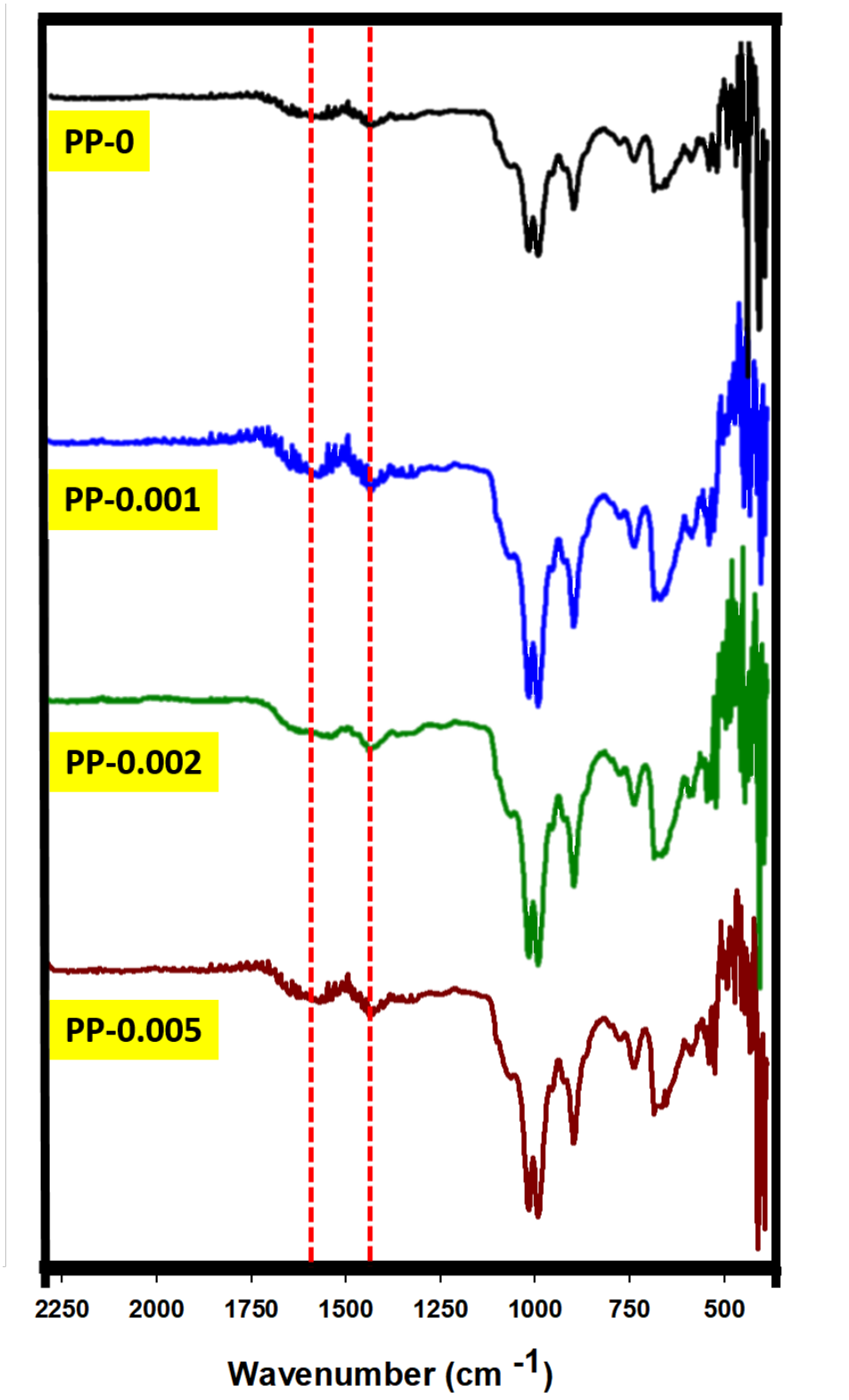

Figure 5.5 FTIR spectra of the TFC (PP-0) and TFN (PP-0.001, PP-0.002, and PP-0.005) PRO membranes

Table 5.2 Properties of the hollow fibre membrane substrate

Property	
Inner diameter (μm)	647 ± 15
Outer diameter (μm)	1309 ± 148
Thickness (μm)	324 ± 12
Elongation at break (%)	48.2 ± 2.3
Tensile strength (mPa)	5.8 ± 0.4
Pure water permeability (L m^{-2} h^{-1} bar^{-1})	319 ± 34
Porosity (%)	68.2 ± 2.3
Mean pore diameter, μ_p (nm)	7.2
Geometric standard deviation, σ_p	1.1

The morphologies of the lumen (inner surface), shell (outer surface), and cross-section of the hollow fibre membrane substrates were characterised using FESEM, and are shown in Figure 5.6. Using the FESEM images, the average thickness, total diameter, and inner diameter of the spun hollow fibre substrates were determined to be 324 ± 12, 1309 ± 148, and 647 ± 29 μm, respectively (shown in Table 5.2, along with the hollow fibre substrate's other properties). The cross-sectional FESEM images show that the hollow fibre is highly porous, with an asymmetrical structure consisting of finger-like pore structures, which are typical of most porous membrane supports for osmotic membranes. The shell and lumen sides of the hollow fibre, on the other hand, show highly different morphologies with each other. The shell side of the hollow fibre membrane substrates was designed to be highly porous for faster transport of water during the osmotic process, thereby reducing ICP effects. The outer surface on the shell side appears rough and highly porous, while the lumen (inner) side, on the contrary, is found to be much denser with the presence of skin layer and much smaller surface pores. This is a result of the instantaneous phase inversion occurring during the simultaneous extrusion of the polymer dope and bore solutions during the hollow fibre spinning process. The use of the bore solution mixture of DI water and NMP, which is a weaker non-solvent than just pure

DI water, caused phase inversion to occur at a slower rate, resulting in the existence of smaller macrovoid structures and more sponge-like surface pores close to the lumen side (Han, Wang & Chung 2013).

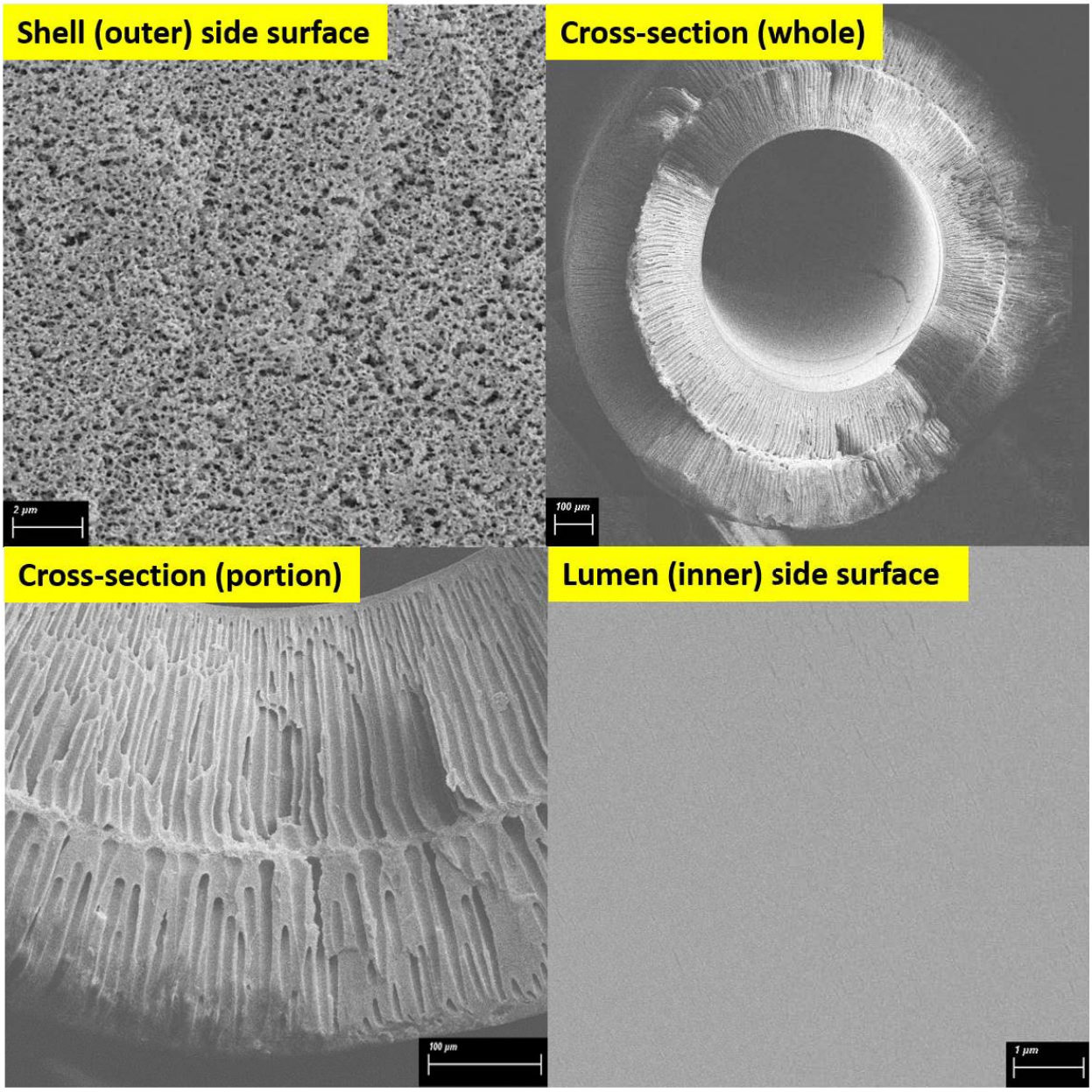

Figure 5.6 The shell (outer) side surface, cross section, and lumen (inner) side surface morphologies of the as-spun hollow fibre membrane substrates using FESEM imaging

Figure 5.7 shows the polyamide selective layer surface of the TFC (PP-0) and TFN (PP-0.001, PP-0.002, and PP-0.005) membranes. All the membranes exhibited the presence of the selective layer, as shown by the ridge-and-valley structures which are characteristics of a polyamide, thus confirming that interfacial polymerisation has occurred between MPD and TMC solutions. The PP-SO_3H nanoparticles are incorporated into the polyamide through the aqueous MPD solution thus appear to be fully embedded well within the polyamide layer.

The presence of hydrophilic nanomaterials, such as sulfonate-functionalised PP-SO_3H, in the polyamide effectively enhances the surface hydrophilicity and affinity of the members to water. To determine if this was the case in this study, the static water contact angle was measured on the membrane surfaces. Lower contact angles generally correspond to higher degree of hydrophilicity; however, the contact angle is not only due to hydrophilicity but also surface roughness, such that smoother surfaces are observed to have lower contact angles (Park et al. 2018). The contact angle measurements can be found in Figure 5.7 (inset). The TFC membrane exhibited a contact angle measurement of 64°, which decreased with the increase in PP-SO_3H loading. Sample PP-0.005, which has a PP-SO_3H loading of 0.005 wt%, showed the lowest contact angle of about 40°. This observed increase in hydrophilicity of the PP-0.005 TFN PRO membrane is a direct result of the presence of the hydrophilic functionalised nanoparticles. The marked decrease in contact angle measurements is not linear or directly proportional to the PP-SO_3H loading rate, because incorporation of nanomaterials likewise increases the surface roughness of the membrane (Liu et al. 2018b).

The degree of sulfonation of the membranes was determined using XPS analysis. Table 5.3 shows the chemical composition of the surfaces of PP-0, PP-0.001, PP-0.002, and PP-0.005 membranes. There was a marked increase in S composition as the PP-SO_3H loading increased, indicating that the degree of sulfonation increased with respect to nanomaterial loading.

Table 5.3 Chemical composition of the TFC and PP-SO_3H-incorporated TFN membrane surfaces

Membrane	C (%)	N (%)	O (%)	S (%)	Others (%)
PP-0	75.33	8.32	15.64	-	0.71
PP-0.001	74.72	10.76	13.18	0.76	0.58
PP-0.002	74.75	11.34	11.93	1.35	0.63
PP-0.005	74.30	12.53	9.72	2.91	0.54

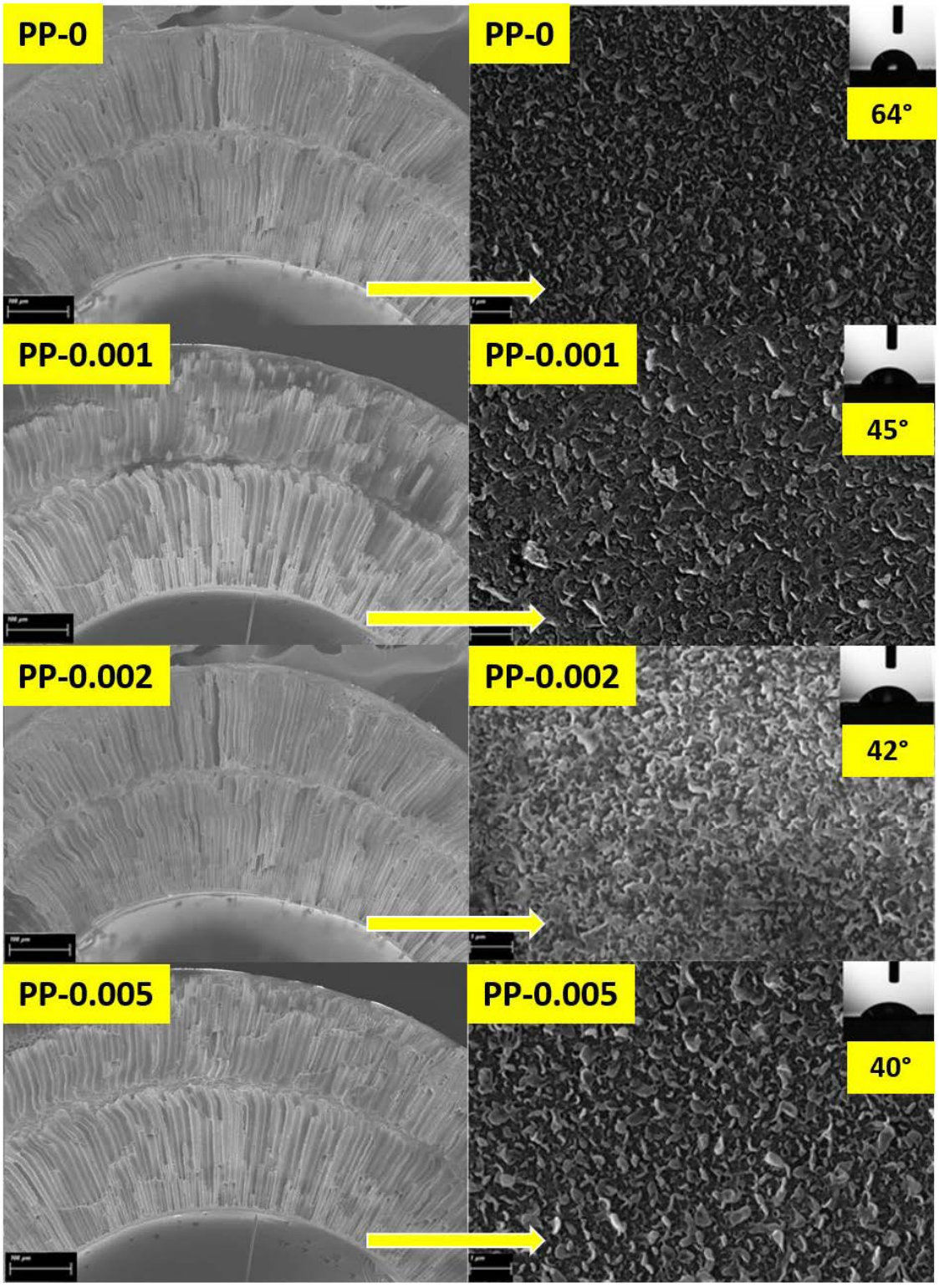

Figure 5.7 The membrane cross section and selective layer morphologies for PP-0, PP-0.001, PP-0.002, and PP-0.005 PRO hollow fibre TFC and TFN membranes using FESEM imaging; Surface contact angle values of each membrane were included inset

5.3.3 Membrane intrinsic transport parameters

The intrinsic membrane transport parameters of the TFC and TFN PRO membranes are presented in Table 5.4. While all the *A* values lie within the range of 1.37 – 1.85 L m^{-2} h^{-1} bar^{-1}, there was a noticeable increase for the PP-SO_3H-incorporated TFN membranes compared to pristine TFC membrane. This is most likely due to enhanced hydrophilicity of the TFN membrane surface as a result of the incorporation of a hydrophilic and porous PP-SO_3H nanomaterial. Also, previous studies noted that there are also interstices between the nanomaterial and the polyamide, providing additional channels for water transport (Wang et al. 2017). The highest *A* value of 1.85 L m^{-2} h^{-1} bar^{-1} was observed for PP-0.002. It was hypothesised that water permeability could increase with nanomaterial loading, due to the effective increase in hydrophilicity and availability of higher number of pores and interstices from the nanomaterial itself. However, this was not observed in this study and hence it can be said that there is an optimal loading rate for nanomaterial incorporation within the polyamide layer that can provide the best membrane permeability.

The *B* values, on the other hand, showed an upward trend as the PP-SO_3H loading increased. PP-0 exhibited a *B* value of 0.35 L m^{-2} h^{-1} which increased to 1.57 L m^{-2} h^{-1} for PP-0.005. Higher water permeability is generally associated with correspondingly higher salt permeability and besides higher porosity of the PP-SO_3H nanoparticles also likely enhanced the transport of solute particles. Consequently, the solute rejection decreased from 96% for PP-0 to 88% for PP-0.005.

Lastly, the *S* value was also evaluated for all the membrane samples, and it was found that the *S* value of 743 μm for PP-0 membrane slightly decreased with the increase

in nanomaterial loading. This can be attributed to the modification of surface chemical composition, which showed significantly higher hydrophilic character.

Table 5.4 Intrinsic membrane transport parameters of the TFC (PP-0) and the PP-SO_3H incorporated TFN (PP-0.001, P-0.002, and P-0.005) membranes

Membrane	A^a (L m^{-2} h^{-1} bar^{-1})	B^b (L m^{-2} h^{-1})	*B/A* (bar)	R^b (%)	*S* (μm)
PP-0	1.37 ± 0.19	0.35	0.26	96.1 ± 1.1	743
PP-0.001	1.51 ± 0.13	0.65	0.43	93.5 ± 0.9	689
PP-0.002	1.85 ± 0.12	1.41	0.76	90.3 ± 1.3	652
PP-0.005	1.76 ± 0.24	1.57	0.89	88.2 ± 1.3	624

[a] Pure water permeability coefficient, *A*, was determined at ΔP = 10 bar with DI water as feed.
[b] Solute permeability coefficient, *B*, and solute rejection, R, were determined at ΔP = 10 bar with 2000 mg L^{-1} NaCl as the feed.

5.3.4 Performance of membranes for PRO process

The TFC and the TFN hollow fibre PRO membranes were pre-stabilised prior to osmotic performance evaluation. The pre-stabilisation step was performed at a hydraulic pressure slightly below the burst pressure to avoid instant breakage of the polyamide selective layer membranes during PRO operation (Gai et al. 2016; Park et al. 2019). The hollow fibre membranes in this study were found to burst between 17 and 18 bar, thus the PRO membranes were pre-stabilised at 15 bar under RO mode (selective layer facing the pressurised stream) for 60 min using DI water as feed. The pre-stabilisation stage allows the simultaneous expansion and compaction of both the hollow fibre membrane substrate and the polyamide layer. These have resulted in elastic stretching of the polymeric substrate and the thinning of both substrate and selective layer, hereby increasing the total effective membrane area (Park et al. 2019). The effective thinning of the membrane then effectively reduces water transport resistance, thus increasing water permeability.

Figures 5.8(a) and 5.8(b) show the membranes' water flux and SRSF performance at varying applied hydraulic pressures. The J_w values at ΔP = 0 were consistent with the *A* values, that there was a marked increase upon incorporation of PP-SO_3H until a 0.002 wt % loading and declined at 0.005 wt% loading. The hydrophilic water-selective channels of PP-SO_3H enhanced the membrane wetting capability of the membrane, and water transport, as well. The –SO_3H functional group of the POP nanomaterial is able to create strong H-bonds with the O–H bonds of water molecules. One drawback of TFC membranes is that the dense polyamide thin film layer usually hinders mass transport due to its lack of solvent transport channels as the PA layer is generally considered non-porous membrane. The incorporation of nanomaterials, such as PP-SO_3H, not only embeds highly porous nanomaterials, but also disrupts the dense structure of the polyamide, making interstices between the nanomaterial and the polyamide, maximising the fractional free volume for water transport (Li, Zhao, Tian, et al. 2018). The highest water flux of 46.3 L m^{-2} h^{-1} was observed for PP-0.002, a dramatic improvement compared to PP-00 with 31.4 L m^{-2} h^{-1}. Incorporation of 0.001 wt% of the PP-SO_3H elevated the J_w to 35.71 L m^{-2} h^{-1}. The J_w decreases slightly for nanomaterial loading above 0.002 wt% and this is conceivably attributed to the agglomeration of the nano-sized particles, ergo reducing permeability as evident from the 42.2 L m^{-2} h^{-1} water flux value of PP-0.005.

As the hydraulic pressure applied during the PRO operation increases, J_w gradually decreases for all membrane samples which is expected due to reduction in the driving force. This continues until the applied hydraulic pressure is identical to the osmotic pressure difference between the draw and feed streams. As pressure is continuously applied on the membrane, the membrane sustained damage from membrane compaction

and stretching, as well as the thinning of the polyamide layer. During the pre-stabilisation step, the membrane was subjected to a pressure less than the burst pressure for it to be compacted and stretched, without breaking; however, due to the elasticity of the polymeric membrane substrate, the membrane bounces back to its original shape and properties. During the continuous PRO operation wherein, hydraulic pressure is constantly applied onto the polyamide selective layer of the membrane, the membrane starts to incur irreversible defects and damage, until it can no longer sustain the damage and eventually bursts. The ability of a membrane to sustain damage despite higher applied hydraulic pressure is a measurement of its robustness, thus the burst pressure is used to evaluate the membrane robustness in previous PRO membrane development studies (Tian et al. 2015). Membrane robustness is an important parameter that needs to be considered for the long-term PRO operation under pressurised environment. Since the incorporation of the sulfonate-functionalised porous polymer is only performed in the polyamide selective layer, this process does not affect the mechanical integrity of the hollow fibre TFC membranes, whose mechanical properties are mostly dependent on the hollow fibre substrate. All the membranes tested in this study have a burst pressure of 17-18 bar regardless of PP-SO_3H incorporation.

Due to the enhanced water permeability of the membranes, one expected trade-off in the form of lower solute rejection due to enhanced solute permeability. Although a trade-off between permeability and selectivity was observed for PP-SO_3H incorporated TFN membranes however, the J_s/J_w values of 0.2 g L^{-1} for PP-0, 0.3 g L^{-1} for PP-0.001, and 0.4 g L^{-1} for PP-0.002 are encouragingly within the ranges reported in the literature. This increasing J_s/J_w trend is in fact consistent with the B values earlier discussed earlier.

In the osmotic process, a much higher amount of water is expected to move from the feed to the DS as compared to the quantity of salt diffusing from the draw to the feed and this perhaps explains the reason for not so significant increase in the J_s/J_w values. This is especially true since water molecules are much smaller than NaCl molecules, so water molecules could penetrate the pores and interfaces of the nanomaterial and the membrane (Yang et al. 2016). Furthermore, the hydrophilic character of the nanomaterial incorporated in the polyamide helps to enhance attraction of water molecules. POP nanomaterials, such as PP-SO_3H are known to be molecular sieves that the molecule has the ability to sieve out other molecules of larger size. This way, despite the supposed drawback of selectivity, we were able to observe that the TFN membranes were able to limit the occurrence of reverse salt permeability and maintain satisfactory salt rejection ability. We can draw from these results that sulfonation concentration could definitely affect PRO membrane performance.

As applied hydraulic pressure on the draw stream increases, it was also observed consistently for all membrane samples that selectivity declines as indicated by the steady increase in the J_s/J_w values. The reverse draw salt transport is a function of concentration difference between the DS and FS which does not change much however the water flux from the feed is retarded due to the presence of applied pressure on the draw stream and hence the J_s/J_w values increases proportionately with the applied pressure. Besides, damage of the polyamide selective layer of the membrane is also highly likely due to compaction, stretching, and thinning out due to the applied pressure thereby allowing more transport channels for solute particles to pass through.

Figure 5.8(c) shows the power density or *W* values of the TFC and TFN membranes at different applied hydraulic pressures. The power density is a straightforward evaluation of the osmotic power generation capacity of the membranes. It is directly related to the water permeability and the applied hydraulic pressure, as well, until a certain point. As the applied hydraulic pressure increases, the power density was found to increase at a hyperbolic trend, until the maximum *W* value is reached, typically at applied hydraulic pressure equals to half the osmotic pressure difference between the draw and feed solutions. Since the PRO hollow fibre membranes in this study were unable to withstand hydraulic pressure beyond 18 bar, hence these membranes could not be tested at the applied hydraulic pressure to achieve maximum *W* value. The highest *W* value obtained for the TFC PRO membrane in this study was 8.2 W m^{-2} at ΔP = 17 bar. Incorporation of 0.002 wt% of PP-SO_3H resulted in a significant increase of the highest *W* value of 14.6 W m^{-2} at the same applied hydraulic pressure.

This membrane performance evaluation results suggest that incorporation of highly porous and hydrophilic nano-sized particles in the polyamide selective layer can effectively enhance water permeability and osmotic power generation of the hollow fibre PRO membranes.

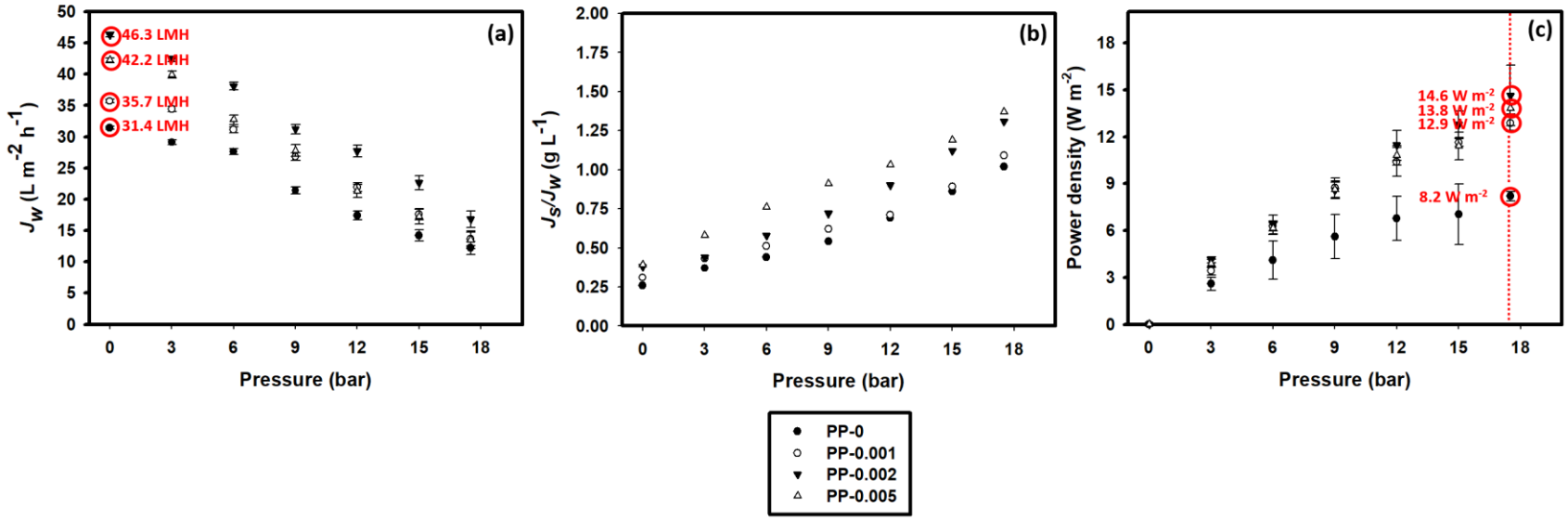

Figure 5.8 The osmotic performance during PRO operation at varying applied hydraulic pressure values, expressed in (a) water flux (J_w), (b) specific reverse salt flux (J_s/J_w), and (c) power density, for PP-0, PP-0.001, PP-0.002, and PP-0.005. DI water and 1.0 M NaCl were the feed and draw, respectively, during PRO operation

5.4 Conclusions

In this study, a hydrophobic porous polymer nanomaterial, PP, was functionalized using chlorosulfonic acid to form sulfonate-functionalized PP-SO_3H with hydrophilic properties. PP-SO_3H was incorporated in the PA layer on PES hollow fiber substrate to develop TFN PRO membrane. The following conclusions are drawn from this study:

1. The incorporation of PP-SO_3H in the polyamide layer effectively modifies the surface chemistry of the selective layer of the osmotic membrane;
2. The presence of highly porous and hydrophilic nanomaterials, such as PP-SO_3H, into the polyamide selective layer significantly enhances water affinity and water permeability of the TFN PRO membranes as a result of enhanced water transport mechanism across the membranes;
3. Despite the enhanced water permeability across the membranes, the salt rejection of the polyamide layer remained satisfactory;

The results suggest that the incorporation of a highly porous and hydrophilic functionalized nanomaterial into the polyamide selective layer is a promising method to develop highly effective TFN membranes for sustainable osmotic power generation. This study has shown that the engineering of the polyamide selective layer by incorporation of a functionalized nano-sized material, such as PP-SO_3H, could effectively result in the functionalization of the TFN membrane surface, as well as enhancement of separation properties. Given the small amounts required of the nanomaterial to be incorporated in the polyamide layer and the enhancement of performance despite the low loading rates, it can be said that functionalized nanomaterial incorporation could be another step toward the development of high-performance membranes and larger-scale application of PRO.

6 Control of antagonistic effects of chlorine oxidative degradation on pressure retarded osmosis thin film composite membrane surface

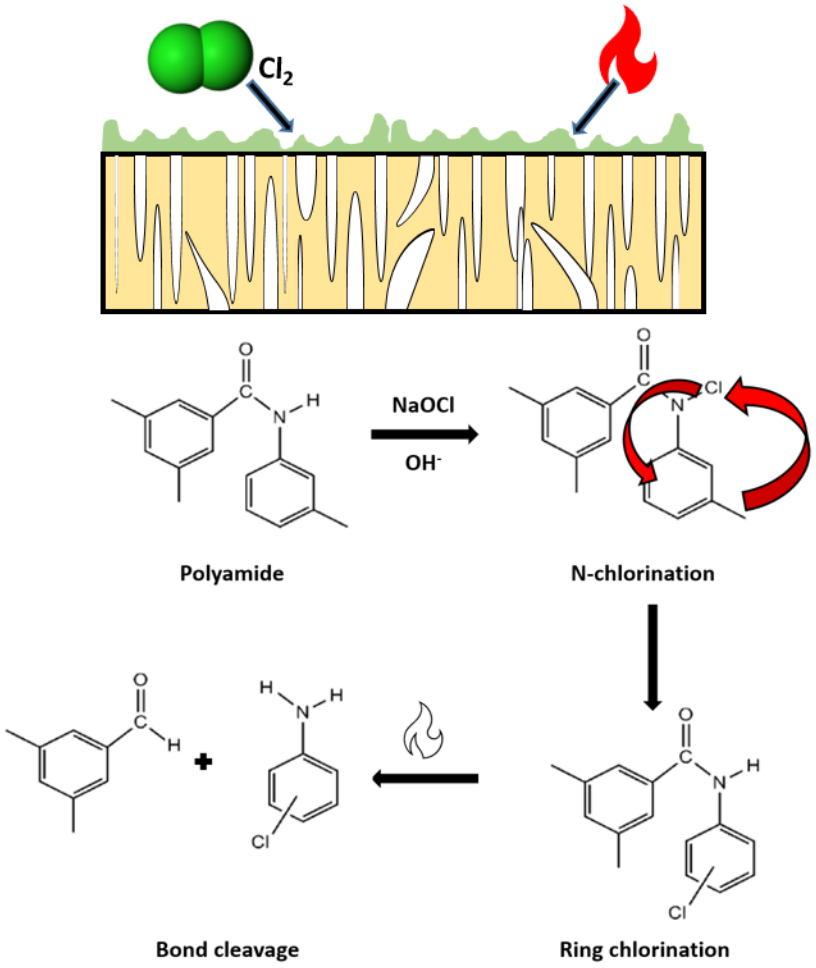

The results of nanomaterial incorporation, as described by the previous two chapters, have shown how alteration of the porosity and hydrophilicity of the polyamide selective layer could enhance the membrane's osmotic generation performance. In this chapter, the polyamide selective layer of the TFC PRO membrane was subjected to oxidative reaction with chlorine (in the form of sodium hypochlorite), a common chemical agent. The exposure of polyamide with chlorine, along with subsequent heat treatment, could result in alteration of the polyamide chemistry and structure. The antagonistic effects of

chlorine and heat treatment were then controlled through optimisation of chlorine oxidation conditions.

6.1 Introduction

PRO is an osmotic-driven membrane process which is known to be able to harvest renewable energy. PRO uses the solute concentration gradient between two streams of different salinities. The FS passes through an asymmetric membrane towards the direction of the DS. Unlike in forward osmosis which applies little to no pressure, hydraulic pressure is applied on the DS side during PRO, against the direction of the solute concentration gradient. This then impedes the flow of water from the FS toward the DS, hence naming the process pressure retarded osmosis. The mixing of the DS and FS leads to production of free energy, which can be converted into mechanical energy (Chung et al. 2017; Volpin et al. 2018).

PRO uses asymmetric semi-permeable membranes, which ideally should be highly porous and hydrophilic to maximise water permeability, highly selective against solute, and mechanically stable enough to withstand the application of hydraulic pressure during PRO operation (Zhang, Sukitpaneenit & Chung 2014). PRO membranes are typically TFC membranes, which are consisted of a porous support and a dense, selective thin film formed on the interface of the porous support (Yip et al. 2011).

Surface modification is a convenient technique to alter the properties of TFC membranes. Surface modification changes the property of the membrane without changing the membrane fabrication process. Properties of the membrane, such as hydrophilicity, surface roughness, surface porosity, and antifouling propensity, can be

altered using surface modification techniques (Ankoliya, Mehta & Raval 2019). Modification of the polyamide selective layer can be done using a number of ways, which include molecular-level design (Li et al. 2019), incorporation of nanomaterials, polyelectrolyte layered interfacial polymerisation (Choi et al. 2017; Gonzales et al. 2018), surface coating or grafting (Saki & Uzal 2019), and chemical modification (Xiong et al. 2019). Chemical modification usually involves exposure of the polyamide selective layer on the modifying agent and removal of the remnant agent via evaporation or drying (Ankoliya, Mehta & Raval 2019). A number of chemical modification studies also required an activation step, usually through application of heat (Zhang et al. 2017).

The chosen modifying agent in this chemical modification study is free chlorine. Free chlorine, a term coined for an aqueous solution containing hypochlorite (OCl^-) and is used generally for membrane recycling, particularly for end-of-life membranes (García-Pacheco et al. 2019). TFC membranes typically have low tolerance to chlorine, such that chlorine resistance has become an important aspect to consider in manufacture of TFC membranes (Chen, Sun, et al. 2019). Chlorine exposure was found to lead to polyamide degradation, and the chlorine attack on the aromatic polyamide is known to be influenced by a number of factors, such as chlorine concentration, exposure time, pH, temperature, and pressure (Donose et al. 2013; Xu et al. 2013). While it had been proven that chlorine leads to deterioration of the polyamide, a controlled degree of chlorination was also found to enhance the membrane performance (Raval et al. 2010; Zhai et al. 2011). It is then highly important to find the best chlorination conditions, in terms of temperature, pH, time, and chlorine concentration.

Response surface methodology (RSM) designs experimental procedures which allow to determine the interactions and the quadratic effects of various factors in an experiment. Statistical analysis and modelling can also be performed using RSM, as well as the evaluation of the significance of the individual experimental factors and of the experimental conditions (Chi et al. 2012). A central composite design (CCD) contains centre points and axial points, which allow estimation of the process response surface.

Unlike variation in chlorine exposure, heat treatment of the membranes exposed in free chlorine was not widely investigated in past membrane chlorine oxidative degradation studies. This study therefore aims to investigate the effect of different factors, pH, chlorine exposure, and heat treatment time, on chlorine oxidative modification of PRO TFC membranes. RSM was employed to develop a central composite face-centred experimental design for the determination of the optimal chlorine oxidative conditions for maximizing the PRO TFC membrane water permeability and osmotic energy harvesting capability, with minimizing detrimental effects on salt rejection, as well as membrane strength and stability.

6.2 Materials and Methods

6.2.1 Materials

Chlorine oxidative degradation was conducted on pristine flat sheet PRO TFC membrane (Toray, South Korea). Sodium hypochlorite (NaOCl, 10-15% available chlorine, Sigma-Aldrich, Australia). Calcium nitrate (tetrahydrate, $Ca(NO_3)_2 \cdot 4H_2O$, Chem-Supply, Pty. Ltd., Australia) was employed for the evaluation of the membrane PRO performance.

6.2.2 Chlorine oxidative degradation

4000 ppm Cl_2 solutions were initially prepared with different pH levels. NaOCl was diluted in 0.1 M CH_3COO^- buffer, 0.1 M $HPO_4^{-2}/H_2PO_4^-$ buffer, and 0.1 M NaOH to achieve pH levels of 5, 9, and 13, respectively. Chlorine exposure is a factor of the Cl_2 concentration, as well as the period of exposure, and is denoted in terms of ppm Cl_2·h. Using a single 4000 ppm Cl_2 solution, the period of membrane exposure was adjusted to vary the chlorine exposure. During the chlorine oxidation process, chlorine exposure was varied to 1000 to 4000 ppm Cl_2·h by exposing the polyamide selective layer of the membranes to 4000 ppm Cl_2 solution for 15 to 60 min. The membranes exposed in Cl_2 solution were afterwards heat-treated in an oven at 90 °C (chosen due to the boiling point of NaOCl which is 101 °C) for a period of 0 to 10 min (0 min means membrane was not heat-treated). After oxidation and the subsequent heat treatment, the membranes were rinsed with and stored in Milli-Q water until use.

6.2.3 Optimisation of chlorine oxidation using response surface methodology

Table 6.1 Full factorial central composite face-centred experimental design for chlorine oxidative degradation of membranes

Run	**Code Values**			**Real Values**		
	X_1	**X_2**	**X_3**	**pH**	**Heating Time (min)**	**Cl_2 Exposure (ppm Cl_2·h)**
0					Pristine	
1	0	0	0	9	5	2500
2	-1	-1	-1	5	0	1000
3	+1	+1	+1	13	10	4000
4	-1	+1	+1	5	10	4000
5	-1	+1	-1	5	10	1000

6	+1	-1	-1	13	0	1000
7	-1	-1	+1	5	0	4000
8	+1	+1	-1	13	10	1000
9	+1	-1	+1	13	0	4000
10	+1	0	0	13	5	2500
11	-1	0	0	5	5	2500
12	0	+1	0	9	10	2500
13	0	-1	0	9	0	2500
14	0	0	+1	9	5	4000
15	0	0	-1	9	5	1000
16	0	0	0	9	5	2500
17	0	0	0	9	5	2500
18	0	0	0	9	5	2500
19	0	0	0	9	5	2500
20	0	0	0	9	5	2500

A central composite face-centred experimental design with replicate centre trials and axial centre points for the three factors, pH, chlorine exposure, and heat treatment period, was used in this study. The experimental design is shown in Table 6.1. A total of 20 experimental trials, consisted of eight trials for cubic points, six for axial points, and six centre points, were performed in this study. The individual and synergistic effects of the oxidation and heat treatment factors were investigated.

6.3 Results and Discussion

6.3.1 Mechanism of chlorine oxidative degradation of polyamide

Several researches have already been performed to elucidate the mechanism of chlorine oxidative degradation (Antony et al. 2010; Gohil & Suresh 2017; Raval et al. 2010). However, these studies simply took account for the mechanism of the chlorine oxidation and did not consider the presence of other factors, such as heat, which was chosen to be a factor in this study.

The mechanistic approach of chemical modification is based on the interaction forces, such as π- π interactions and hydrogen bonding, between the chemical agent and the organic membrane surface, as shown in Figure 6.1, modified from an earlier chlorine oxidation mechanism (Zhai et al. 2011). The chlorine oxidation of the polyamide aromatic ring subsequently allows the deterioration of the H-bonds. The N-H bond is broken as a chlorinated N intermediate is formed; hydrogen is replaced by chlorine, prior to the rearrangement into a chlorinated ring product. As most oxidative processes, chlorine oxidation occurs mainly at a specific pH level, in this case, in alkaline conditions. At harsher chlorine oxidation conditions, it is possible that bond cleavage at the chlorinated ring would occur. The breaking of H-bonds of the polyamide will also lead to increased rotational freedom and of the polymer chains, which could contribute to the increased water permeability (Zhai et al. 2011).

Upon exposure to free chlorine, the amide nitrogen (-C(=O)-N=) is first chlorinated, then the chlorine moves towards the aromatic ring via the intramolecular mechanism Orton rearrangement. Moreover, the amide group is simultaneously hydrolysed during the process, producing carboxylate and either amine or ammonia. These groups are known to be more hydrophilic, compared to polyamide, enhancing the membrane's water permeability (Do et al. 2012).

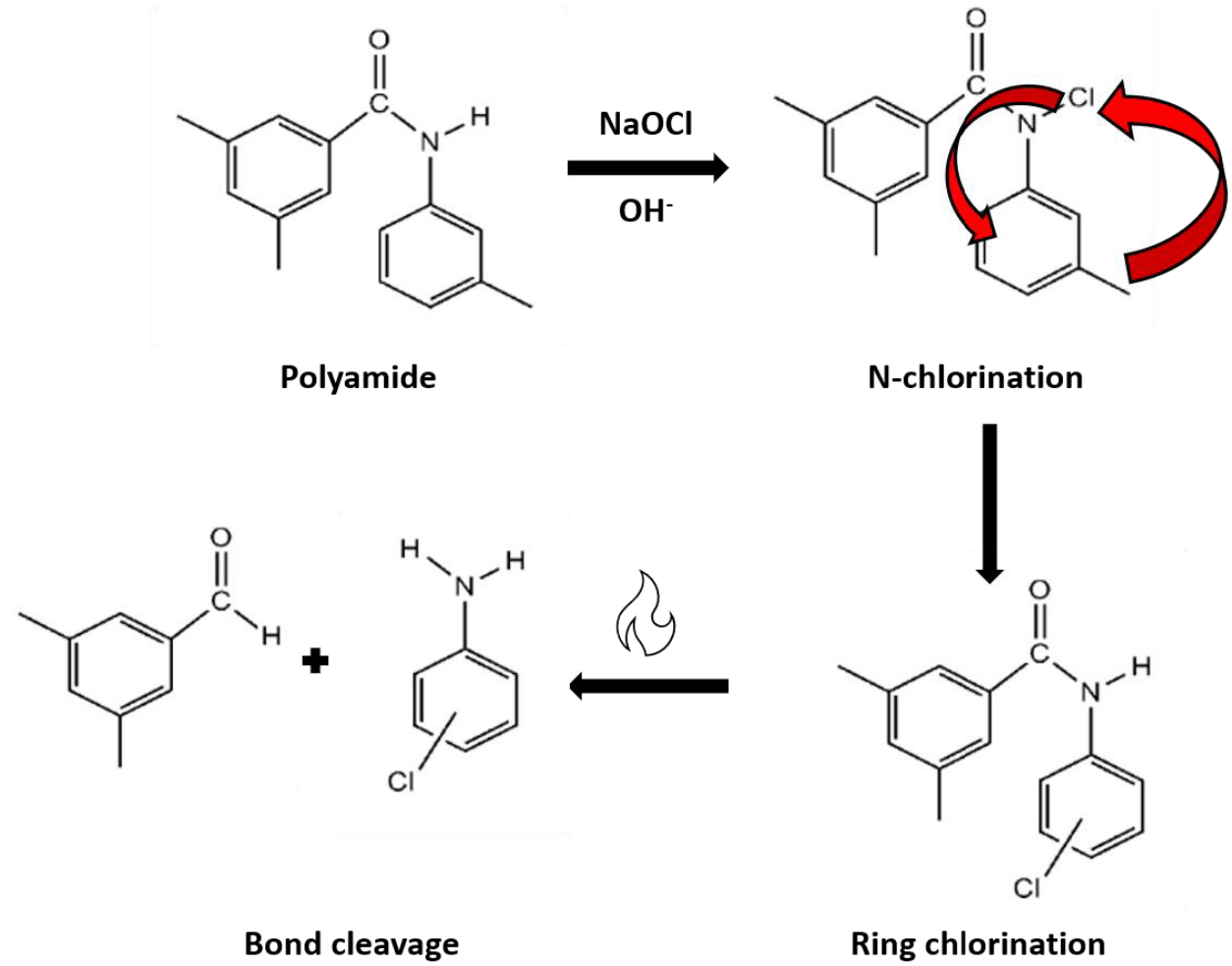

Figure 6.1 Proposed mechanism of chlorine oxidative degradation and heat treatment on polyamide

Due to the hydrolysis of amide functional groups occurring during chlorine oxidation, the acyl groups of polyamide are dissociated into ionised species, making the polyamide layer looser and more susceptible to the passage of water molecules, as well as hydrated ions. This is among the reasons why chlorine oxidation leads to enhancement of both water and solute permeability. This dissociation of the acyl groups is even facilitated further by heat treatment, resulting to scission and bond cleavage.

6.3.2 Influence of chlorine oxidative degradation on TFC membrane stability

The TFC membrane stability and mechanical properties were first evaluated. It is highly important to determine how the chemical treatment affects the stability of TFC PRO membranes and their ability to withstand the application of hydraulic pressure, especially that degradation occurs directly on the polyamide selective layer. The burst pressure was first determined for the pristine and modified membranes and shown in Figure 6.2.

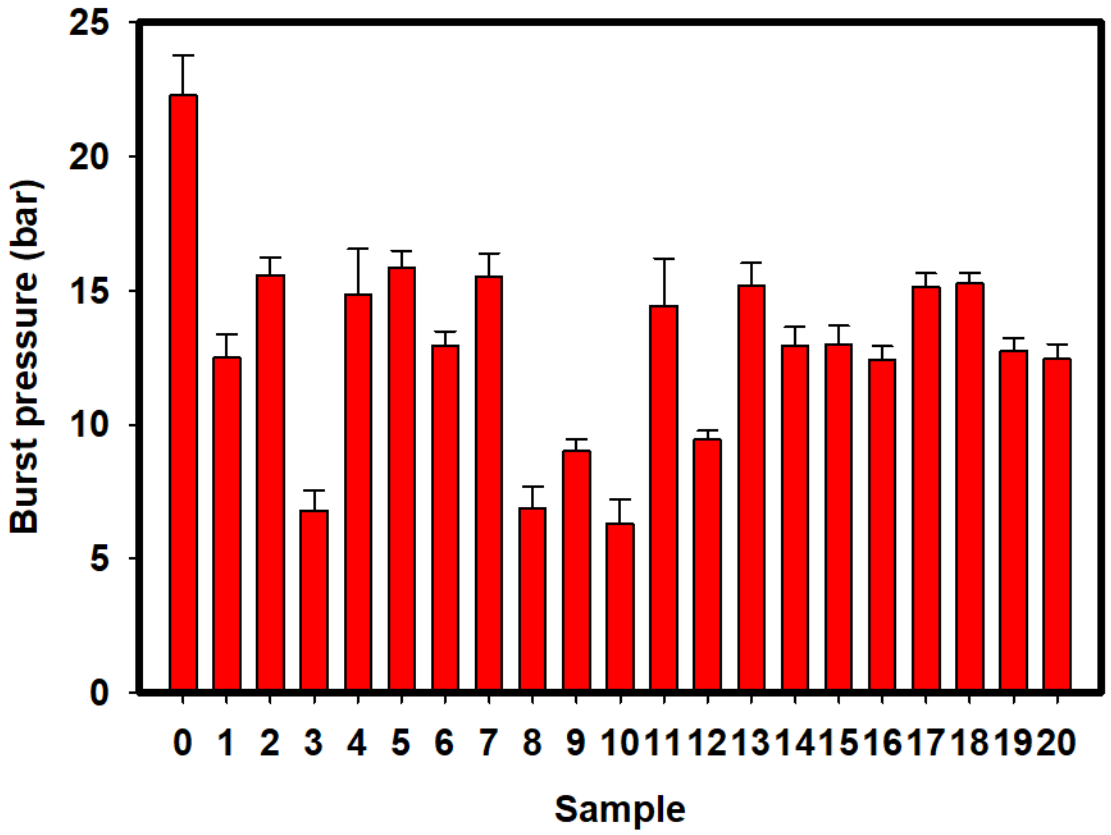

Figure 6.2 Burst pressures of the PRO TFC membranes subjected to chlorine oxidative degradation; Three membranes sustained critical damage on the polyamide layer and were observed to burst after application of hydraulic pressure of 6 bar: membranes 3 (pH 13, 4000 ppm Cl_2·h, and 10 min heating time), 8 (pH 13, 1000 ppm Cl_2·h, and 10 min heating time), and 10 (pH 13, 2500 ppm Cl_2·h, and 5 min heating time)

As shown in Figure 6.2, the membranes resulting from the chemical oxidative degradation process exhibited burst pressures in the range of 6 to 15 bar. These were significantly lower hydraulic pressure values compared to the burst pressure of the pristine PRO TFC membrane, which is 22 bar. Among the membranes, three membranes burst after application of 6 bar: membranes 3 (pH 13, 4000 ppm Cl_2·h, and 10 min heating time), 8 (pH 13, 1000 ppm Cl_2·h, and 10 min heating time), and 10 (pH 13, 2500 ppm Cl_2·h, and 5 min heating time). This is interesting to note, since all three membranes were treated at an extremely alkaline pH. As earlier mentioned, chlorine oxidation mainly occurs at alkaline conditions, and the oxidation process mainly attacks the integrity of the H-bonds of the polyamide. This leads to a thinner polyamide layer, membrane compaction during PRO operation, and eventual collapse of the membrane (Donose et al. 2013). Following the determination of the burst pressure, the membranes were all uniformly tested at 5 bar to comparatively determine the power density of the membranes for the succeeding tests. It is safe to note that for membranes which can withstand higher hydraulic pressures, the power density can increase at higher hydraulic pressures applied.

A previous study correlated the changes in mechanical properties of aromatic polyamide upon chlorine treatment (Lee et al. 2013). Aromatic polyamide is known to be more susceptible to chlorine oxidation due to the presence of π—π interactions, resulting to increased brittleness and fragility of polyamide. Furthermore, in cases of extreme chlorine oxidation conditions, the chain breakage of PSf is possible (Regula et al. 2013), leading to a significant decrease in membrane stability. This was not observed in this study, due to the controlled chlorine oxidative degradation conditions applied.

6.3.3 Optimisation of chlorine oxidative degradation conditions

In this study, the following conditions were controlled in optimisation of chlorine oxidative degradation: free chlorine exposure (a factor of free chlorine dosage and exposure period), solution pH, and heat treatment period. A fixed dose of 4000 ppm free chlorine was utilised for all runs, and the exposure period was varied to demonstrate the effect of chlorine exposure on the TFC membranes. At a fixed dosage of chlorine, a longer exposure time leads to a higher total free chlorine exposure, expressed in terms of ppm Cl_2·h. RSM was used to find the best conditions to ensure enhancement of permeability, while still having satisfactory rejection.

6.3.3.1 Influence of pH and free chlorine exposure at constant heating time

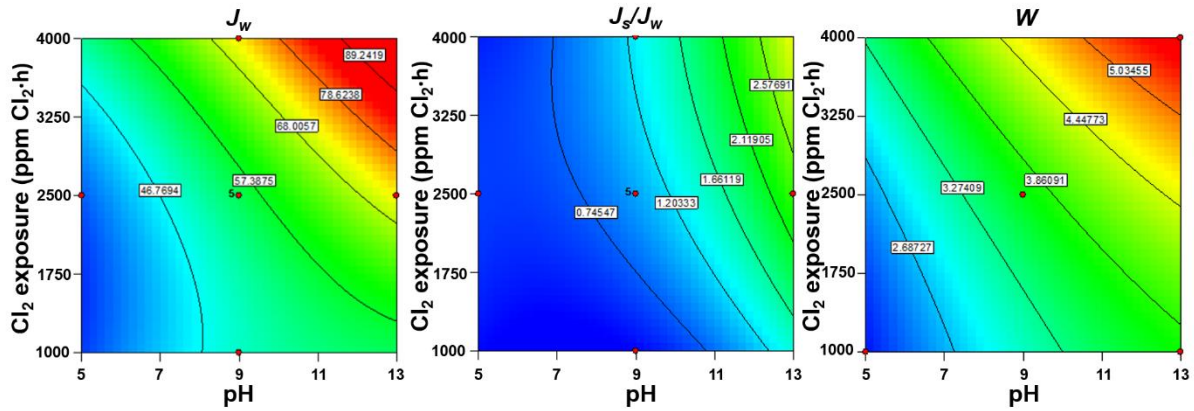

Figure 6.3 Contour plots showing the influence of pH and free chlorine exposure on the water flux, specific reverse salt flux, and power density, at constant heating time of 5 min

Since it was earlier established that chlorine oxidative degradation occurs specifically at alkaline pH, we first examine the influence of pH and free chlorine exposure on the PRO TFC membranes at a constant heating time of 5 min (middle factor in the

RSM design). The influence of pH and free chlorine exposure on the osmotic performance of the membranes are shown in Figure 6.3.

Previous studies of Donose et al. (Donose et al. 2013) and Kang et al. (Kang et al. 2007) had shown the effect of pH on RO membrane ageing after exposure to hypochlorite. In this study, it was found that the effect of hypochlorite (OCl^-) treatment on polyamide is preferred in alkaline environment, just as most oxidation reactions occur preferably at a specific pH. At pH levels over 8, the researchers found that the OCl^- allows the swelling in the polyamide structure.

It is clearly seen from Figure 6.3 that at acidic pH (pH 5), the membranes showed particularly low water flux and power density at 5 bar, regardless of free chlorine exposure. This indicates the possibility that chlorine oxidation did not proceed due to the acidic nature of the solution. However, at higher pH, it can be seen that the water flux and power density values dramatically increased until pH 13, with highest water flux and power density values when the membrane was also exposed at 4000 ppm Cl_2·h. The specific reverse salt flux, on the other hand, is found to be moderately affected by both pH and free chlorine exposure. Albeit typically high J_s/J_w values were observed at higher pH and free chlorine exposure (0.75 to 2.57 g L^{-1}), these were not the highest J_s/J_w values in this study, indicating that the decrease in selectivity of the membranes are mainly due to the occurrence of oxidation reaction.

6.3.3.2 Influence of pH and heating time at constant free chlorine exposure

The influence of pH and heating time on the osmotic performance of the PRO TFC membranes at constant free chlorine exposure of 2500 ppm Cl_2·h (middle factor in RSM design) is shown in Figure 6.4.

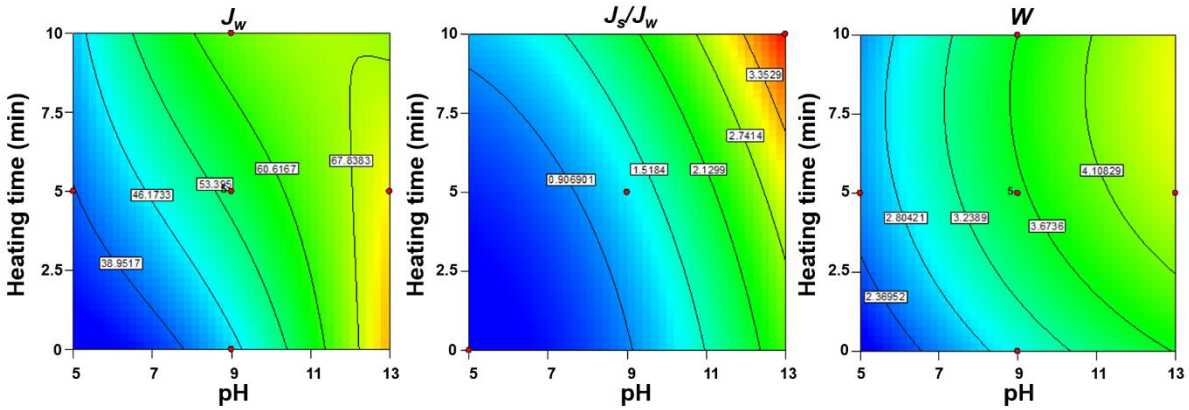

Figure 6.4 Contour plots showing the influence of pH and heating time on the water flux, specific reverse salt flux, and power density, at constant free chlorine exposure of 2500 ppm

Figure 6.4 shows that both pH and heating time have moderate influence on the osmotic performance of the membranes exposed to free chlorine at 2500 ppm Cl_2·h. Moderate increase (indicated by blue- and green-coloured regions in the contour plots) indicate a lower degree of polyamide degradation. For membranes exposed to high concentration of free chlorine and shorter exposure times, the polyamide is not fully degraded. Consistently with pH being an important parameter in oxidative reactions, it can also be seen from these results that at acidic pH, low water flux and power density at 5 bar were observed. Interestingly, we can see that the selectivity of the membranes significantly dropped to a high J_s/J_w value of 3.36 g L^{-1} at 10 min heating time. The rejection of the chlorine oxidised membranes is like that of nanofiltration (NF) membranes,

indicating that the polyamide selective layer had been almost completely deteriorated. This sharp drop in solute rejection is a clear sign that the polyamide layer has sustained damage not only from chlorine oxidation, but also due to the bond breaking during heating.

6.3.3.3 Influence of free chlorine exposure and heating time at constant pH

Lastly, the influence of free chlorine exposure and heating time on the osmotic performance of the PRO TFC membranes at constant pH of 9 (middle factor in RSM design) is shown in Figure 6.5.

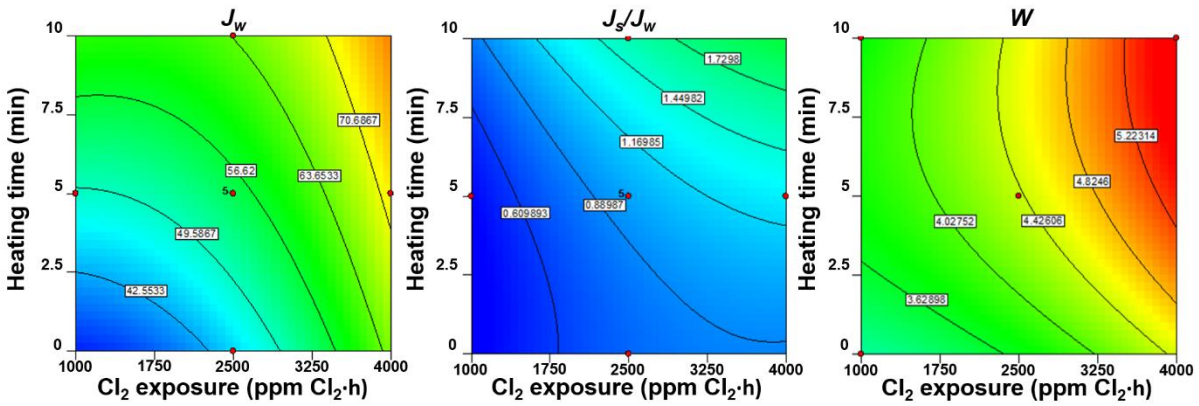

Figure 6.5 Contour plots showing the influence of free chlorine exposure and heating time on the water flux, specific reverse salt flux, and power density, at constant pH of 9

At a constant alkaline pH of 9, we can now see how free chlorine exposure and the downstream heat treatment affect the membranes' osmotic performance. It is interesting to note that at lower free chlorine exposure and short to no heat treatment, chlorine oxidation increased the membrane water permeability and osmotic energy harvesting capability, without affecting the membrane selectivity. Garcia-Pacheco et al (García-Pacheco et al. 2019) earlier reported that low chlorine exposure levels (around 50 – 1000

ppm Cl_2·h) would lead to an increase in the water permeability of the membrane without affecting the solute rejection significantly. At high free chlorine exposure and long heating period, there was definitely a marked increase in both water flux and power density at 5 bar, while keeping solute rejection moderately affected.

6.3.3.4 Synergistic effect of the chlorine oxidation factors and optimisation of chlorine oxidation

The membrane performance is presented in two-dimensional contour plots (Figures 6.3 to 6.5) which model the synergistic effects of two experimental factors when a third factor is held constant. The contour plots show that all three factors — free chlorine exposure, pH, and heat treatment time — have significant individual impacts on the PRO TFC membrane performance. These results indicate that tuning the structure of the polyamide selective via chemical modification can affect membrane performance.

RSM was used to optimise the chlorine oxidative degradation conditions and model their synergistic effect on the following osmotic performance parameters: water flux, specific reverse salt flux, and power density. The following are the regression equations of J_w, J_s/J_w, and W obtained during RSM optimization:

$$J_w = 16.20 + 4.07\,x - 6.56\,y + 1.64\,z + 5.35\,xy + 0.05\,xz + 1.42x10^{-4}\,yz - 0.13\,x^2 + 1.46x10^{-6}\,y^2 - 0.12\,z^2 \quad R^2 = 0.9971 \qquad \textbf{6.1}$$

$$J_s/J_w = 2.29 - 0.55\,x - 5.89x10^{-5}\,y - 0.13\,z + 6.31x10^{-5}\,xy + 9.5x10^{-3}\,xz + 2.18x10^{-5}\,yz - 0.03\,x^2 - 6.67x10^{-8}\,y^2 + 6.79x10^{-3}\,z^2 \quad R^2 = 0.9473 \qquad \textbf{6.2}$$

$$W = 0.55 + 0.32\,x - 3.17x10^{-4}\,y + 0.11\,z + 2.75x10^{-5}\,xy + 2.87x10^{-3}\,xz + 2.07x10^{-5}\,yz - 9.41x10^{-3}\,x^2 + 7.53x10^{-8}\,y^2 - 0.01\,z^2 \quad R^2 = 0.9650 \qquad \textbf{6.3}$$

All modelled regression equations have regression coefficient values (R^2) values over 0.94, indicating that the regression models were fit for the experimental data. ANOVA results showed that the computed F-values (119.11, 13.98, and 21.44 for J_w, J_s/J_w, and W, respectively) are all greater than the tabular F-value of 2.76 at the 5% confidence interval. Moreover, the low p-values (0.0002, 0.0011, and 0.0003 for J_w, J_s/J_w, and W, respectively) tell us that the regression was statistically significant.

According to the optimised regression models, the membrane should be treated at the following conditions: pH 10.89, 4000 ppm Cl_2·h exposure, and 3.6 min heat treatment, to maximise J_w to 84.7 L m^{-2} h^{-1} and power density to 4.7 W m^{-2}, while keeping the specific reverse salt flux (J_s J_w^{-1}) to 1.81 g L^{-1}. These optimised chemical modification conditions could be used for industrial preparation of high-flux membranes for low-pressure PRO operation, when trying to avoid high energy expenditure from application of high hydraulic pressures.

6.3.4 Membrane characterisation

Polyamide degradation and the membrane surface chemistry was confirmed using ATR-FTIR spectroscopy. Figure 6.6 shows the FTIR spectra of the pristine PRO TFC membrane and three chosen membranes: membrane 2 (all factors corresponding to -1; pH 5, 1000 ppm Cl_2·h, no heating), membrane 1 (all factors corresponding to 0; pH 9, 2500 ppm Cl_2·h, 5 min heating), and membrane 3 (all factors corresponding to +1; pH 13, 4000 ppm Cl_2·h, 10 min heating).

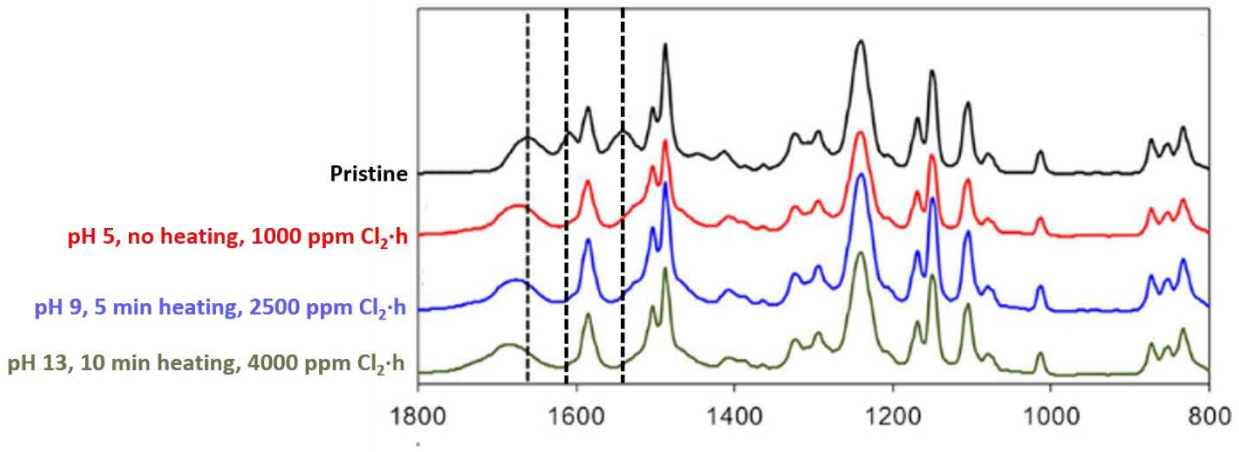

Figure 6.6 FTIR spectra of the pristine PRO TFC membrane and three chosen membranes with different severity of chlorine oxidative degradation conditions

Figure 6.6 shows the difference in the surface chemistry of the membranes treated at different chlorine oxidation severity, compared with the pristine PRO TFC membrane. The following peaks were observed to decrease in intensity as severity increases: 1664 cm^{-1} corresponding to amide, 1610 cm^{-1} corresponding to the C=C stretching vibrations from aromatic polyamide, and 1541 cm^{-1} corresponding to the amide N—H bond. The strength decrease at these peaks indicates that the H-bonds of the amide groups are broken due to the chlorination of N. (Do et al. 2012; Ettori et al. 2011)

Hydrophilicity of the membranes could be examined through sessile drop contact angle measurements. As shown in Figure 6.7, contact angle values significantly decreased after all chlorination experiments, indicating that the chlorine oxidation increased the hydrophilicity of the TFC membrane surface.

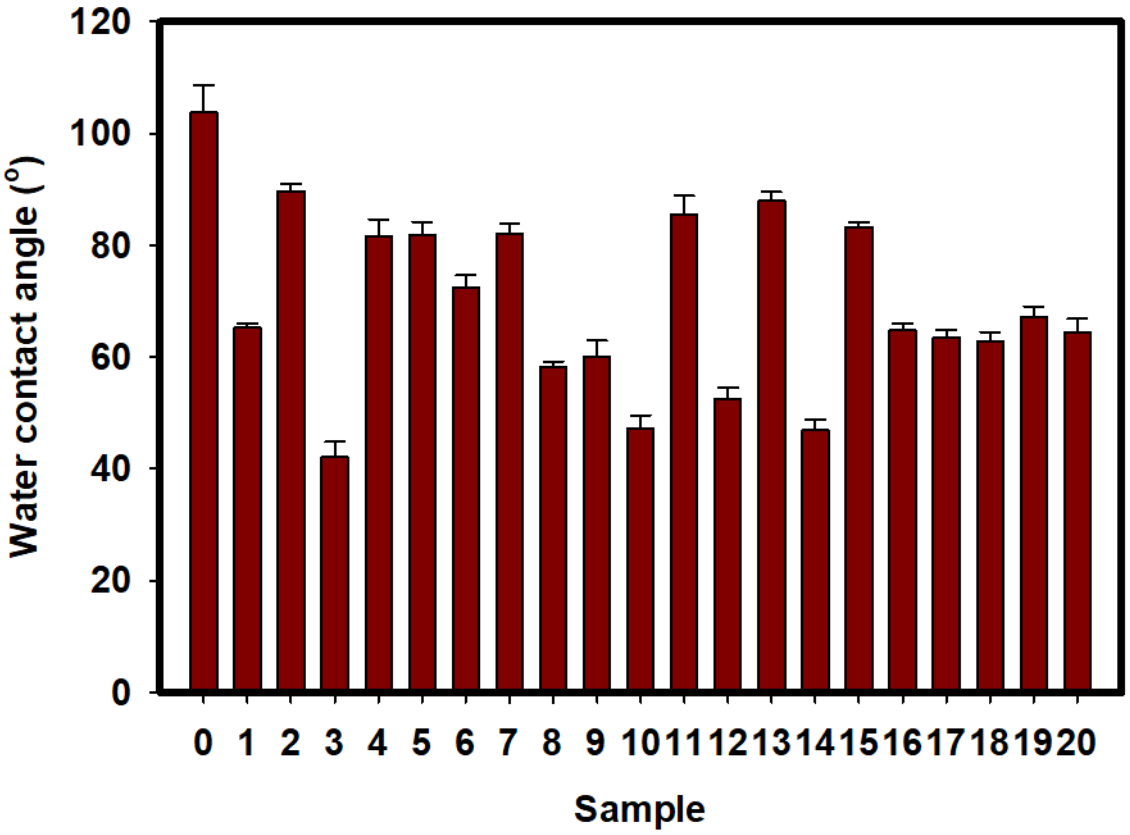

Figure 6.7 Sessile water contact angle measurements of the membrane samples subjected to chlorine oxidative degradation

Figure 6.8 shows the polyamide selective layer surface of the pristine PRO TFC membrane and three chosen membranes with varying degree of severity of chlorine oxidative degradation conditions: membrane 2 (all factors corresponding to -1; pH 5, 1000 ppm Cl_2·h, no heating), membrane 1 (all factors corresponding to 0; pH 9, 2500 ppm Cl_2·h, 5 min heating), and membrane 3 (all factors corresponding to +1; pH 13, 4000 ppm Cl_2·h, 10 min heating).

The surface morphologies of the PRO TFC membranes shown in Figure 6.8 exhibit various degrees of polyamide degradation as the condition severity increased. The PRO

TFC membrane treated at acidic pH, low free chlorine exposure and no heat treatment show almost similar ridge-and-valley structure with that of the pristine PRO TFC membrane, indicating little to no degradation of the polyamide structure. As the severity of the conditions increase, we observe the loosening of the polyamide structure, indicating the damage sustained by the polyamide due to the degradation process. The membrane treated at the extreme chlorine oxidative degradation conditions (pH 13, 4000 ppm Cl_2·h exposure, and 10 min heat treatment) was observed to sustain a high degree of polyamide degradation.

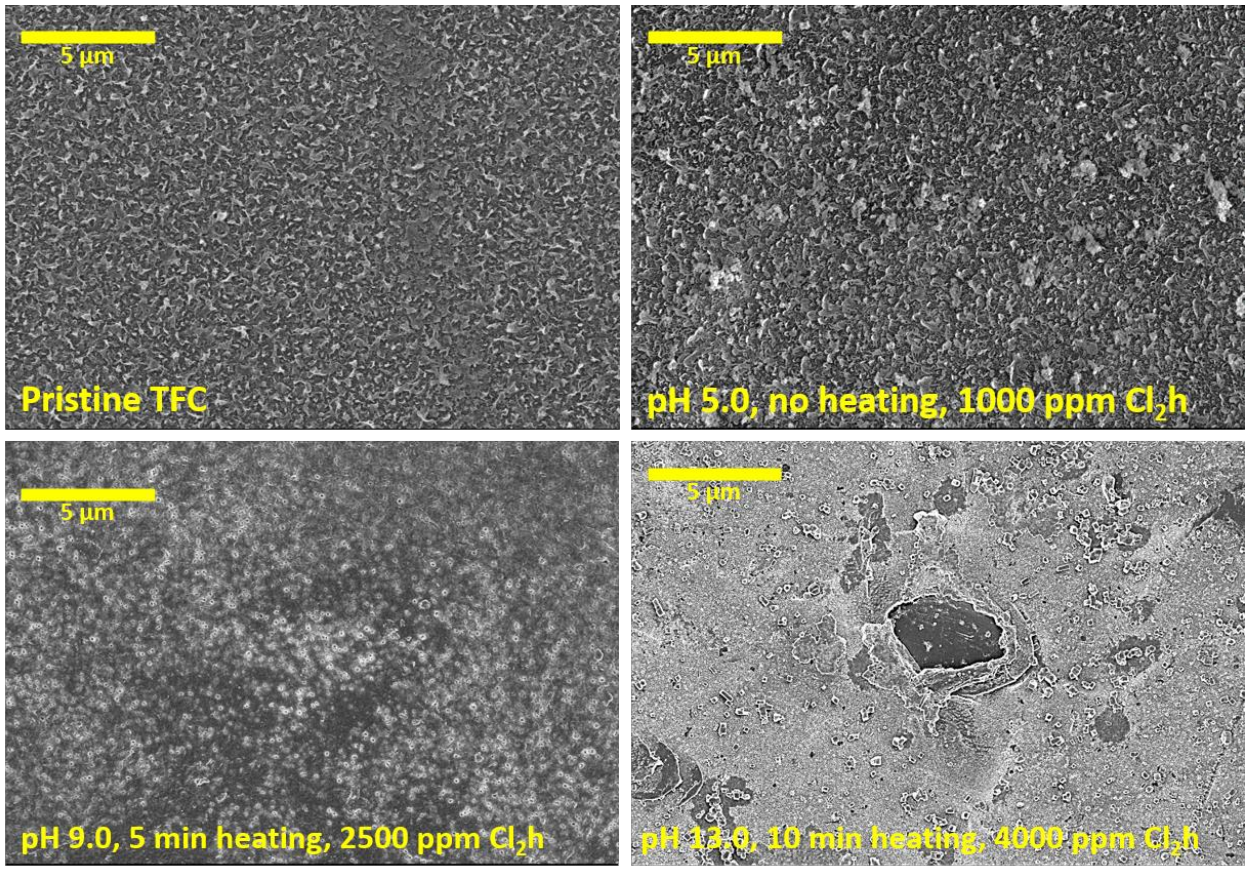

Figure 6.8 Surface morphology of the pristine PRO TFC membrane and three chosen membranes with different severity of chlorine oxidative degradation conditions

6.4 Conclusions

Chlorine oxidation of the TFC membrane surface can lead to degradation of the polyamide selective layer. However, the antagonistic effects of chlorine oxidative degradation can be controlled when performed under optimal conditions, after which, the membranes can be tailored to exhibit enhanced water permeability without significantly affecting solute rejection and without sacrificing its mechanical strength, to obtain a higher extractable osmotic energy from PRO membranes. These are the main conclusions from this study:

1. Significant increase in water flux and power density values were observed for membranes subjected to chlorine oxidation, but only under alkaline conditions;
2. Mechanical defects and polyamide degradation caused enhanced water and solute permeability of the membranes;
3. Chlorine oxidation degrades the polyamide through a chlorination on the aromatic group of the polyamide, leading to dissociation and scission; and
4. Downstream heat treatment of the membranes will further cause bond cleavage on the polyamide structure.

7 Aliphatic polyketone-based thin film composite membranes with mussel-inspired polydopamine interlayer for high performance osmotic power generation

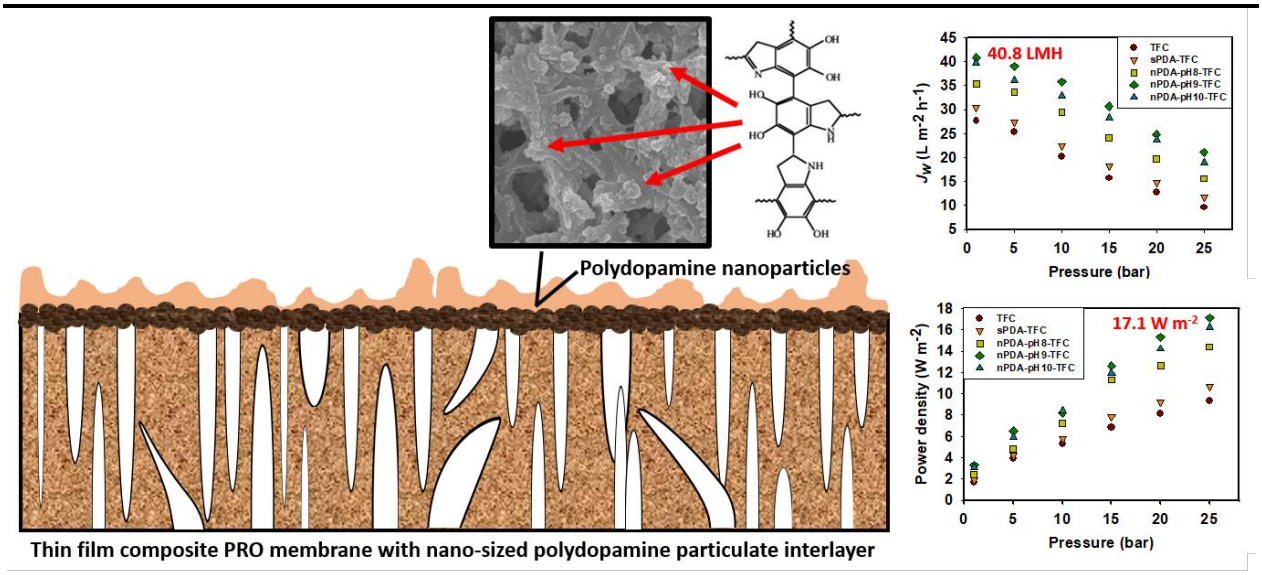

The previous chapters have described direct polyamide engineering via nanomaterial incorporation, surface functionalisation, and chemical modification. This final technical chapter then describes how the polyamide selective layer could be engineered after alteration of the TFC membrane substrate via introduction of an intermediate layer between the substrate and the polyamide. This chapter also incorporates the previous techniques performed, chemical modification using dopamine and incorporation of nano-sized polydopamine particles.

7.1 Introduction

Currently, alternative sources of energy are needed to augment the world's continuously increasing energy requirements due to increased population and advanced economic development (Achilli & Childress 2010). Until present, most of the earth's

energy is obtained from vastly depleting fossil fuel reserves, which also causes greenhouse gas emissions contributing to global warming. As a result of this energy crisis, scientific research from all over the world has looked into the following more sustainable energy sources: solar, wind, geothermal, biomass, and osmotic power (Achilli & Childress 2010; Gonzales & Kim 2017; Klaysom et al. 2013).

Osmotic power generation using pressure retarded osmosis (PRO) is achieved due to the natural occurrence of osmosis between two solutions of different salinities and osmotic pressures separated by a semi-permeable membrane (Volpin et al. 2018). The osmotic pressure difference allows water permeation from the less concentrated FS toward the pressurized more concentrated DS. Osmotic power can then afterwards be harvested by delivering the pressurized DS to a hydro turbine, which produces electrical energy (Loeb 2002).

Alongside the development of PRO as a commercially-viable and technologically-feasible process is the manufacture of membranes specifically for PRO application. Recently, research on PRO membrane development has shown a tangible progress, especially for the development of TFC membranes.

TFC membranes are consisted of a porous substrate and a dense thin film active layer, typically polyamide, formed on top of the porous substrate through IP. Previous research efforts have explored the engineering of PRO TFC membranes, using a variety of methods, modifying agents, and nanomaterial fillers. These techniques aimed to improve the water permeability, selectivity, and mechanical strength of the membranes, in order to improve overall osmotic power generation capability.

Among the chemical agents used in modifying PRO TFC membranes is polydopamine (PDA) (Ingole, Choi, Kim, Park, et al. 2014). This polymer formed from the self-polymerization of dopamine (3,4-dihydroxyphenylalanine) in alkaline conditions. The properties of PDA are known to be similar to the phenolic protein that are found in mussels, causing PDA to be called a bio-inspired or mussel-inspired material. PDA is mainly used for coating a wide range of materials, from nanomaterials to huge surfaces, and it is also widely used as an adhesive. PDA is highly hydrophilic, owing to the presence of hydrophilic hydroxyl and amine groups. Therefore, this polymer has been used for modification of membranes utilized in water-based technologies to enhance separation performance and even fouling resistance (Lee et al. 2007). PDA has become a versatile and efficient engineering agent in membrane development, and it can be applied on membranes using any of the following techniques: (a) surface deposition (Guo et al. 2018), (b) addition in polymer dope solution prior to casting (Jiang et al. 2014), (c) covalent linkage with other molecules by exploitation of Michael or Schiff base reactions (Li et al. 2014), and (d) intermediate layer formation (Zhang et al. 2020). PDA has been widely used to facilitate the formation of intermediate layer and reinforce the incorporation of nano-sized inorganic fillers, such as graphene oxide (Choi et al. 2019), silica (Lv et al. 2017), taurine-modified hydroxyapatite (Mu et al. 2019), halloysite nanotubes (Shah et al. 2019), and covalent organic framework (Wu et al. 2019).

Recent studies have revealed the formation of nano-sized PDA particles when, instead of Tris-HCl buffer, ammonia is used to initiate the dopamine self-polymerization. This method is different from the conventional PDA modification which uses an aqueous PDA and Tris-HCl buffer solution on the surface to form a smooth film. In this study, both

smooth and particulate PDA interlayers were formed between an aliphatic polyketone substrate and the polyamide selective layer. Furthermore, it has been long established that the catechol and amine groups present in PDA can react with the acyl chloride precursor during IP. The introduction of a PDA interlayer between the membrane substrate and selective layer has been found to facilitate excellent formation of mechanically-strong thin film, as caused by the adhesive properties of the said polymer.

The introduction of nanomaterials in TFC membranes for PRO has led to a new class of membranes known as TFN membranes. PRO TFN membranes are developed by incorporating nano-sized materials, like graphene oxide (Park et al. 2019), carbon quantum dots (Gai, Zhao & Chung 2018; Zhao, Das & Chung 2017), and carbon nanotubes (Kim, Yang, et al. 2020), either in the membrane substrate or the polyamide selective layers. TFN membranes have exhibited enhanced water permeability due to the presence of the highly porous and hydrophilic nanomaterials. The incorporation of nanomaterials in the intermediate layer of PRO TFC membranes has not yet fully been explored, and this study aims to exploit nano-sized particulate PDA as an intermediate media for PRO TFC membranes.

This study aimed to discover whether the formation of particulate PDA interlayer could retain the high permselectivity of the pristine TFC and TFC membrane with smooth PDA interlayer, and how the interlayer structure could affect polyamide formation and the subsequent PRO operation performance. Furthermore, ammonia-initiated polymerization of dopamine was also investigated in terms of varying alkaline pH. While research on TFC membrane modification using PDA has been abound, this manuscript provides

insight on how changes in polymerization agent and alkalinity could influence a technique as simple as PDA modification and the PRO performance.

7.2 Experimental

7.2.1 Chemicals

The membrane substrate was prepared using aliphatic PEK and PET nonwoven fabric. Membrane modification was conducted using dopamine hydrochloride (dopamine HCl, Sigma-Aldrich, Japan), Tris(hydroxymethyl) aminomethane (Tris, Sigma Aldrich, Japan), hydrochloric acid (HCl, 1 mol/L, Wako Pure Chemical Industries, Ltd., Japan), ammonia (25.0~27.9%, in solution, Fujifilm Wako Pure Chemical Corp., Japan), and ethanol (99.5%, Fujifilm Wako Pure Chemical Corp., Japan).

7.2.2 Membrane preparation

7.2.2.1 Membrane casting and polydopamine interlayer formation

Flat sheet PK membrane substrate was fabricated by conventional NIPS, as described in Chapter 3.

PDA interlayer was formed *in situ* on the top side of the PK membrane substrate. Two types of PDA interlayer were formed: the conventional smooth PDA and the nano-sized particulate PDA, afterwards denoted as PK-sPDA and PK-nPDA, respectively.

The typical PDA layer formation method required 2 mg mL^{-1} of dopamine HCl dissolved in a 0.01 M Tris-HCl solution (pH 8.5). The membrane substrate surface was immersed in the solution for 8 h while agitating at 400 rpm using a shaker (Eyela, Japan) in room temperature (Han et al. 2012).

For the formation of particulate PDA interlayer, a 2 mg mL^{-1} dopamine HCl was dissolved in an aqueous 30% (v/v) ethanol solution (Zhang et al. 2020). The pH of the solution was adjusted by dropwise addition of 25% ammonia solution. The membrane substrate surface was immersed in the solution for 8 h at light agitating conditions.

All PDA-coated membrane substrates were washed with copious DI water prior to interfacial polymerization.

7.2.2.2 In situ formation of polyamide selective layer via interfacial polymerisation

The polyamide selective thin film layer was prepared *in situ* on top of the PDA-coated membrane substrate by interfacial polymerisation (IP) of MPD and TMC.

7.3 Results and discussion

7.3.1 Polydopamine modification and formation of smooth and nanoparticle polydopamine interlayer

Figure 7.1 shows the FTIR spectra of the membrane substrates, comparing the plain polyketone with the PDA-coated ones. All the PDA-coated membrane substrates exhibited peaks attributed to the presence of PK and PDA groups, indicating the successful incorporation of the PDA interlayer. The peaks at around 1570 cm^{-1} and 1650 cm^{-1} respectively correspond to the N-H and C=C groups of PDA formed during the self-polymerization of dopamine (Kwon et al. 2019). There was no notable difference from the FTIR spectra of the membranes coated with PDA, whether smooth or particulate.

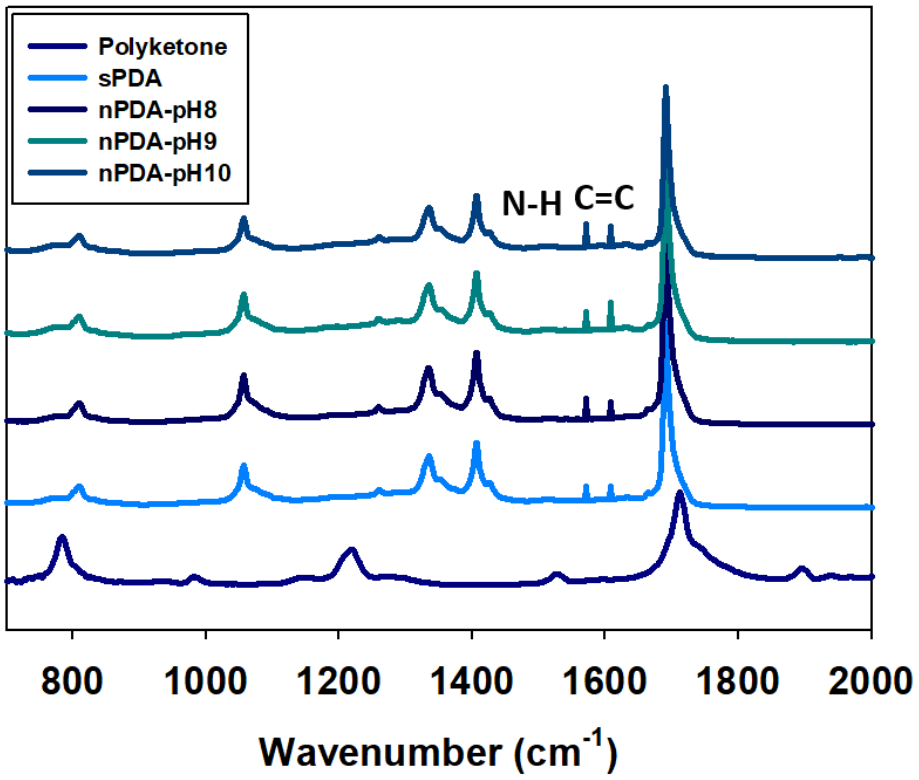

Figure 7.1 FTIR spectra of the pristine polyketone and PDA-modified membrane substrates

To further analyse the surface chemistry of the PDA-coated membrane substrates, XPS analysis was performed, and the elemental XPS analysis results are shown in Table 7.1. The elemental composition of the membrane substrate surface confirms that there was indeed the presence of the PDA coating on top of the polyketone, as evidenced by the increase in N content, starting from *nil* in pristine polyketone to the 5.28 % N content of nPDA-pH10, or the membrane substrate modified with PDA at pH 10. The self-polymerization of dopamine to polydopamine is highly controlled by the pH of the reaction medium, with OH^- ions acting as the catalyst. Typically, the pH of the self-polymerization reaction is controlled using a buffer to ensure the gradual polymerization and facilitate the

formation of a smooth polydopamine coating onto a surface. In the case of this study, the self-polymerization was catalyzed by ammonia, and the pH of the solution influenced the reaction. At lower pH (pH 8), the self-polymerization reaction was not fully catalyzed, as the reaction mostly takes place between pH 8.5 to 9, thus the dopamine which has not polymerized during the reaction period might have been washed off from the membrane surface, resulting in a lower N content, as seen from the XPS characterization, indicating the presence of less polydopamine on the membrane substrate surface. The higher reaction pH of the succeeding samples ensured that the self-polymerization reaction took place and resulted in the formation of the PDA nanoparticles which were embedded within the membrane substrate, and led to higher N content.

Table 7.1 Surface elemental analysis of the PDA intermediate layer using X-ray photoelectron spectrometry

Membrane substrate	C (%)	N (%)	O (%)	Others (%)
Polyketone	70.63	-	29.01	0.36
sPDA	72.34	3.12	24.27	0.27
nPDA-pH8	71.89	2.74	25.03	0.34
nPDA-pH9	73.87	4.59	21.19	0.22
nPDA-pH10	75.26	5.28	19.23	0.23

The morphology of the membrane substrates characterised using FE-SEM are shown in Figure 7.2. In general, PDA modification results in enhancement of hydrophilicity and smoothness of the surface; however, in this study, it could be seen that while hydrophilicity was definitely enhanced upon introduction of the PDA interlayer (Ingole, Choi, Kim, Park, et al. 2014), surface smoothness was only achieved when the conventional PDA modification technique was performed. The smooth PDA interlayer appeared to be a smooth coating on the fibril-like structures of polyketone, still revealing

the intrinsic highly porous structure of the membrane substrate. In the case of formation of PDA nanoparticles as an interlayer, the roughness of the membrane substrate was observed to be increased as self-polymerisation pH increased. The particulate PDA interlayer was observed to exhibit granular surface with open pore structure. As dopamine self-polymerisation pH increased, there was an observed increase in the presence of particulate PDA structure attached onto the fibrous polyketone substrate. The nPDA-pH10 substrate has clearly shown aggregation of the PDA nanoparticles, which was known to be more prevalent at elevated pH, thus self-polymerisation of dopamine is not performed at pH values higher than 10.

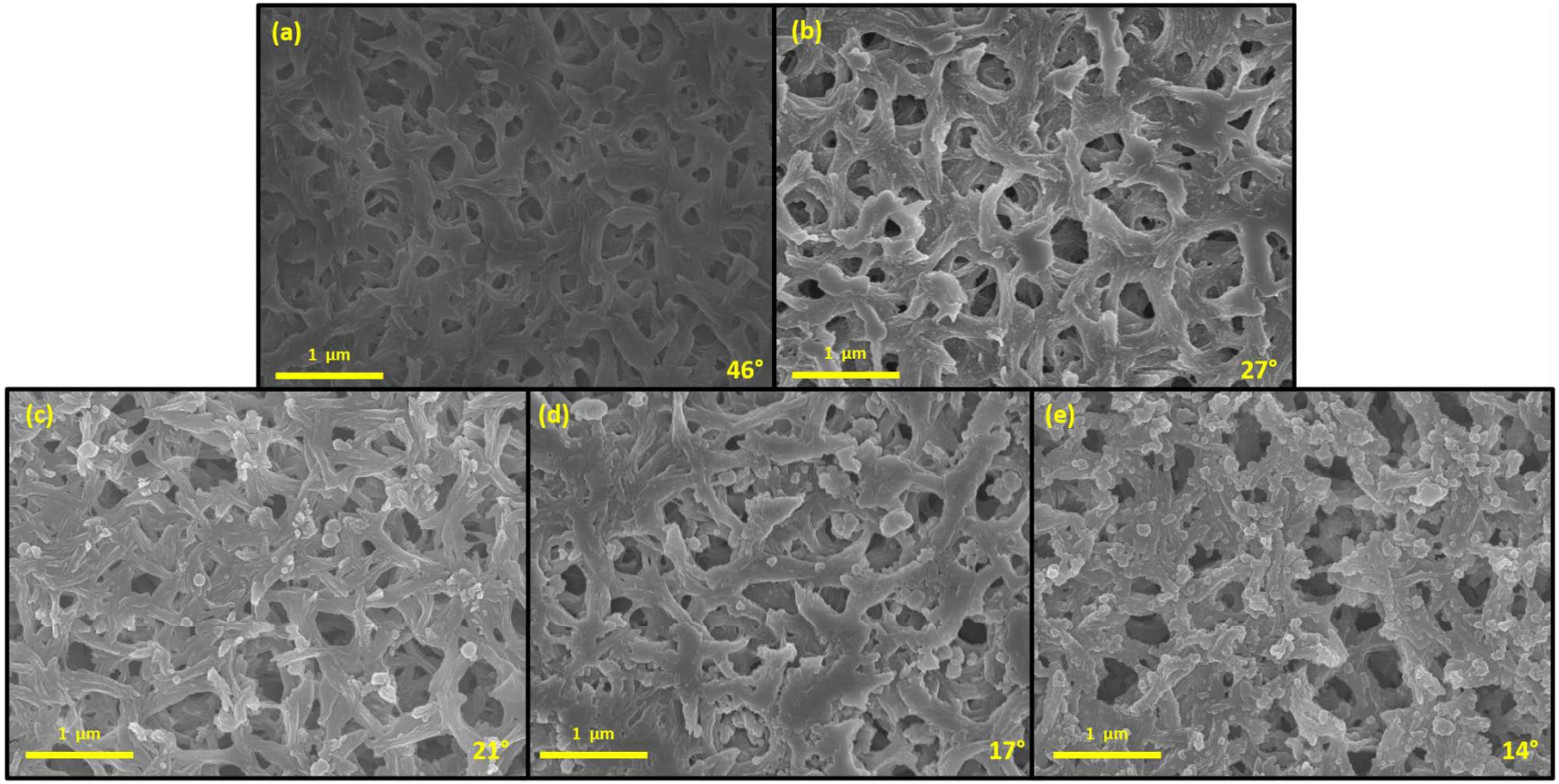

Figure 7.2 Surface morphology of the (a) pristine polyketone and PDA-coated membrane substrates: (b) sPDA, (c) nPDA-pH8, (d) nPDA-pH9, and (e) nPDA-pH10; Average water contact angles are included inset

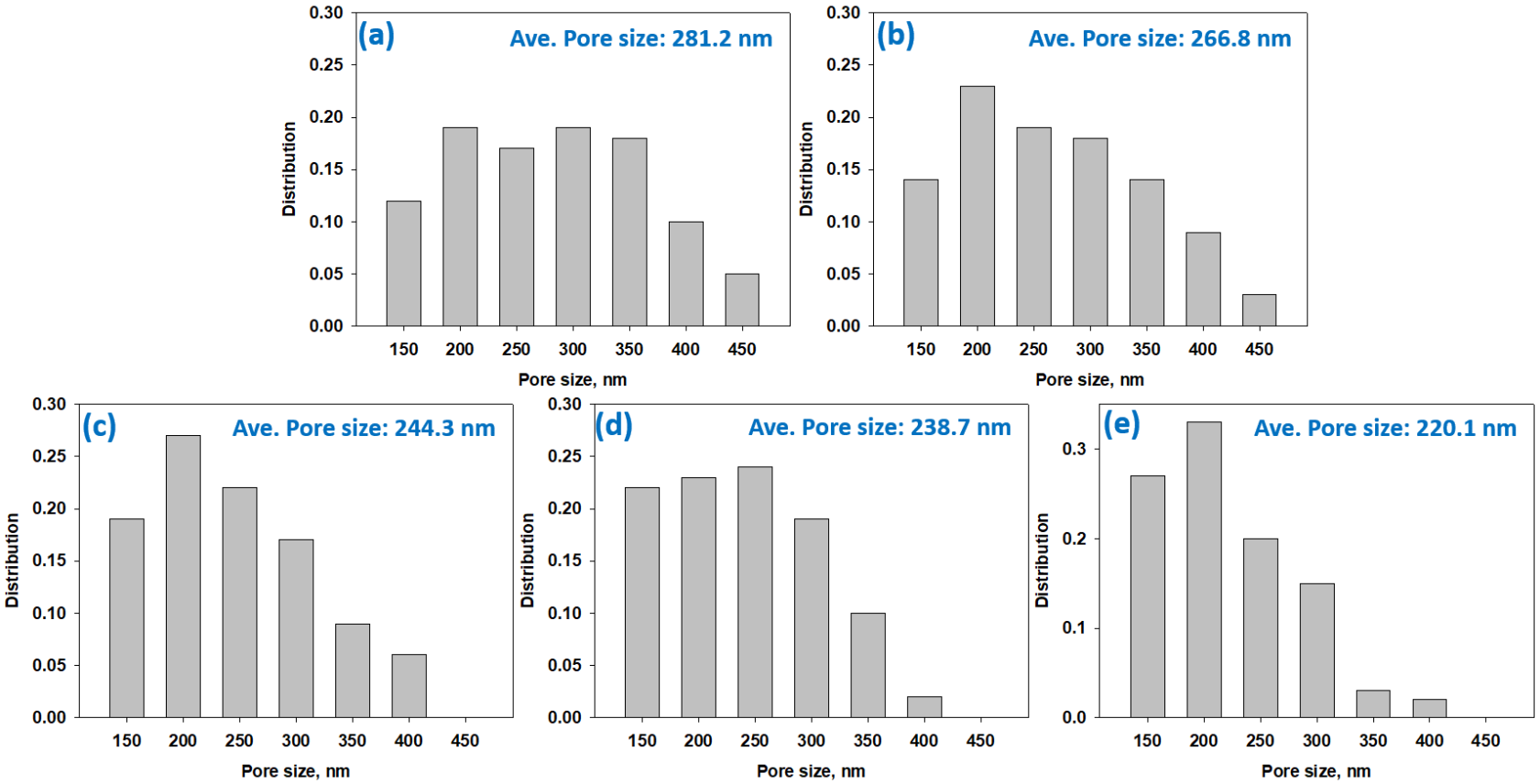

Figure 7.3 Pore size distribution and average pore size of the (a) pristine polyketone and PDA-coated membrane substrates: (b) sPDA, (c) nPDA-pH8, (d) nPDA-pH9, and (e) nPDA-pH10

The membrane substrate roughness was also characterized using AFM. Figure 7.4 and Table 7.2 show the average surface roughness of the prepared polyketone and PDA-coated membrane substrates. The surface roughness of both pristine polyketone and sPDA samples showed statistically similar average R_{ms} values, with sPDA having a lower average, indicating how the conventional PDA coating could result in the formation of a smooth coating on top of the membrane substrate. The surface roughness, however, increased as pH increased during the self-polymerization of dopamine. The surface roughness was heavily influenced by the formation of the nano-sized PDA particles, which have been formed upon exposure of dopamine monomer with NH_3 initiator.

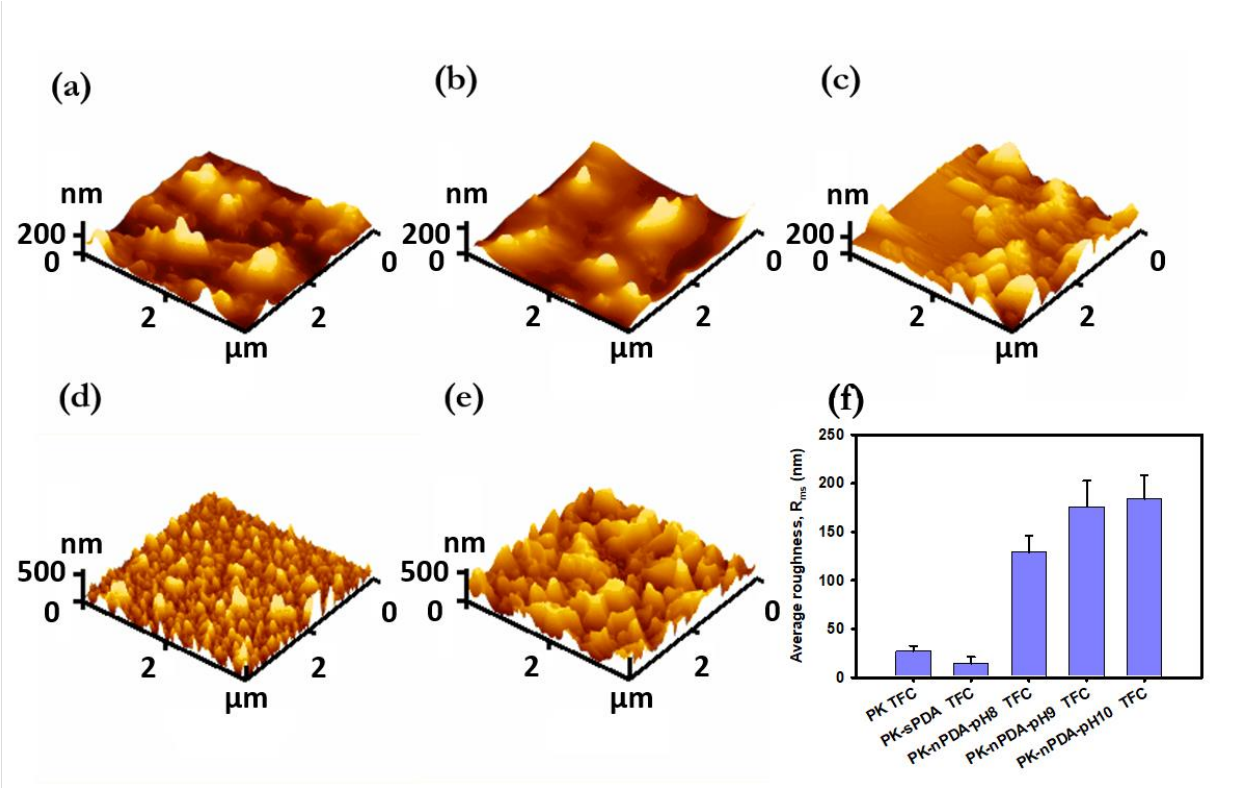

Figure 7.4 Surface roughness characterization of (a) pristine polyketone and PDA-coated membrane substrates: (b) sPDA, (c) nPDA-pH8, (d) nPDA-pH9, and (e) nPDA-pH10

Table 7.2 Average roughness (R_{ms}) of the membrane substrates characterized

Membrane substrate	Average Roughness, R_{ms} (nm)
Polyketone	59.3 ± 10.2
sPDA	48.2 ± 8.4
nPDA-pH8	96.6 ± 17.1
nPDA-pH9	129.3 ± 21.6
nPDA-pH10	159.7 ± 33.6

It is also interesting to note that PDA modification of the membrane substrates resulted to smaller surface pores and narrower pore size distribution, as shown in Figure 7.3. It was expected that PDA modification could cause partial blockage of the surface pores (Han et al. 2012); however, the PDA coating makes up for it by providing higher functionality and hydrophilicity to the membrane substrate. Also included inset are the contact angle measurements of the plain and PDA-modified polyketone substrates. Due to the functional groups present in the structure of PDA, the membrane substrate surfaces were also effectively functionalized upon coating and the hydrophilicity of the surfaces were effectively enhanced as well (Arena et al. 2014).

It is interesting then to know whether the PDA interlayer morphology could have an effect on the *in situ* polyamide formation during IP and the PRO membrane performance.

7.3.2 TFC membrane characterisation

The morphology of the TFC membranes observed using FE-SEM are shown in Figure 7.5 (cross section) and Figure 7.6 (surface). The cross-section images show that a thin dense selective layer was formed on top of the porous substrate. There was a noticeable change in the polyamide layer thickness for the samples. Polyamide has a

typical thickness of 100 to 150 nm, and the measured thickness of the polyamide selective layer of the plain TFC membrane was well within this range. The same observation was true for the polyamide thickness of the TFC membrane with a smooth PDA interlayer; however, the polyamide layer of sPDA-TFC was observed to be even thinner than that of the plain TFC membrane. This shows that the smooth PDA interlayer forms denser and thinner selective layers. Aside from being caused by the smoothness of the membrane substrate, this phenomenon is also most likely due to the ability of PDA to penetrate into the pores of the membrane substrate, enhancing its hydrophilicity (Yang et al. 2014) and improving the retention of the MPD precursor during IP, leading to the formation of denser, yet thinner polyamide. On the other hand, there was an increase, albeit slightly, in the polyamide thickness observed for the membranes modified with a nanoparticulate PDA interlayer. Furthermore, upon inspection of the polyamide surface morphology of the membrane samples, it is interesting that the polyamide of the plain TFC and the one with smooth PDA interlayer were observed to be highly dense, while the polyamide of the membranes with nanoparticle PDA interlayer were observed to be less dense, which may indicate the formation of looser polyamide structure. This difference in the morphology of the polyamide formed is highly attributed to the properties of the intermediate layer between the substrate and the polyamide.

To further characterize the polyamide selective layer of the TFC membranes and how its formation was influenced by the introduction of the intermediate layer, XPS analysis was performed to determine the atomic composition and degree of cross-linking of the polyamide layer in each membrane. Based on the atomic composition analysis, the

ratio of O and N can provide the degree of cross-linkage of the polyamide layer. The O/N ratio is inversely proportional to the degree of cross-linkage, be calculated using:

$$a + b = 1 \quad \textbf{7.1}$$

$$\frac{O}{N} = \frac{3a+4b}{2a+2b} \quad \textbf{7.2}$$

where a and b are the crosslinked structure and linear structure components of polyamide, respectively (Chi et al. 2018).

Table 7.3 Atomic composition and the degree of cross-linking of the polyamide selective layer of the TFC membranes

Membrane	C (%)	N (%)	O (%)	O/N	*a* value
Polyketone TFC	72.29	13.07	14.64	1.12	83.0 %
sPDA TFC	72.14	13.33	14.53	1.09	87.1 %
nPDA-pH8 TFC	71.73	12.79	15.48	1.21	71.5 %
nPDA-pH9 TFC	72.56	12.14	15.30	1.26	65.5 %
nPDA-pH10 TFC	73.04	11.72	15.24	1.3	60.9 %

Table 7.3 shows the atomic composition and degree of cross-linking of the polyamide layers of the TFC membranes in this study. The XPS analysis shows and confirms that the introduction of intermediate PDA layer could influence formation of the polyamide selective layer. Both the pristine TFC and sPDA TFC membranes show a high degree of cross-linkage of 83.0 and 87.1%, respectively, while those with nanoparticulate PDA intermediate layer exhibited lower degree of cross-linkage between 60 and 72%. The presence of the embedded PDA nanoparticles increased roughness of the membrane substrate, causing a less even distribution of the MPD and TMC monomers during IP and resulting in lower degrees of cross-linkage. The lower degree of cross-linkage then explains the appearance of seemingly looser polyamide layer of the nPDA TFC membranes, as shown by the FE-SEM images (Figure 7.5 and 7.6).

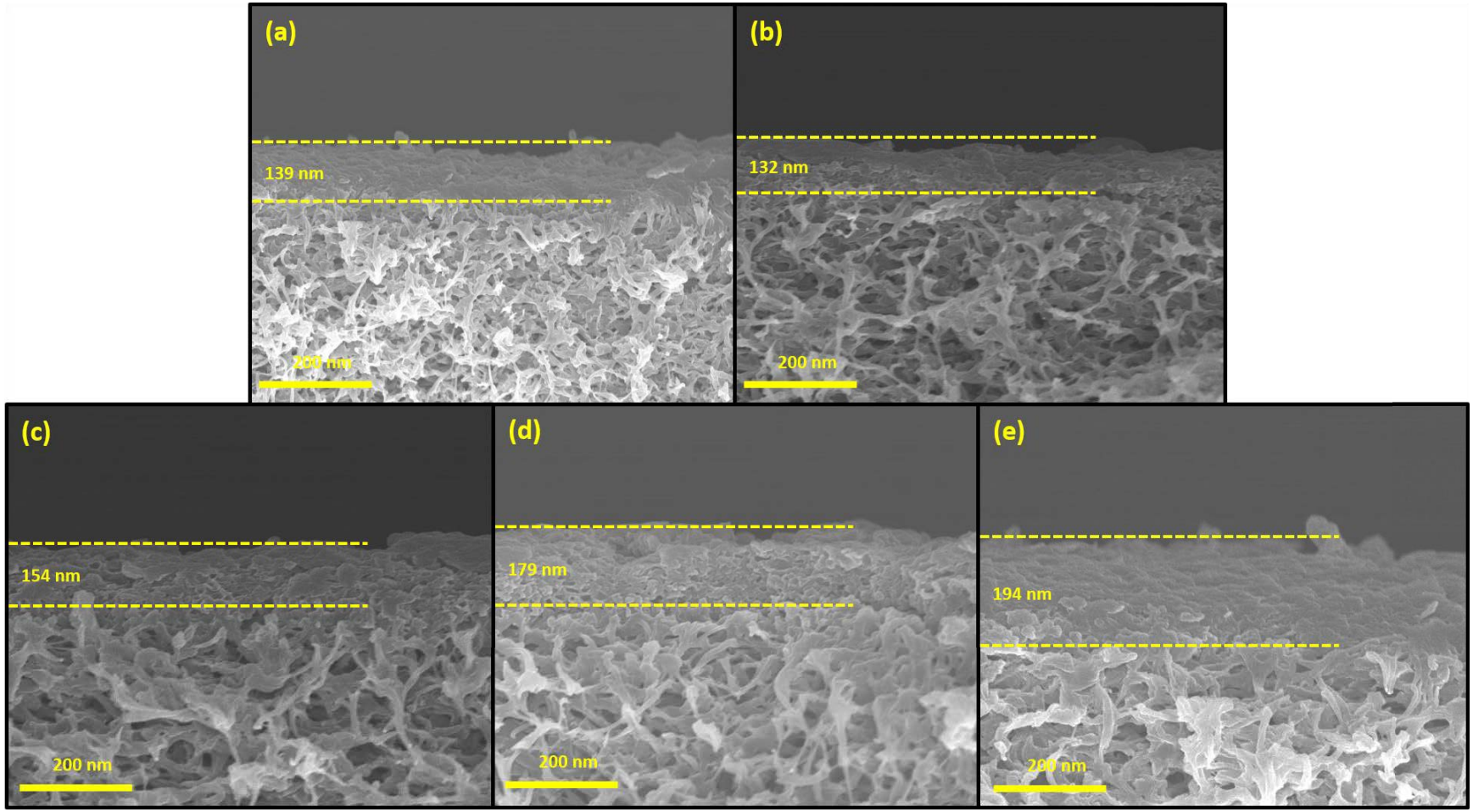

Figure 7.5 Cross-section FE-SEM images of the TFC membranes with the polyamide layer thickness: (a) plain TFC, (b) sPDA-TFC, (c) nPDA-pH8-TFC, (d) nPDA-pH9-TFC, and (e) nPDA-pH10-TFC

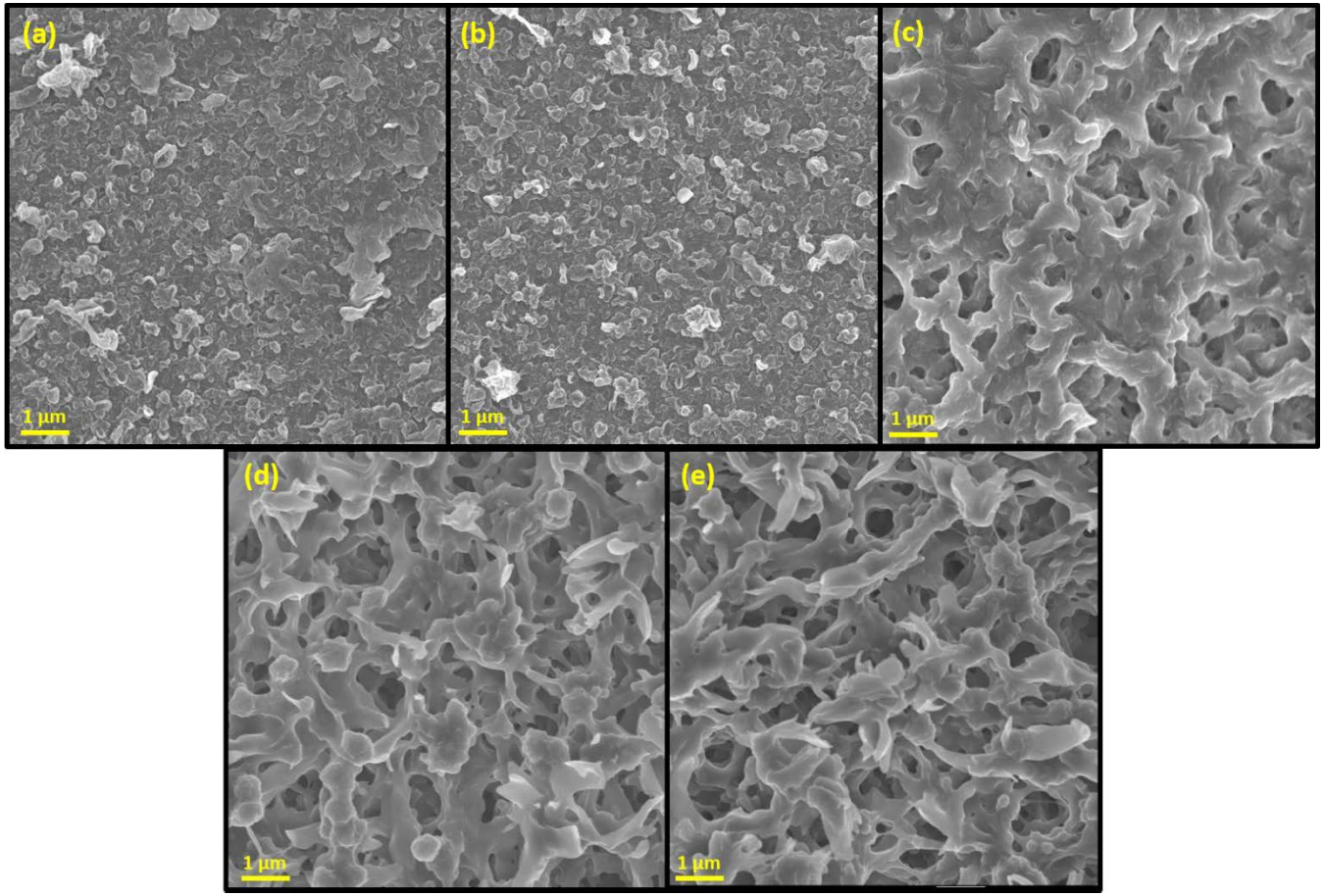

Figure 7.6 Polyamide selective layer surface FE-SEM images of the TFC membranes: (a) plain TFC, (b) sPDA-TFC, (c) nPDA-pH8-TFC, (d) nPDA-pH9-TFC, and (e) nPDA-pH10-TFC

7.3.3 Membrane intrinsic transport properties

Pure water permeability (*A*) and salt permeability (*B*) of the membrane samples were evaluated, and the membrane intrinsic transport properties can be seen in Table 7.4.

Table 7.4 Intrinsic transport properties of the TFC membranes

Membrane	*A* (L m^{-2} h^{-1} bar^{-1})	*B* (L m^{-2} h^{-1})	B/A (bar)	R (%)
TFC	1.36 ± 0.13	0.33 ± 0.05	0.24	97.5 ± 0.3
sPDA-TFC	2.12 ± 0.08	0.39 ± 0.12	0.18	98.3 ± 0.4
nPDA-pH8-TFC	2.58 ± 0.15	0.87 ± 0.18	0.34	95.3 ± 0.4
nPDA-pH9-TFC	2.76 + 0.19	1.08 ± 0.11	0.39	94.7 ± 0.6
nPDA-pH10-TFC	2.41 ± 0.23	1.44 ± 0.16	0.60	92.8 ± 0.8

The membranes exhibited higher water permeability upon PDA modification, when compared to the plain TFC membrane. There was also an increase in the water permeability upon increasing pH of the self-polymerization of dopamine from pH 8 to 9. However, the membrane modified with particulate PDA interlayer at pH 10 showed a sharp drop in the water permeability, which can most likely be explained by the surface pore blockage occurred due to the presence of the PDA nanoparticles (Choi et al. 2019). The highest *A* value of 2.76 L m^{-2} h^{-1} bar^{-1} was observed for the sample nPDA-pH9-TFC. The increase in the water permeability is likely caused by the satisfactory coating on top of the membrane surface, without blocking the porous structure of the polyketone, while enhancing the surface hydrophilicity, and the presence of higher free volume of the looser polyamide thin film.

The increase in water permeability was expected to be met with a likewise increase in solute permeability. The membranes with thinner and denser selective layers exhibited high solute rejection values, while those with looser, less cross-linked, and quite thicker polyamide layers exhibited a decrease in rejection and increase in solute permeability.

7.3.4 Membrane osmotic performance and energy generation capability

Membrane performance during PRO operation was evaluated using DI water and 1.0 M NaCl as the FS and DS, respectively. Figure 7.7 shows the water flux, specific reverse salt flux (J_s/J_w, g L^{-1}), and power density (W m^{-2}) of the TFC membranes. Water flux dramatically increased upon the introduction of the PDA interlayer, indicating the enhanced hydrophilicity of the membrane substrate, which facilitated water transport. The highly hydrophilic nature of the intermediate layer complemented the microporous structure of the polyketone membrane substrate, thereby resulting in better water transport during osmotic operation. Consistently with the pure water permeability data, nPDA-pH9-TFC showed the highest initial water flux of 40.8 L m^{-2} h^{-1}, with a sharp flux decline at nPDA-pH10-TFC.

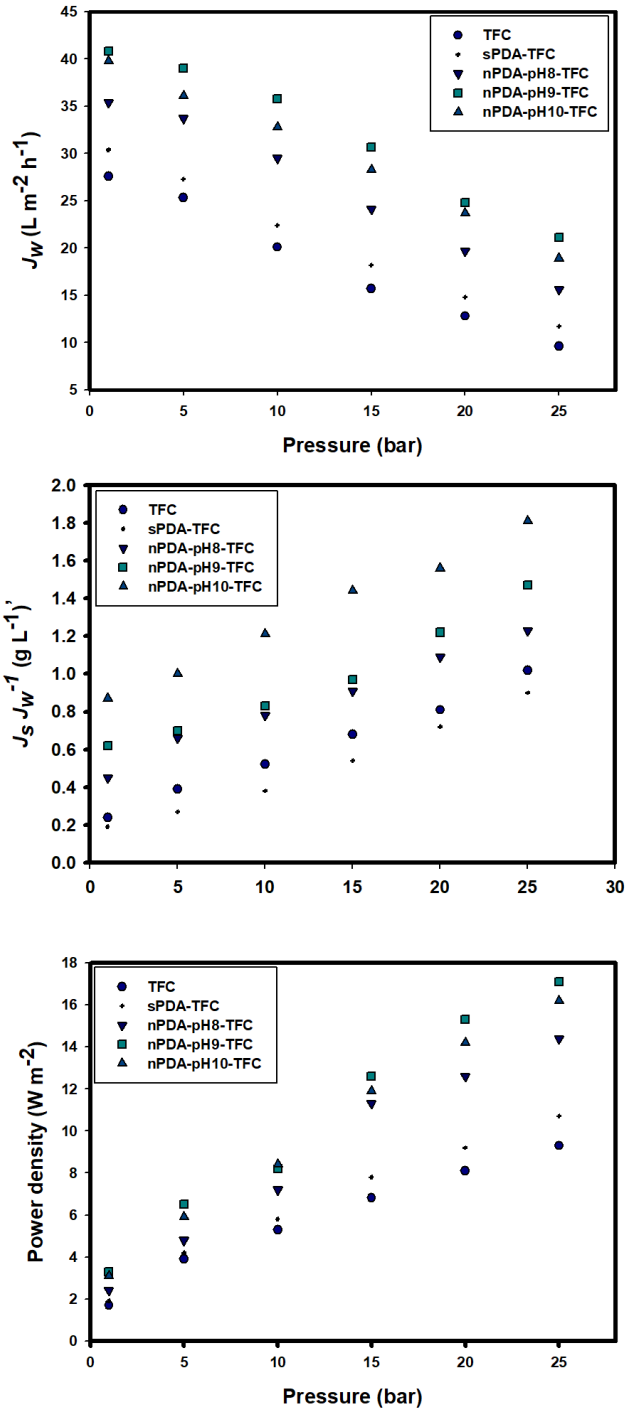

Figure 7.7 Osmotic performance, in terms of water flux (J_w), specific reverse salt flux (J_s/J_w), and power density, of the TFC membranes during PRO operation at different applied hydraulic pressures using DI water as FS and 1.0 M NaCl as DS

The introduction of nanoparticulate PDA intermediate layer and the subsequent production of looser polyamide selective layer caused decline of the membrane selectivity and an increase of reverse salt diffusion during PRO operation. These were not observed for the plain TFC membrane and the smooth PDA interlayer-modified TFC membrane, which both exhibited specific reverse salt flux values lower than 0.3 g L^{-1} for osmotic operation at minimal applied hydraulic pressure. With the formation of looser polyamide atop the nanoparticulate PDA intermediate layer, even at minimal applied hydraulic pressure, the specific reverse salt flux increased dramatically to 0.45 g L^{-1} for nPDA-pH8-TFC and increased to 0.87 g L^{-1} for nPDA-pH10-TFC. As applied pressure increased during PRO operation, the specific reverse salt flux values were observed to increase as well. The formation of nanoparticulate PDA intermediate layer significantly affected the selectivity of the TFC membranes; thus, the PDA nanoparticle formation should be optimized to enhance the water permeability, without sacrificing the membrane selectivity which may cause considerable loss of osmotic driving force by severe concentration polarization during operation.

In terms of power density, the highest power density of 17.1 W m^{-2} was obtained from nPDA-pH-9-TFC at an applied hydraulic pressure of 25 bar. The increase in the power density was dramatic compared to that of the plain TFC membrane, whose power density at 25 bar was 8.6 W m^{-2}. In this study, the maximum power density has yet to be achieved, as the membrane mechanical strength hindered the use of the PRO TFC membranes at applied hydraulic pressures over 25 bar.

7.4 Conclusions

In this study, PDA intermediate layer was formed in between the aliphatic polyketone membrane substrate and the polyamide selective layer of a PRO TFC membrane. Two types of PDA interlayer were formed and compared: the conventional smooth PDA and particulate PDA. Furthermore, the effect of pH during the self-polymerization of dopamine was investigated and evaluated in terms of the ease of PDA nanoparticle formation and its subsequent effect to the polyamide formation during interfacial polymerization and the membrane performance during PRO process operation. The following conclusions can be drawn from this study:

1. The morphology of the PDA intermediate layer significantly influences the formation of polyamide selective layer. Both the pristine TFC and sPDA-TFC (modified with smooth PDA interlayer) membranes exhibited highly dense and thinner polyamide layer, while those with the particulate PDA interlayer were observed to have formed looser and quite thicker polyamide layers.
2. Not only does the structure of the polyamide selective layer was affected by the intermediate layer morphology, the membrane performance was likewise affected. Introduction of the particulate PDA interlayer created more free volume and transport channels, which compensated the pore-blocking phenomenon of the nano-sized PDA particles. This resulted in higher water permeability for nPDA-pH8-TFC and nPDA-pH9-TFC. However, for nPDA-pH10-TFC, the more alkaline environment during dopamine self-polymerization resulted in better nucleation of the PDA nanoparticles, which as evidenced by the membrane characterization techniques.

3. The looser polyamide selective layer formed on top of the particulate PDA intermediate layer also led to slight decrease in the membrane selectivity, compared with the pristine and sPDA-TFC samples.
4. The membrane performance was evaluated using deionized water and 1.0 M NaCl as FS and DS, respectively. The TFC membrane with nanoparticulate PDA layer formed at pH 9.0 exhibited the best initial water flux of 40.8 L m^{-2} h^{-1}, and this membrane also showed the highest power density of 17.1 W m^{-2} at 25 bar.

This study was able to prove that a simple, facile, and versatile technique such as the ammonia-initialized introduction of nanoparticulate PDA intermediate layer, at controlled conditions, could significantly improve the water transport properties of a TFC membrane, while maintaining satisfactory rejection ability.

8 Conclusions and recommendations

8.1 Conclusions

In the first study, novel PET open mesh fabric-reinforced SNW-1 COF-incorporated TFN PRO membranes were fabricated in this study. The mode of incorporation of SNW-1 was also investigated using two different precursors of the interfacial polymerisation process. Incorporation of the porous and hydrophilic nanomaterial resulted in significant enhancement of the surface hydrophilicity and water flux of the TFN membranes, due to the hydrophilic secondary amine functional groups of SNW-1. Maximum pure water permeability was 3.87 $Lm^{-2}h^{-1}bar^{-1}$ for the membrane with 0.1 wt% SNW-1 incorporated through the MPD solution. 0.02 wt% was the optimum loading of the nanomaterial, beyond which the loading affects the stability of the membrane at higher applied pressures. The highest water flux and power density for the membrane incorporated with 0.02 wt% SNW-1 through MPD were 42.5 $Lm^{-2}h^{-1}$ and 12.1 Wm^{-2} (at 20 bar), respectively.

In the second study, a hydrophobic porous polymer nanomaterial, PP, was functionalised using chlorosulfonic acid to form sulfonate-functionalised PP-SO_3H with hydrophilic properties. PP-SO_3H was incorporated in the polyamide layer on PES hollow fibre membrane substrate to develop TFN PRO membranes. The incorporation of functionalised nanomaterials, such as PP-SO_3H, in the polyamide layer effectively modifies the surface chemistry of the selective layer of the osmotic membrane. The TFN membrane with 0.002 wt% of PP-SO_3H loading showed the highest J_w of 46.3 L m^{-2} h^{-1}, with a J_s/J_w value of 0.4 g L^{-1}, using 1.0 M NaCl and DI water as draw and feed,

respectively. The *W* value of the best performing PRO membrane was 14.6 Wm^{-2}, obtained at 17.5 bar.

Chlorine oxidation of the TFC membrane surface can lead to degradation of the polyamide selective layer. However, the antagonistic effects of chlorine oxidative degradation can be controlled when performed under optimal conditions, after which, the membranes will exhibit enhancement in permeability, without sacrificing mechanical strength and solute rejection, to obtain a higher extractable osmotic energy from PRO membranes. Significant increase in water flux and power density values were observed for membranes subjected to chlorine oxidation. Mechanical defects and polyamide degradation cause the enhanced water and solute permeability of the membranes. Downstream heat treatment of the membranes will further cause bond cleavage on the polyamide structure.

In the last chapter, PDA intermediate layer was formed in between the aliphatic polyketone membrane substrate and the polyamide selective layer of a PRO TFC membrane. Two types of PDA interlayer were formed and compared: the conventional smooth PDA and particulate PDA. Furthermore, the effect of pH during the self-polymerisation of dopamine was investigated and evaluated in terms of the ease of PDA nanoparticle formation and its subsequent effect to the polyamide formation during interfacial polymerisation and the membrane performance during PRO operation. The morphology of the PDA intermediate layer heavily influences the formation of polyamide. Both the pristine TFC and sPDA-TFC (modified with smooth PDA interlayer) membranes exhibited highly dense and thinner polyamide, whilst those with the particulate PDA interlayer was observed to have formed looser and quite thicker polyamide layers. The

highest initial water flux of 40.8 L m^{-2} h^{-1} was observed for the nPDA-pH9-TFC sample. After PRO operation at an applied hydraulic pressure of 25 bar, the highest power density of 17.1 W m^{-2} was likewise achieved by nPDA-pH9-TFC.

This thesis was able to demonstrate, through the four technical chapters, that engineering of the polyamide selective layer of the TFC membrane could significantly enhance the membrane osmotic performance and salinity gradient energy generation capacity. The techniques presented in this thesis, (1) nanomaterial incorporation, (2) surface functionalisation, (3) chlorine oxidation, and (4) introduction of nanoparticulate intermediate layer, were all proven to be simple, facile, and versatile techniques to improve the water transport properties and power density of the TFC membrane, while maintaining satisfactory rejection ability.

8.2 Comparison with commercial PRO membrane standard and comparison of techniques in this thesis

Four different techniques were performed to develop the set of new PRO TFC membranes presented in this thesis. The goal of the different techniques employed was to develop membranes which are better than the current commercial PRO membrane, which can be used as the benchmarking standard to compare the membranes developed in this thesis with.

Toray, a company specialising in industrial products and polymer chemistry, has been among the biggest membrane manufacturers for osmotic processes. Toray was involved in the Japanese RO-PRO Mega-ton project, which was among the most recent efforts in commercialisation of PRO. In its effort to develop and commercialise its spiral wound module for PRO, it has made available its flat sheet PRO membrane for the purpose of preliminary studies and benchmark tests. In this thesis, the flat sheet TFC PRO membrane by Toray was used as the benchmark commercial membrane. Table 8.1 lists down the intrinsic transport properties and osmotic performance of the said membrane. It should be noted, however, that the Toray flat sheet TFC membrane used as a benchmark in this thesis belongs in the earlier generations of Toray flat sheet TFC PRO membranes. The company has since continued to develop the membrane and further enhance the membrane osmotic performance, but not necessarily reflected in the results shown.

Comparison of the intrinsic membrane transport properties and osmotic membrane performance of the membranes developed in this thesis with the commercial flat-sheet TFC membrane by Toray shows that the membranes developed in this thesis, regardless

of polyamide engineering technique, performed better than the commercial standard. However, it can also be noted that all the membranes developed marked lower selectivity compared with the commercial standard, reflecting the modifications performed on the polyamide selective layer which could affect the solute selectivity.

Comparing all the techniques performed in this thesis with each other offers interesting insights regarding the development of TFC membranes for PRO. In this study, nanomaterial incorporation, simultaneous nanomaterial incorporation and functionalisation, oxidative degradation, and introduction of intermediate layer were performed, and each technique proved to be highly versatile and effective in changing the TFC membrane properties and performance. Among the four techniques, the membranes treated with oxidative degradation showed the biggest enhancement in water permeability, with the optimised chlorine oxidative degradation conditions yielding an initial J_w of 84.7 L m^{-2} h^{-1}. This super-water permeability of the chlorine oxidized membrane, however, suffered from a severe decline in selectivity and mechanical strength, posting high reverse salt flux values and low burst pressures. Based on the results of this thesis, this particular method can be applied in future membrane development, should both ultra-high water permeability and low pressure PRO operation are desired, without special consideration for selectivity. This technique, considered highly simple and facile, is particularly useful for suggested PRO configurations, wherein simultaneous FS and DS mixing and pressure exchange and recovery are performed. The first two methods presented in this thesis, which both involved the incorporation of nano-sized porous polymeric fillers, both resulted in development of TFN membranes which provided enhanced permeability without a huge impact on the membrane selectivity,

granted that the nanomaterial loading was optimised. However, as the results from these two studies suggest, the osmotic performance of nanomaterial-incorporated TFN membranes highly depend on the water permeability of the membrane substrate, with the polyamide selective layer engineering merely supplementing the membrane performance. It is interesting to see how the incorporation of SNW-1 and PP-HSO_3 could further enhance the performance of a membrane whose substrate is mechanically-strong, highly porous and water permeable, and able to mitigate the performance-limiting effects of ICP. Other drawbacks of nanomaterial incorporation are (1) the underlying cost of nanomaterial synthesis, which could prove not to be economical and practical methods for PRO membrane development, especially for efforts towards commercialisation, and (2) the large-scale incorporation of the nanomaterial which ensures the uniform distribution of the nanomaterials on the polyamide selective layer. Despite these drawbacks, nanomaterial incorporation and functionalisation are still worth to be investigated, especially for their other advantages, which include ease of downstream modification and fouling mitigation. Lastly, the introduction of the PDA intermediate layer showed similar performance with the nanomaterial-incorporated ones; however, the ease of preparation and control of optimised conditions proved to be its biggest advantage. PDA was known to be a highly versatile and effective chemical agent to enhance the performance of membranes for a wide array of processes.

Table 8.1 Intrinsic transport properties and osmotic performance of commercial flat-sheet PRO TFC membrane by Toray, compared with those developed in this thesis

Parameter	Membrane				
	Toray TFC	**SNW TFN**	**PP TFN**	**Cl_2 TFC**	**PK-PDA TFC**
Intrinsic transport properties					
A **(L m^{-2} h^{-1} bar^{-1})**	1.23 ± 0.48	3.23	1.51		2.76
B **(L m^{-2} h^{-1})**	0.39 ± 0.12	1.20	0.65	Not	1.08
B/A **(bar)**	0.32 ± 0.04	0.38	0.43	determined	0.39
R **(%)**	96.2	94.7	93.5		94.7
Osmotic performance					
Initial J_w (at ΔP ~ 0 bar) (L m^{-2} h^{-1})	20.3 ± 2.4	42.46	46.3	84.7	40.8
Initial J_s/J_w (g L^{-1})	0.19 ± 0.06	0.21	0.37	1.81	0.61
Burst pressure (bar)	27	27	18	5	25
W_{max} (W m^{-2})	4.28	12.1	14.6	4.7	17.1

8.3 Recommendations

After establishing the methods presented in this thesis in effective engineering of the polyamide selective layer to enhance the osmotic and energy-harnessing properties and performance of PRO TFC membranes, the following are recommended for future studies on membrane development for PRO:

8.3.1 Development and optimisation of membrane substrate

As shown in the different studies included in this thesis, the morphology, mechanical properties, and chemical nature of the membrane substrate influence the performance of the membrane and the formation of the polyamide selective layer. Polyamide selective layer engineering techniques, such as nanomaterial incorporation or chemical grafting, can effectively enhance membrane performance, but not greatly, as these techniques can only improve the intrinsic separation and transport properties of the membrane substrate. Membrane substrate preparation optimisation and polyamide engineering should go hand in hand in order to develop the desired PRO TFC membrane with outstanding performance.

8.3.2 Larger-scale membrane development

All the membranes prepared in this thesis are laboratory-scale, designed for bench-scale PRO experiments. In the growing efforts for commercialisation and larger-scale demonstration of the PRO process, it is imperative to develop larger-scale PRO membrane modules, whether hollow fibre or flat sheet. The challenge is to apply the established polyamide engineering techniques presented in this thesis and devise a

streamlined method through which the said techniques can be applied in a larger-scale membrane development process. As mentioned in the literature review, modulation studies for PRO membranes have been ongoing; although, no significant progress has been marked since the demonstration of the RO-PRO pilot plants in Japan (Megaton) (Tanioka, Kurihara & Sakai 2018) and Korea (GMVP) (Lee, Park, et al. 2020), which both utilized early generations of PRO modules developed by membrane manufacturing companies. Other significant larger-scale module efforts have been reported, putting together more than 100 hollow fibres in a module (Chen et al. 2018). Aside from hollow fibre modules with high packing density, roll-to-roll manufacturing can also be performed for flat-sheet membranes.

8.3.3 Extended studies on controlled polyamide degradation via chemical treatment

In this thesis, oxidative degradation of polyamide via chemical treatment was performed using chlorine. Aside from chlorine, a number of other chemical agents can be utilized for controlled polyamide modification. Among these chemical agents are alcohols, ionic liquids, and deep eutectic solvents. All these chemical agents have shown chemical reactions which could alter the chemical makeup of the polyamide selective layer (Ankoliya, Mehta & Raval 2019; Meng et al. 2014; Zhang et al. 2017). It is expected that these chemical agents are not as destructive and disruptive as chlorine, which was used in the third study, but these agents are nonetheless interesting to investigate.

8.3.4 Other methods of nanomaterial and functional material incorporation

In the first two studies, SNW-1 and PP-HSO_3 were incorporated in the polyamide *via* delivery through the MPD precursor. Aside from *in situ* incorporation, nanomaterials and functional materials can also be used to modify the polyamide through surface grafting (Huang, Marsh, et al. 2016; Le et al. 2017; Zhao et al. 2012) and molecular layer-by-layer assembly (Choi et al. 2013; Liu et al. 2014; Tsai et al. 2020).

8.3.5 Evaluation of membrane integrity under chlorine cleaning regime

Following the results obtained from Chapter 6, it is interesting to use Cl_2 treatment as a standard cleaning regime for membranes and evaluation method of membrane integrity.

8.3.6 Use of developed membranes for niche PRO applications

All the membranes developed in this thesis were tested using model seawater brine (1.0 M NaCl) and DI water. It would be interesting to know the behaviour and performance of the membranes when other DS and FS are used. As earlier mentioned in the literature review, PRO can have a variety of niche applications, which can exhaust the power generation capacity of the process with the presence of two streams of varying salinities. FS used for PRO applications can vary from real river water, brackish water, irrigation water, or even wastewater. The DS, on the other hand, can be any stream with high salinity, such as real seawater, seawater brine, fertiliser, and oil-produced water.

References

A. Altaee, J.Z., A. A. Alanezi, G. Zaragoza 2017, 'Pressure retarded osmosis process for power generation: Feasibility, energy balance and controlling parameters', *Applied Energy*, vol. 206, pp. 303–11.

Abbasi-Garravand, E., Mulligan, C.N., Laflamme, C.B. & Clairet, G. 2016, 'Role of two different pretreatment methods in osmotic power (salinity gradient energy) generation', *Renewable Energy*, vol. 96, pp. 98-119.

Achilli, A., Cath, T.Y. & Childress, A.E. 2009, 'Power generation with pressure retarded osmosis: An experimental and theoretical investigation', *Journal of Membrane Science*, vol. 343, no. 1, pp. 42-52.

Achilli, A. & Childress, A.E. 2010, 'Pressure retarded osmosis: From the vision of Sidney Loeb to the first prototype installation - Review', *Desalination*, vol. 261, pp. 205-11.

Achilli, A., Prante, J.L., Hancock, N.T., Maxwell, E.B. & Childress, A.E. 2014, 'Experimental results from RO-PRO: A next generation system for low-energy desalination', *Environmental Science & Technology*, vol. 48, pp. 6437-43.

Adham, S., Hussain, A., Minier-Matar, J., Janson, A. & Sharma, R. 2018, 'Membrane applications and opportunities for water management in the oil & gas industry', *Desalination*, vol. 440, pp. 2-17.

Ahmad, N.A., Goh, P.S., Wong, K.C., Zulhairun, A.K. & Ismail, A.F. 2020, 'Enhancing desalination performance of thin film composite membrane through layer by layer assembly of oppositely charged titania nanosheet', *Desalination*, vol. 476, p. 114167.

Alsvik, I. & Hägg, M.-B. 2013, 'Pressure retarded osmosis and forward osmosis membranes: Materials and methods', *Polymers*, vol. 5, no. 1, p. 303.

Altaee, A. & Cipolina, A. 2019, 'Modelling and optimization of modular system for power generation from a salinity gradient', *Renewable Energy*, vol. 141, pp. 139-47.

Altaee, A. & Hilal, N. 2014, 'Dual-stage forward osmosis/pressure retarded osmosis process for hypersaline solutions and fracking wastewater treatment', *Desalination*, vol. 350, pp. 79-85.

Altaee, A., Palenzuela, P., Zaragoza, G. & AlAnezi, A.A. 2017, 'Single and dual stage closed-loop pressure retarded osmosis for power generation: Feasibility and performance', *Applied Energy*, vol. 191, pp. 328-45.

Altaee, A., Sharif, A., Zaragoza, G. & Hilal, N. 2014, 'Dual stage PRO process for power generation from different feed resources', *Desalination*, vol. 352, pp. 118-27.

Altaee, A., Zaragoza, G. & Sharif, A. 2014, 'Pressure retarded osmosis for power generation and seawater desalination: Performance analysis', *Desalination*, vol. 344, pp. 108-15.

Alvarez-Silva, O. & Osorio, A.F. 2015, 'Salinity gradient energy potential in Colombia considering site specific constraints', *Renewable Energy*, vol. 74, pp. 737-48.

Amini, M., Jahanshani, M. & Rahimpour, A. 2013, 'Synthesis of novel thin film nanocomposite (TFN) forward osmosis membranes using functionalized multi-walled carbon nanotubes', *Journal of Membrane Science*, vol. 435, pp. 233-41.

Ankoliya, D., Mehta, B. & Raval, H. 2019, 'Advances in surface modification techniques of reverse osmosis membrane over the years', *Separation Science and Technology*, vol. 54, no. 3, pp. 293-310.

Antony, A., Fudianto, R., Cox, S. & Leslie, G. 2010, 'Assessing the oxidative degradation of polyamide reverse osmosis membrane—Accelerated ageing with hypochlorite exposure', *Journal of Membrane Science*, vol. 347, no. 1, pp. 159-64.

Arena, J.T., Manickam, S.S., Reimund, K.K., Freeman, B.D. & McCutcheon, J.R. 2014, 'Solute and water transport in forward osmosis using polydopamine modified thin film composite membranes', *Desalination*, vol. 343, pp. 8-16.

Arena, J.T., McCloskey, B., Freeman, B.D. & McCutcheon, J.R. 2011, 'Surface modification of thin film composite membrane support layers with polydopamine: Enabling use of reverse osmosis membranes in pressure retarded osmosis', *Journal of Membrane Science*, vol. 375, no. 1, pp. 55-62.

Arias, F.J. & De Las Heras, S. 2020, 'Pool pressure-retarded osmosis', *International Journal of Energy Research*, vol. 44, no. 9, pp. 7841-5.

Attarde, D., Jain, M., Chaudhary, K. & Gupta, S.K. 2015, 'Osmotically driven membrane processes by using a spiral wound module — Modeling, experimentation and numerical parameter estimation', *Desalination*, vol. 361, pp. 81-94.

Bar-Zeev, E., Perreault, F., Straub, A.P. & Elimelech, M. 2015, 'Impaired performance of pressure-retarded osmosis due to irreversible biofouling', *Environmental Science & Technology*, vol. 49, no. 21, pp. 13050-8.

Belfer, S., Purinson, Y. & Kedem, O. 1998, 'Surface modification of commercial polyamide reverse osmosis membranes by radical grafting: An ATR-FTIR study', *Acta Polymerica*, vol. 49, no. 10-11, pp. 574-82.

Blankert, B., Kim, Y., Vrouwenvelder, H. & Ghaffour, N. 2020, 'Facultative hybrid RO-PRO concept to improve economic performance of PRO: Feasibility and maximizing efficiency', *Desalination*, vol. 478, p. 114268.

Brotzel, F., Chu, Y.C. & Mayr, H. 2007, 'Nucleophilicities of primary and secondary amines in water', *The Journal of Organic Chemistry*, vol. 72, no. 10, pp. 3679-88.

Bui, N.-N., Lind, M.L., Hoek, E.M.V. & McCutcheon, J.R. 2011, 'Electrospun nanofiber supported thin film composite membranes for engineered osmosis', *Journal of Membrane Science*, vol. 385-386, pp. 10-9.

Bui, N.-N. & McCutcheon, J.R. 2014, 'Nanofiber supported thin-film composite membrane for pressure-retarded osmosis', *Environmental Science & Technology*, vol. 48, pp. 4129-36.

Burheim, O.S., Liu, F., Sales, B.B., Schaetzle, O., Buisman, C.J.N. & Hamelers, H.V.M. 2012, 'Faster Time Response by the Use of Wire Electrodes in Capacitive Salinity Gradient Energy Systems', *The Journal of Physical Chemistry C*, vol. 116, no. 36, pp. 19203-10.

Cai, T., Li, X., Wan, C. & Chung, T.-S. 2016, 'Zwitterionic polymers grafted poly (ether sulfone) hollow fiber membranes and their antifouling behaviors for osmotic power generation', *Journal of Membrane Science*, vol. 497, pp. 142-52.

Cath, T.Y., Childress, A.E. & Elimelech, M. 2006a, 'Forward osmosis: Principles, applications, and recent developments', *Journal of Membrane Science*, vol. 281, pp. 70-87.

Cath, T.Y., Childress, A.E. & Elimelech, M. 2006b, 'Forward osmosis: Principles, applications, and recent developments: Review', *Journal of Membrane Science*, vol. 281, no. 2006, pp. 70-87.

Chae, H.S., Kim, M.Y., Park, H., Seo, J., Lim, J.S. & Kim, H.J. 2019, 'Modeling and simulation studies analyzing the pressure-retarded osmosis (PRO) and PRO-hybridized processes', *Energies*, vol. 12, no. 2.

Chae, S.H., Seo, J., Kim, J., Kim, Y.M. & Kim, J.H. 2018, 'A simulation study with a new performance index for pressure-retarded osmosis processes hybridized with seawater reverse osmosis and membrane distillation', *Desalination*, vol. 444, pp. 118-28.

Chandra, S., Kundu, T., Dey, K., Addicoat, M., Heine, T. & Banerjee, R. 2016, 'Interplaying Intrinsic and Extrinsic Proton Conductivities in Covalent Organic Frameworks', *Chemistry of Materials*, vol. 28, no. 5, pp. 1489-94.

Chekli, L., Phuntsho, S., Kim, J.E., Kim, J., Choi, J.Y., Choi, J.-S., Kim, S., Kim, J.H., Hong, S., Shon, J. & Shon, H.K. 2016, 'A comprehensive review of hybrid forward osmosis systems: Performance, applications and future prospects', *Journal of Membrane Science*, vol. 497, pp. 430-49.

Chekli, L., Phuntsho, S., Shon, H.K., Vigneswaran, S., Kandasamy, J. & Chanan, A. 2012, 'A review of draw solutes in forward osmosis process and their use in modern applications', *Desalination and Water Treatment*, vol. 43, pp. 167-84.

Chen, Q., Sun, F., Zhou, J., Lu, Y., Li, Y.-Y., Yu, H.-Y. & Gu, J.-S. 2019, 'Chlorine-resistant and internal-concentration-polarization-mitigated polyamide membrane via tethering poly(ethylene glycol) methacrylate', *Journal of Applied Polymer Science*, vol. 136, no. 20, p. 47406.

Chen, S.C., Amy, G.L. & Chung, T.-S. 2016, 'Membrane fouling and anti-fouling strategies using RO retentate from a municipal water recycling plant as the feed for osmotic power generation', *Water Research*, vol. 88, pp. 144-55.

Chen, S.C., Fu, X.Z. & Chung, T.-S. 2014, 'Fouling behaviors of polybenzimidazole (PBI)–polyhedral oligomeric silsesquioxane (POSS)/polyacrylonitrile (PAN) hollow fiber membranes for engineering osmosis processes', *Desalination*, vol. 335, no. 1, pp. 17-26.

Chen, S.C., Wan, C.F. & Chung, T.-S. 2015, 'Enhanced fouling by inorganic and organic foulants on pressure retarded osmosis (PRO) hollow fiber membranes under high pressures', *Journal of Membrane Science*, vol. 479, pp. 190-203.

Chen, Y., Alanezi, A.A., Zhou, J., Altaee, A. & Shaheed, M.H. 2019, 'Optimization of module pressure retarded osmosis membrane for maximum energy extraction', *Journal of Water Process Engineering*, vol. 32, pp. 100935-45.

Chen, Y., Liu, C., Setiawan, L., Wang, Y.-N., Hu, X. & Wang, R. 2017, 'Enhancing pressure retarded osmosis performance with low-pressure nanofiltration pretreatment: Membrane fouling analysis and mitigation', *Journal of Membrane Science*, vol. 543, pp. 114-22.

Chen, Y., Loh, C.H., Zhang, L., Setiawan, L., She, Q., Fang, W., Hu, X. & Wang, R. 2018, 'Module scale-up and performance evaluation of thin film composite hollow fiber membranes for pressure retarded osmosis', *Journal of Membrane Science*, vol. 548, pp. 398-407.

Chen, Y., Setiawan, L., Chou, S., Hu, X. & Wang, R. 2016, 'Identification of safe and stable operation conditions for pressure retarded osmosis with high performance hollow fiber membrane', *Journal of Membrane Science*, vol. 503, pp. 90-100.

Cheng, Z.L., Li, X. & Chung, T.-S. 2018, 'The forward osmosis-pressure retarded osmosis (FO-PRO) hybrid system: A new process to mitigate membrane fouling for sustainable osmotic power generation', *Journal of Membrane Science*, vol. 559, pp. 63-74.

Cheng, Z.L., Li, X., Feng, Y., Wan, C.F. & Chung, T.-S. 2017, 'Tuning water content in polymer dopes to boost the performance of outer-selective thin-film composite (TFC) hollow fiber membranes for osmotic power generation', *Journal of Membrane Science*, vol. 524, pp. 97-107.

Cheng, Z.L., Li, X., Liu, Y.D. & Chung, T.-S. 2016, 'Robust outer-selective thin-film composite polyethersulfone hollow fiber membranes with low reverse salt flux for renewable salinity-gradient energy generation', *Journal of Membrane Science*, vol. 506, pp. 119-29.

Chi, G., Hu, S., Yang, Y. & Chen, T. 2012, 'Response surface methodology with prediction uncertainty: A multi-objective optimisation approach', *Chemical Engineering Research and Design*, vol. 90, no. 9, pp. 1235-44.

Chi, X.-Y., Xia, B.-G., Xu, Z.-L. & Zhang, M.-X. 2018, 'Impact of cross-linked chitosan sublayer structure on the performance of TFC FO PAN nanofiber membranes', *ACS Omega*, vol. 3, no. 10, pp. 13009-19.

Cho, Y.H., Kim, S.D., Kim, J.F., Choi, H.-g., Kim, Y., Nam, S.-E., Park, Y.-I. & Park, H. 2019, 'Tailoring the porous structure of hollow fiber membranes for osmotic power generation applications via thermally assisted nonsolvent induced phase separation', *Journal of Membrane Science*, vol. 579, pp. 329-41.

Choi, H.-g., Shah, A.A., Nam, S.-E., Park, Y.-I. & Park, H. 2019, 'Thin-film composite membranes comprising ultrathin hydrophilic polydopamine interlayer with graphene oxide for forward osmosis', *Desalination*, vol. 449, pp. 41-9.

Choi, H.-g., Son, M. & Choi, H. 2017, 'Integrating seawater desalination and wastewater reclamation forward osmosis process using thin-film composite mixed matrix membrane with functionalized carbon nanotube blended polyethersulfone support layer', *Chemosphere*, vol. 185, no. Supplement C, pp. 1181-8.

Choi, W., Choi, J., Bang, J. & Lee, J.-H. 2013, 'Layer-by-layer assembly of graphene oxide nanosheets on polyamide membranes for durable reverse-osmosis applications', *ACS Applied Materials & Interfaces*, vol. 5, pp. 12510-9.

Choi, W., Jeon, S., Kwon, S.J., Park, H., Park, Y.-I., Nam, S.-E., Lee, P.S., Lee, J.S., Choi, J., Hong, S., Chan, E.P. & Lee, J.-H. 2017, 'Thin film composite reverse osmosis membranes prepared via layered interfacial polymerization', *Journal of Membrane Science*, vol. 527, pp. 121-8.

Choi, Y., Vigneswaran, S. & Lee, S. 2016, 'Evaluation of fouling potential and power density in pressure retarded osmosis (PRO) by fouling index', *Desalination*, vol. 389, no. Supplement C, pp. 215-23.

Chou, S., Shi, L., Wang, R., Tang, C.Y., Qiu, C. & Fane, A.G. 2010, 'Characteristics and potential applications of a novel forward osmosis hollow fiber membrane', *Desalination*, vol. 261, no. 3, pp. 365-72.

Chou, S., Wang, R. & Fane, A.G. 2013, 'Robust and high performance hollow fiber membranes for energy harvesting from salinity gradients by pressure retarded osmosis', *Journal of Membrane Science*, vol. 448, pp. 44-54.

Chou, S., Wang, R., Shi, L., She, Q., Tang, C. & Fane, A.G. 2012a, 'Thin-film composite hollow fiber membranes for pressure retarded osmosis (PRO) process with high power density', *Journal of Membrane Science*, vol. 389, pp. 25-33.
Chou, S., Wang, R., Shi, L., She, Q., Tang, C. & Fane, A.G. 2012b, 'Thin-film composite hollow fiber membranes for pressure retarded osmosis (PRO) process with high power density', *Journal of Membrane Science*, vol. 389, no. Supplement C, pp. 25-33.
Chun, Y., Mulcahy, D., Zou, L. & Kim, I.S. 2017, 'A short review of membrane fouling in forward osmosis processes', *Membranes*, vol. 7, no. 2, p. 30.
Chung, H.W., Banchik, L.D., Swaminathan, J. & Lienhard V, J.H. 2017, 'On the present and future economic viability of stand-alone pressure-retarded osmosis', *Desalination*, vol. 408, pp. 133-44.
Chung, T.-S., Li, X., Ong, R.C., Ge, Q., Wang, H. & Han, G. 2012, 'Emerging forward osmosis (FO) technologies and challenges ahead for clean water and clean energy applications', *Current Opinion in Chemical Engineering*, vol. 1, no. 3, pp. 246-57.
Chung, T.-S., Luo, L., Wan, C.F., Cui, Y. & Amy, G. 2015, 'What is next for forward osmosis (FO) and pressure retarded osmosis (PRO)', *Separation and Purification Technology*, vol. 156, pp. 856-60.
Chung, T.-S., Zhang, S., Wang, K.Y., Su, J. & Ling, M.M. 2012, 'Forward osmosis processes: Yesterday, today and tomorrow', *Desalination*, vol. 287, pp. 78-81.
Cui, Y., Liu, X.-Y. & Chung, T.-S. 2014, 'Enhanced osmotic energy generation from salinity gradients by modifying thin film composite membranes', *Chemical Engineering Journal*, vol. 242, pp. 195-203.
D. I. Kim, J.K., H. K. Shon, S. Hong 2015, 'Pressure retarded osmosis (PRO) for integrating seawater desalination and wastewater reclamation: Energy consumption and fouling', *Journal of Membrane Science* vol. 483, pp. 34–41.
D. Johnson, N.H. 2015, 'Characterisation and quantification of membrane surface properties using atomic force microscopy: A comprehensive review', *Desalination*, vol. 356, pp. 149–64.
Deng, L., Wang, Q., An, X., Li, Z. & Hu, Y. 2020, 'Towards enhanced antifouling and flux performances of thin-film composite forward osmosis membrane via constructing a sandwich-like carbon nanotubes-coated support', *Desalination*, vol. 479, p. 114311.
Ding, S.-Y. & Wang, W. 2013, 'Covalent organic frameworks (COFs): From design to applications', *Chemical Society Reviews*, vol. 42, no. 2, pp. 548-68.
Do, V.T., Tang, C.Y., Reinhard, M. & Leckie, J.O. 2012, 'Degradation of polyamide nanofiltration and reverse osmosis membranes by hypochlorite', *Environmental Science & Technology*, vol. 46, no. 2, pp. 852-9.
Donose, B.C., Sukumar, S., Pidou, M., Poussade, Y., Keller, J. & Gernjak, W. 2013, 'Effect of pH on the ageing of reverse osmosis membranes upon exposure to hypochlorite', *Desalination*, vol. 309, pp. 97-105.
Elimelech, M. & Phillip, W.A. 2011, 'The future of seawater desalination: Energy, technology, and the environment', *Science*, vol. 333, no. 6043, p. 712.
Emadzadeh, D., Lau, W.J. & Ismail, A.F. 2013, 'Synthesis of thin film nanocomposite forward osmosis membrane with enhancement in water flux without sacrificing salt rejection', *Desalination*, vol. 330, pp. 90-9.

Emadzadeh, D., Lau, W.J., Matsuura, T., Ismail, A.F. & Rahbari-Sisakht, M. 2014, 'Synthesis and characterization of thin film nanocomposite forward osmosis membrane with hydrophilic nanocomposite support to reduce internal concentration polarization', *Journal of Membrane Science*, vol. 449, pp. 74-85.

Emadzadeh, D., Lau, W.J., Matsuura, T., Rahbari-Sisakht, M. & Ismail, A.F. 2014, 'A novel thin film composite forward osmosis membrane prepared from PSf-TiO2 nanocomposite substrate for water desalination', *Chemical Engineering Journal*, vol. 237, pp. 70-80.

Ettori, A., Gaudichet-Maurin, E., Schrotter, J.-C., Aimar, P. & Causserand, C. 2011, 'Permeability and chemical analysis of aromatic polyamide based membranes exposed to sodium hypochlorite', *Journal of Membrane Science*, vol. 375, no. 1, pp. 220-30.

Fu, F.-J., Sun, S.-P., Zhang, S. & Chung, T.-S. 2014, 'Pressure retarded osmosis dual-layer hollow fiber membranes developed by co-casting method and ammonium persulfate (APS) treatment', *Journal of Membrane Science*, vol. 469, pp. 488-98.

Fu, F.-J., Zhang, S., Sun, S.-P., Wang, K.-Y. & Chung, T.-S. 2013, 'POSS-containing delamination-free dual-layer hollow fiber membranes for forward osmosis and osmotic power generation', *Journal of Membrane Science*, vol. 443, pp. 144-55.

Gai, W., Li, X., Xiong, J.Y., Wan, C.F. & Chung, T.-S. 2016, 'Evolution of micro-deformation in inner-selective thin film composite hollow fiber membranes and its implications for osmotic power generation', *Journal of Membrane Science*, vol. 516, pp. 104-12.

Gai, W., Zhao, D.L. & Chung, T.-S. 2018, 'Novel thin film composite hollow fiber membranes incorporated with carbon quantum dots for osmotic power generation', *Journal of Membrane Science*, vol. 551, pp. 94-102.

Gao, H., Chen, W., Xu, C., Liu, S., Tong, X. & Chen, Y. 2020, 'Two-dimensional Ti3C2Tx MXene/GO hybrid membranes for highly efficient osmotic power generation', *Environmental Science & Technology*, vol. 54, no. 5, pp. 2931-40.

Gao, X., Zou, X., Ma, H., Meng, S. & Zhu, G. 2014, 'Highly selective and permeable porous organic framework membrane for CO2 capture', *Advanced Materials*, vol. 26, no. 22, pp. 3644-8.

García-Pacheco, R., Landaburu-Aguirre, J., Lejarazu-Larrañaga, A., Rodríguez-Sáez, L., Molina, S., Ransome, T. & García-Calvo, E. 2019, 'Free chlorine exposure dose (ppm·h) and its impact on RO membranes ageing and recycling potential', *Desalination*, vol. 457, pp. 133-43.

Geise, G.M., Lee, H.-S., Miller, D.J., Freeman, B.D., McGrath, J.E. & Paul, D.R. 2010, 'Water purification by membranes: The role of polymer science', *Journal of Polymer Science Part B: Polymer Physics*, vol. 48, pp. 1685-718.

Gerstandt, K., Peinemann, K.V., Skilhagen, S.E., Thorsen, T. & Holt, T. 2008, 'Membrane processes in energy supply for an osmotic power plant', *Desalination*, vol. 224, no. 1, pp. 64-70.

Ghanbari, M., Emadzadeh, D., Lau, W.J., Matsuura, T., Davoody, M. & Ismail, A.F. 2015, 'Super hydrophilic TiO2/HNT nanocomposites as a new approach for fabrication of high performance thin film nanocomposite membranes for FO application', *Desalination*, vol. 371, pp. 104-14.

Gohil, J.M. & Suresh, A.K. 2017, 'Chlorine attack on reverse osmosis membranes: Mechanisms and mitigation strategies', *Journal of Membrane Science*, vol. 541, pp. 108-26.
Gonzales, R.R., Kim, J.S. & Kim, S.-H. 2019, 'Optimization of dilute acid and enzymatic hydrolysis for dark fermentative hydrogen production from the empty fruit bunch of oil palm', *International Journal of Hydrogen Energy*, vol. 44, no. 4, pp. 2191-202.
Gonzales, R.R. & Kim, S.-H. 2017, 'Dark fermentative hydrogen production following the sequential dilute acid pretreatment and enzymatic saccharification of rice husk', *International Journal of Hydrogen Energy*, vol. 42, no. 45, pp. 27577-83.
Gonzales, R.R., Kumar, G., Sivagurunathan, P. & Kim, S.-H. 2017, 'Enhancement of hydrogen production by optimization of pH adjustment and separation conditions following dilute acid pretreatment of lignocellulosic biomass', *International Journal of Hydrogen Energy*, vol. 42, no. 45, pp. 27502-11.
Gonzales, R.R., Park, M.J., Tijing, L., Han, D.S., Phuntsho, S. & Shon, H.K. 2018, 'Modification of nanofiber support layer for thin film composite forward osmosis membranes via layer-by-layer polyelectrolyte deposition', *Membranes*, vol. 8, no. 3, pp. 70-84.
Gonzales, R.R., Sivagurunathan, P. & Kim, S.-H. 2016, 'Effect of severity on dilute acid pretreatment of lignocellulosic biomass and the following hydrogen fermentation', *International Journal of Hydrogen Energy*, vol. 41, no. 46, pp. 21678-84.
Gonzales, R.R., Sivagurunathan, P., Parthiban, A. & Kim, S.-H. 2016, 'Optimization of substrate concentration of dilute acid hydrolyzate of lignocellulosic biomass in batch hydrogen production', *International Biodeterioration and Biodegradation*, vol. 113, pp. 22-7.
Greenlee, L.F., Lawler, D.F., Freeman, B.D., Marrot, B. & Moulin, P. 2009, 'Reverse osmosis desalination: Water sources, technology, and today's challenges', *Water Research*, vol. 43, pp. 2317-48.
Guo, H., Yao, Z., Wang, J., Yang, Z., Ma, X. & Tang, C.Y. 2018, 'Polydopamine coating on a thin film composite forward osmosis membrane for enhanced mass transport and antifouling performance', *Journal of Membrane Science*, vol. 551, pp. 234-42.
Guo, W., Ngo, H.-H. & Li, J. 2012, 'A mini-review on membrane fouling', *Bioresource Technology*, vol. 122, pp. 27-34.
Han, G., Cheng, Z.L. & Chung, T.-S. 2017, 'Thin-film composite (TFC) hollow fiber membrane with double-polyamide active layers for internal concentration polarization and fouling mitigation in osmotic processes', *Journal of Membrane Science*, vol. 523, pp. 497-504.
Han, G. & Chung, T.-S. 2014, 'Robust and high performance pressure retarded osmosis hollow fiber membranes for osmotic power generation', *AIChE Journal*, vol. 60, no. 3, pp. 1107-19.
Han, G., Liu, J.T., Lu, K.J. & Chung, T.-S. 2018, 'Advanced anti-fouling membranes for osmotic power generation from wastewater via pressure retarded osmosis (PRO)', *Environmental Science & Technology*, vol. 52, no. 11, pp. 6686-94.
Han, G., Wang, P. & Chung, T.-S. 2013, 'Highly robust thin-film composite pressure retarded osmosis (PRO) hollow fiber membranes with high power densities for renewable salinity-gradient energy generation', *Environmental Science & Technology*, vol. 47, no. 14, pp. 8070-7.

Han, G., Zhang, S., Li, X. & Chung, T.-S. 2013, 'High performance thin film composite pressure retarded osmosis (PRO) membranes for renewable salinity-gradient energy generation', *Journal of Membrane Science*, vol. 440, pp. 108-21.
Han, G., Zhang, S., Li, X. & Chung, T.-S. 2015, 'Progress in pressure retarded osmosis (PRO) membranes for osmotic power generation', *Progress in Polymer Science*, vol. 51, pp. 1-27.
Han, G., Zhang, S., Li, X., Widjojo, N. & Chung, T.-S. 2012, 'Thin film composite forward osmosis membranes based on polydopamine modified polysulfone substrates with enhancements in both water flux and salt rejection', *Chemical Engineering Science*, vol. 80, pp. 219-31.
Han, G., Zhou, J., Wan, C., Yang, T. & Chung, T.-S. 2016, 'Investigations of inorganic and organic fouling behaviors, antifouling and cleaning strategies for pressure retarded osmosis (PRO) membrane using seawater desalination brine and wastewater', *Water Research*, vol. 103, pp. 264-75.
Han, G., Zuo, J., Wan, C. & Chung, T.-S. 2015, 'Hybrid pressure retarded osmosis-membrane distillation (PRO-MD) process for osmotic power and clean water generation', *Environmental Science: Water Research & Technology*, vol. 1, no. 4, pp. 507-15.
He, W., Wang, Y. & Shaheed, M.H. 2015, 'Enhanced energy generation and membrane performance by two-stage pressure retarded osmosis (PRO)', *Desalination*, vol. 359, pp. 186-99.
Hegab, H.M., ElMekawy, A., Barclay, T.G., Michelmore, A., Zou, L., Saint, C.P. & Ginic-Markovic, M. 2015, 'Fine-tuning the surface of forward osmosis membranes via grafting graphene oxide: Performance patterns and biofouling propensity', *ACS Applied Materials & Interfaces*, vol. 7, no. 32, pp. 18004-16.
Helfer, F., Lemckert, C. & Anissimov, Y.G. 2014, 'Osmotic power with pressure retarded osmosis: Theory, performance and trends – A review', *Journal of Membrane Science*, vol. 453, pp. 337-58.
Hickenbottom, K.L., Vanneste, J. & Cath, T.Y. 2016, 'Assessment of alternative draw solutions for optimized performance of a closed-loop osmotic heat engine', *Journal of Membrane Science*, vol. 504, pp. 162-75.
Higa, M., Shigefuji, D., Shibuya, M., Izumikawa, S., Ikebe, Y., Yasukawa, M., Endo, N. & Tanioka, A. 2017, 'Experimental study of a hollow fiber membrane module in pressure-retarded osmosis: Module performance comparison with volumetric-based power outputs', *Desalination*, vol. 420, pp. 45-53.
Huang, L., Arena, J.T., Meyering, M.T., Hamlin, T.J. & McCutcheon, J.R. 2016, 'Tailored multi-zoned nylon 6,6 supported thin film composite membranes for pressure retarded osmosis', *Desalination*, vol. 399, pp. 96-104.
Huang, X., Marsh, K.L., McVerry, B.T., Hoek, E.M.V. & Kaner, R.B. 2016, 'Low-fouling antibacterial reverse osmosis membranes via surface grafting of graphene oxide', *ACS Applied Materials & Interfaces*, vol. 8, no. 23, pp. 14334-8.
Idarraga-Mora, J.A., Ladner, D.A. & Husson, S.M. 2018, 'Thin-film composite membranes on polyester woven mesh with variable opening size for pressure-retarded osmosis', *Journal of Membrane Science*, vol. 549, pp. 251-9.

Ingole, P.G., Choi, W., Kim, K.-H., Jo, H.-D., Choi, W.-K., Park, J.-S. & Lee, H.-K. 2014, 'Preparation, characterization and performance evaluations of thin film composite hollow fiber membrane for energy generation', *Desalination*, vol. 345, pp. 136-45.
Ingole, P.G., Choi, W., Kim, K.H., Park, C.H., Choi, W.K. & Lee, H.K. 2014, 'Synthesis, characterization and surface modification of PES hollow fiber membrane support with polydopamine and thin film composite for energy generation', *Chemical Engineering Journal*, vol. 243, pp. 137-46.
Ingole, P.G., Kim, K.H., Park, C.H., Choi, W.K. & Lee, H.K. 2014, 'Preparation, modification and characterization of polymeric hollow fiber membranes for pressure-retarded osmosis', *RSC Advances*, vol. 4, no. 93, pp. 51430-9.
International Renewable Energy Agency, I. 2014, *Salinity Gradient Energy*, International Renewable Energy Agency, Abu Dhabi.
Janson, A., Dardor, D., Al Maas, M., Minier-Matar, J., Abdel-Wahab, A. & Adham, S. 2020, 'Pressure-retarded osmosis for enhanced oil recovery', *Desalination*, vol. 491, p. 114568.
Jellinek, H.H.G. & Masuda, H. 1981, 'Osmo-power. Theory and performance of an osmo-power pilot plant', *Ocean Engineering*, vol. 8, no. 2, pp. 103-28.
Jiang, J.-H., Zhu, L.-P., Zhang, H.-T., Zhu, B.-K. & Xu, Y.-Y. 2014, 'Improved hydrodynamic permeability and antifouling properties of poly(vinylidene fluoride) membranes using polydopamine nanoparticles as additives', *Journal of Membrane Science*, vol. 457, pp. 73-81.
K. Yang, Z.L., H. Zhang, J. Qian, G. Chen 2010, 'Municipal wastewater phosphorus removal by coagulation', *J. Environ. Sci.*, vol. 31, pp. 601–9.
Kadhom, M., Hu, W. & Deng, B. 2017, 'Thin film nanocomposite membranes filled with metal-organic frameworks UiO-66 and MIL-125 nanoparticles for water desalination', *Membranes*, vol. 7, no. 2, p. 31.
Kalogirou, S.A. 2005, 'Seawater desalination using renewable energy sources', *Progress in Energy and Combustion Science*, vol. 31, no. 3, pp. 242-81.
Kang, G.-D., Gao, C.-J., Chen, W.-D., Jie, X.-M., Cao, Y.-M. & Yuan, Q. 2007, 'Study on hypochlorite degradation of aromatic polyamide reverse osmosis membrane', *Journal of Membrane Science*, vol. 300, no. 1, pp. 165-71.
Kang, Y., Obaid, M., Jang, J. & Kim, I.S. 2019, 'Sulfonated graphene oxide incorporated thin film nanocomposite nanofiltration membrane to enhance permeation and antifouling properties', *Desalination*, vol. 470, p. 114125.
Kim, D.I., Gonzales, R.R., Dorji, P., Gwak, G., Phuntsho, S., Hong, S. & Shon, H. 2020, 'Efficient recovery of nitrate from municipal wastewater via MCDI using anion-exchange polymer coated electrode embedded with nitrate selective resin', *Desalination*, vol. 484, p. 114425.
Kim, D.I., Kim, J. & Hong, S. 2016, 'Changing membrane orientation in pressure retarded osmosis for sustainable power generation with low fouling', *Desalination*, vol. 389, no. Supplement C, pp. 197-206.
Kim, D.I., Kim, J., Shon, H.K. & Hong, S. 2015, 'Pressure retarded osmosis (PRO) for integrating seawater desalination and wastewater reclamation: Energy consumption and fouling', *Journal of Membrane Science*, vol. 483, pp. 34-41.

Kim, H., Choi, J.S. & Lee, S. 2012, 'Pressure retarded osmosis for energy production: Membrane materials and operating conditions', *Water Science and Technology*, vol. 65, no. 10, pp. 1789-94.
Kim, J., Jeong, K., Park, M.J., Shon, H.K. & Kim, J.H. 2015, 'Recent advances in osmotic energy generation via pressure-retarded osmosis (PRO): A review', *Energies*, vol. 8, pp. 11821-45.
Kim, J., Park, M., Snyder, S.A. & Kim, J.H. 2013, 'Reverse osmosis (RO) and pressure retarded osmosis (PRO) hybrid processes: Model-based scenario study', *Desalination*, vol. 322, pp. 121-30.
Kim, J., Park, M.J., Park, M., Shon, H.K., Kim, S.-H. & Kim, J.H. 2016, 'Influence of colloidal fouling on pressure retarded osmosis', *Desalination*, vol. 389, pp. 207-14.
Kim, J., Suh, D., Kim, C., Baek, Y., Lee, B., Kim, H.J., Lee, J.-C. & Yoon, J. 2016, 'A high-performance and fouling resistant thin-film composite membrane prepared via coating TiO2 nanoparticles by sol-gel-derived spray method for PRO applications', *Desalination*, vol. 397, pp. 157-64.
Kim, J.H., Moon, S.J., Park, S.H., Cook, M., Livingston, A.G. & Lee, Y.M. 2018, 'A robust thin film composite membrane incorporating thermally rearranged polymer support for organic solvent nanofiltration and pressure retarded osmosis', *Journal of Membrane Science*, vol. 550, pp. 322-31.
Kim, S.W., Han, S.O., Sim, I.N., Cheon, J.Y. & Park, W.H. 2015, 'Fabrication and characterization of cellulose acetate/montmorillonite composite nanofibers by electrospinning', *Journal of Nanomaterials*, vol. 2015, pp. 1-8.
Kim, Y., Yang, E., Park, H. & Choi, H. 2020, 'Anti-biofouling effect of a thin film nanocomposite membrane with a functionalized-carbon-nanotube-blended polymeric support for the pressure-retarded osmosis process', *RSC Advances*, vol. 10, no. 10, pp. 5697-703.
Kim, Y.C. & Elimelech, M. 2012, 'Adverse impact of feed channel spacers on the performance of pressure retarded osmosis', *Environmental Science & Technology*, vol. 46, no. 8, pp. 4673-81.
Kim, Y.C. & Elimelech, M. 2013, 'Potential of osmotic power generation by pressure retarded osmosis using seawater as feed solution: Analysis and experiments', *Journal of Membrane Science*, vol. 429, pp. 330-7.
Kim, Y.C., Kim, Y., Oh, D. & Lee, K.H. 2013, 'Experimental investigation of a spiral-wound pressure-retarded osmosis membrane module for osmotic power generation', *Environmental Science & Technology*, vol. 47, no. 6, pp. 2966-73.
Kishimoto, M., Tanaka, Y., Yasukawa, M., Goda, S., Higa, M. & Matsuyama, H. 2019, 'Optimization of pressure-retarded osmosis with hollow-fiber membrane modules by numerical simulation', *Industrial & Engineering Chemistry Research*, vol. 58, no. 16, pp. 6687-95.
Kitagawa, S., Kitaura, R. & Noro, S.-i. 2004, 'Functional porous coordination polymers', *Angewandte Chemie International Edition*, vol. 43, no. 18, pp. 2334-75.
Klaysom, C., Cath, T.Y., Depuydt, T. & Vankelecom, I.F.J. 2013, 'Forward and pressure retarded osmosis: potential solutions for global challenges in energy and water supply', *Chemical Society Reviews*, vol. 42, no. 16, pp. 6959-89.
Kruyt, B., van Vuuren, D.P., de Vries, H.J.M. & Groenenberg, H. 2009, 'Indicators for energy security', *Energy Policy*, vol. 37, no. 6, pp. 2166-81.

Kurihara, M., Sakai, H., Tanioka, A. & Tomioka, H. 2016, 'Role of pressure-retarded osmosis (PRO) in the mega-ton water project', *Desalination and Water Treatment*, vol. 57, no. 55, pp. 26518-28.
Kwon, S.J., Park, K., Kim, D.Y., Zhan, M., Hong, S. & Lee, J.-H. 2021, 'High-performance and durable pressure retarded osmosis membranes fabricated using hydrophilized polyethylene separators', *Journal of Membrane Science*, vol. 619, p. 118796.
Kwon, S.J., Park, S.-H., Shin, M.G., Park, M.S., Park, K., Hong, S., Park, H., Park, Y.-I. & Lee, J.-H. 2019, 'Fabrication of high performance and durable forward osmosis membranes using mussel-inspired polydopamine-modified polyethylene supports', *Journal of Membrane Science*, vol. 584, pp. 89-99.
Le, N.L., Bettahalli, N., Nunes, S.P. & Chung, T.-S. 2016, 'Outer-selective thin film composite (TFC) hollow fiber membranes for osmotic power generation', *Journal of Membrane Science*, vol. 505, pp. 157-66.
Le, N.L., Quilitzsch, M., Cheng, H., Hong, P.-Y., Ulbricht, M., Nunes, S.P. & Chung, T.-S. 2017, 'Hollow fiber membrane lumen modified by polyzwitterionic grafting', *Journal of Membrane Science*, vol. 522, pp. 1-11.
Lee, C., Chae, S.H., Yang, E., Kim, S., Kim, J.H. & Kim, I.S. 2020, 'A comprehensive review of the feasibility of pressure retarded osmosis: Recent technological advances and industrial efforts towards commercialization', *Desalination*, vol. 491, p. 114501.
Lee, E.S.H., Xiong, J.Y., Han, G., Wan, C.F., Chong, Q.Y. & Chung, T.-S. 2017, 'A pilot study on pressure retarded osmosis operation and effective cleaning strategies', *Desalination*, vol. 420, pp. 273-82.
Lee, H., Dellatore, S.M., Miller, W.M. & Messersmith, P.B. 2007, 'Mussel-inspired surface chemistry for multifunctional coatings', *Science*, vol. 318, no. 5849, p. 426.
Lee, J.-G., Kim, Y.-D., Shim, S.-M., Im, B.-G. & Kim, W.-S. 2015, 'Numerical study of a hybrid multi-stage vacuum membrane distillation and pressure-retarded osmosis system', *Desalination*, vol. 363, pp. 82-91.
Lee, J.-H., Chung, J.Y., Chan, E.P. & Stafford, C.M. 2013, 'Correlating chlorine-induced changes in mechanical properties to performance in polyamide-based thin film composite membranes', *Journal of Membrane Science*, vol. 433, pp. 72-9.
Lee, K.L., Baker, R.W. & Lonsdale, H.K. 1981, 'Membranes for power generation by pressure-retarded osmosis', *Journal of Membrane Science*, vol. 8, no. 2, pp. 141-71.
Lee, S., Kim, S.-H. & Park, Y.-G. 2018, 'High-Salinity Pressure Retarded Osmosis Using Seawater Reverse Osmosis Brine', in S. Sarp & N. Hilal (eds), *Membrane-Based Salinity Gradient Processes for Water Treatment and Power Generation*, Elsevier.
Lee, S., Kim, Y.C., Park, S.-J., Lee, S.-K. & Choi, H.-C. 2016, 'Experiment and modeling for performance of a spiral-wound pressure-retarded osmosis membrane module', *Desalination and Water Treatment*, vol. 57, no. 22, pp. 10101-10.
Lee, S., Park, T.-s., Park, Y.-G., Lee, W.-i. & Kim, S.-H. 2020, 'Toward scale-up of seawater reverse osmosis (SWRO) – pressure retarded osmosis (PRO) hybrid system: A case study of a 240 m3/day pilot plant', *Desalination*, vol. 491, p. 114429.
Li, J., Wang, X., Chen, G., Li, D., Zhou, Y., Yang, X. & Wang, J. 2015, 'Hypercrosslinked organic polymer based carbonaceous catalytic materials: Sulfonic acid

functionality and nano-confinement effect', *Applied Catalysis B: Environmental*, vol. 176-177, pp. 718-30.
Li, J.L., Zhang, Y., Zhang, S., Liu, M., Li, X. & Cai, T. 2019, 'Hyperbranched poly(ionic liquid) functionalized poly(ether sulfone) membranes as healable antifouling coatings for osmotic power generation', *Journal of Materials Chemistry A*, vol. 7, pp. 8167-76.
Li, X.-M., He, T., Dou, P. & Zhao, S. 2010, *Forward Osmosis and Forward Osmosis Membranes*, Elsevier.
Li, X., Cai, T., Amy, G.L. & Chung, T.-S. 2017, 'Cleaning strategies and membrane flux recovery on anti-fouling membranes for pressure retarded osmosis', *Journal of Membrane Science*, vol. 522, pp. 116-23.
Li, X., Cai, T. & Chung, T.-S. 2014, 'Anti-fouling behavior of hyperbranched polyglycerol-grafted poly(ether sulfone) hollow fiber membranes for osmotic power generation', *Environmental Science & Technology*, vol. 48, no. 16, pp. 9898-907.
Li, X. & Chung, T.-S. 2014, 'Thin-film composite P84 co-polyimide hollow fiber membranes for osmotic power generation', *Applied Energy*, vol. 114, pp. 600-10.
Li, X., Zhang, S., Fu, F. & Chung, T.-S. 2013, 'Deformation and reinforcement of thin-film composite (TFC) polyamide-imide (PAI) membranes for osmotic power generation', *Journal of Membrane Science*, vol. 434, pp. 204-17.
Li, Y., Qi, S., Wang, Y., Setiawan, L. & Wang, R. 2017, 'Modification of thin film composite hollow fiber membranes for osmotic energy generation with low organic fouling tendency', *Desalination*, vol. 424, pp. 131-9.
Li, Y., Su, Y., Zhao, X., He, X., Zhang, R., Zhao, J., Fan, X. & Jiang, Z. 2014, 'Antifouling, high-flux nanofiltration membranes enabled by dual functional polydopamine', *ACS Applied Materials & Interfaces*, vol. 6, no. 8, pp. 5548-57.
Li, Y., Wang, R., Qi, S. & Tang, C.Y. 2015, 'Structural stability and mass transfer properties of pressure retarded osmosis (PRO) membrane under high operating pressures', *Journal of Membrane Science*, vol. 488, pp. 142-53.
Li, Y., Zhao, S., Setiawan, L., Zhang, L. & Wang, R. 2018, 'Integral hollow fiber membrane with chemical cross-linking for pressure retarded osmosis operated in the orientation of active layer facing feed solution', *Journal of Membrane Science*, vol. 550, pp. 163-72.
Li, Y., Zhao, Y., Tian, E. & Ren, Y. 2018, 'Preparation and characterization of novel forward osmosis membrane incorporated with sulfonated carbon nanotubes', *RSC Advances*, vol. 8, no. 71, pp. 41032-9.
Lim, S., Park, M.J., Phuntsho, S., Mai-Prochnow, A., Murphy, A.B., Seo, D. & Shon, H. 2018, 'Dual-layered nanocomposite membrane incorporating graphene oxide and halloysite nanotube for high osmotic power density and fouling resistance', *Journal of Membrane Science*, vol. 564, pp. 382-93.
Lim, S., Park, M.J., Phuntsho, S., Tijing, L.D., Nisola, G.M., Shim, W.-G., Chung, W.-J. & Shon, H.K. 2017, 'Dual-layered nanocomposite substrate membrane based on polysulfone/graphene oxide for mitigating internal concentration polarization in forward osmosis', *Polymer*, vol. 110, pp. 36-48.
Lin, S., Straub, A.P. & Elimelech, M. 2014, 'Thermodynamic limits of extractable energy by pressure retarded osmosis', *Energy & Environmental Science*, vol. 7, no. 8, pp. 2706-14.

Lin, S., Yip, N.Y., Cath, T.Y., Osuji, C.O. & Elimelech, M. 2014, 'Hybrid pressure retarded osmosis–membrane distillation system for power generation from low-grade heat: Thermodynamic analysis and energy efficiency', *Environmental Science & Technology*, vol. 48, no. 9, pp. 5306-13.
Liu, C., Li, X., Liu, T., Liu, Z., Li, N., Zhang, Y. & Xiao, C. 2016, 'Microporous CA/PVDF membranes based on electrospun nanofibers with controlled crosslinking induced by solvent vapor', *Journal of Membrane Science*, vol. 2016, pp. 1-12.
Liu, L., Son, M., Park, H., Celik, E., Bhattacharjee, C. & Choi, H. 2014, 'Efficacy of CNT-bound polyelectrolyte membrane by spray-assisted layer-by-layer (LbL) technique on water purification', *RSC Advances*, vol. 4, pp. 32858-65.
Liu, T.-Y., Yuan, H.-G., Liu, Y.-Y., Ren, D., Su, Y.-C. & Wang, X. 2018, 'Metal-organic framework nanocomposite thin films with interfacial bindings and self-standing robustness for high water flux and enhanced ion selectivity', *ACS Nano*.
Liu, X., Foo, L.-X., Li, Y., Lee, J.-Y., Cao, B. & Tang, C.Y. 2016, 'Fabrication and characterization of nanocomposite pressure retarded osmosis (PRO) membranes with excellent anti-biofouling property and enhanced water permeability', *Desalination*, vol. 389, pp. 137-48.
Liu, X., Qi, S., Li, Y., Yang, L., Cao, B. & Tang, C.Y. 2013, 'Synthesis and characterization of novel antibacterial silver nanocomposite nanofiltration and forward osmosis membranes based on layer-by-layer assembly', *Water Research*, vol. 47, no. 9, pp. 3081-92.
Loeb, S. 1975, *Method and apparatus for generating power utilizing pressure-retarded-osmosis*, United States.
Loeb, S. 1976, 'Production of energy from concentrated brines by pressure-retarded osmosis: I. Preliminary technical and economic correlations', *Journal of Membrane Science*, vol. 1, pp. 49-63.
Loeb, S. 1981, 'The Loeb-Sourirajan Membrane: How It Came About', *Synthetic Membranes:*, vol. 153, AMERICAN CHEMICAL SOCIETY, pp. 1-9.
Loeb, S. 1998, 'Energy production at the Dead Sea by pressure-retarded osmosis: challenge or chimera?', *Desalination*, vol. 120, no. 3, pp. 247-62.
Loeb, S. 2001, 'One hundred and thirty benign and renewable megawatts from Great Salt Lake? The possibilities of hydroelectric power by pressure-retarded osmosis', *Desalination*, vol. 141, no. 1, pp. 85-91.
Loeb, S. 2002, 'Large-scale power production by pressure-retarded osmosis, using river water and sea water passing through spiral modules', *Desalination*, vol. 143, no. 2, pp. 115-22.
Loeb, S. & Mehta, G.D. 1978, 'A two-coefficient water transport equation for pressure-retarded osmosis', *Journal of Membrane Science*, vol. 4, pp. 351-62.
Loeb, S. & Norman, R.S. 1975, 'Osmotic power plants', *Science*, vol. 189, no. 4203, p. 654.
Loeb, S., Van Hessen, F. & Shahaf, D. 1976, 'Production of energy from concentrated brines by pressure-retarded osmosis: II. Experimental results and projected energy costs', *Journal of Membrane Science*, vol. 1, pp. 249-69.
Logan, B.E. & Elimelech, M. 2012, 'Membrane-based processes for sustainable power generation using water', *Nature*, vol. 488, p. 313.

Lu, W., Yuan, D., Sculley, J., Zhao, D., Krishna, R. & Zhou, H.C. 2011, 'Sulfonate-grafted porous polymer networks for preferential CO2 adsorption at low pressure', *J Am Chem Soc*, vol. 133, no. 45, pp. 18126-9.

Lv, Y., Du, Y., Qiu, W.-Z. & Xu, Z.-K. 2017, 'Nanocomposite membranes via the codeposition of polydopamine/ polyethylenimine with silica nanoparticles for enhanced mechanical strength and high water permeability', *ACS Applied Materials & Interfaces*, vol. 9, no. 3, pp. 2966-72.

Ma, D., Peh, S.B., Han, G. & Chen, S.B. 2017, 'Thin-film nanocomposite membranes incorporated with super-hydrophilic metal-organic framework (MOF) UiO-66: Toward enhancement of water flux and salt rejection', *ACS Applied Materials & Interfaces*, vol. 9, no. 8, pp. 7523-34.

Ma, N., Wei, J., Liao, R. & Tang, C.Y. 2012, 'Zeolite-polyamide thin film nanocomposite membranes: Towards enhanced performance for forward osmosis', *Journal of Membrane Science*, vol. 405, pp. 149-57.

Madsen, H.T., Bruun Hansen, T., Nakao, T., Goda, S. & Søgaard, E.G. 2020, 'Combined geothermal heat and pressure retarded osmosis as a new green power system', *Energy Conversion and Management*, vol. 226, p. 113504.

McCutcheon, J.R. & Elimelech, M. 2006, 'Influence of concentrative and dilutive internal concentration polarization on flux behavior in forward osmosis', *Journal of Membrane Science*, vol. 284, pp. 237-47.

McCutcheon, J.R. & Elimelech, M. 2008, 'Influence of membrane support layer hydrophobicity on water flux in osmotically driven membrane processes', *Journal of Membrane Science*, vol. 318, no. 1, pp. 458-66.

McGinnis, R.L., McCutcheon, J.R. & Elimelech, M. 2007, 'A novel ammonia–carbon dioxide osmotic heat engine for power generation', *Journal of Membrane Science*, vol. 305, no. 1, pp. 13-9.

Mehta, G.D. & Loeb, S. 1978, 'Internal polarization in the porous substructure of a semipermeable membrane under pressure-retarded osmosis', *Journal of Membrane Science*, vol. 4, pp. 261-5.

Mehta, G.D. & Loeb, S. 1979, 'Performance of permasep B-9 and B-10 membranes in various osmotic regions and at high osmotic pressures', *Journal of Membrane Science*, vol. 4, pp. 335-49.

Meng, H., Gong, B., Geng, T. & Li, C. 2014, 'Thinning of reverse osmosis membranes by ionic liquids', *Applied Surface Science*, vol. 292, pp. 638-44.

Meng, M., Liu, S. & Wang, X. 2020, 'Pressure retarded osmosis coupled with activated sludge process for wastewater treatment: Performance and fouling behaviors', *Bioresource Technology*, vol. 307, p. 123224.

Moon, S.J., Kim, J.H., Seong, J.G., Lee, W.H., Park, S.H., Noh, S.H., Kim, J.H. & Lee, Y.M. 2020, 'Thin film composite on fluorinated thermally rearranged polymer nanofibrous membrane achieves power density of 87 W m−2 in pressure retarded osmosis, improving economics of osmotic heat engine', *Journal of Membrane Science*, vol. 607, p. 118120.

Moon, S.J., Lee, S.M., Kim, J.H., Park, S.H., Wang, H.H., Kim, J.H. & Lee, Y.M. 2020, 'A highly robust and water permeable thin film composite membranes for pressure retarded osmosis generating 26 W·m−2 at 21 bar', *Desalination*, vol. 483, p. 114409.

Mu, Y., Zhu, K., Luan, J., Zhang, S., Zhang, C., Na, R., Yang, Y., Zhang, X. & Wang, G. 2019, 'Fabrication of hybrid ultrafiltration membranes with improved water separation properties by incorporating environmentally friendly taurine modified hydroxyapatite nanotubes', *Journal of Membrane Science*, vol. 577, pp. 274-84.

N. Hilal, A.F.I., M. Kh. Souhaimi, D. Johnson 2020, *Osmosis engineering*, Elsevier, Oxford.

Nagy, E., Hegedüs, I., Tow, E.W. & Lienhard V, J.H. 2018, 'Effect of fouling on performance of pressure retarded osmosis (PRO) and forward osmosis (FO)', *Journal of Membrane Science*, vol. 565, pp. 450-62.

Nicolaisen, B. 2003, 'Developments in membrane technology for water treatment', *Desalination*, vol. 153, no. 1, pp. 355-60.

Norman, R.S. 1974, 'Water salination: A source of energy', *Science*, vol. 186, no. 4161, p. 350.

Oh, Y., Lee, S., Elimelech, M., Lee, S. & Hong, S. 2014, 'Effect of hydraulic pressure and membrane orientation on water flux and reverse solute flux in pressure assisted osmosis', *Journal of Membrane Science*, vol. 465, pp. 159-66.

Park, M.J., Gonzales, R.R., Abdel-Wahab, A., Phuntsho, S. & Shon, H.K. 2018, 'Hydrophilic polyvinyl alcohol coating on hydrophobic electrospun nanofiber membrane for high performance thin film composite forward osmosis membrane', *Desalination*, vol. 426, pp. 50-9.

Park, M.J., Lim, S., Gonzales, R.R., Phuntsho, S., Han, D.S., Abdel-Wahab, A., Adham, S. & Shon, H.K. 2019, 'Thin-film composite hollow fiber membranes incorporated with graphene oxide in polyethersulfone support layers for enhanced osmotic power density', *Desalination*, vol. 464, pp. 63-75.

Park, M.J., Phuntsho, S., He, T., Nisola, G.M., Tijing, L.d., Li, X.-M., Chen, G., Chung, W.-J. & Shon, H.K. 2015, 'Graphene oxide incorporated polysulfone substrate for the fabrication of flat-sheet thin-film composite forward osmosis membranes', *Journal of Membrane Science*, vol. 493, pp. 496-507.

Patel, R., Chi, W.S., Ahn, S.H., Park, C.H., Lee, H.-K. & Kim, J.H. 2014, 'Synthesis of poly(vinyl chloride)-g-poly(3-sulfopropyl methacrylate) graft copolymers and their use in pressure retarded osmosis (PRO) membranes', *Chemical Engineering Journal*, vol. 247, pp. 1-8.

Pattle, R.E. 1954, 'Production of electric power by mixing fresh and salt water in the hydro-electric pile', *Nature*, vol. 174, no. 4431, pp. 660-.

Peng, N., Widjojo, N., Sukitpaneenit, P., Teoh, M.M., Lipscomb, G.G., Chung, T.-S. & Lai, J.-Y. 2012, 'Evolution of polymeric hollow fibers as sustainable technologies: Past, present, and future', *Progress in Polymer Science*, vol. 37, no. 10, pp. 1401-24.

Phuntsho, S., Shon, H.K., Majeed, T., El Saliby, I., Vigneswaran, S., Kandasamy, J., Hong, S. & Lee, S. 2012, 'Blended fertilizers as draw solutions for fertilizer-drawn forward osmosis desalination', *Environmental Science & Technology*, vol. 46, pp. 4567-75.

Post, J.W., Veerman, J., Hamelers, H.V.M., Euverink, G.J.W., Metz, S.J., Nymeijer, K. & Buisman, C.J.N. 2007, 'Salinity-gradient power: Evaluation of pressure-retarded osmosis and reverse electrodialysis', *Journal of Membrane Science*, vol. 288, no. 1, pp. 218-30.

Prante, J.L., Ruskowitz, J.A., Childress, A.E. & Achilli, A. 2014, 'RO-PRO desalination: An integrated low-energy approach to seawater desalination', *Applied Energy*, vol. 120, pp. 104-14.
Qiu, S., Wu, L., Zhang, L., Chen, H. & Gao, C. 2009, 'Preparation of reverse osmosis composite membrane with high flux by interfacial polymerization of MPD and TMC', *Journal of Applied Polymer Science*, vol. 112, no. 4, pp. 2066-72.
Raval, H.D., Trivedi, J.J., Joshi, S.V. & Devmurari, C.V. 2010, 'Flux enhancement of thin film composite RO membrane by controlled chlorine treatment', *Desalination*, vol. 250, no. 3, pp. 945-9.
Reali, M., Dassie, G. & Jonsson, G. 1990, 'Computation of salt concentration profiles in the porous substrate of anisotropic membranes under steady pressure-retarded-osmosis conditions', *Journal of Membrane Science*, vol. 48, no. 2, pp. 181-201.
Regula, C., Carretier, E., Wyart, Y., Sergent, M., Gésan-Guiziou, G., Ferry, D., Vincent, A., Boudot, D. & Moulin, P. 2013, 'Ageing of ultrafiltration membranes in contact with sodium hypochlorite and commercial oxidant: Experimental designs as a new ageing protocol', *Separation and Purification Technology*, vol. 103, pp. 119-38.
Root, T.L., Price, J.T., Hall, K.R., Schneider, S.H., Rosenzweig, C. & Pounds, J.A. 2003, 'Fingerprints of global warming on wild animals and plants', *Nature*, vol. 421, no. 6918, pp. 57-60.
Saito, K., Irie, M., Zaitsu, S., Sakai, H., Hayashi, H. & Tanioka, A. 2012, 'Power generation with salinity gradient by pressure retarded osmosis using concentrated brine from SWRO system and treated sewage as pure water', *Desalination and Water Treatment*, vol. 41, no. 1-3, pp. 114-21.
Saki, S. & Uzal, N. 2019, 'Surface coating of polyamide reverse osmosis membranes with zwitterionic 3-(3,4-dihydroxyphenyl)-l-alanine (l-DOPA) for forward osmosis', *Water and Environment Journal*, vol. 0, no. 0.
Sarp, S., Li, Z. & Saththasivam, J. 2016, 'Pressure Retarded Osmosis (PRO): Past experiences, current developments, and future prospects', *Desalination*, vol. 389, pp. 2-14.
Schwab, M.G., Fassbender, B., Spiess, H.W., Thomas, A., Feng, X. & Müllen, K. 2009, 'Catalyst-free preparation of melamine-based microporous polymer networks through Schiff Base chemistry', *Journal of the American Chemical Society*, vol. 131, no. 21, pp. 7216-7.
Schwinge, J., Neal, P.R., Wiley, D.E., Fletcher, D.F. & Fane, A.G. 2004, 'Spiral wound modules and spacers: Review and analysis', *Journal of Membrane Science*, vol. 242, no. 1, pp. 129-53.
Sgouridis, S. & Csala, D. 2014, 'A Framework for Defining Sustainable Energy Transitions: Principles, Dynamics, and Implications', *Sustainability*, vol. 6, no. 5.
Shafiee, S. & Topal, E. 2009, 'When will fossil fuel reserves be diminished?', *Energy Policy*, vol. 37, no. 1, pp. 181-9.
Shah, A.A., Cho, Y.H., Choi, H.-g., Nam, S.-E., Kim, J.F., Kim, Y., Park, Y.-I. & Park, H. 2019, 'Facile integration of halloysite nanotubes with bioadhesive as highly permeable interlayer in forward osmosis membranes', *Journal of Industrial and Engineering Chemistry*, vol. 73, pp. 276-85.

Shannon, M.A., Bohn, P.W., Elimelech, M., Georgiadis, J.G., Marinas, B.J. & Mayes, A.M. 2008, 'Science and technology for water purification in the coming decades', *Nature*, vol. 452, no. 7185, pp. 301-10.
Shaulsky, E., Boo, C., Lin, S. & Elimelech, M. 2015, 'Membrane-based osmotic heat engine with organic solvent for enhanced power generation from low-grade heat', *Environmental Science & Technology*, vol. 49, no. 9, pp. 5820-7.
She, Q., Hou, D., Liu, J., Tan, K.H. & Tang, C.Y. 2013, 'Effect of feed spacer induced membrane deformation on the performance of pressure retarded osmosis (PRO): Implications for PRO process operation', *Journal of Membrane Science*, vol. 445, pp. 170-82.
She, Q., Jin, X. & Tang, C.Y. 2012, 'Osmotic power production from salinity gradient resource by pressure retarded osmosis: Effects of operating conditions and reverse solute diffusion', *Journal of Membrane Science*, vol. 401, pp. 262-73.
She, Q., Wei, J., Ma, N., Sim, V., Fane, A.G., Wang, R. & Tang, C.Y. 2016, 'Fabrication and characterization of fabric-reinforced pressure retarded osmosis membranes for osmotic power harvesting', *Journal of Membrane Science*, vol. 504, pp. 75-88.
She, Q., Wong, Y.K.W., Zhao, S. & Tang, C.Y. 2013, 'Organic fouling in pressure retarded osmosis: Experiments, mechanisms and implications', *Journal of Membrane Science*, vol. 428, pp. 181-9.
She, Q., Zhang, L., Wang, R., Krantz, W.B. & Fane, A.G. 2017, 'Pressure-retarded osmosis with wastewater concentrate feed: Fouling process considerations', *Journal of Membrane Science*, vol. 542, pp. 233-44.
Sivertsen, E., Holt, T., Thelin, W. & Brekke, G. 2012, 'Modelling mass transport in hollow fibre membranes used for pressure retarded osmosis', *Journal of Membrane Science*, vol. 417-418, pp. 69-79.
Sivertsen, E., Holt, T., Thelin, W. & Brekke, G. 2013, 'Pressure retarded osmosis efficiency for different hollow fibre membrane module flow configurations', *Desalination*, vol. 312, pp. 107-23.
Skilhagen, S.E., Dugstad, J.E. & Aaberg, R.J. 2008, 'Osmotic power — power production based on the osmotic pressure difference between waters with varying salt gradients', *Desalination*, vol. 220, no. 1, pp. 476-82.
Skråmestø, Ø.S., Skilhagen, S.E. & Nielsen, W.K. 2008, *Power production based on osmotic pressure*, Statkraft, Norway.
Son, M., Park, H., Liu, L., Choi, H., Kim, J.H. & Choi, H. 2016, 'Thin-film nanocomposite membrane with CNT positioning in support layer for energy harvesting from saline water', *Chemical Engineering Journal*, vol. 284, pp. 68-77.
Song, X., Liu, Z. & Sun, D.D. 2013, 'Energy recovery from concentrated seawater brine by thin-film nanofiber composite pressure retarded osmosis membranes with high power density', *Energy & Environmental Science*, vol. 6, no. 4, pp. 1199-210.
Song, X., Wang, L., Tang, C.Y., Wang, Z. & Gao, C. 2015, 'Fabrication of carbon nanotubes incorporated double-skinned thin film nanocomposite membranes for enhanced separation performance and antifouling capability in forward osmosis process', *Desalination*, vol. 369, pp. 1-9.
Soroush, A., Ma, W., Cyr, M., Rahaman, M.S., Asadishad, B. & Tufenkji, N. 2016, 'In situ silver decoration on graphene oxide-treated thin film composite forward osmosis

membranes: Biocidal properties and regeneration potential', *Environmental Science & Technology Letters*, vol. 3, no. 1, pp. 13-8.
Soroush, A., Ma, W., Silvino, Y. & Rahaman, M.S. 2015, 'Surface modification of thin film composite forward osmosis membrane by silver-decorated graphene-oxide nanosheets', *Environmental Science: Nano*, vol. 2, no. 4, pp. 395-405.
Sorribas, S., Gorgojo, P., Téllez, C., Coronas, J. & Livingston, A.G. 2013, 'High flux thin film nanocomposite membranes based on metal-organic frameworks for organic solvent nanofiltration', *Journal of the American Chemical Society*, vol. 135, no. 40, pp. 15201-8.
Stenzel, P. & Wagner, H.-J. 2010, 'Osmotic power plants: Potential analysis and site criteria', paper presented to the 3rd International Conference on Ocean Energy, Bilbao, Spain.
Strathmann, H. 2001, 'Membrane separation processes: Current relevance and future opportunities', *AIChE Journal*, vol. 47, no. 5, pp. 1077-87.
Straub, A.P., Deshmukh, A. & Elimelech, M. 2015, 'Pressure-retarded osmosis for power generation from salinity gradients: Is it viable?', *Energy Environ. Sci.*
Straub, A.P., Deshmukh, A. & Elimelech, M. 2016, 'Pressure-retarded osmosis for power generation from salinity gradients: is it viable?', *Energy & Environmental Science*, vol. 9, no. 1, pp. 31-48.
Straub, A.P., Lin, S. & Elimelech, M. 2014, 'Module-scale analysis of pressure retarded osmosis: Performance limitations and implications for full-scale operation', *Environmental Science & Technology*, vol. 48, no. 20, pp. 12435-44.
Straub, A.P., Osuji, C.O., Cath, T.Y. & Elimelech, M. 2015, 'Selectivity and mass transfer limitations in pressure-retarded osmosis at high concentrations and increased operating pressures', *Environmental Science & Technology*, vol. 49, no. 20, pp. 12551-9.
Sun, S.-P. & Chung, T.-S. 2013, 'Outer-selective pressure-retarded osmosis hollow fiber membranes from vacuum-assisted interfacial polymerization for osmotic power generation', *Environmental Science & Technology*, vol. 47, no. 22, pp. 13167-74.
Sun, Y., Cheng, L., Shintani, T., Tanaka, Y., Takahashi, T., Itai, T., Wang, S., Fang, L. & Matsuyama, H. 2018, 'Development of high-flux and robust reinforced aliphatic polyketone thin-film composite membranes for osmotic power generation: Role of reinforcing materials', *Industrial & Engineering Chemistry Research*, vol. 57, no. 40, pp. 13528-38.
Tan, C.H. & Ng, H.Y. 2008, 'Modified models to predict flux behavior in forward osmosis in consideration of external and internal concentration polarizations', *Journal of Membrane Science*, vol. 324, pp. 209-19.
Tan, C.H. & Ng, H.Y. 2013, 'Revised external and internal concentration polarization models to improve flux prediction in forward osmosis process', *Desalination*, vol. 309, pp. 125-40.
Tanioka, A. 2016, 'Preface to the special issue on “Pressure Retarded Osmosis in Megaton Water System Project”', *Desalination*, vol. 389, pp. 15-7.
Tanioka, A., Kurihara, M. & Sakai, H. 2018, 'Megaton Water System: High Salinity Pressure Retarded Osmosis', in S. Sarp & N. Hilal (eds), *Membrane-Based Salinity Gradient Processes for Water Treatment and Power Generation*, Elsevier.

Thelin, W.R., Sivertsen, E., Holt, T. & Brekke, G. 2013, 'Natural organic matter fouling in pressure retarded osmosis', *Journal of Membrane Science*, vol. 438, pp. 46-56.
Thorsen, T. & Holt, T. 2009, 'The potential for power production from salinity gradients by pressure retarded osmosis', *Journal of Membrane Science*, vol. 335, no. 1, pp. 103-10.
Tian, M., Wang, R., Goh, K., Liao, Y. & Fane, A.G. 2015, 'Synthesis and characterization of high-performance novel thin film nanocomposite PRO membranes with tiered nanofiber support reinforced by functionalized carbon nanotubes', *Journal of Membrane Science*, vol. 486, pp. 151-60.
Tian, M., Wang, Y.-N. & Wang, R. 2015, 'Synthesis and characterization of novel high-performance thin film nanocomposite (TFN) FO membranes with nanofibrous substrate reinforced by functionalized carbon nanotubes', *Desalination*, vol. 370, pp. 79-86.
Tian, M., Wang, Y.-N., Wang, R. & Fane, A.G. 2017, 'Synthesis and characterization of thin film nanocomposite forward osmosis membranes supported by silica nanoparticle incorporated nanofibrous substrate', *Desalination*, vol. 401, pp. 142-50.
Tiraferri, A., Yip, N.Y., Phillip, W.A., Schiffman, J.D. & Elimelech, M. 2011a, 'Relating performance of thin-film composite forward osmosis membranes to support layer formation and structure', *Journal of Membrane Science*, vol. 367, no. 1-2, pp. 340-52.
Tiraferri, A., Yip, N.Y., Phillip, W.A., Schiffman, J.D. & Elimelech, M. 2011b, 'Relating performance of thin-film composite forward osmosis membranes to support layer formation and structure', *Journal of Membrane Science*, vol. 367, pp. 340-52.
Tiscornia, I., Kumakiri, I., Bredesen, R., Téllez, C. & Coronas, J. 2010, 'Microporous titanosilicate ETS-10 membrane for high pressure CO2 separation', *Separation and Purification Technology*, vol. 73, no. 1, pp. 8-12.
Tong, X., Wang, X., Liu, S., Gao, H., Xu, C., Crittenden, J. & Chen, Y. 2018, 'A freestanding graphene oxide membrane for efficiently harvesting salinity gradient power', *Carbon*, vol. 138, pp. 410-8.
Touati, K., Salamanca, J., Tadeo, F. & Elfil, H. 2017, 'Energy recovery from two-stage SWRO plant using PRO without external freshwater feed stream: Theoretical analysis', *Renewable Energy*, vol. 105, pp. 84-95.
Touati, K. & Tadeo, F. 2016, 'Study of the reverse salt diffusion in pressure retarded osmosis: Influence on concentration polarization and effect of the operating conditions', *Desalination*, vol. 389, pp. 171-86.
Touati, K. & Tadeo, F. 2017, 'Green energy generation by pressure retarded osmosis: State of the art and technical advancement—review', *International Journal of Green Energy*, vol. 14, no. 4, pp. 337-60.
Touati, K., Usman, H.S., Mulligan, C.N. & Rahaman, M.S. 2020, 'Energetic and economic feasibility of a combined membrane-based process for sustainable water and energy systems', *Applied Energy*, vol. 264, p. 114699.
Tow, E.W., McGovern, R.K. & Lienhard V, J.H. 2015, 'Raising forward osmosis brine concentration efficiency through flow rate optimization', *Desalination*, vol. 366, pp. 71-9.

Tsai, M.-t., Chung, L.-h., Lin, G.-y., Chang, M.-c., Lee, C.-y. & Tai, N.-h. 2020, 'Layered carbon nanotube/polyacrylonitrile thin-film composite membrane for forward osmosis application', *Separation and Purification Technology*, vol. 241, p. 116683.
Volpin, F., Gonzales, R.R., Lim, S., Pathak, N., Phuntsho, S. & Shon, H.K. 2018, 'GreenPRO: A novel fertiliser-driven osmotic power generation process for fertigation', *Desalination*, vol. 447, pp. 158-66.
W. A. Suwaileh, D.J.J., S. Sarp, N. Hilal 2018, 'Advances in forward osmosis membranes: Altering the sub-layer structure via recent fabrication and chemical modification approaches', *Desalination* vol. 436, pp. 176–201.
Wan, C.F. & Chung, T.-S. 2016a, 'Energy recovery by pressure retarded osmosis (PRO) in SWRO–PRO integrated processes', *Applied Energy*, vol. 162, pp. 687-98.
Wan, C.F. & Chung, T.-S. 2016b, 'Maximize the operating profit of a SWRO-PRO integrated process for optimal water production and energy recovery', *Renewable Energy*, vol. 94, pp. 304-13.
Wan, C.F., Jin, S. & Chung, T.-S. 2019, 'Mitigation of inorganic fouling on pressure retarded osmosis (PRO) membranes by coagulation pretreatment of the wastewater concentrate feed', *Journal of Membrane Science*, vol. 572, pp. 658-67.
Wan, C.F., Li, B., Yang, T. & Chung, T.-S. 2017, 'Design and fabrication of inner-selective thin-film composite (TFC) hollow fiber modules for pressure retarded osmosis (PRO)', *Separation and Purification Technology*, vol. 172, pp. 32-42.
Wan, C.F., Yang, T., Gai, W., Lee, Y.D. & Chung, T.-S. 2018, 'Thin-film composite hollow fiber membrane with inorganic salt additives for high mechanical strength and high power density for pressure-retarded osmosis', *Journal of Membrane Science*, vol. 555, pp. 388-97.
Wang, C., Li, Z., Chen, J., Li, Z., Yin, Y., Cao, L., Zhong, Y. & Wu, H. 2017, 'Covalent organic framework modified polyamide nanofiltration membrane with enhanced performance for desalination', *Journal of Membrane Science*, vol. 523, pp. 273-81.
Wang, L., Song, X., Wang, T., Wang, S., Wang, Z. & Gao, C. 2015, 'Fabrication and characterization of polyethersulfone/carbon nanotubes (PES/CNTs) based mixed matrix membranes (MMMs) for nanofiltration application', *Applied Surface Science*, vol. 330, pp. 118-25.
Wang, Y., Luo, S., Guo, J., Liu, M., Wang, J., Yan, J. & Luo, T. 2020, 'LIS-PRO: A new concept of power generation from low temperature heat using liquid-phase ion-stripping-induced salinity gradient', *Energy*, vol. 200, p. 117593.
Wang, Y., Ou, R., Ge, Q., Wang, H. & Xu, T. 2013, 'Preparation of polyethersulfone/carbon nanotube substrate for high-performance forward osmosis membrane', *Desalination*, vol. 330, pp. 70-8.
Wang, Y., Ou, R., Wang, H. & Xu, T. 2015, 'Graphene oxide modified graphitic carbon nitride as a modifier for thin film composite forward osmosis membrane', *Journal of Membrane Science*, vol. 475, pp. 281-9.
Wei, J., Li, Y., Setiawan, L. & Wang, R. 2016, 'Influence of macromolecular additive on reinforced flat-sheet thin film composite pressure-retarded osmosis membranes', *Journal of Membrane Science*, vol. 511, pp. 54-64.
Wei, J., Qiu, C., Tang, C.Y., Wang, R. & Fane, A.G. 2011, 'Synthesis and characterization of flat-sheet thin film composite forward osmosis membranes', *Journal of Membrane Science*, vol. 372, no. 1-2, pp. 292-302.

Wu, M., Yuan, J., Wu, H., Su, Y., Yang, H., You, X., Zhang, R., He, X., Khan, N.A., Kasher, R. & Jiang, Z. 2019, 'Ultrathin nanofiltration membrane with polydopamine-covalent organic framework interlayer for enhanced permeability and structural stability', *Journal of Membrane Science*, vol. 576, pp. 131-41.

Xie, M., Lee, J., Nghiem, L.D. & Elimelech, M. 2015, 'Role of pressure in organic fouling in forward osmosis and reverse osmosis', *Journal of Membrane Science*, vol. 493, pp. 748-54.

Xiong, J.Y., Cai, D.J., Chong, Q.Y., Lee, S.H. & Chung, T.-S. 2017, 'Osmotic power generation by inner selective hollow fiber membranes: An investigation of thermodynamics, mass transfer, and module scale modelling', *Journal of Membrane Science*, vol. 526, pp. 417-28.

Xiong, S., Xu, S., Phommachanh, A., Yi, M. & Wang, Y. 2019, 'Versatile surface modification of TFC membrane by layer-by-layer assembly of phytic acid-metal complexes for comprehensively enhanced FO performance', *Environmental Science & Technology*, vol. 53, pp. 3331-41.

Xu, J., Wang, Z., Wei, X., Yang, S., Wang, J. & Wang, S. 2013, 'The chlorination process of crosslinked aromatic polyamide reverse osmosis membrane: New insights from the study of self-made membrane', *Desalination*, vol. 313, pp. 145-55.

Yang, H.-C., Liao, K.-J., Huang, H., Wu, Q.-Y., Wan, L.-S. & Xu, Z.-K. 2014, 'Mussel-inspired modification of a polymer membrane for ultra-high water permeability and oil-in-water emulsion separation', *Journal of Materials Chemistry A*, vol. 2, no. 26, pp. 10225-30.

Yang, H., Wu, H., Pan, F., Li, Z., Ding, H., Liu, G., Jiang, Z., Zhang, P., Cao, X. & Wang, B. 2016, 'Highly water-permeable and stable hybrid membrane with asymmetric covalent organic framework distribution', *Journal of Membrane Science*, vol. 520, pp. 583-95.

Yang, T., Wan, C.F., Xiong, J.Y. & Chung, T.-S. 2019, 'Pre-treatment of wastewater retentate to mitigate fouling on the pressure retarded osmosis (PRO) process', *Separation and Purification Technology*, vol. 215, pp. 390-7.

Yang, Y., Chuah, C.Y., Nie, L. & Bae, T.-H. 2019, 'Enhancing the mechanical strength and CO_2/CH_4 separation performance of polymeric membranes by incorporating amine-appended porous polymers', *J. Membr. Sci.*, vol. 569, pp. 149-56.

Yin, J., Kim, E.-S., Yang, J. & Deng, B. 2012, 'Fabrication of a novel thin-film nanocomposite (TFN) membrane containing MCM-41 silica nanoparticles (NPs) for water purification', *Journal of Membrane Science*, vol. 423-424, pp. 238-46.

Yip, N.Y. & Elimelech, M. 2011, 'Performance limiting effects in power generation from salinity gradients by pressure retarded osmosis', *Environmental Science & Technology*, vol. 45, no. 23, pp. 10273-82.

Yip, N.Y. & Elimelech, M. 2013, 'Influence of natural organic matter fouling and osmotic backwash on pressure retarded osmosis energy production from natural salinity gradients', *Environmental Science & Technology*, vol. 47, no. 21, pp. 12607-16.

Yip, N.Y. & Elimelech, M. 2014, 'Comparison of energy efficiency and power density in pressure retarded osmosis and reverse electrodialysis', *Environmental Science & Technology*, vol. 48, no. 18, pp. 11002-12.

Yip, N.Y., Tiraferri, A., Phillip, W.A., Schiffman, J.D., Hoover, L.A., Kim, Y.C. & Elimelech, M. 2011, 'Thin-film composite pressure retarded osmosis membranes for

sustainable power generation from salinity gradients', *Environmental Science & Technology*, vol. 45, no. 10, pp. 4360-9.
Yun, T., Kim, Y.-J., Lee, S., Hong, S. & Kim, G.I. 2014, 'Flux behavior and membrane fouling in pressure-assisted forward osmosis', *Desalination and Water Treatment*, vol. 52, no. 4-6, pp. 564-9.
Zhai, X., Meng, J., Li, R., Ni, L. & Zhang, Y. 2011, 'Hypochlorite treatment on thin film composite RO membrane to improve boron removal performance', *Desalination*, vol. 274, no. 1, pp. 136-43.
Zhang, J., Qin, Z., Yang, L., Guo, H. & Han, S. 2017, 'Activation promoted ionic liquid modification of reverse osmosis membrane towards enhanced permeability for desalination', *Journal of the Taiwan Institute of Chemical Engineers*, vol. 80, pp. 25-33.
Zhang, L., Lin, Y., Wang, S., Cheng, L. & Matsuyama, H. 2020, 'Engineering of ultrafine polydopamine nanoparticles in-situ assembling on polyketone substrate for highly-efficient oil-water emulsions separation', *Journal of Membrane Science*, vol. 613, p. 118501.
Zhang, L., She, Q., Wang, R., Wongchitphimon, S., Chen, Y. & Fane, A.G. 2016, 'Unique roles of aminosilane in developing anti-fouling thin film composite (TFC) membranes for pressure retarded osmosis (PRO)', *Desalination*, vol. 389, pp. 119-28.
Zhang, M., Hou, D., She, Q. & Tang, C.Y. 2014, 'Gypsum scaling in pressure retarded osmosis: Experiments, mechanisms and implications', *Water Research*, vol. 48, pp. 387-95.
Zhang, S., Fu, F. & Chung, T.-S. 2013, 'Substrate modifications and alcohol treatment on thin film composite membranes for osmotic power', *Chemical Engineering Science*, vol. 87, pp. 40-50.
Zhang, S., Sukitpaneenit, P. & Chung, T.-S. 2014, 'Design of robust hollow fiber membranes with high power density for osmotic energy production', *Chemical Engineering Journal*, vol. 241, pp. 457-65.
Zhang, S., Zhang, Y. & Chung, T.-S. 2016, 'Facile preparation of antifouling hollow fiber membranes for sustainable osmotic power generation', *ACS Sustainable Chemistry & Engineering*, vol. 4, no. 3, pp. 1154-60.
Zhang, Y., Li, J.L., Cai, T., Cheng, Z.L., Li, X. & Chung, T.-S. 2018, 'Sulfonated hyperbranched polyglycerol grafted membranes with antifouling properties for sustainable osmotic power generation using municipal wastewater', *Journal of Membrane Science*, vol. 563, pp. 521-30.
Zhao, D., Qiu, G., Li, X., Wan, C., Lu, K. & Chung, T.-S. 2016, 'Zwitterions coated hollow fiber membranes with enhanced antifouling properties for osmotic power generation from municipal wastewater', *Water Research*, vol. 104, pp. 389-96.
Zhao, D.L., Das, S. & Chung, T.-S. 2017, 'Carbon quantum dots grafted antifouling membranes for osmotic power generation via pressure-retarded osmosis process', *Environmental Science & Technology*, vol. 51, no. 23, pp. 14016-23.
Zhao, J., Milanova, M., Warmoeskerken, M.M.C.G. & Dutschk, V. 2012, 'Surface modification of TiO2 nanoparticles with silane coupling agents', *Colloids and Surfaces A: Physicochemical and Engineering Aspects*, vol. 413, pp. 273-9.

Zhou, Z., Lee, J.Y. & Chung, T.-S. 2014, 'Thin film composite forward-osmosis membranes with enhanced internal osmotic pressure for internal concentration polarization reduction', *Chemical Engineering Journal*, vol. 249, pp. 236-45.

Zornoza, B., Tellez, C., Coronas, J., Gascon, J. & Kapteijn, F. 2013, 'Metal organic framework based mixed matrix membranes: An increasingly important field of research with a large application potential', *Microporous and Mesoporous Materials*, vol. 166, no. Supplement C, pp. 67-78.

Zou, L., Sun, Y., Che, S., Yang, X., Wang, X., Bosch, M., Wang, Q., Li, H., Smith, M., Yuan, S., Perry, Z. & Zhou, H.C. 2017, 'Porous organic polymers for post-combustion carbon capture', *Adv. Mater.*, vol. 29, no. 37, p. 1700229.